Interannual variability and predictability of the Indian Summer Monsoon - El Niño Southern Oscillation system

Ghyslaine Boschat

THESE DE DOCTORAT
DE L'UNIVERSITE PIERRE ET MARIE CURIE

Ecole Doctorale des sciences de l'environnement d'Ile de France

Spécialité
Océanographie Physique - Sciences Atmosphériques

Présentée par
Ghyslaine BOSCHAT

Pour obtenir le grade de
Docteur de l'Université Pierre et Marie CURIE

Interannual variability and predictability of the Indian Summer Monsoon – El Niño Southern Oscillation system

---

pour soutenir le 10 Février 2012, devant le jury composé de :

Pr Hervé LETREUT	Président	IPSL
Dr Pascale DELECLUSE	Rapporteur	Météo-France CNRM
Dr Thierry DELCROIX	Rapporteur	LEGOS
Dr Hervé DOUVILLE	Examinateur	CNRM
Dr Annalisa CHERCHI	Examinateur	INGV (Italy)
Dr Pascal TERRAY	Directeur de thèse	LOCEAN
Dr Sébastien MASSON	Co-Directeur de thèse	LOCEAN

Thèse préparée au laboratoire LOCEAN

Université Pierre & Marie Curie - Paris 6
Bureau d'accueil, inscription des doctorants et base de données
Esc G, 2ème étage
15 rue de l'école de médecine, 75270-PARIS CEDEX 06

Tél. Secrétariat : 01 42 34 68 35
Fax : 01 42 34 68 40
E-mail : scolarite.doctorat@upmc.fr

Acknowledgment

It may not come to a surprise for some that I have left this section to write at the very last minute... nevertheless I hope I will be able to convey here my most sincere gratitude to those who have made these three last years so special.

My first thank you goes to Pascal and Sébastien who have always been there for me in spite of the twists and turns that may have animated my PhD. Pascal, thank you for everything that you have taught me on the Indian monsoon, on El Niño, and on the bright and dark sides of the research world. Thank you for your advice and guidance in times of need, and for having been so available throughout these three years. Sébastien thank you for trusting me, for teaching me how to use a computer and write a script. Thank you for making me laugh, for your optimism and unconditional patience! You both have done much more than simply « supervise » me over the years, and I feel privileged to have worked with you.

I am also grateful to the jury members of my thesis who have been ever so kind to read this manuscript and to come to Paris for my PhD defense. Dr Pascale Delecluse, Thierry Delcroix, Hervé Douville, Annalisa Cherchi thank you for your insightful comments and many thanks to Professor Hervé Letreut for accepting to preside this jury.

I cannot continue here without acknowledging that my experience in the field of oceanography and climate science began in 2006 in the remote town of Tallahassee in Florida, where I was lucky to meet and work with two amazing people Dr William K Dewar and Nicolas Wienders. A part of who am I stems from this experience. Nico, thank you for teaching me the redneck lifestyle (especially how to hunt deers!), and for being the source of motivation for my professional future.

During my stay at the LOCEAN, I feel privileged to have also met many special people. I would like to thank in particular Christine Provost and Nathalie Sennechael for believing in me and for allowing me to experience such a thrilling adventure on board the Polarstein to Antarctica. I will be ever so grateful..

Finally, these years would not have been the same without the many friends I made at the LOCEAN. In their order of appearance:

Pascaline – thank you for your friendship. I hope we will continue sharing our life experiences and that you will always keep that passionate sparkle in your eye. Who knows maybe we'll meet up in Noeux-Les-Mines one day ;-)

Kristell – if we had written as many articles as long daily emails, we would definitely be sharing an impressive list of publications by now! Thank you for being such a supportive and trustworthy friend.

Agnès – thank you for all the chit-chat, the chocolate fondants, your headstands against the wall, and for your infinite smile and courage.

Gaëlle – thank you for bearing with my ups and downs, for your constant technical or moral support. These years would never had been the same without our coffee breaks.

Simon – whats the craic mate? thanks for your nutritious tips and for helping me acquire that inner balance between guinness and chocolate.

Audrey – I'm not quite sure how to thank you. Tu penses que ça craint? thank you for your good humour and for teaching me to put things well into perspective :-)

I also have to thank my lunch break buddies, Marion, Laetitia, Pierre, and the other friends I was lucky to make along the way, at the 4th *and* 5th floors: Camille M, Chloé, Dorotea, Kamala, Manu, Rym, Fer, Aurélie, Benoît, Cédric, Kyla, Manu. Without forgetting those, outside, who never failed to believe in me: Jemmy, Anne-Lise, Alex, Camille.

I would like to finish by expressing my full and uttermost gratitude to my Ma and Da for their love and emotional support. Despite the distance, your persistent confidence in me has taken the load off my shoulder.

My last – but by no means least – words are dedicated to the person who has been my source of encouragement, motivation and joy throughout the years. Guillaume, I owe you everything.

Abstract

Interannual variability and predictability of the Indian Summer Monsoon - El Niño Southern Oscillation system

El Niño-Southern Oscillation (ENSO) and the Indian Summer Monsoon (ISM) are two of the most energetic and influential climatic phenomena on the planet. Although they originate in the tropical Indo-Pacific region, they can extend their reach well beyond, through atmospheric teleconnnections that can affect patterns of climate variability worldwide. This thesis takes part in a global effort to improve our understanding of the potential predictability of ISM rainfall and ENSO, by exploring the large-scale teleconnections associated with the whole monsoon-ENSO system on interannual timescales, as well as the role played by leading modes of coupled variability, particularly in tropical and extratropical parts of the Indo-Pacific region. Based on statistical diagnoses of observations before and after the 1976-77 climate shift, and numerical experiments with the SINTEX-F coupled model, our results highlight the importance of mid-latitudes in the predictability of the ISM-ENSO system. Indeed, significant and robust precursors are identified in the North Pacific and South Indian Oceans during the previous boreal winter/early spring, and have the potential to predict ISM and ENSO events with longer lead-times than their traditional tropical predictors. Besides, this predictability is stronger for the 'late' ISM rainfall during August-September. This second part of the ISM season is also characterized by the occurrence of ocean-atmospheric processes in the Indian Ocean, which compete with the effect of ENSO on the monsoon. The enhancement of these local feedbacks could explain the apparent weakening of the seasonal ENSO-monsoon relationship observed in recent decades.

Keywords: variability, predictability, monsoon, ENSO, teleconnection, ocean-atmospheric coupling, extratropical forcing.

Résumé

Variabilité interannuelle et prévisibilité du système Mousson Indienne d'Eté - El Niño Oscillation Australe

La Mousson Indienne d'été (ISM) et l'Oscillation Australe El Niño (ENSO) sont parmi les phénomènes climatiques les plus énergétiques et importants de la planète. Bien qu'ils soient localisés dans la région tropicale Indo-Pacifique, ces deux phénomènes peuvent avoir des répercussions climatiques à l'échelle globale via les téléconnections atmosphériques. Cette thèse vise à améliorer notre compréhension et la prévisibilité interannuelle d'ENSO et de l'ISM, en analysant leurs téléconnections grandes échelles, et en déterminant le rôle, dans cette prévisibilité, des modes majeurs de variabilité interannuelle observés dans les régions tropicales et extratropicales de l'Indo-Pacifique. A partir de diagnostiques statistiques d'observations sur les périodes 1950-1976 et 1979-2007, et d'expériences de sensibilité réalisées à l'aide du modèle couplé SINTEX-F, nous montrons l'importance des latitudes tempérées dans la prévisibilité du système ENSO-mousson. Des précurseurs robustes des évènements ENSO et ISM sont identifiés dans les régions du Pacific Nord et de l'Océan Indien Sud pendant l'hiver boréal précédent, apportant ainsi de la prévisibilité plus tôt que leurs traditionnels précurseurs tropicaux. De plus, cette prévisibilité de la mousson d'été est accrue pour les pluies en *fin* de saison (Août-Septembre). Cette deuxième partie de la saison de mousson se caractérise également par l'émergence de processus couplés océan-atmosphère dans l'Océan Indien, pouvant contrecarrer l'effet d'ENSO sur la mousson. Une amplification de ces rétroactions locales pourrait expliquer l'affaiblissement de la relation ENSO-mousson observé lors des dernières décennies.

Mots clés : variabilité, prévisibilité, mousson, ENSO, téléconnection, couplage océan-atmosphère, forçage extratropical.

Contents

Chapter I

INTRODUCTION

Contents

Tropical oceans play a major role in the natural variability of the world climate, as they give rise to large-scale ocean-atmosphere interactions, and some of the most energetic and influential climatic phenomena on the planet. The El Niño Southern Oscillation (ENSO) in the tropical Pacific Ocean is one of such phenomenon [*Philander*, 1990; *Clarke*, 2008]. It is recognized as being a dominant source of interannual climate variability, and can produce global atmospheric and oceanic circulation changes that influence regional climate conditions even in remote areas [*Trenberth et al.*, 1998; *Alexander et al.*, 2002]. The seasonal Asian Summer Monsoon system is another vigorous climatic signal in the tropics, and source of tremendous energy, also for both tropical and extratropical regions of the globe [*Krishnamurthi et al.*, 1973]. The direct and indirect climate signatures – or 'teleconnections' – associated with these two tropical phenomena have large socio-economical impacts and affect more than 60% of the earth's population [*Philander*, 1990; *Webster et al.*, 1998; *Wang*, 2006a]. With such significant and far-reaching effects, it is no wonder the ENSO-monsoon system has received so much attention from the world climate community over the past few decades and will continue to do so in the present global warming context. Indeed, deeper understanding of the mechanisms regulating this tropical system and the associated teleconnections, may have significant repercussions for long-term seasonal prediction of regional climates, both in tropical and extratropical areas of the globe [*Alexander et al.*, 2002].

In this introductory chapter, we will start by defining and describing some of the main salient features of ENSO and the Asian Summer Monsoon system, as to better apprehend the global importance of these modes of variability, how they interact with each other, as well as our current understanding and the remaining challenging issues regarding their long-term seasonal predictability. The purpose of the next few pages is to set the general context of the thesis and describe only the basic large-scale characteristics of ENSO and the Asian monsoon, which, we believe, are essential for the understanding of the following chapters. A much more detailed and, certainly much better, account of the Asian Summer Monsoon and ENSO may be found in the recent literature (*e.g.* [*Wang*, 2006a; *Clarke*, 2008]).

I.1 A brief overview of the Indian Summer Monsoon

Definition

As the word 'monsoon' indicates (derived from the Arabic word for 'season'), the South Asian Monsoon is part of a seasonally-reversing wind system characterized by wet summers and dry winters [*Webster et al.*, 1998; *Ding and Chan*, 2005; *Trenberth et al.*, 2006; *Wang*, 2006a]. Throughout this thesis, we will be focusing on the **Indian Summer Monsoon** (ISM hereafter) component of the monsoonal region, since the Indian subcontinent experiences large seasonal variations in wind direction from boreal winter to boreal summer (Fig I.3) and some of the largest seasonal rainfall

during boreal summer (Fig I.1), which has drastic impacts on the resources of the South Asian countries and livelihood of their population. The summer monsoon accounts for about 80% of the annual rainfall received over the South Asian region, particularly over the Indian subcontinent, and these rains have a crucial impact on the economy of India since this country is still largely dependent on its rain-fed agriculture representing 25% of the Gross Domestic Product and 70% of total employment [*Selvaraju*, 2003].

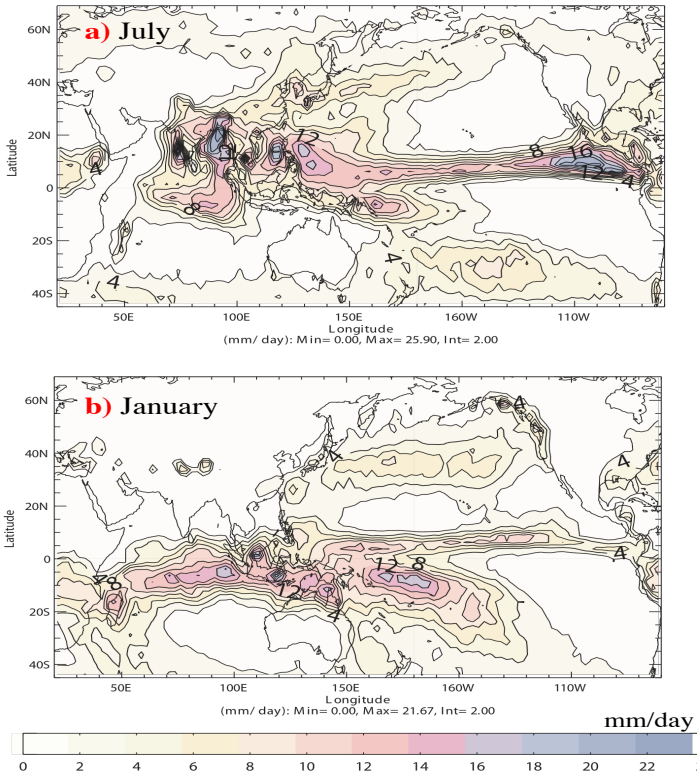

Figure I.1: Rainfall climatology derived from the CMAP dataset (during 1979-2000) for the months of July **(a)** and January **(b)**, from [*Terray et al.*, 2005b].

An understanding of some of the mean large-scale features of the monsoon annual cycle is necessary before examining the variability and predictability of the ISM at the interannual timescale.

ISM annual cycle

Traditionally, monsoons are considered as large-scale 'land-sea breezes', where the seasonal wind reversal is driven by land-ocean thermal contrasts, caused by the different responses of land and sea to seasonal solar heating, and resulting in the development of a thermal low over the continent [*Halley*, 1686; *Webster et al.*, 1998]. The seasonal change of winds and rainfall in the ISM region is also often interpreted as a result of the northward seasonal migration of the east-west oriented

precipitation belt or InterTropical Convergence Zone (ITCZ), from the southern hemisphere in boreal winter to the northern hemisphere in boreal summer [*Gadgil*, 2003]. The largest northward excursion of the rain belt associated with the ITCZ takes place over this Indian monsoon region where it moves from a mean position of about 5°S in winter to about 20°N during boreal summer (see Fig I.1 and I.2).

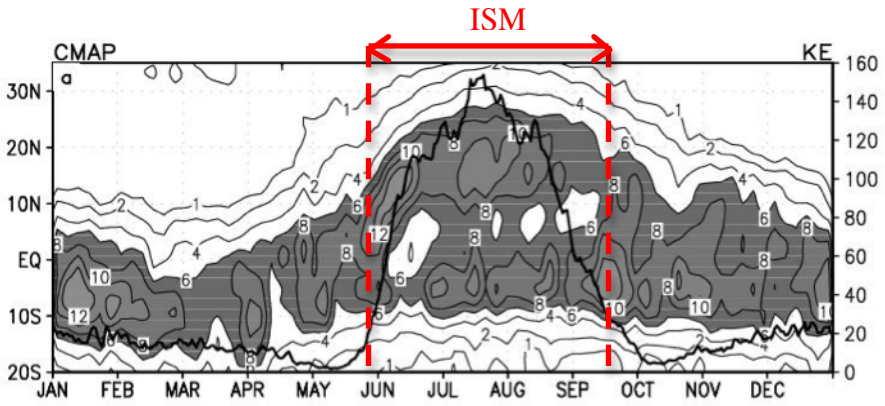

Figure I.2: Annual evolution of the ITCZ over the Indian monsoon region, defined by climatological precipitation (mm/day) averaged between 70°E and 90°E (shaded) and kinetic energy (thick solid line) of the Low-Level Jet (winds at 850hPa averaged over 50°E-65°E, 5°N-15°N), from [*Goswami*, 2005].

In boreal winter, the southward position of this ITCZ induces a convergence of low-level winds south of the equator, around 5°- 10°S, which creates strong northeasterly winds over the northern Indian Ocean (IO) (DJF season, in Fig I.3). During the spring intermediate season, the Indian landmass begins to heat up (inducing a heat low over the northwestern part of the continent) and the warmest Sea Surface Temperatures (SST) are observed over most of the IO, north of 10 °S (Fig I.3). This northward SST gradient tends to intensify the trade winds in the south IO, and this time incites a convergence of seasonal winds from the *southern* hemisphere towards the *northern* hemisphere. The southeasterly winds in the south IO are deflected by the Coriolis force while crossing the equator and become southwesterlies in the northern IO. By boreal summer (JJA season, in Fig I.3), these southwesterly winds are a dominant feature of the whole north IO, and are particularly strong over the western Arabian Sea, where an intense low-level jet (*e.g.* the Findlater jet) has developed along the African coast. The Findlater jet is associated with one of the most intense upwellings in the world. The colder waters upwelled along this coastline act to further enhance the SST gradient in the north Arabian Sea and in turn sustain/reinforce the strength of this low-level jet near the Indian subcontinent. The onset of the monsoon is characterized by a sharp increase in the kinetic energy of this low-level jet over the Arabian Sea (see Fig I.2), as well as a rapid northward transition of the wind convergence and high precipitation zone between the end of May and early June.

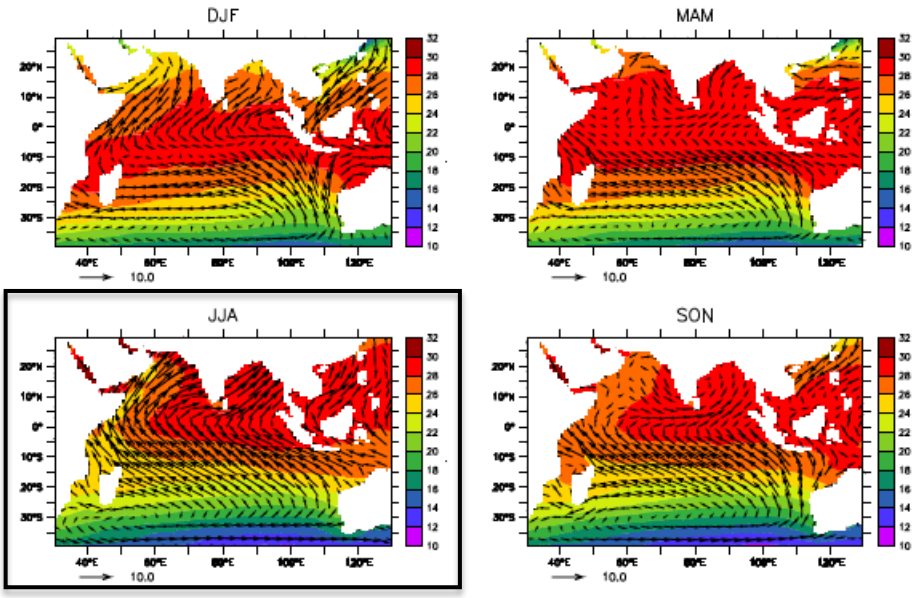

Figure I.3: SST and 10m wind climatological fields in the Indian Ocean, calculated from Hadley centre SST dataset [*Rayner et al.*, 2003] and from ERA40 reanalysis wind data [*Uppala et al.*, 2005] during the 1958-2001 period (from *Manuel de météorologie tropicale : des alizés au cyclone*, by Florent Beucher).

The seasonal reversal of the wind direction from boreal winter to summer brings copious moisture from the warm waters of the tropical IO towards the Indian subcontinent, through two branches :

- the *Arabian Sea branch* (A), which first hits the Western Ghats on the coastal state of Kerala and then moves northwards along the western coast, providing this western region with maximum rainfall during the summer

- the *Bay of Bengal branch* (B), which gathers moisture from the Bay of Bengal then flows towards North-East India and Bengal, to arrive at the Eastern Himalayas with large amounts of rain, and then travel westwards over the Indo-Gangetic Plains. The northeastern hilly regions are characterized by another maximum of rainfall, and thereby illustrate the considerable spatial variability of mean summer monsoon rainfall over India.

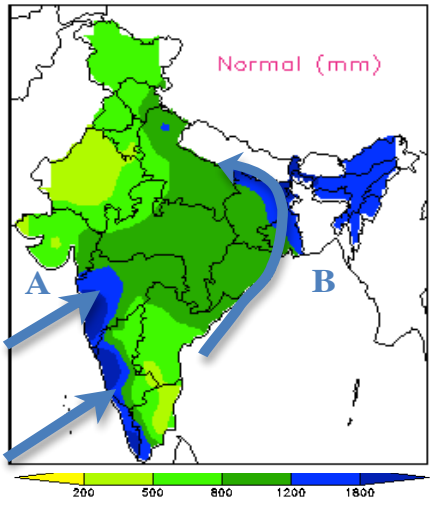

Figure I.4: Spatial distribution of long-term mean cumulated ISM rainfall from June to September (based on the Iindian Meteorological Department subdivisional rainfall data).

The climatological date of monsoon onset over Kerala has been defined as the 1^{st} June with a standard deviation of 8 days [*Pai and Rajeevan*, 2007]. However, a delay of even a few days in the arrival of the monsoon could have dire economic and social consequences for India. This strong reliance of the population on monsoon characteristics raises the issue of ISM predictability, and calls on the necessity to understand the variations in ISM rainfall, to be able to foresee them in a timely and accurate manner.

ISM variability

Two remarkable features of the summer monsoon are its *regular* occurrence every year from June to September, and the *irregular* variation in the timing and amount of seasonal mean rainfall that it brings to India from one year to the other. The ISM rainfall thus exhibits some 'interannual' variability, with some years characterized by excessive seasonal rainfall (or floods) and others marked by deficient rainfall (or droughts) over a large part of the country, as it is illustrated during the 1871-2009 period in Fig I.5. There are also considerable variations of rainfall within the summer season, due to the occurrence of 'active' and 'break' phases, which are associated with intraseasonal oscillations on timescales of 10-20 days and 30-60 days [*Goswami*, 1998; *Annamalai and Slingo*, 2001; *Kripalani et al.*, 2004]. Thus, the ISM exhibits oscillations on time scales ranging from days to decades, but the physical mechanisms that contribute to the existence of these specific modes of ISM oscillations and their mutual interactions are not yet fully understood.

Therefore, as part of the broader effort to develop useful forecasts, in this thesis we will be focusing on the year-to-year variations of ISM rainfall. Earlier works have shown that this interannual variability is non periodic and may result from the inherent atmospheric dynamics (*e.g.* instabilities in the form of synoptic scale disturbances, non linear interactions among various scales of motion), but may also be influenced by slowly varying forcings such as SST, soil moisture, sea ice or snow at the surface [*Charney and Shukla*, 1981; *Webster et al.*, 1998]. These global boundary forcings have the potential to modify the location and intensity of heat sources and circulation, which control the monsoon. Understanding the teleconnection between ISM rainfall and these potential sources of forcing may thus have interesting implications for our understanding of ISM predictability at the interannual timescale.

As an illustration, Fig I.5 indicates that a majority of deficient (excessive) ISM events during 1871-2009 seem to occur during El Niño (La Niña) years, thereby introducing a well-known connection between extreme ISM seasons and manifestations of the ENSO mode of variability in the tropical Pacific.

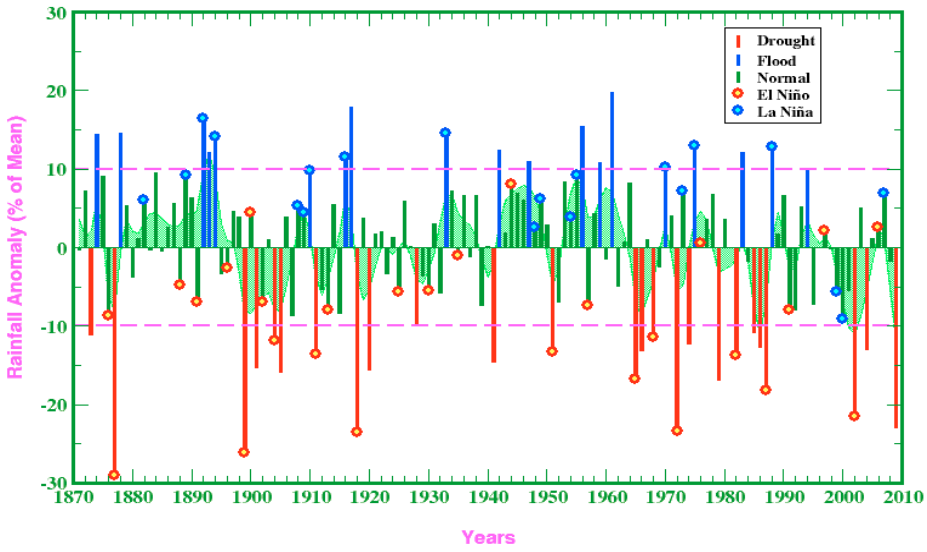

Figure I.5: Interannual variability in the observed record of the ISM seasonal rainfall from 1871 to 2009, based on the Indian Institute of Tropical Meteorology (IITM) Homogeneous Indian Monthly Rainfall Dataset (http://www.tropmet.res.in/ kolli/mol/Monsoon/frameindex.html). Associations with El Niño or La Niña conditions in the east Pacific are also indicated by red and blue circles respectively.

I.2 A brief overview of ENSO

El Niño Southern Oscillation, or ENSO, can be schematically defined as a coupled ocean-atmosphere phenomenon, which combines changes in the atmosphere, referred to as the 'Southern Oscillation' (SO), and changes in the Pacific Ocean represented by the 'El Niño/La Niña' phenomenon.

Interestingly, it was while searching for predictors of the Indian Monsoon, that Sir Gilbert Walker (1923, 1924) first discovered the Southern Oscillation, a sea-saw of atmospheric pressure between the Indian and Pacific sections (in Darwin and Tahiti), premise of a larger east-west circulation which *Bjerknes* [1969] later named the "Walker circulation". During a 'normal year' (see Fig I.6b), this circulation is caused by a zonal equatorial pressure gradient between the higher surface pressures in the eastern Pacific and the lower pressures over the warmer waters of the western Pacific and eastern Indian Oceans. A weaker/reversed (stronger) Walker circulation modifies the ocean surface conditions in the tropical Pacific, which leads to an El Niño (La Niña) event.

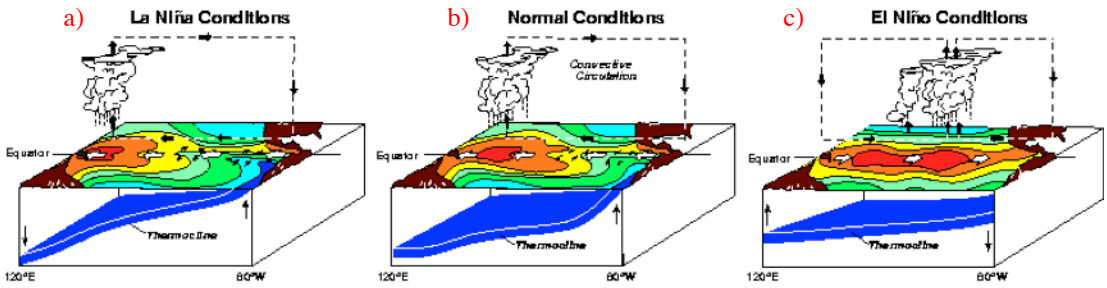

Figure I.6: Schematic view of the tropical Pacific ocean during a La Niña **(a)**, normal **(b)** and El Niño year **(c)**. Figure courtesy of NOAA PMEL.

At the simplest level, El Niño's growth is the result of the Bjerknes feedback [*Bjerknes*, 1966], a positive ocean-atmosphere interaction that links the strength of easterly trade winds to surface temperature in the Pacific cold tongue. A warm anomaly in the central Pacific induces an eastward displacement of the atmospheric deep convection, and westerly wind anomalies in the central and western Pacific (Fig I.6c). The westerly wind anomaly drives an ocean response that reinforces the initial SST anomaly by pushing the warm pool to the east; furthermore the excited downwelling Kelvin wave depresses the thermocline in the east. This positive feedback loop eventually leads to anomalous conditions such as those displayed in Fig I.6c, culminating during boreal winter. La Niña, the opposite phase to El Niño, features cooling in the central to east Pacific region also peaking during boreal winter, and is associated with enhanced easterly trade winds and a steeper thermocline with more upwelling in the east (Fig I.6a).

Historically, El Niño events occur about every 3 to 7 years [*Chang et al.*, 2006] and are quite regularly followed by the opposite La Niña phases of below-average temperatures in the eastern tropical Pacific (although the reversed La Niña – El Niño transitions are less systematic). In other words, ENSO oscillates between warm phases and cold phases. Several theories have been proposed in order to explain the mechanism of oscillation embedded in ENSO events [*Battisti and Hirst*, 1989; *Weisberg and Wang*, 1997; *Jin*, 1997; *Picaut et al.*, 1997]. In most of these theories, oceanic equatorial waves (Rossby and Kelvin waves) and upper-ocean heat content play an important role in explaining the oscillatory characteristics of the ENSO dynamics. One of the challenging questions in most of these ENSO theories is the triggering mechanisms for the onset of El Niño events and the phase locking of the ENSO cycle to the annual cycle which is characterized by a reduced persistence of equatorial Pacific SST anomalies during boreal spring [*Torrence and Webster*, 1998; *Chang et al.*, 2006].

Although ENSO originates in the tropical Pacific, it can extend its reach well beyond, through atmospheric teleconnections that can affect patterns of climate variability worldwide, especially over the Indian Ocean and Asia (see Fig I.7 for an illustration of some of El Niño worldwide effects).

Understanding and predicting ENSO is thus crucial to both the scientific community and the public [*McPhaden et al.*, 2006].

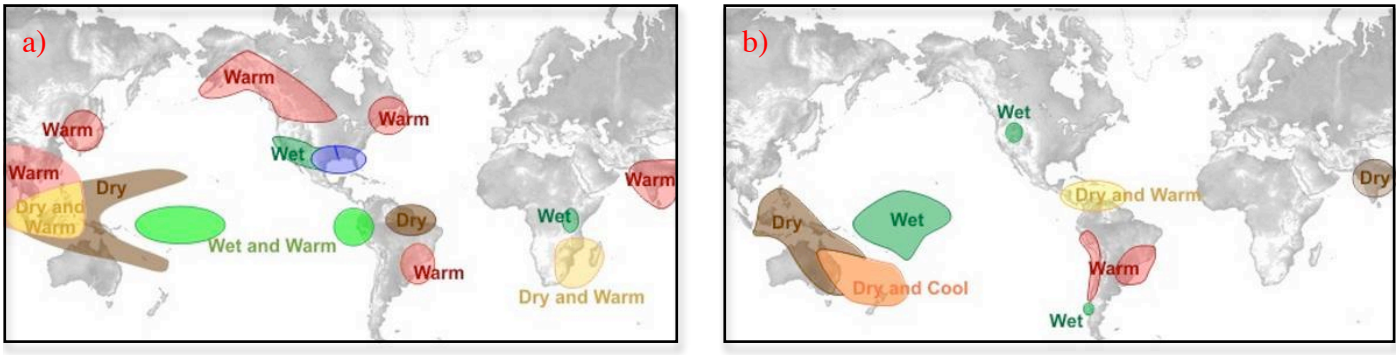

Figure I.7: El Niño effects in worldwide regions **a)** during December through February, and **b)** during June through August. Source: http://www.srh.noaa.gov/jetstream.

I.3 Our current understanding of the ENSO-monsoon system

For nearly a century, research has been done to attempt to quantify the nature and origins of large-scale connections between the interannual variability of the ISM system and ENSO. Most studies agree on the existence of a strong synchronous relationship between ISM and ENSO (with a significant -0.5 correlation between ISM rainfall in JJAS and the Niño3.4 SST during the following DJ, see red cross in Fig I.10), according to which a deficient (excessive) ISM rainfall season is associated with the warm (cold) phase of ENSO ([*Rasmusson and Carpenter*, 1982; *Ju and Slingo*, 1995; *Webster et al.*, 1998] among many others; see Fig I.5). The exact mechanism of interactions between ENSO and ISM, however, is still not clear.

Influence of ENSO on ISM:

Since the pioneering works of *Walker* [1924], ENSO has been used in ISM forecasts [*Rajeevan et al.*, 2006], and various ENSO-related predictors have been developed, representing the strengths of both its atmospheric component (the Southern Oscillation) and its ocean component (El Niño SST). ENSO influences the ISM not by direct subsidence over the Indian continental region but through an interaction between the equatorial Walker circulation and the regional monsoon (reversed) Hadley circulation. Indeed, during El Niño events, the shift of the climatological Walker circulation results in enhanced low-level convergence over the equatorial IO and in driving an anomalous Hadley circulation with descent over the Indian continent and decreased monsoon rainfall [*Goswami*, 1998]. Recent studies have also provided evidence that ENSO may even shorten the length of the ISM rainy

season, in particular by delaying the timing of its onset [*Xavier et al.*, 2007; *Annamalai et al.*, 2005a; *Boschat et al.*, 2011a].

Influence of ISM on ENSO:

Meanwhile, there have been suggestions that the ISM, in return, may also affect the following ENSO events, in particular by modulating the zonal wind variability in the equatorial Pacific during boreal summer and fall [*Wu and Kirtman*, 2004]: in this case, a weak (strong) monsoon results in a weakening (strengthening) of the trade winds over the tropical Pacific.

A Tropical Biennial Oscillation:

Finally, the ISM has been shown to be strongly linked to ENSO in the framework of the Tropical Biennial Oscillation (TBO), a dominant biennial component of interannual tropical variability. More precisely, the TBO is defined as the tendency for strong ISMs to be followed by a strong North Australian Summer Monsoon six months later and by a relatively weak ISM one year later [*Yasunari*, 1991; *Meehl*, 1987, 1997]. *Meehl and Arblaster* [2002a], *Meehl and Arblaster* [2002b] and *Meehl et al.* [2003] have suggested that ENSO, the ISM, and the tropical Indian Ocean Dipole (IOD mode, see [*Chang et al.*, 2006] and Fig I.8) are all integral parts of the TBO. In this scenario, strong ISMs lead to the development of a negative phase of the IOD mode, and a subsequent acceleration of the Pacific trade winds, leading in turn, to the development of a La Niña phase, and an increase in the strength of the Walker circulation during the following boreal winter. The ISM weakens in response to these changes, thereby setting the conditions for an opposite second annual cycle to begin.

Meehl and Arblaster [2002a,b] have pointed out that the TBO transitions are related to three factors: 500hPa height-Asian land temperature, and tropical Indian and Pacific SSTs. Coupled air-sea processes in the tropical Indian Ocean play an important role in forming and sustaining SST anomalies in the whole Indo-Pacific sector at the biennial timescale [*Loschnigg et al.*, 2003]. Moreover, there is now pervasive evidence that the Indian Ocean plays a critical role in the TBO transitions [*Yu et al.*, 2003]. It has even been suggested that the origin of the TBO may arise from coupled processes within the tropical Indian Ocean [*Chang and Li*, 2000; *Li et al.*, 2001a]. Collectively, these studies are important because they suggest that there are coupled modes of variability inherent to the Indian Ocean-monsoon system, independent of ENSO to some extent, which may be used to increase our ability to predict tropical variability on interannual timescales.

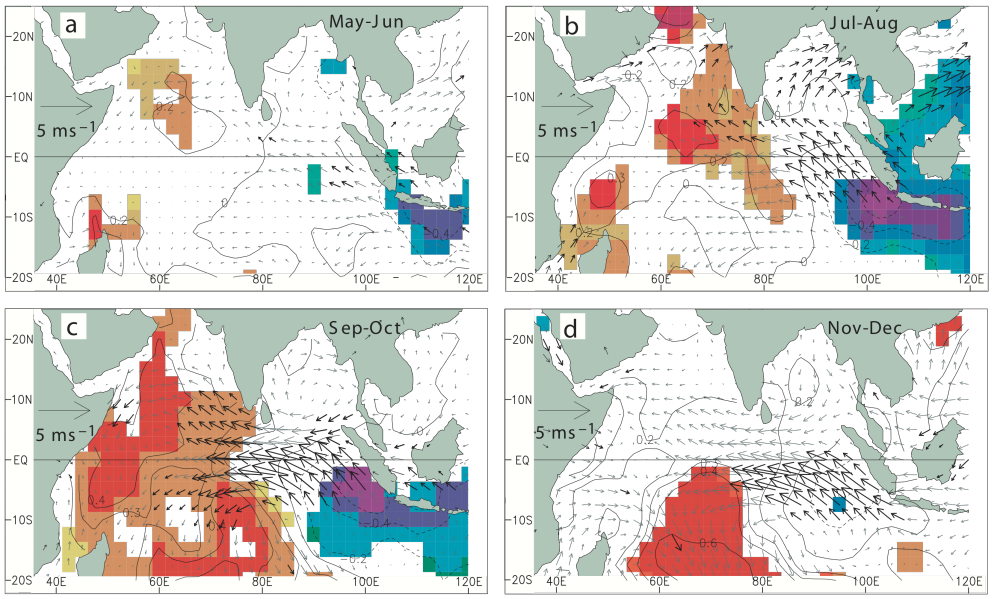

Figure I.8: A composite positive IOD mode event (a coupled ocean-atmosphere phenomenon in the IO, characterized by anomalous SST cooling in the southeastern equatorial IO and anomalous SST warming in the western equatorial IO, which usually peaks during boreal fall). Evolution of composite SST and surface wind anomalies from May-June **(a)** to Nov-Dec **(d)**. The statistical significance of the analyzed anomalies were estimated by the two-tailed t-test. Anomalies of SSTs and winds exceeding 90% significance are indicated by shading and bold arrows, respectively, from [*Saji et al.*, 1999].

However, despite of the fully interactive nature of the monsoon-ENSO system highlighted above, the relationship between ENSO and ISM is not always systematic. Though the probability of occurrence of a weak ISM during an El Niño event and that of a strong ISM during a La Niña event is large, ENSO can explain only about 35% of ISM rainfall variance at the interannual timescale [*Webster et al.*, 1998]. Figure I.9 illustrates some exceptional failures of this relationship, such as the strongest El Niño event which occurred during the boreal winter of 1997-98, but was not preceded by a significant Indian drought during the boreal summer of 1997. The recent extreme ISM drought in 2009, on the other hand, was accompanied by relatively weaker El Niño conditions during the following winter. Finally, as a simple illustration of the recent 2011 conditions, we can notice that the western coast of India experienced wet conditions during the past summer, and this (consistently) seems to be associated with the development of moderate La Niña-like SST conditions in the tropical Pacific during the boreal winter of 2011.

Furthermore, this relationship is not very useful for seasonal forecasting purposes since the lead and lag relationships between the two phenomena, shown in Fig I.10, are rather weak (or at least weaker than the synchronous connection). As an illustration, ISM's onset occurs during the developing phase of ENSO, at the end of boreal spring, but ENSO forecasts show a very significant drop off in skill during this period of the year, the so-called 'spring predictability barrier', so that the

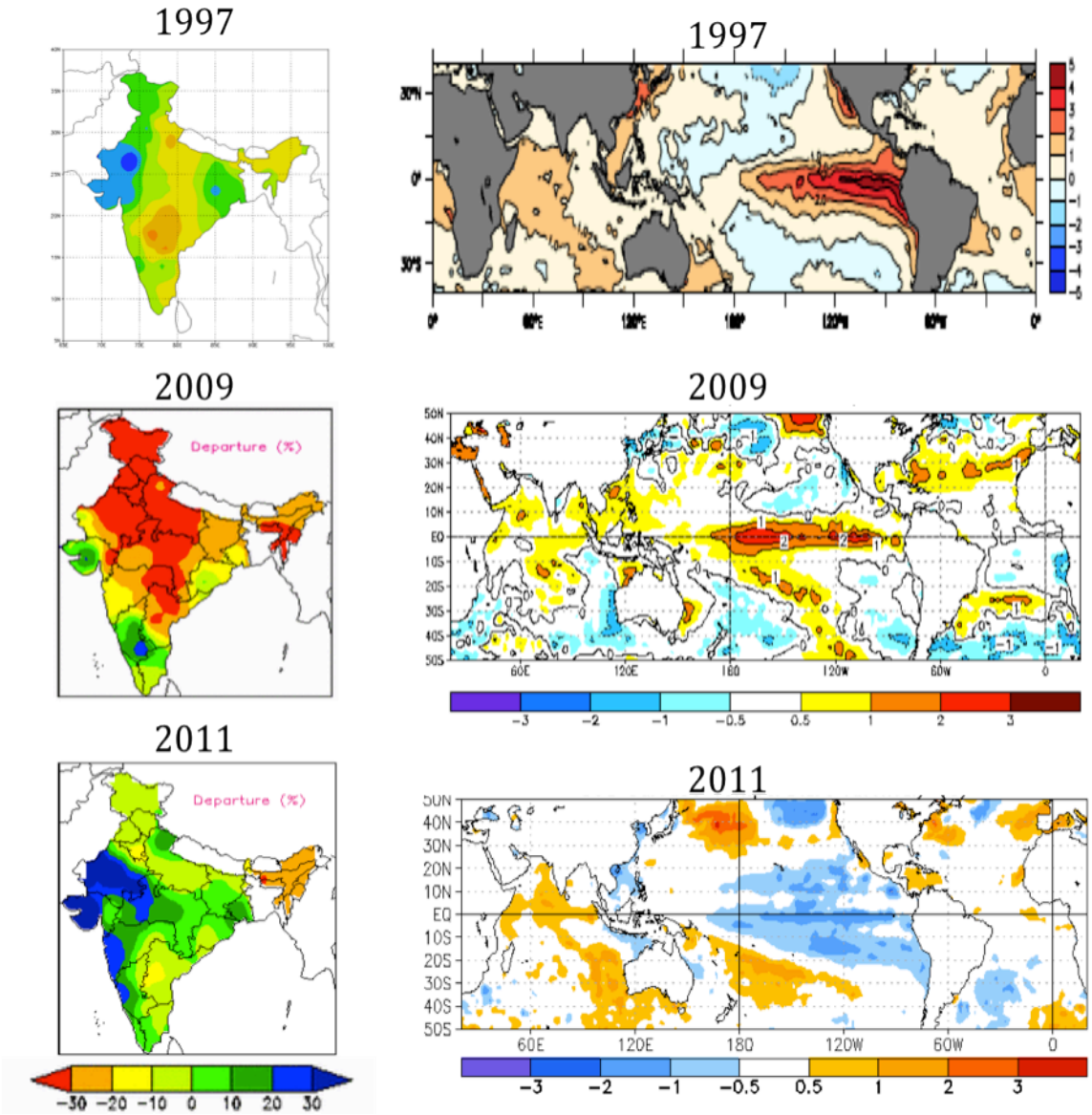

Figure I.9: Anomalous conditions observed during extreme El Niño or ISM years in 1997 and 2009 compared to the recent conditions in 2011: departures (%) from long-term ISM rainfall during JJAS season *(left panels)* and global SST anomalies (°C) during boreal winter *(right panels)* (IITM and NOAA websites)

Pacific SSTs cannot be used as an efficient and simple predictor for the monsoon [*Webster and Yang*, 1992; *McPhaden*, 2003]. Even a perfect forecast after spring would be of limited value, because by spring it is too late to allow farmers to prepare adequately for a weaker (or stronger) than average ISM season. Likewise, the monsoon alone, despite of its strong links with ENSO in the framework of the TBO is not an efficient ENSO predictor. Since ENSO and the monsoon are integral parts of the same interactive system, it thus seems rather difficult to simply use one to forecast the other.

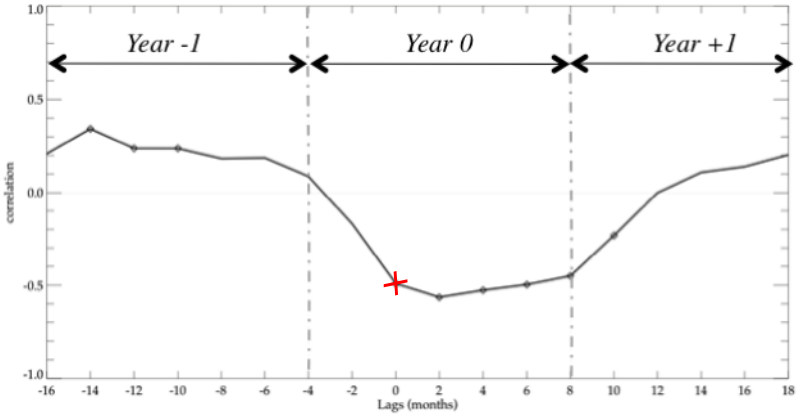

Figure I.10: Lead-lag correlation between bimonthly Niño3.4 SST timeseries and fixed ISM rainfall in JJAS (lag 0), during the 1950-2006 period, based on HadISST1 dataset [*Rayner et al.*, 2003] and ISM rainfall data derived from the rain gauge in situ observations [*Parthasarathy et al.*, 1995]. Correlation values exceeding the 10% probability level according to the phase scrambling bootstrap test of *Ebisuzaki* [1997] with 999 samples are marked by a diamond.

Finally, this ISM-ENSO relationship is not stationary in time: it exhibits strong multi-decadal variability and even seems to have considerably weakened during recent decades [*Kripalani and Kulkarni*, 1997; *Kumar et al.*, 1999; *Kinter et al.*, 2002]. Is this weakening caused by changes in the characteristics of ENSO or the monsoon after the 1976-77 climate-shift [*Wang*, 1995; *Terray and Dominiak*, 2005], or can it be attributed to the influence of other external factors? So far, a broad range of phenomena have been proposed in the literature, ranging from changes in atmospheric fields due to global warming [*Kumar et al.*, 1999], stochastic noise [*Gershunov et al.*, 2001], to changes in tropical Pacific SST patterns [*Kumar et al.*, 2006] or tropical Atlantic during boreal summer [*Kucharski et al.*, 2007, 2008, 2009], to the more frequent co-occurrence of positive IODs and El Niño events during recent decades [*Ashok et al.*, 2001, 2004; *Krishnan and Swapna*, 2009], possibly also due to global warming [*Abram et al.*, 2008; *Ihara et al.*, 2008, 2009; *Cai et al.*, 2009a,b]. However, no general consensus has yet been reached to explain this apparent weakening of the ISM-ENSO relationship. Collectively, these studies have drawn on the need to explore the possible influence from other tropical and extratropical regions on the ISM-ENSO system, with the hope to identify some relevant and perhaps new potential sources of forcing/predictability for ENSO and the monsoon.

I.4 Prediction of the ENSO-monsoon system: tropical sources of predictability?

It is faced with this difficulty in understanding the changes in the monsoon-ENSO relationship, that many studies started to examine the role of the tropical IO or Atlantic Ocean on the ISM and ENSO, and generally found stronger relationships with these tropical SSTs than in earlier studies [*Harzallah and Sadourny*, 1997; *Clark et al.*, 2000; *Li et al.*, 2001b; *Meehl and Arblaster*, 2002a,b].

The tropical IO SSTs have been shown to affect ENSO through the modulation of the Pacific and IO Walker circulations [*Wu and Kirtman*, 2004], or by hastening the transition from El Niño to La Niña events, through the excitement of an anomalous anticyclone in the North Pacific Ocean that drives easterly wind stress anomalies in the western Pacific [*Watanabe and Jin*, 2002; *Annamalai et al.*, 2005b; *Kug and Kang*, 2006]. These IO SSTs also seem to play an important role for the ISM, since recent studies have shown the existence of an intrinsic tropical IO basin mode (IOB), maintained by local air-sea interactions during the spring and summer seasons following major El Niño events [*Du et al.*, 2009; *Xie et al.*, 2009], and positively correlated with ISM rainfall a few months later [*Yang et al.*, 2007; *Park et al.*, 2010]. However, the links between the ISM and IOB SSTs are not yet fully understood: does the IOB affect ISM variability *directly* via local processes in the IO, or *indirectly* by accelerating the ENSO transition in the Pacific Ocean [*Ohba and Ueda*, 2007]? Besides, there is some doubt regarding the intrinsic nature of this recent IOB forcing and the added value it may carry for ISM predictability, since the IOB mode is strongly linked to the previous ENSO event, which has the potential to provide longer-lead prediction, *i.e.* beyond the spring predictability barrier.

The frequent occurrence of IOD events during the last two decades has also generated considerable interest to probe the role of the IOD in the coupled monsoon-ENSO system [*Yamagata et al.*, 2004; *Lau and Nath*, 2004; *Izumo et al.*, 2010], although there are still many contradictory results on this matter in today's literature. Indeed, there are suggestions that the IOD may be important for ISM prediction, but some studies support the existence of a *positive* relationship between IOD and ISM events [*Krishnan and Swapna*, 2009], while others insist the IOD-ISM relationship is closely tied with the TBO, according to which wet ISMs are this time associated with *negative* IOD events during the same year [*Meehl and Arblaster*, 2002a; *Loschnigg et al.*, 2003; *Webster and Hoyos*, 2010]. Recently, the IOD has also been recognized as a significant predictor for ENSO, able to provide accurate forecasts of ENSO events 14 months in advance, well beyond the spring predictability barrier [*Izumo et al.*, 2010]. Nevertheless, there is still considerable debate regarding the intrinsic nature of the IOD mode of variability, and the general cause-and-effect relationships between the IOD, ISM and ENSO phenomena. Is the IOD an intrinsic source of forcing or does it strongly depend on ENSO or the ISM? For example, what is the role of ENSO in the potential forcing of IOD on the ISM,

and inversely, what role does the ISM play in the forcing of IOD on ENSO? According to [*Ashok et al.*, 2001, 2004], the IOD-ISM relationship may vary complementarily to the ENSO-ISM relationship.

Although numerous studies have been devoted to the influence of the tropical IO on the ISM-ENSO system, recent studies have also been interested in the role played by the Atlantic Ocean. Inclusion of summer tropical Atlantic SSTs has even been shown to improve the ENSO forecast skill in some studies [*Jansen et al.*, 2009], with suggestions that these SSTs act as a forcing for the equatorial Pacific via the inter-basin SST gradient variability associated with the Atlantic-Pacific Walker circulation [*Wang*, 2006b; *Rodriguez-Fonseca et al.*, 2009]. However, the physical processes involved in these teleconnections have yet to be clarified.

Overall, the literature seems to provide some fragmented and at times even contradictory results on the influence of tropical regions on the ISM-ENSO system. Although there is evidence that SST in the tropical IO may exert a significant forcing on the ISM-ENSO relationship, further work is needed to elucidate the physical processes responsible for each of these associations. Besides, there are no conclusive results regarding the relative importance and contribution of each of these factors in terms of ISM and ENSO predictability. Finally, the interannual IO SST modes identified in these studies (*e.g.* IOB and IOD) are shown to interact in a quite complicated manner with one another, and particularly with the ISM and ENSO. It seems important to reach a better understanding of their inter-relations/inter-dependence, as to gain further insight into their relevance and respective merits as ISM or ENSO predictors.

I.5 An increasing role of the extratropics?

Although it is generally accepted that extratropical latitudes play a significant role in climate variability at decadal and longer timescales, their influence on shorter timescales is a more debated matter [*Chang et al.*, 2006]. At the interannual timescale, for instance, it is commonly believed that mid-latitudes exert a much weaker forcing on tropical regions. However, recently, this potential extratropical influence has begun to probe the interest of many scientists, and to provide hopes for a longer-term seasonal prediction of the ISM-ENSO system.

So far, there have been various suggestions of significant extratropical influence on ISM variability, from the North Pacific [*Peings et al.*, 2009], the North and South Atlantic [*Srivastava et al.*, 2002; *Kucharski et al.*, 2007, 2008, 2009; *Rajeevan and Sridhar*, 2008] or the South IO [*Terray et al.*, 2003, 2005a, 2007]. These predictive relationships are mostly significant during recent decades, and highlight the existence of potential long-term ISM predictors - such as the winter-to-spring Pacific

North America (PNA) oscillation [*Peings et al.*, 2009] - most of which have also been recognized as significant ENSO precursors. Among these predictors, the Indian Ocean Subtropical Dipole mode [*Behera and Yamagata*, 2001] has been shown to play a significant role in influencing ISM, but also the IOD and ENSO [*Fischer et al.*, 2005; *Terray et al.*, 2005a, 2007; *Terray*, 2011], particularly after the so-called 1976–1977 climate shift [*Terray and Dominiak*, 2005].

Meanwhile, there has also been growing interest in the importance of extratropical climate modes for ENSO itself. Recent works suggest that mid-latitude coupled variability during late boreal winter may play a significant role in the onset and development of ENSO events: in the North Pacific [*Vimont et al.*, 2001, 2003a,b, 2009], or in the South Atlantic or Indian Oceans [*Terray and Dominiak*, 2005; *Terray*, 2011]. These subtropical forcings are shown to operate through various coupled feedbacks, linked to the North Pacific Oscillation [*Vimont et al.*, 2001] or to the occurrence of subtropical dipole events in the southern IO [*Behera and Yamagata*, 2001], and affecting ENSO mainly through a modulation of the zonal wind variability during boreal spring in the western tropical Pacific.

Altogether, these recent studies thus suggest that potential sources of ISM and ENSO forcing may also exist *outside* of tropical regions, and give rise to prospects of long-term seasonal predictability of the ISM-ENSO system (even beyond the spring predictability barrier). However, there are several remaining questions concerning, in particular, the mechanisms involved in this extratropical forcing. For instance, does this extratropical forcing on ENSO systematically operate through a modulation of wind variability in the tropical Pacific? Do the extratropical ISM predictors affect the monsoon *indirectly* through this forcing on ENSO or are there more *direct* means of forcing the ISM? Finally, it seems important again to evaluate the relative contribution from each of these extratropical sources of forcing on the ISM-ENSO system. Can they provide additional or more efficient seasonal forecasts than traditional tropical predictors?

In this framework, it would be also interesting to examine whether these extratropical modes of variability are in any way related to each other (or inter-dependent), and investigate their possible interaction with the tropical modes of variability also of relevance to the ISM-ENSO predictability issue (*e.g.* IOB or IOD).

New physical understanding of these tropical-extratropical interactions would allow longer-range forecasts of La Niña and El Niño by somehow transcending the spring predictability barrier, and could help with monsoon predictions and with climate forecasts in other regions where ENSO and the monsoon have a strong influence.

I.6 Questions addressed in this thesis

Although significant progress has been made in our understanding of ENSO and ISM predictability, the state of this current research yields results that are still fragmented, thus severely hampering our ability to predict these phenomena accurately and with sufficient lead-time (*e.g.* recent failures in the prediction of ISM droughts such as in 2009). This thesis takes part in a global effort to improve our understanding of the potential predictability of ISM rainfall and ENSO, and attempts to answer some of the unresolved questions on this matter.

Q1) ***What are the most robust ISM and ENSO SST precursors (in observations)? How are these precursors related to each other and through which pathways do they impact the ISM-ENSO system?***
Over the past recent decades, many studies have strived to explore new potential sources of forcing for ISM and ENSO, and have shown the existence of significant tropical and extratropical SST precursors. But what are the dynamical properties of each of these precursors? Are they in any way inter-related or inter-dependent?

Q2) ***What are the relative roles played by these tropical and extratropical precursors on the ISM-ENSO system? Which are the most promising predictors?***
It seems important to evaluate and compare the respective contribution from each of these SST precursors, in order to assess their pertinence for ISM and ENSO prediction. Do the ISM and ENSO have precursors in common? What are the implications in terms of ISM and ENSO predictability?

Q3) ***What are the inter-decadal or long-term modulations of these teleconnections and predictive relationships?***
In the context of a weakened ISM-ENSO relationship, it seems important to assess the (time) robustness of the predictive relationships which have previously been established. Are these predictive relationships a unique characteristic of the recent period? Are they stationary on longer periods? Have the associated mechanisms recently changed? Finally, we will examine the epochal changes in the ENSO-ISM relationship (*e.g.* before and after the 1976-77 climate shift), in order to understand why this relationship has been weakening in recent decades, and what physical processes may be involved in this modulation.

In an attempt to address these questions, this thesis explores the large-scale teleconnections associated with the whole monsoon-ENSO system on interannual timescales and the role played by leading modes of coupled variability, particularly in tropical and extratropical parts of the Indo-Pacific region. We will be focusing here on the importance of *ocean-atmospheric coupling* and *fast atmospheric teleconnections* for the predictability of the monsoon and ENSO [*Dommenget*, 2010;

Clement et al., 2011]. Besides, it seems important to remind here that our intention is not to detail the small-scale processes inherent to the monsoon or to ENSO, but rather to approach this problem from a global point of view, and gather in a single conceptual and more comprehensive framework some of the fragmented and conflicting results currently found in the literature on this subject.

The thesis has been divided into five chapters, and the major contents of each chapter are discussed briefly in the following paragraphs.

Chapters 2 and 3 in this thesis are devoted to the study of ISM variability and predictability, and based on statistical diagnoses of observations (of SST, Sea Level Pressure, Outgoing Longwave Radiation, winds at 850hPa and 200hPa and surface heat fluxes). **Chapter 2** explores ISM-SST relationships during the recent 1979-2007 period, and compares the respective merits and dynamic properties of key SST precursors for the monsoon in the Indo-Pacific region (**Q1** and **Q2**). In **Chapter 3**, we test the spatial and temporal robustness of these predictive relationships during the 1950-1976 and 1979-2007 periods, and examine the implications of these results for ISM predictability (**Q2** and **Q3**). We also provide a possible explanation for the apparent weakening of the ENSO-monsoon relationship in recent decades (**Q3**). Finally, **Chapter 4** addresses the issue of ENSO predictability in observations and in a coupled model: in Part I, we assess the respective role of potential tropical and extratropical SST predictors, and then test their robustness and pertinence for the prediction of El Niño events though numerical experiments in Part II (**Q1** and **Q2**). The main conclusions and perspectives drawn from this work are given in **Chapter 5**.

Chapter II

Relationships between ISM rainfall and key SST indices in the Indo-Pacific region during recent decades

Contents

II.1 Introduction

The predictability of the Indian Summer Monsoon (ISM) rainfall has been at the core of much research since the pioneering works of Blanford (1884) and Walker (1923), and so far various SST indices have been proposed as potential ISM predictors in the literature. Most of these studies agree on the importance of tropical Pacific and IO SSTs for ISM variability, however there are still many contradictory results on the interactions between these coupled modes of variability, and their relative role in the variability of ISM rainfall.

The purpose of this chapter is to come to a better understanding (and comparison) of these SST-ISM linkages on interannual timescales. The present work examines and compares the relationship between ISM rainfall and major SST modes of variability in the Indo-Pacific region, using observations over the recent 1979-2007 period. Based on recent findings in the literature, we will be exploring the influence of:

- **ENSO**, using the Niño3.4 SST index during the boreal winter both preceding [Nino(-1)] and following the ISM season [Nino(0)] (*e.g.* [*Webster et al.*, 1998])
- **the Indian Ocean Dipole mode** during the boreal fall, also both preceding [IOD(-1)] and following the ISM season [IOD(0)] (*e.g.* [*Saji et al.*, 1999; *Ashok et al.*, 2001, 2004; *Krishnan and Swapna*, 2009; *Izumo et al.*, 2010])
- **the Indian Ocean Basin mode** (IOB), reflecting the occurrence of a basin-wide warming of the IO in the boreal spring following most El Niño events (*e.g.* [*Yang et al.*, 2007; *Park et al.*, 2010])
- **the South East Indian Ocean** (SEIO) SST in late boreal winter, recognized as being a significant and common precursor of the whole ENSO-IOD and ISM system, particularly after the 1976-77 climate-shift [*Terray et al.*, 2003, 2007].

The spatial definition and peaking seasons of these key SST indices are illustrated in Fig II.1 below.

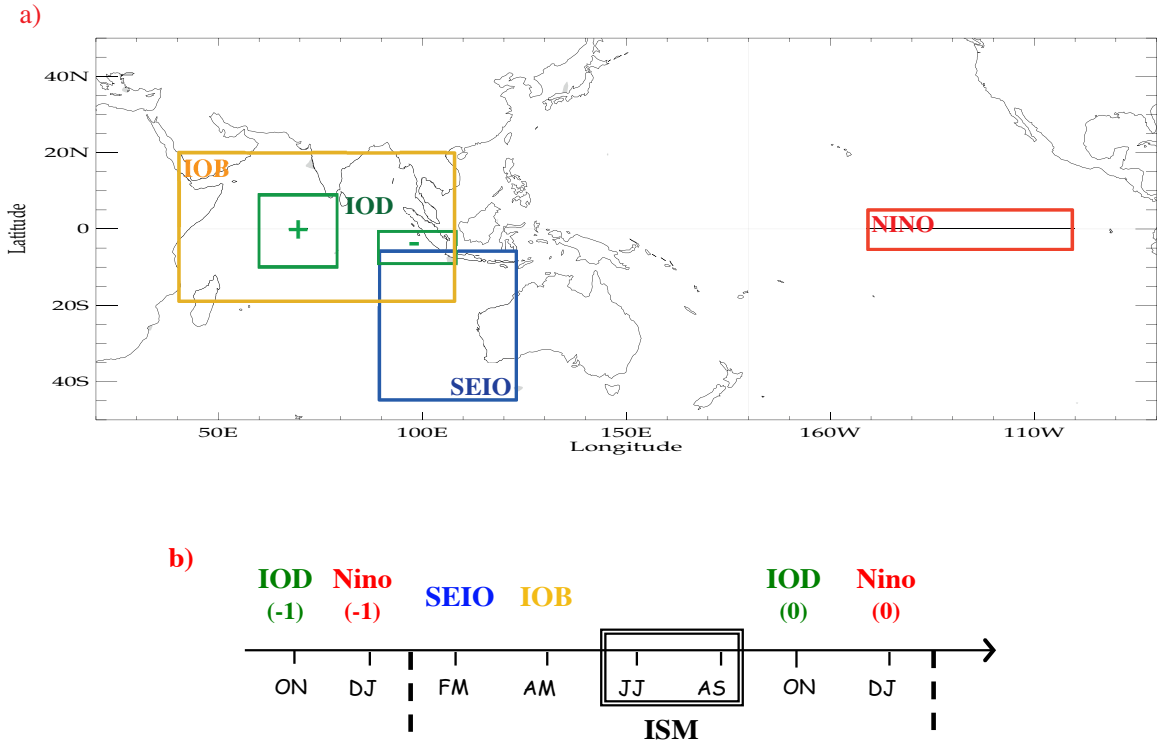

Figure II.1: **a)** Spatial definitions **b)** and peaking seasons of each selected SST index in this work. The Nino index is computed in December-January over the [170°W-120°W; 5°S-5°N] domain, the IOD index in September-October-November over the domain marked by the west box [50°E-70°E; 10°S-10°N] minus east box [90°E-110°E; 10°S-0°], the SEIO index in February-March over the [90°E-122°E; 5°S-45°S] domain, and the IOB index in April-May over the [40°E-110°E; 20°S-20°N] domain.

Although these indices have been carefully selected, our intention is not necessarily to improve or question the pertinence of their definitions in the literature. We simply wish to compare their dynamical properties, as well as their respective merits and potential compatibility as far as ISM predictability and variability are concerned . The questions we will be addressing are:

(i) Are each of these SST indices statistically linked to ISM rainfall variability?
(ii) If so, by which means can they affect ISM rainfall variability?
(iii) What are their respective merits for the long-range predictability of ISM?

In an attempt to answer these questions, we have first examined the statistical significance of these SST-ISM relationships in recent observations. Lead-lag correlation analyses have then been carried out to elucidate the physical processes which may be responsible for these statistical associations. Finally, we have discussed the implications of this work for the long-range seasonal predictability of ISM rainfall.

II.2 Article published in *Climate Dynamics*

Our results are based on statistical analyses of observations over the recent 1979-2007 time period, and are detailed in the following article.

Reference: Boschat, G., P. Terray, and S. Masson (2011a) Interannual relationships between indian Summer Monsoon and Indo-Pacific coupled modes of variability during recent decades, *Climate Dynamics*, 37, 1019–1043, Doi 10.1007/s00382-010-0887-y.

Clim Dyn
DOI 10.1007/s00382-010-0887-y

Interannual relationships between Indian Summer Monsoon and Indo-Pacific coupled modes of variability during recent decades

Ghyslaine Boschat · Pascal Terray · Sébastien Masson

Received: 26 March 2010 / Accepted: 20 July 2010

Abstract Various SST indices in the Indo-Pacific region have been proposed in the literature in light of a long-range seasonal forecasting of the Indian Summer Monsoon (ISM). However, the dynamics associated with these different indices have never been compared in detail. To this end, the present work re-examines the variabilities of ISM rainfall, onset and withdrawal dates at interannual timescales and explores their relationships with El Niño-Southern Oscillation (ENSO) and various modes of coupled variability in the Indian Ocean. Based on recent findings in the literature, five SST indices are considered here: Niño3.4 SST index in December–January both preceding [Nino(−1)] and following the ISM [Nino(0)], South East Indian Ocean (SEIO) SST in February–March, the Indian Ocean Basin (IOB) mode in April–May and, finally, the Indian Ocean Dipole (IOD) averaged from September to November, also, both preceding [IOD(−1)] and following the ISM [IOD(0)]. The respective merits and associated dynamics of the selected indices are compared through various correlation and regression analyses. Our first result is a deceptive one: the statistical relationships with the ISM rainfall at the continental and seasonal scales are modest and only barely significant, particularly for the IOD, IOB and Nino(−1) indices. However, a detailed analysis shows that statistical relationships with the ISM rainfall time series are statistically biased as the ISM rainfall seems to be shaped by much intraseasonal variability, linked in particular to the timing of the onset and withdrawal of the ISM. Surprisingly, analysis within the ISM season shows that Nino(−1), IOB and SEIO indices give rise to prospects of comparatively higher ISM previsibility for both the ISM onset and the amount of rainfall during the second half of the ISM season. The IOD seems to play only a secondary role. Moreover, our work shows that these indices are associated with distinct processes occurring within the Indian Ocean from late boreal winter or early spring onwards. The regression analyses also illustrate that these (local) mechanisms are dynamically and remotely linked to different phases of ENSO in the equatorial Pacific, a result which may have useful implications in terms of forecasting strategies since the choice of the better indices then hinges on the concurrent phasing of the ENSO cycle.

Keywords Indian Summer Monsoon · Indian Ocean · ENSO · Long-range predictability · Ocean–atmosphere interactions

1 Introduction

Almost three decades ago, Krishnamurti (1971) first demonstrated that the Asian summer monsoon is one of the most energetic features of the climate system and that latent heat release by monsoon rainfall plays an important role in forcing the global atmospheric circulation even at midlatitudes. During the months of June through September, the rainfall associated with the Asian summer monsoon provides the main source of fresh water for millions of people in the Indian subcontinent. Furthermore, the countries of South Asia are primarily based on agricultural economy, which is again closely linked to the monsoon rainfall (Pant and Rupa Kumar 1997). Therefore, the prediction of Indian Summer Monsoon (ISM) rainfall is not

G. Boschat (✉) · P. Terray · S. Masson
LOCEAN-IPSL, CNRS/IRD/MNHN, Université Pierre et Marie Curie, BP100, 4 place Jussieu, 75252 Paris Cedex 05, France
e-mail: gbolod@locean-ipsl.upmc.fr

Published online: 04 August 2010

only scientifically challenging but is also important for planning and devising agricultural strategies.

Though the probability of occurrence of a weak ISM during an El Niño event and that of a strong ISM during a La Niña event is large, El Niño-Southern Oscillation (ENSO) can explain only about 35% variance of ISM rainfall (Webster et al. 1998). Moreover, the ISM–ENSO relationship has considerably weakened during recent decades (Kinter et al. 2002). Therefore it is natural to explore the possible influence of the neighboring Indian Ocean on ISM rainfall variability (Krishnan et al. 2003; Krishnan and Swapna 2009; Clark et al. 2000; Terray et al. 2003, 2007; Yang et al. 2007; Izumo et al. 2008; Park et al. 2010; among many others).

The relationship between tropical Indian Ocean Sea Surface Temperature (SST) and ISM has been the subject of many observational studies before the end of the twentieth century (Shukla and Misra 1977; Weare 1979; Shukla 1987; Joseph and Pillai 1984; Rao and Goswami 1988; Terray 1995; Harzallah and Sadourny 1997; Clark et al. 2000). While several of these studies have found that some precursory SST signals exist before the ISM onset (Harzallah and Sadourny 1997; Rao and Goswami 1988; Nicholls 1995; Clark et al. 2000; Sahai et al. 2003), others have found that it is very difficult to establish a clear relationship between Indian Ocean SSTs and ISM variability during the boreal summer (e.g. after the ISM onset). It is also fair to say that some of these earlier studies have obtained quite different and at times contradictory results. Indeed, based on these first studies (Shukla 1987), many authors have suggested that tropical Indian Ocean SST may be considered as a passive element of the ISM system at the interannual time scale.

On the other hand, recent studies also suggest the existence of coupled dynamics in the Indian Ocean, which may be partly independent of ENSO and give rise to strong interannual anomalies over the Indian Ocean.

The so-called Indian Ocean SST Zonal/Dipole mode (Saji et al. 1999; Webster et al. 1999; IOD hereafter), which peaks during boreal fall is one of such phenomena. The frequent occurrence of IOD events during the last two decades has generated considerable interest to probe the role of IOD in the coupled monsoon-ENSO system (Lau and Nath 2004; Yamagata et al. 2004; Izumo et al. 2010). However, there is a lot of contradicting results in the literature on the cause and effect relationships, *if any*, between the two phenomena. First, a number of studies have suggested that the IOD may be a natural part of the Asian summer monsoon and the Tropospheric Biennial Oscillation (TBO, e.g. Meehl and Arblaster 2002, 2003; Loschnigg et al. 2003, Li et al. 2006; Webster and Hoyos 2010). Here, the IOD is argued to arise from the ocean–atmosphere interactions within the Indian Ocean with links to the Pacific involved with the TBO. In this framework, strong ISMs are followed by negative IOD events and strong Australian monsoons and negative IOD events precede both El Niño and weak ISMs (Meehl et al. 2003; Izumo et al. 2010; Webster and Hoyos 2010). Another suggestion is that positive IOD events coincide with wet conditions over the Indian subcontinent (Behera et al. 1999; Ashok et al. 2001, 2004; Li et al. 2003; Gadgil et al. 2004; Swapna and Krishnan 2008; Krishnan and Swapna 2009). However, Li et al. (2003) argue that the strong ISM will then tend to damp the original IOD event while Swapna and Krishnan (2008) and Krishnan and Swapna (2009) suggest the opposite: the existence of positive feedbacks between positive IOD events and strong ISMs. Furthermore, Ashok et al. (2001, 2004) suggest that the influence of IOD on the ISM is opposite to the effect of ENSO, and that the IOD–monsoon rainfall relationship varies complementarily to that between ENSO and monsoon rainfall. Therefore, a better understanding of the linkages between ISM rainfall and IOD events will be a welcome contribution to the literature.

Another SST dipole mode in the southern Indian Ocean, seasonally phase-locked to the austral summer, has also been documented (Behera and Yamagata 2001; Hermes and Reason 2005; Chiodi and Harrison 2007). Recent studies using observed data and coupled models have demonstrated that this Indian Ocean Subtropical Dipole (IOSD) mode plays a significant role in influencing the monsoon, IOD and ENSO (Fischer et al. 2005; Terray et al. 2003, 2005, 2007; Terray 2010). More precisely, these works suggest that the IOSD events play a significant role in the variability of Indo-Pacific Tropical climate, and interact with ISM and ENSO after the so-called 1976–1977 climate shift (Nitta and Yamada 1989; Terray and Dominiak 2005), highlighting the possible role of global warming or decadal variability on the interannual variability of the tropical climate. Consideration of this dipole may improve long-range forecasts of ISM rainfall (Terray et al. 2003) or ENSO (Dominiak and Terray 2005; Terray 2010).

The interannual SST anomalies in the Indian Ocean during boreal winter are largely due to the remote ENSO forcing through the atmospheric bridge mechanism (Lau and Nath 2000, 2003; Alexander et al. 2002) or El Niño-induced westward-propagating oceanic Rossby waves in the south Indian Ocean (Xie et al. 2002). However, the existence of an intrinsic tropical Indian Ocean Basin (IOB) mode, maintained by local air-sea interactions during the spring and summer seasons following major El Niño events has also drawn great attention recently (Du et al. 2009; Xie et al. 2009). Since this basin-wide Indian Ocean warming persists well into the following boreal spring and summer, its influence on ISM variability has also been the focus of several recent studies (Annamalai et al. 2005; Yang et al.

2007; Park et al. 2010). However, the physical mechanisms which explain the links between ISM and IOB related SSTs are, as yet, not well understood and deserve further studies.

In summary, the relationships between the different modes of Indian Ocean coupled variability and their respective merits as far as the long-range predictability of the ISM is concerned have yet to be explored in a systematic manner from observational or modeling perspectives. This necessity is further recognized by the fact that these interannual modes interact in a complicated manner with both the Asian monsoon and ENSO. Thus, the primary goal of this study is to further investigate the spatiotemporal characteristics of Indian Ocean SSTs and their relationships with ISM, with a special focus on coupled modes of variability such as IOD, IOSD and IOB modes. Diagnostic analysis of observations is carried out, first to test the statistical significance of the relationships between ISM and these specific modes of Indian Ocean coupled variability and, secondly for elucidating the physical processes responsible for these statistical associations. In terms of long-range predictability of ISM, it is also important to clarify the lead-lag relationships among these various coupled modes and ENSO. This is a necessary step if we wish to demonstrate that these modes are useful for improving the long-range forecasting of the ISM beyond ENSO.

This paper is organized as follows. Data and methods are described in Sect. 2. Using a simple correlation analysis, we first identify and describe the main statistical associations between the ISM rainfall, onset and withdrawal date time series and specific indices of IOD, IOSD and IOB modes in Sect. 3. We then turn to our main result, the relationships between the evolution of these coupled patterns of variability and ISM in Sect. 4. The conclusions and some discussions are given in Sect. 5.

2 Data and statistical techniques

2.1 Datasets

The monthly ISM rainfall is provided by the Indian Institute of Tropical Meteorology (IITM) through their website. This ISM rainfall monthly time series covers the period 1871–2005 and consists of an area-weighted average of 306 rain gauges distributed evenly across India (Parthasarathy et al. 1995).

The onset and withdrawal time series used in the correlation analyses cover the 1979–2005 period and are derived from objective definitions in relation to tropospheric seasonal warming (Xavier et al. 2007). More precisely, the ISM onset and withdrawal dates are estimated from the NCEP/NCAR reanalysis, based on the change of sign in the meridional gradient of upper tropospheric temperature (averaged between 700 and 200 hPa) between a northern box (40°–100°E; 5°–35°N) and a southern box (40°–100°E; 15°S–5°N) over the Asian Monsoon region. For comparison, we have also used the dates of ISM onset as derived by the India Meteorology Department (IMD), although these dates are available to us over a shorter period from 1979 to 2001.

To complement the IITM rainfall time series, our analysis also makes use of outgoing longwave radiation (OLR), which is a widely used indicator of convective precipitation in the Tropics. The OLR used here covers the period from 1979 to the present and is the interpolated OLR data provided by the National Oceanic and Atmospheric Administration-Cooperative Institute for Research in Environmental Sciences (NOAA-CIRES; Liebmann and Smith 1996).

We use the NCEP-Department of Energy (DOE) Atmospheric Model Intercomparison Project (AMIP-II) reanalysis (Kanamitsu et al. 2002, hereinafter NCEP2) to examine the ISM atmospheric circulation. The period analyzed runs from January 1979 to December 2005. Although data exist over a longer period for the previous NCEP-NCAR reanalysis (Kalnay et al. 1996), we choose to use only the second NCEP reanalysis, since it is considered as more reliable for at least two reasons: first, many of the known problems found in the earlier reanalysis have been corrected and, secondly, use is made of satellite data for the whole period (possible shifts due to their use or not are therefore avoided).

The observed SST dataset selected for the study is the Hadley Centre sea ice and sea surface temperature dataset (HadISST1.1) developed by Rayner et al. (2003). Using a unique combination of monthly globally complete fields of SST on a 1° latitude–longitude gridded mesh and improved bias corrections, quality of HadISST1.1 has been found to compare well with other historical SST analyses (Rayner et al. 2003). Due to uncertainties in the first part of the record and to be consistent with the NCEP2 and OLR datasets, we have used only the period from 1979 to the present as a basis for our correlation analyses in the following sections. However, the full SST record is used to remove the long-term trends of Indian Ocean SSTs before further statistical analyses (see below).

SST and atmospheric fields are linked with each other through processes at the air–sea interface like surface turbulent and radiative fluxes. The surface heat fluxes analyzed here are derived from products of the objectively analyzed air–sea fluxes (OAFlux) for the Global Oceans project (Yu et al. 2008) and are obtained from the Woods Hole Oceanographic Institute through ftp://ftp.whoi.edu/pub/science/oaflux/data. These fluxes are used to identify the processes that are important for the generation or attenuation of SST anomalies in the Indian Ocean.

Table 1 Description of the different indices used in this study and their standard deviation, based of HadISST1.1 SST data over the 1979–2007 period

	ENSO	IOD	IOSD	IOB
Index name (reference)	NINO index (Nino3.4 index)	IOD index (Saji et al. 1999)	SEIO index (Terray and Dominiak 2005)	IOB index (Yang et al. 2007)
Geographical domain	Eastern tropical Pacific Ocean: (5°N–5°S; 170°W–120°W)	Equatorial Indian Ocean: West box (50°E–70°E; 10°N–10°S) minus East box (90°E–110°E;10°S–0°S)	South East Indian Ocean: (90°–122°E; 5°–45°S)	Tropical Indian Ocean: (40°–110°E; 20°S–20°N)
Temporal definition	December–January	September–October–November	February–March	April–May
Standard deviation (°C)	1.10	0.40	0.31	0.21

The Simple Ocean Data Assimilation (SODA) product (Carton and Giese 2008; Version 2.023) is also used in this study, in particular to follow the evolution of heat content in the first 130 m layer of the Indian Ocean, during the 1979–2004 period. SODA is available at 0.45° × 1° latitude–longitude resolution in the Tropics, and has 20 vertical levels with 15-m resolution near the surface.

Finally, the coupled modes examined here (namely ENSO, IOD, IOSD and IOB) will be represented by SST indices, defined as SST anomalies averaged over various regions and during specific seasons. Each index is based on a specific criterion taken from the literature (see Table 1). Note that this analysis considers two different Nino indices, Nino(−1) and Nino(0), which both peak during boreal winter but one index [Nino(−1)] preceeds while the other [Nino(0)] follows the ISM. The denominations (0) and (−1) thus refer to the ISM season rather than the evolution of the ENSO event itself. Based on recent findings (Izumo et al. 2010; Webster and Hoyos 2010) and the same index denomination as for ENSO, the IOD index is also defined during the boreal fall, both preceding and following the ISM [IOD(−1) and IOD(0) hereafter]. Finally, we have decided to limit our analysis of the IOSD to its variability in the South East Indian Ocean (SEIO) in agreement with the results of Terray et al. (2003, 2005, 2007) and Terray and Dominiak (2005).

2.2 Statistical methods

SST variations in the Indian Ocean occur over a wide range of time scales (Schott et al. 2009). In particular, analysis of long-term time series shows that the monthly tropical Indian Ocean SST has experienced an average warming trend of 0.01°C year^{-1} since 1945 (Nitta and Yamada 1989; Terray 1994) with a significant 0.3 or 0.5°C shift to a warmer state that occurred around 1976–1977 (Clark et al. 2000; Terray and Dominiak 2005). This gradual, but significant warming of the Indian Ocean may be largely attributed to the global warming as many of the historical simulations using the IPCC coupled climate models also indicate a substantial warming of the Indian Ocean in response to increasing greenhouse gases during the recent decades (Alory et al. 2007). However, similar low-frequency fluctuations are absent in the observed all-India rainfall time series as well as in the all-India rainfall time series computed from the recent IPCC coupled simulations (Rupa Kumar et al. 2002). In light of these results, it is clear that the trend in Indian Ocean SSTs is probably detracting from the relationship between interannual variations of ISM rainfall and Indian Ocean SSTs. More precisely, the existence of a non-stationary, externally forced, component of SST Indian Ocean variability may be masking the Indian Ocean SST–ISM rainfall relationships at the interannual time scale since observed SST anomalies over the Indian Ocean are relatively small (Schott et al. 2009).

It is, thus, important to eliminate the influence of this Indian Ocean warming trend before addressing the problem of Indian Ocean SSTs–ISM relationships at the interannual time scale. To achieve this goal, the annual cycle, trend and very low-frequency variations were removed from the historical SST monthly fields using the STL (Seasonal-Trend decomposition procedure based on Loess) additive scheme developed by Cleveland et al. (1990). The STL procedure is a powerful statistical technique for describing a discrete time series (Cleveland et al. 1990). In the STL procedure, the analyzed X_t monthly time series is decomposed into three terms:

$$X_t = T_t + A_t + R_t$$

The T_t term is used to quantify the trend and low-frequency variations in the time series. The A_t term describes the annual cycle and its modulation through time, while the R_t term is the remaining variation in the data beyond the annual and trend components. The STL procedure is particularly useful

for extracting the interannual signal from non-stationary and noisy climate observations, as illustrated by Cleveland et al. (1990) or Terray (2010). The interannual SST monthly anomalies analyzed here are obtained as the departures from the extracted seasonal cycle, A_t, and trend, T_t, components estimated by the STL procedure for each grid-point time series in the SST datasets from 1979 to 2007.

Standard regression and correlation analyses are used to describe the life cycle of coupled patterns of variability in the Indo-Pacific areas. Note that none of the fields used in these regression exercises have been filtered by the STL procedure in order to give an exact overview of the long-range predictability associated with our key indices. To account for the effects of autocorrelation, the statistical significance levels for the correlation and regression coefficients are estimated using the method proposed by Ebisuzaki (1997) with 999 samples.

3 Relationship between ISM rainfall and Indo-Pacific SST indices

The aim of this part is to assess the potential predictability of ISM rainfall provided by the key SST indices defined in the previous section. The statistical relationships, based on correlation analyses, are examined over the 1979–2007 period and are summarized in Table 2.

During the conventional June to September (JJAS) season, the ISM rainfall is significantly correlated with the SEIO and Nino(0) indices, whereas results are generally weak and poorly significant with other indices. Table 2 is able to capture some well-known features of the ENSO–ISM relationship, as the ISM rainfall is out-of-phase with the development phase of ENSO in the Pacific [correlation of −0.4 with Nino(0) index] and in-phase with its mature and decaying phases [correlation of 0.18 with Nino(−1) index]. In spite of recent findings (see Sect. 1) which show a weakening of the ISM–ENSO relationship during recent decades, the best result at the seasonal time scale is here obtained with the Nino(0) index. Meanwhile, seasonal correlations also fail to reproduce the known merits of the Nino(−1), IOB and IOD indices for the seasonal prediction of ISM rainfall suggested by recent studies (Yang et al. 2007; Krishnan and Swapna 2009; Webster and Hoyos 2010). This apparent weak seasonal previsibility may be related to the subseasonal ISM variability and draws on the need to examine these relationships at shorter timescales. To this end, we have completed these seasonal analyses by monthly correlations between each index and ISM rainfall (Table 2). We have also computed correlation coefficients between SST indices and the ISM onset and withdrawal dates time series (Table 3), as ISM onset and withdrawal dates are important aspects of ISM variability which contribute to make each monsoon unique and have a significant practical value (Ramesh Kumar et al. 2008). The timing of the onset and withdrawal are particularly important as they statistically influence the amount of rainfall during the early and late monsoon seasons as we will illustrate below. Understanding the influence of each index on these specific components of ISM intraseasonal variability thus becomes a key element to the more global assessment of predictive relationships with the ISM.

Surprisingly, our analysis (Tables 2, 3) shows the importance of Nino(−1) and IOB indices for the ISM onset phase. More precisely, the IOB and Nino(−1) indices are, on one hand, significantly and negatively correlated to the June ISM rainfall (correlations of −0.32 and −0.46, respectively, in Table 2) and, on the other hand, significantly and positively correlated with the ISM onset dates (correlations of 0.47 and 0.63, respectively, in Table 3). The ISM onset thus tends to be significantly delayed during the decaying El Niño years. These robust results are consistent with earlier studies which have recorded a 1-week delay of the ISM onset following the mature phase of El Niño events and its subsequent Indian Ocean warming (Joseph et al. 1994; Annamalai et al. 2005). Moreover, this leads to the hypothesis that the delayed ISM onset is partly responsible for the negative correlations of the IOB and

Table 2 Cross-correlations between the key SST indices (defined in Table 1) and the ISM rainfall (ISMR) in seasonal and monthly mean from June to September, for the 1979–2007 period

	ISMR (JJAS)	ISMR (June)	ISMR (July)	ISMR (August)	ISMR (September)
IOB	0.19	−0.32*	0.03	0.23	0.44**
Nino(−1)	0.18	−0.46**	0.05	0.32*	0.45**
SEIO	0.39**	−0.19	0.21	0.27	0.56***
Nino(0)	−0.40**	0.06	−0.44**	0.11	−0.52**
IOD(0)	−0.16	−0.01	−0.21	0.15	−0.24
IOD(−1)	0.24	−0.30	0.19	0.25	0.34*

The coefficients exceeding the 10%, 5% and 5‰ confidence levels according to the phase-scrambling bootstrap test of Ebisuzaki (1997) with 999 samples are followed by one asterisk (*), two asterisks (**) and three asterisks (***), respectively

* $P < 0.1$, ** $P < 0.05$, *** $P < 0.005$

Table 3 Cross-correlations between the key SST indices (defined in Table 1) and the onset and withdrawal dates of the ISM, for the 1979–2005 period

	Onset dates		Withdrawal dates
	NCEP	IMD	
IOB	0.47**	0.22	0.36*
Nino(−1)	0.63***	0.34	0.34*
SEIO	0.08	0.13	0.63***
Nino(0)	0.22	0.22	−0.55***
IOD(0)	0.18	0.08	−0.44**
IOD(−1)	0.30	0.22	0.43**

The onset and withdrawal dates are estimated from NCEP/NCAR reanalysis, using the objective definitions of Xavier et al. (2007). Note that the IMD onset dates (based on rainfall over Kerala) available during the 1979–2001 period are also used for comparison purpose. The coefficients exceeding the 10%, 5% and 5‰ confidence levels according to the phase-scrambling bootstrap test of Ebisuzaki (1997) with 999 samples are followed by one asterisk (*), two asterisks (**) and three asterisks (***), respectively

* $P < 0.1$, ** $P < 0.05$, *** $P < 0$ .005

Nino(−1) indices with ISM rainfall in June. The statistically significant and negative correlation (−0.4) between the June ISM rainfall and the ISM onset dates is in agreement with this suggestion. In other words, the rainfall over the Indian subcontinent is reduced in June after the mature phase of El Niño, mainly because of the delayed onset and not necessarily because the monsoon circulation is weak *after the onset*. On the other hand, correlations of SEIO, Nino(0) and IOD (0 or −1) indices with ISM rainfall in June (see Table 2) or the onset date (see Table 3) are weak and insignificant. This suggests no significant impact of El Niño, during its development phase, or IOD, during the preceding year, on ISM onset. However, we will illustrate below that ENSO, *during its development phase*, has a larger influence on the withdrawal of the monsoon.

We next focus on the evolution of the statistical relationships within JJAS. Despite weak and poorly significant values during mid ISM season, results of the IOB, Nino(−1), IOD(−1) and SEIO indices in Table 2 are characterized by a steady increase in the amplitude of correlations from July to September. This low-frequency evolution is not as clear for the other indices, as correlation values remain weak for the IOD(0) index throughout the season, and fluctuate from 1 month to another with the Nino(0) index. Statistics linked to these two indices are overall difficult to interpret. The ISM–Nino(0) relationship, in particular, seems to be modulated by important intraseasonal activity, a fact which may even control its global nature over the JJAS season. Nevertheless, in September, correlations between ISM rainfall and the SST indices are generally enhanced. Indeed, results are statistically significant for nearly all indices [except the IOD(0) index], with maximum values obtained for the SEIO and Nino(0) indices (0.56 and −0.52, respectively). Note that, September rainfall is also strongly linked to ISM withdrawal dates (0.71 correlation), which, in turn, is significantly associated with both SEIO and Nino(0) indices (correlations of 0.63 and −0.55, respectively). Therefore, in an analogous way as during the onset phase, the positive (negative) correlation value obtained with ISM rainfall in September may be explained by SEIO's [Nino(0)'s] tendency to postpone (advance) the withdrawal of the monsoon. It is also interesting to observe here that this statistical association is the strongest with the SEIO index.

These preliminary results show that monthly statistics are significantly influenced by the timing of the onset (withdrawal) of the monsoon rains, particularly in June (September), and that this could account for the generally negative (positive) correlations obtained during the early (late) part of the ISM season. This temporal dichotomy within the ISM season had already been observed by Terray (1995), Ailikun and Yasunari (2001), Terray et al. (2003) and Park et al. (2010). It is also clearly illustrated here by Fig. 1, which shows the lead-lag correlations between all the key SST indices and ISM rainfall taken separately in June–July (JJ) and August–September (AS). Note that, for this analysis exclusively, the SST indices are not only considered during their specific peaking season (as defined in the previous section) but throughout the years preceding and following the monsoon. Figure 1 is therefore presented as an alternative approach to our first analysis, and helps highlight the statistical dichotomy between the early and late summer season.

Indeed, Fig. 1a illustrates once again a globally poor statistical association of ISM rainfall in JJ with all indices. The only significant correlation coefficient is obtained with the Nino time series in April–May, just before the monsoon onset (significant value of −0.39). Note that this spring Nino index, which probably combines the effects of both early developing and slowly decaying El Nino events, is also influencing the ISM onset (correlation of 0.56 with onset dates). However, by AS predictability is enhanced (Fig. 1b), with important precursory signals for ISM rainfall in the preceding winter and spring. The maximum correlation values are obtained in DJ with Nino, in FM with IOB and AM with SEIO, which are quite consistent with the definitions of each index found in literature. The IOD index seems to have continuously weaker correlations with ISM rainfall, suggesting it could only play a secondary role in comparison to other indices for the ISM prediction.

In conclusion, this first analysis has shed a light on the importance of subseasonal features, such as the timing of ISM onset and withdrawal, in the assessment of predictive relationships with ISM rainfall. The monthly correlations in Table 2 and Fig. 1 illustrate the temporal dichotomy

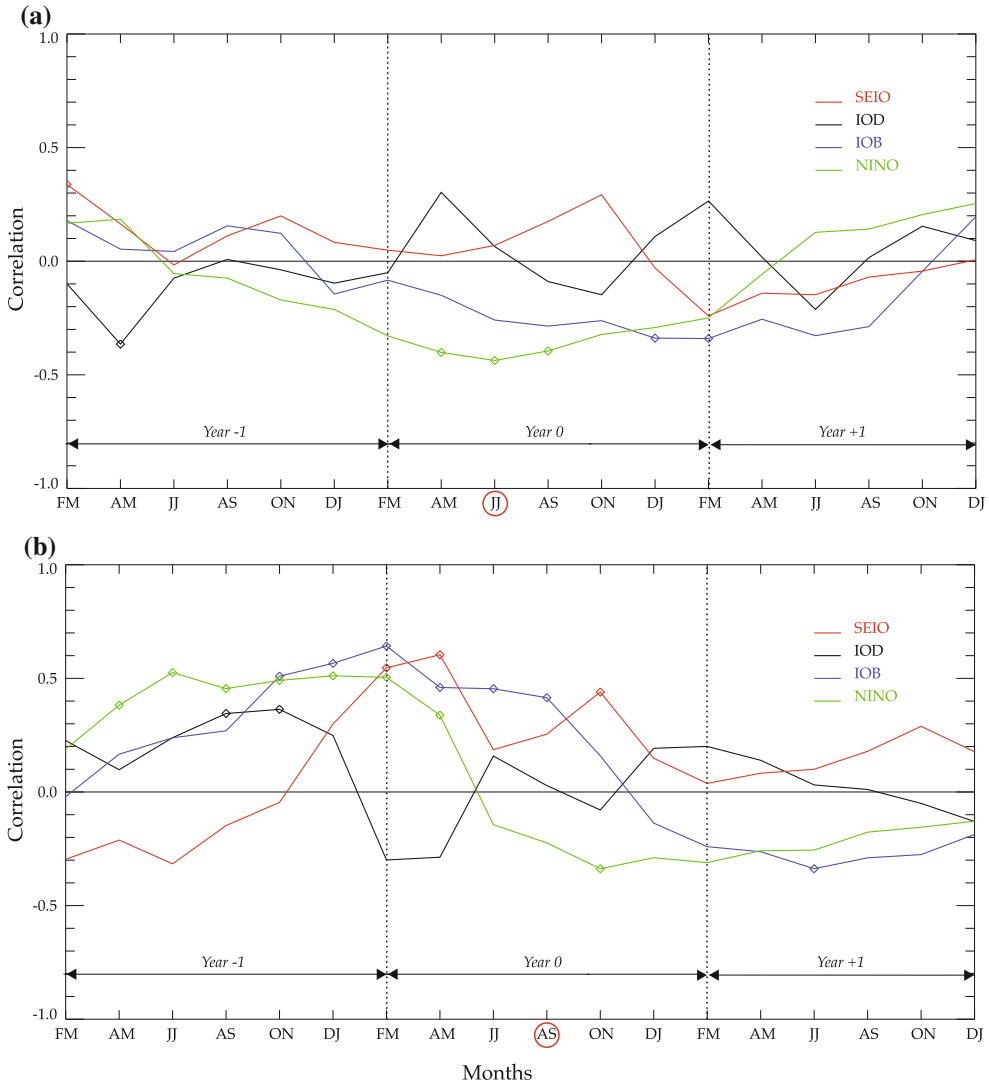

Fig. 1 Lead-lag correlations between bimonthly SST indices and the ISM rainfall in **a** June–July and **b** August–September for the 1979–2007 period. The correlation with the Nino index is plotted in *green*, the IOB in *blue*, the SEIO in *red* and the IOD in *black*. Correlation values exceeding the 10% probability level according to the phase-scrambling bootstrap test of Ebisuzaki (1997) with 999 samples are marked by a *diamond*

often observed within the ISM season in the literature, as well as the existence of low-frequency variations *inside the ISM season* as mentioned before (Buermann et al. 2004; Park et al. 2010; Terray 1995). This analysis has also suggested a parallel between the Nino(−1) and IOB indices during the earlier part of the season, and between the Nino(0) and SEIO indices in the later part. However, all these results need now to be interpreted on a more physical basis. For instance, we need to understand which physical processes explain the similarities between Nino(−1) and IOB or Nino(0) and SEIO indices. What are the physical roots of the temporal evolution of the correlations between SST indices and the ISM rainfall within the JJAS season? We also need to know if and how distinct indices, such as the IOB, Nino(−1) and SEIO, can offer complementary potential ISM predictability (since they have correlation values which peak with a comparable amplitude, and during approximately the same period). The answer to these questions requires a closer examination of the dynamics associated with the Nino, IOB and SEIO indices.

4 Dynamics associated with each index during the ISM season

The aim of this section is thus to investigate the mechanisms that govern the evolution of these coupled modes of variability in relation to the ISM seasonal march. Note, however, that we have eliminated the IOD index from this analysis, given its statistically weaker association with ISM rainfall (e.g. Sect. 3). As a result, the analysis will focus on the dynamics associated with the Nino(−1), Nino(0), IOB and SEIO indices and their low-frequency evolution before and during the development of the ISM season.

4.1 Nino(−1) and IOB indices

We examine first the mechanisms associated with the Nino(−1) and IOB indices. Bimonthly SST regression patterns onto these two indices are shown in Fig. 2, and present remarkably similar evolutions from February–March (FM) to August–September (AS). This striking resemblance is also captured by the regression with other variables (not shown), and thereby corroborates the parallel which was previously suggested between both indices in Sect. 3, but illustrated here from winter to the end of the following summer. Therefore, based on this robust analogy and the premise of an earlier

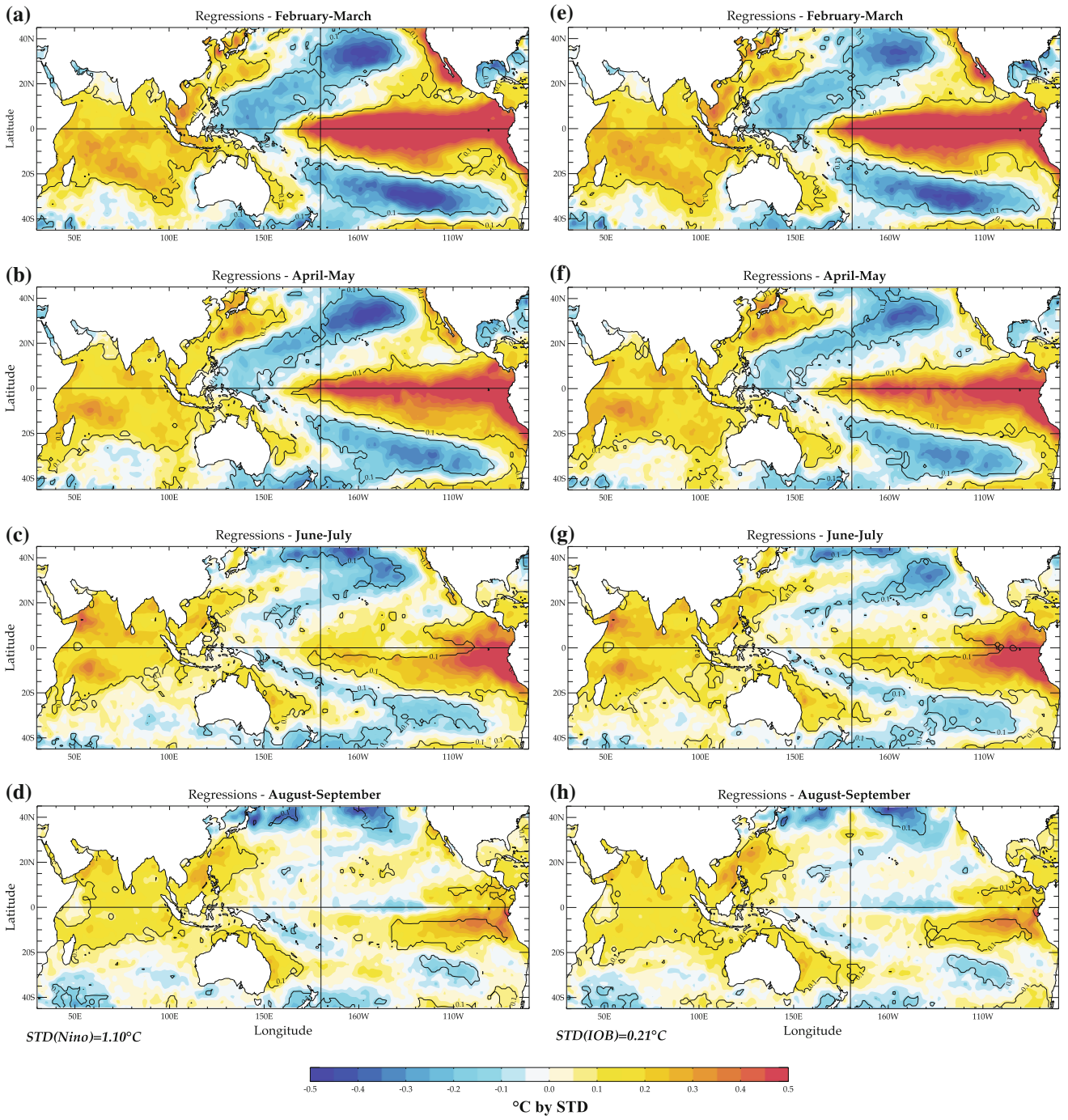

Fig. 2 Bimonthly SST anomalies regressed onto the Nino(−1) index (**a**–**d**) and IOB index (**e**–**h**) from February–March (FM) to August–September (AS). Regressions that are above the 90% confidence level estimated with a phase-scrambling bootstrap test with 999 sampled are encircled. The standard deviation of the Niño3.4 (IOB) index is given at the *bottom* of the *left* (*right*) panels

ISM forecast with the Niño34 index in the preceding winter, we will focus on the regression patterns associated with the Nino(−1) index.

The distribution of SST anomalies from FM to JJ is marked by strong positive SST anomalies in the central and eastern Pacific Ocean, which are out of phase with anomalies in the west part of the basin, consistent with the decaying phase of an El Niño event (Fig. 2). Meanwhile, the tropical Indian Ocean is characterized by a significant warming which persists well into the ISM season when SST anomalies in the central Pacific have almost completely faded away (Yang et al. 2007; Li et al. 2008; Du et al. 2009; Schott et al. 2009). Interestingly, Fig. 2 suggests a stronger warming in the southwest and equatorial Indian Ocean from FM to AM, consistent with the significant positive heat content anomalies found in this region and associated with the Nino(−1) index during spring in Fig. 3a. It has already been shown that the ENSO-induced atmospheric changes in the West Pacific during boreal fall and winter force slow downwelling Rossby waves to propagate in the Indian Ocean, which deepen the thermocline and raise SST specifically in the South-West Indian Ocean (SWIO), a region where the mean thermocline is shallow (Xie et al. 2002; Schott et al. 2009). On the other hand, the equatorial heat content anomalies probably stem from the changes in the Indo-Pacific Walker circulation occurring, this time, during the mature phase of El Niño. Indeed, the modulated Indian Walker cell and the well-organized subtropical Northwest Pacific anticyclone favor anomalous low-level easterlies in the equatorial Indian Ocean (Fig. 3b), which weaken the seasonal westerly Wyrtki jet and thus help maintain warm waters in the western part of the basin until boreal spring (Fig. 3a). This lagged SST response to ENSO has already been well documented (Klein et al. 1999; Reason et al. 2000; Alexander et al. 2002; Lau and Nath 2003; Xie et al. 2002; Huang and Kinter 2002; Wang et al. 2003; Annamalai et al. 2005). Our analysis is in line with these works and further shows that the warm SST anomalies in the south Indian Ocean are dominant and robust features of the Indian Ocean variability in the late boreal spring following an El Niño event.

Interestingly, by AM, the SWIO warming is collocated with intense local convection (shown by negative OLR anomalies in Fig. 4a) and incites the convergence of northerly winds onto this region (Fig. 3b). The induced low-level flow is, however, influenced by the Coriolis force when crossing the equator, which leads to the "C-shaped" wind pattern observed in Fig. 3b, with northeasterly (northwesterly) wind anomalies north (south) of the equator. By suppressing evaporation south and north of the equator (not shown), this wind pattern is then able to sustain the initial warm SST anomalies in the south Indian

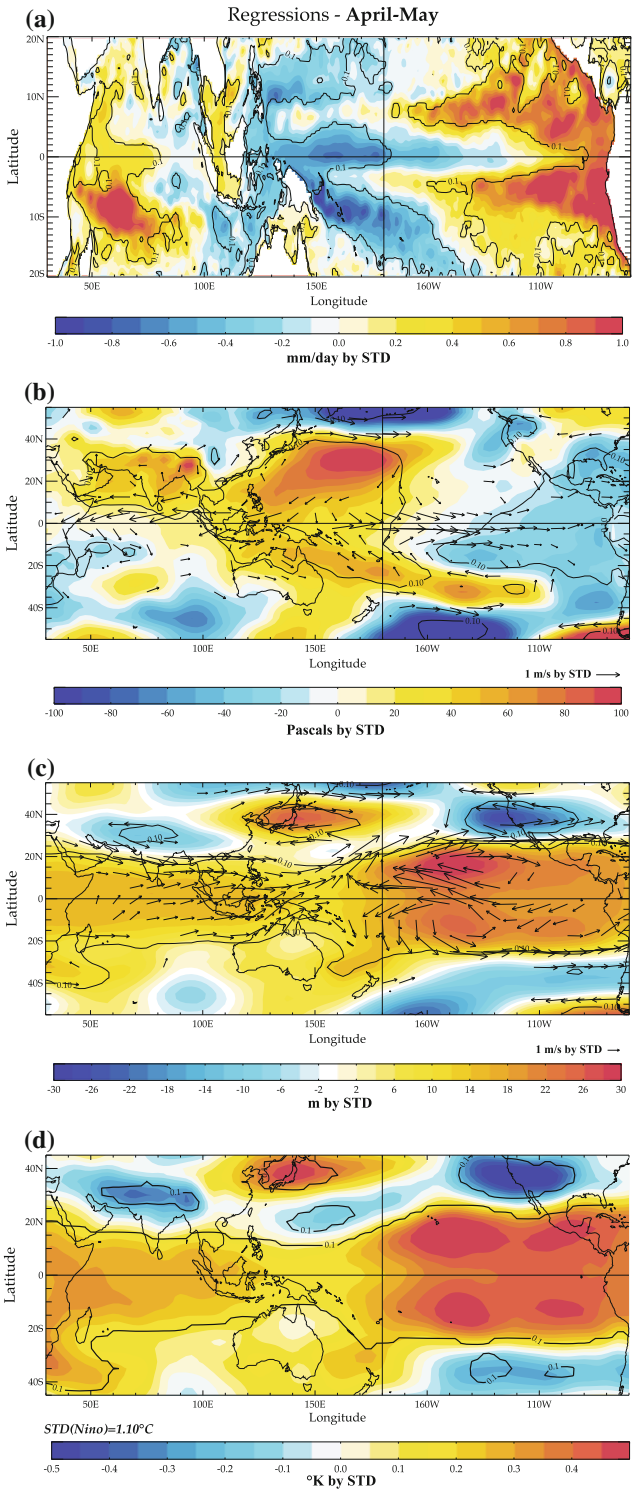

Fig. 3 Regression of Nino(−1) index onto bimonthly **a** heat content anomalies averaged over the first 130 m layer of the ocean, **b** wind anomalies at 10 m, **c** geopotential (*shading*) and 200 hPa wind anomalies (*arrows*), and **d** tropospheric mean temperatures (averaged from 850 to 200 hPa), all in April–May (AM). Regressions that are above the 90% confidence level estimated with a phase-scrambling bootstrap test with 999 sampled are encircled. Only wind anomalies that are above the 90% confidence level are shown. The standard deviation of the Niño3.4 index is given at the *bottom* of the panels

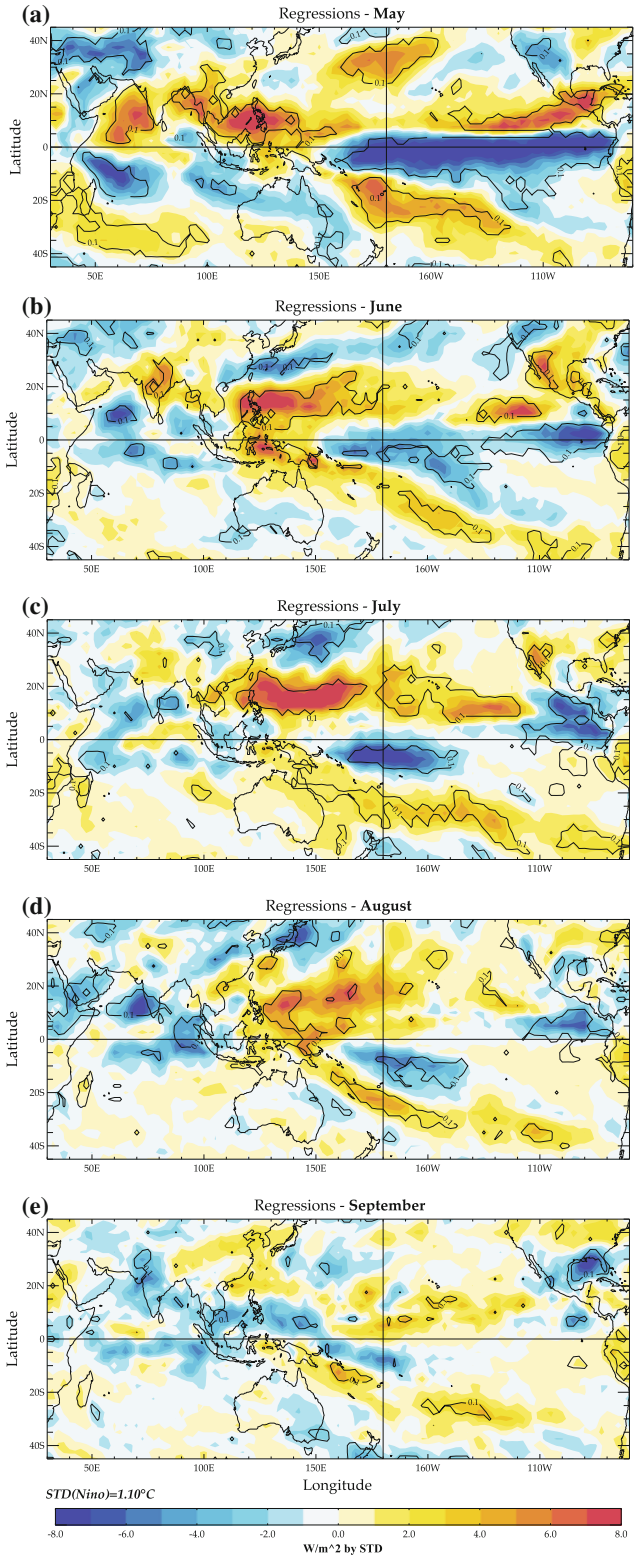

Fig. 4 Regression of Nino(−1) index onto monthly OLR anomalies from May to September. Regressions that are above the 90% confidence level estimated with a phase-scrambling bootstrap test with 999 sampled are *encircled*. The standard deviation of the Niño3.4 index is given at the *bottom* of the panels

Ocean and allows the northward propagation of the warm SST anomalies, a process partly consistent with a positive Wind-Evaporation-SST (WES) feedback. At the same time, convective activity is largely decreased north of the equator from the Arabian Sea to the Northwest Pacific suggesting a remote forcing from the subtropical Northwest Pacific anticyclone (see Figs. 3b, 4a). Previous works have already recognized the presence of this asymmetric atmospheric pattern during boreal spring over the tropical Indian Ocean (Kawamura et al. 2001; Wu et al. 2008; Du et al. 2009). Altogether, Figs. 3 and 4 confirm that the asymmetric atmospheric pattern tends to occur during the decaying phase of El Niño and is able to persist through early summer induced by the SWIO warming and possibly anchored by the subtropical Northwest Pacific anticyclone.

Nevertheless, we must bear in mind that traditionally at this time of the year (e.g. in AM), the monsoon is preparing to set in over India. Climatology conditions over the Indian Ocean are thus typical of this pre-onset phase, with the warmest area of the Indian Ocean lying in the Arabian Sea. Indeed, this region of high SST can usually cause large-scale moisture convergence, leading to the local build-up of deep convection, with a heating of the tropospheric column, a lowering of the surface pressure and a strengthening of low-level westerly winds, giving rise to a local Hadley circulation over the western Indian Ocean (Joseph et al. 2003). The ISM onset date is directly linked to the timing of this deep convection and the setup of this local Hadley cell: therefore the earlier the SST peak in the Arabian Sea, the earlier the monsoon onset (Soman and Krishnakumar 1993; Joseph et al. 1994; Ramesh Kumar et al. 2008). However, in the spring following an El Niño event, the strongest warming is located south of the equator in the SWIO (Fig. 2). The increased SST, decreased OLR and SLP in this region can reduce the strength or even induce a reversal of the local Hadley cell over the western Indian Ocean in AM as illustrated by cross-equatorial northerly (southerly) wind anomalies at 850 hPa (200 hPa) in this region (see Fig. 3b, c). Consistent with the work of Joseph et al. (2003) and Annamalai et al. (2005), this anomalous cell suppresses convection over the Arabian Sea and maintains the convective activity in the south, causing a delayed northward migration of the InterTropical Convergence Zone (ITCZ) and a late ISM onset. Consequently, the asymmetric atmospheric mode observed in AM over the tropical Indian Ocean after an El Niño presents unfavorable conditions for the ISM onset. Note that this ISM pre-onset phase may also be influenced by larger-scale features, such as the substantial warming of the troposphere often associated with an El Niño (Chiang and Sobel 2002; He et al. 2003 among others). As illustrated in Fig. 3d, these warm tropospheric temperature anomalies are able to

persist from winter to the following spring and spread across the entire tropical belt (between 20°S and 20°N). Moreover, negative temperature anomalies associated with Nino(−1) have set up over North India by AM. This leads to the establishment of a significant meridional gradient between 15°S and 35°N, a large-scale tropospheric feature which is reminiscent of Goswami and Xavier Prince's (2005) definition of ISM onset (see Sect. 2a). Therefore, by setting up persistent negative (positive) anomalies over North (South) India in the following spring, an El Niño creates unfavorable conditions for the reversal of the tropospheric temperature gradient over the monsoon region which delays the subsequent ISM onset.

Altogether, these results thus corroborate the positive correlation obtained in Table 3 between the Nino(−1) and IOB indices and the ISM onset dates.

In May–June, the anomalous patterns are consistent with this delayed ISM onset (Figs. 4, 5). Indeed, the "C-shaped" wind anomalies at 850 hPa in the western Indian Ocean (Fig. 5a) indicate a deceleration of the cross-equatorial low-level jet stream (LLJ) (Findlater 1969; Joseph and Sijikumar 2004), and a delay in the ensuing moisture transport, which is usually known to maintain the monsoon over the Indian subcontinent once it gets established. Meanwhile, the subsident branch of the anomalous reversed Hadley cell over the south Arabian Sea is associated with a cloudless sky, reduced upwelling and evaporation along the African coast (consistent with short wave and latent heat fluxes not shown) and induces a significant warming of the south Arabian Sea (Fig. 2c). This anomalous warming is subsequently collocated (in June) with a low pressure anomaly and cyclonic cell at 850 hPa (Fig. 5b) as well as increased wind speed and evaporation just to the north of the equator (Fig. 6a, d), which suggests it may enhance in situ convection over the south Arabian Sea and thus cause the northward shift observed in OLR anomalies from the SWIO in May to the south Arabian Sea in June (Fig. 4a, b). This shift in convection marks the collapse of the asymmetric atmospheric pattern, the onset of the monsoon over the ocean, but also causes a delay in the ISM onset over India, since convection at this time is favored over its adjacent oceanic regions. The positive OLR anomalies prevailing over the Indian subcontinent in June (Fig. 4b) are consistent with this hypothesis, and may also account for the negative correlation obtained between the Nino(−1) index and ISMR in June in Table 2.

From June onwards, the evolution of OLR anomalies shows a quite distinctive northeastward propagation from the Arabian Sea to the Indian subcontinent (Fig. 4). Indeed, after being maintained for a significant time over the south Arabian Sea, significant negative convection anomalies are able to reach the west coast of India later in the season, in August, and spread over the entire subcontinent by

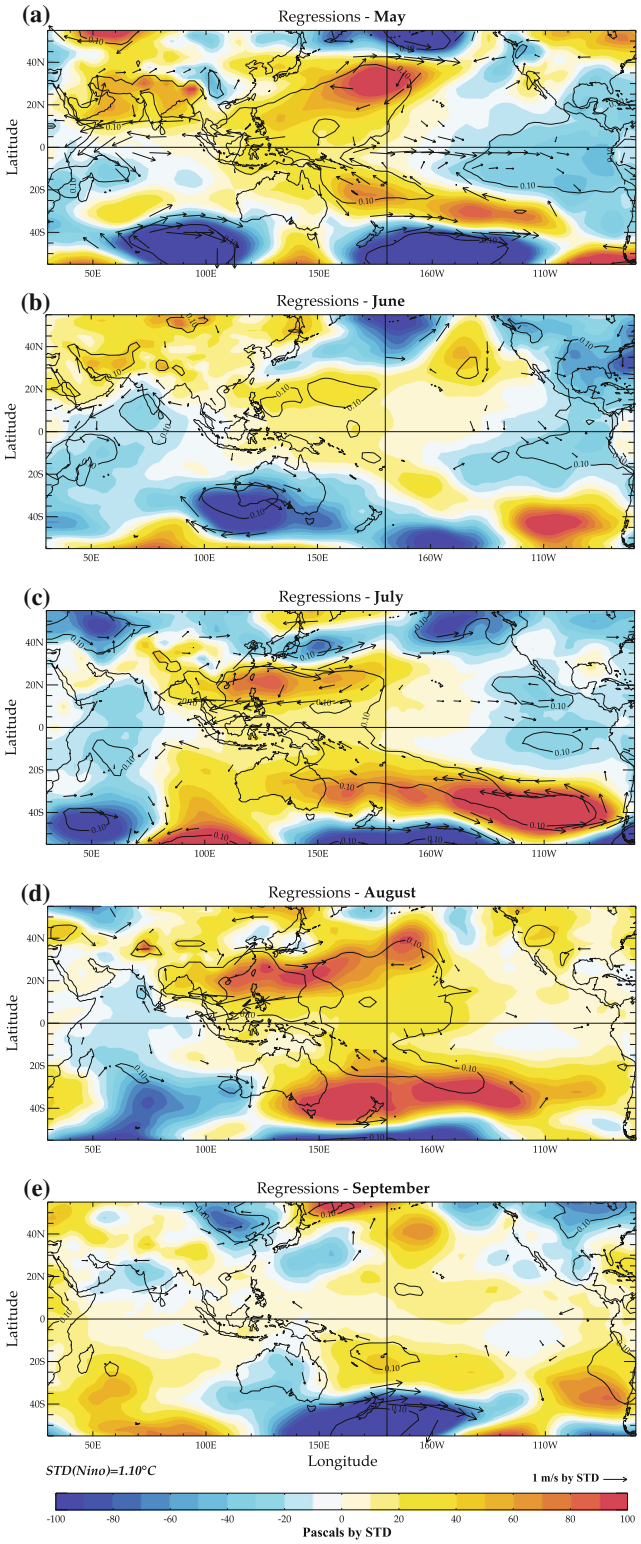

Fig. 5 Regression of Nino(−1) index onto monthly SLP (*shading*) and 850 hPa wind anomalies (*arrows*) from May to September. Regressions that are above the 90% confidence level estimated with a phase-scrambling bootstrap test with 999 sampled are *encircled*. Only wind anomalies that are above the 90% confidence level are shown. The standard deviation of the Niño3.4 index is given at the *bottom* of the panels

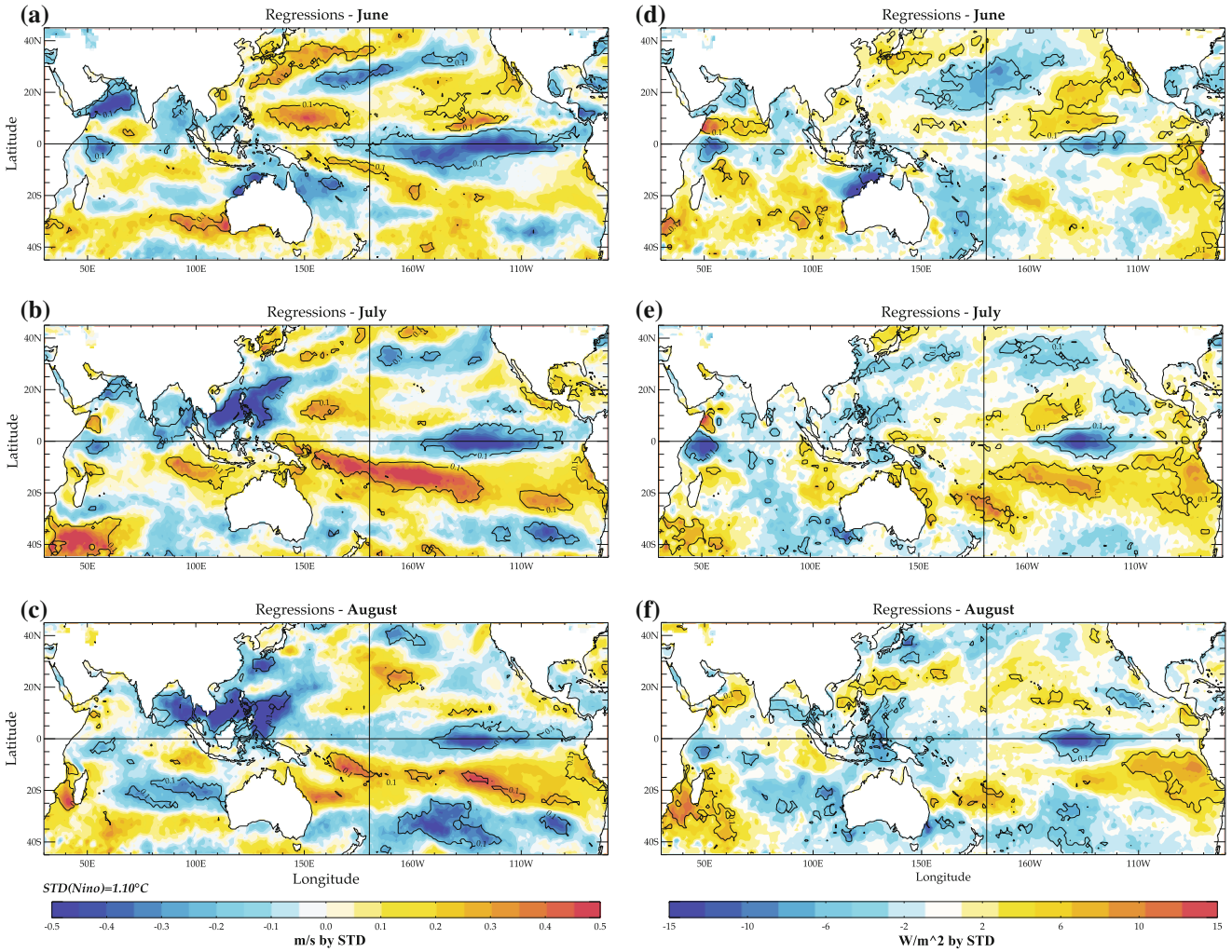

Fig. 6 Regression of Nino(−1) index onto monthly wind speed (**a**–**c**) and upward latent heat flux anomalies (**d**–**f**) from June to August. Regressions that are above the 90% confidence level estimated with a phase-scrambling bootstrap test with 999 sampled are *encircled*. The standard deviation of the Niño3.4 index is given at the *bottom* of the left panels

September. Although this evolution of convective activity during the ISM season is not yet fully understood, our observational analysis points towards a possible interaction with both local and remote dynamical coupling processes associated to the end of an El Niño. The processes we suggest below may also help understand the gradual increase in correlations with ISM rainfall from June to September in Table 2.

Our first hypothesis is based on the existence of a local feedback between convection and temperature anomalies in the Indian areas. The preceding analysis suggests that while convection is favored over the south Arabian Sea in the early ISM season, SST tends to cool from June to July (see Fig. 7). Indeed, by July, the SST has returned to climatology and the cyclonic wind anomalies have disappeared (Fig. 5c). This result is consistent with the observed rebound to climatological winds noted in Park et al. (2010). Meanwhile, Fig. 7 also indicates a significant rise from June to July in 2 m air temperatures over India, thereby sustaining the thermal contrast between land and ocean. This suggests that, from June to September, the low-frequency northeastward propagation of the convection anomalies in the Indian region is thus partly driven by the modulated temperature gradient from the south Arabian Sea towards the Indian subcontinent, by processes similar to those governing the propagation of rainfall over the land during the onset of the monsoon (Webster et al. 1998).

Our second hypothesis is based on the possible remote influence of the Northwest Pacific region on the development of the ISM. In our analysis, this region stands out as a statistically prominent feature of the decay of an El Niño, characterized by robust positive OLR anomalies (see Fig. 4), collocated in July and August with a highly significant positive SLP anomaly and a vigorous low-level anticyclonic anomalous wind pattern (Fig. 5c, d). The origin and persistence of this anticyclone have often been

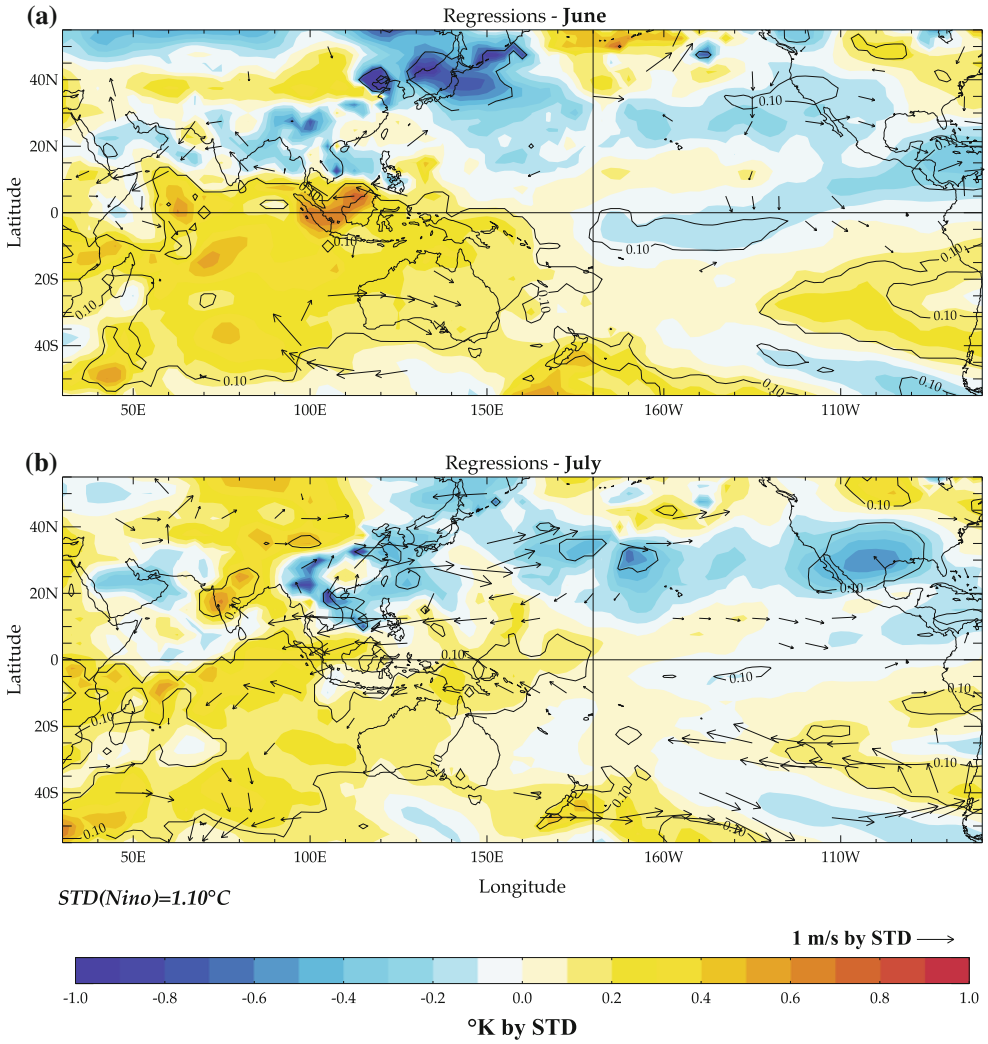

Fig. 7 Regression of Nino(−1) index onto monthly air temperature at 2 m (*shading*) and 850 hPa wind anomalies (*arrows*) in June and July. Regressions that are above the 90% confidence level estimated with a phase-scrambling bootstrap test with 999 sampled are *encircled*. Only wind anomalies that are above the 90% confidence level are shown. The standard deviation of the Niño3.4 index is given at the *bottom* of the panels

linked to ENSO and its subsequent warming in the tropical Indian Ocean. In particular, Xie et al. (2009) explain that this warming excites a warm atmospheric Kelvin wave, which propagates into the western Pacific along the equator. The consecutive decrease in equatorial SLP drives northeasterly wind anomalies, induces surface wind divergence and suppresses convection over the subtropical Northwest Pacific. In our analysis, an interesting out-of-phase relationship in convection is observed between the Northwest Pacific and the Indian Ocean during the ISM season. Indeed, Fig. 4 shows that while the convective cell is maintained over the Arabian Sea, from June to August, convection is simultaneously suppressed over the Northwest Pacific Ocean, suggesting that the anomalous Northwest Pacific anticyclone may also play an important role in the transitory blocking of convection over the Arabian Sea during early boreal summer. The low-level wind and pressure anomalies during this period seem consistent with this hypothesis (Fig. 5). Indeed, Fig. 5c shows that, by July, the northeasterly wind anomalies have disappeared over the Arabian Sea, allowing for the moist-laden monsoonal winds to develop and strengthen from this region to the west coast of India. Meanwhile, the circulation over the Bay of Bengal seems to be significantly influenced by the strengthening and eastward extension of the anomalous Northwest Pacific anticyclone. Easterly wind anomalies originating from the southern branch of the anomalous anticyclone, are seen to penetrate into the Bay of Bengal and even extend to the west coast of India by August. During July and August, the local reduction in wind speed and evaporation associated with the suppressed convection over the eastern Indian

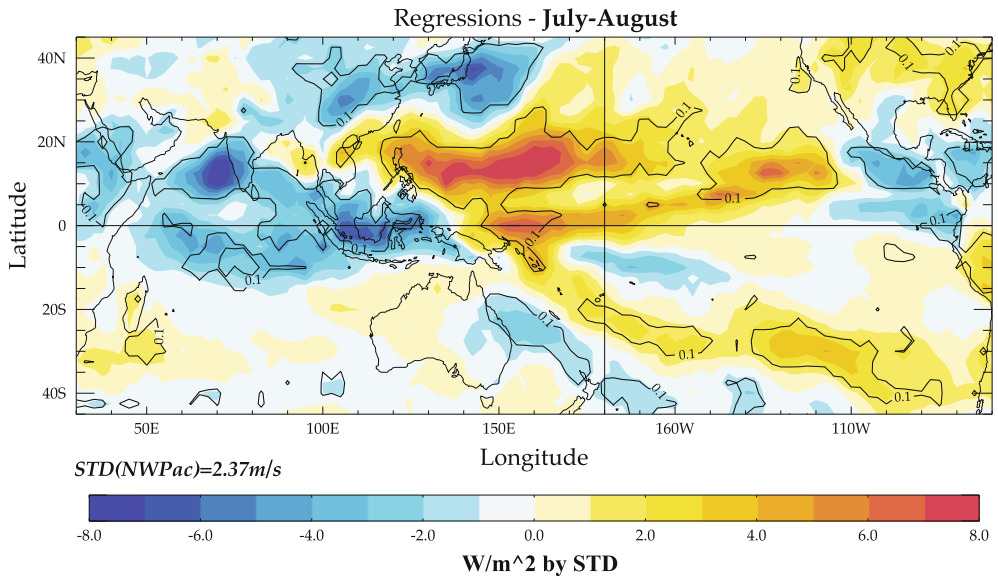

Fig. 8 Regression of a Northwest Pacific summer monsoon dynamical index onto bimonthly OLR anomalies in July–August. The Northwest Pacific monsoon index is defined as the meridional difference of 850 hPa zonal wind anomalies between a northern (20°–30°N, 110°–140°E) and a southern region (5°–15°N, 100°–130°E) averaged over June–July–August, following Wang et al. (2001). The standard deviation of this index is given at the bottom of the panel. Regressions that are above the 90% confidence level estimated with a phase-scrambling bootstrap test with 999 sampled are encircled

region north of the equator (Fig. 6b, c, e, f), are in opposition with the concurrent build-up of moist air and upward motions over the Arabian Sea where the wind is near climatology. In other words, we here suggest that the weakening of the monsoon winds in the eastern Indian region (north of the equator) associated with the Northwest Pacific anticyclone may also play a significant role in sustaining the convection over the Arabian Sea during July and August by dynamically strengthening upward motions. The OLR anomalies associated with a Northwest Pacific summer monsoon dynamical index, as defined in Wang et al. (2001), agree with this suggestion as significant negative anomalies are seen to prevail over the Arabian Sea, indicating the blocking of local convection during July–August (Fig. 8). Note also that, consistently with this hypothesis, the disappearance of the anomalous Northwest Pacific anticyclone in September coincides with the unlocking of convection over the Arabian Sea and its propagation over the Indian subcontinent in the Nino(−1)/OLR regression patterns (Fig. 4e).

4.2 Nino(0) and SEIO indices

Anomalous fields regressed onto the Nino(0) and SEIO indices generally display very similar evolutions during the ISM. Figure 9, in particular, illustrates how SST anomalies regressed onto the SEIO index are opposite in sign but comparable in amplitude and pattern with those associated with Nino(0), and this more specifically in JJ and AS. This resemblance is also in good agreement with previous works, which have recognized the SEIO index as a significant precursor of ENSO after the 1976–1977 climate shift (Terray et al. 2005; Terray and Dominiak 2005; Dominiak and Terray 2005; Terray 2010). Given the general acknowledgment of an inverse ENSO–ISM relationship corroborated by the results in Table 2, even for the period after the 1976–1977 climate shift, it may thus be eligibly inferred that the SEIO index is first linked to the ISM via its forcing on ENSO. However, the coupled experiments of Terray et al. (2007) have also demonstrated that SEIO SSTs in FM are able to significantly influence the ISM, regardless of the concurrent ENSO state in the Pacific: this suggests that local processes within the Indian Ocean may also be playing an important role before and during the ISM season. Our correlation analysis in Sect. 3 stands in line with this hypothesis, as it distinguishes the SEIO and Nino(0) indices in their relationship with the ISM, by showing that the monthly correlations associated with Nino(0) are quite chaotic, in contrast with the steady strengthening of the SEIO–ISM relationship from June to September (see Table 2). Therefore, given the long-range ISM forecast offered by the SEIO in FM and the apparently higher robustness of the SEIO–ISM relationship, we will focus on the regressions with the SEIO index and examine the local dynamical processes through which it may impact the ISM rainfall and atmospheric circulation.

The distribution of SST anomalies in Fig. 9e shows that in FM, the SEIO index is significantly linked to a decaying El Niño event in the equatorial Pacific Ocean and to an

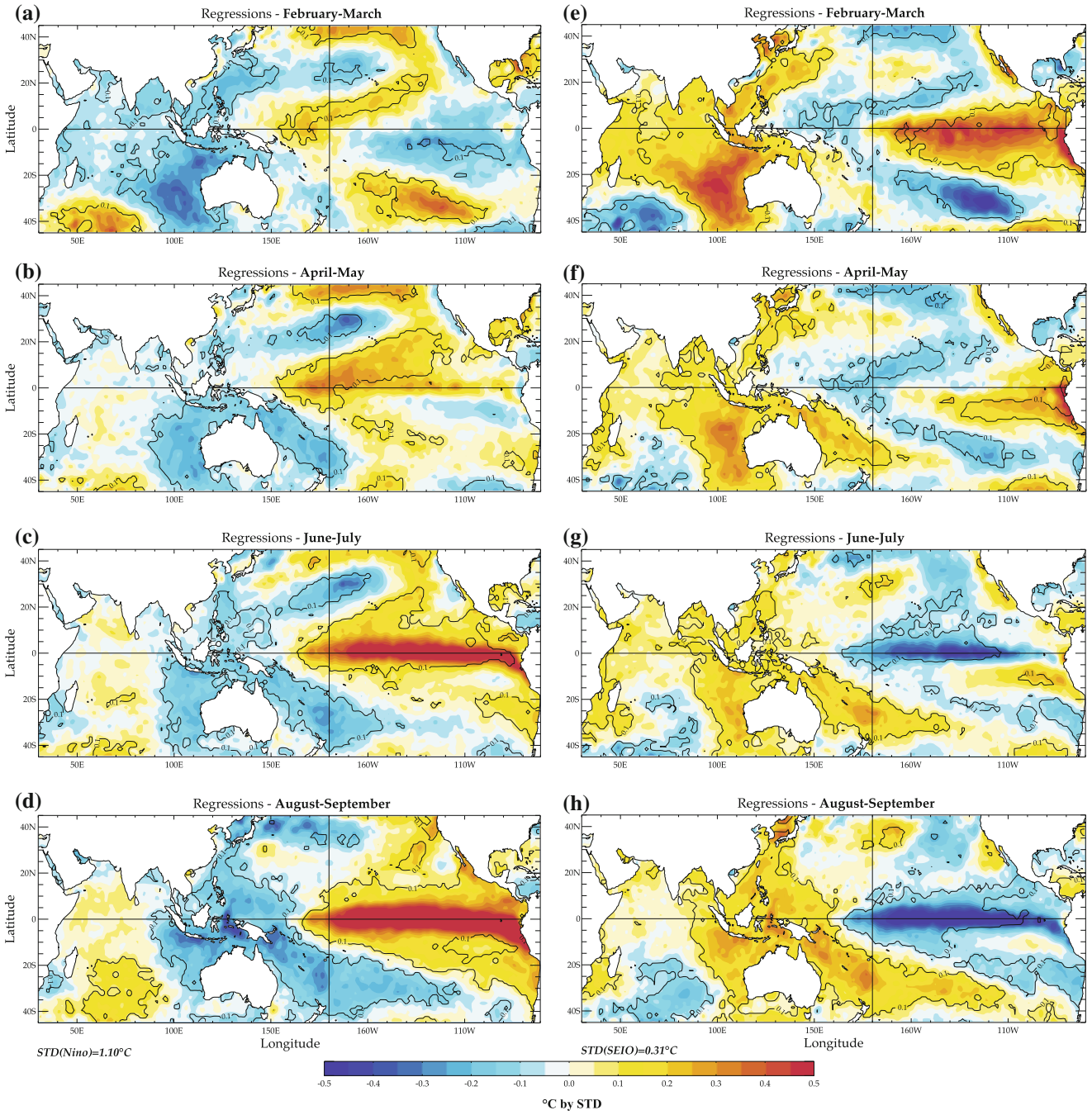

Fig. 9 Bimonthly SST anomalies regressed onto the Nino(0) index (**a**–**d**) and SEIO index (**e**–**h**) from February–March (FM) to August–September (AS). Regressions that are above the 90% confidence level estimated with a phase-scrambling bootstrap test with 999 sampled are encircled. The standard deviation of the Niño3.4 (SEIO) index is given at the *bottom* of the *left* (*right*) panels

anomalous subtropical SST gradient in the south Indian Ocean. Previous studies have shown that such subtropical dipole events are generated by Mascarene high pulses during boreal winter, and can occur independently from ENSO, producing significant climate anomalies in southern Africa (Behera and Yamagata 2001; Reason et al. 2002), and over the entire Indo-Pacific region (Terray et al. 2005; Terray and Dominiak 2005; Terray 2010). In FM, this anomalous dipole is located between 20°S and 40°S in the Indian Ocean, and is seen to persist until the end of the ISM season (Fig. 9e–h).

During boreal spring, the SST patterns show a decay of this anomalous dipole in the south Indian Ocean (Fig. 9f). However, the warm anomalies in the SEIO are still significant and have shifted northward, suggesting that ocean–atmosphere feedbacks may be operating at this time to

allow the persistence of these SST anomalies (from FM to AM). The atmospheric response to the SEIO index in AM is consistent with this hypothesis and shows that the anomalous SST gradient in the south Indian Ocean forces the low-level flow to converge towards the anomalously warm region (Fig. 10). In Fig. 10a, b, negative OLR and cyclonic wind anomalies are consistently collocated with the warm anomaly in the SEIO, as opposed to the positive OLR anomaly and anomalous anticyclonic cell over the cooler southwest Indian Ocean region, a pattern consistent with an ocean-to-atmosphere forcing. At this stage, the northwesterly wind anomalies, observed on the eastern flank of the SEIO cyclonic circulation, tend to reduce the seasonal wind speed (Fig. 10b, d) and suppress local evaporation (Fig. 10c), which, in turn, sustains the initial warm anomaly and allows its northward propagation. On the other hand, wind anomalies on the western side of the SEIO convective perturbation strengthen the southeasterly trade winds (Fig. 10d). The increased wind speed is this time collocated with upward latent heat fluxes in the central part of the south Indian Ocean (Fig. 10c), suggesting a cooling of SST anomalies via enhanced evaporation. As a result, the SST gradients are maintained in the south Indian Ocean and these gradients favor again the atmospheric convergence over the initial warm anomaly, a process consistent with a positive WES feedback. During the same period, convection is increased just over the warm SST anomaly, and along a latitudinal band between 5°S and 15°S, which thus affects the seasonal position of the ITCZ (Fig. 10a). The increased cloudiness over this region is associated with upward short wave flux anomalies and a subsequent cooling of surface temperatures while the reversed processes are operating to the south (figures not shown). Hence, surface shortwave radiation anomalies associated with the SEIO index provides, by contrast, a negative feedback on SST anomalies during spring.

By June, there is a generally weak response to the SEIO index over the Indian Ocean. SST anomalies have lost statistical significance in the south Indian Ocean, suggesting that, at this stage, the negative feedback provided by the short wave radiation is more active and has significantly damped the SST fluctuations. Although the SEIO index has an overall weak impact on the ISM onset (see also Table 3), it seems able to trigger a significant atmospheric response in the eastern part of the IO basin. Indeed, strong convective anomalies are observed over the Maritime Continent and eastern Indian Ocean (Fig. 11a), collocated with reduced wind speed near the west coast of Sumatra (Fig. 12a), an area which is usually shaped by intense coastal upwelling (Schott et al. 2009). Surface latent heat flux anomalies are not significant or are even of the wrong sign to sustain the warm SST anomaly in this region (Fig. 12e). This supports the idea that ocean

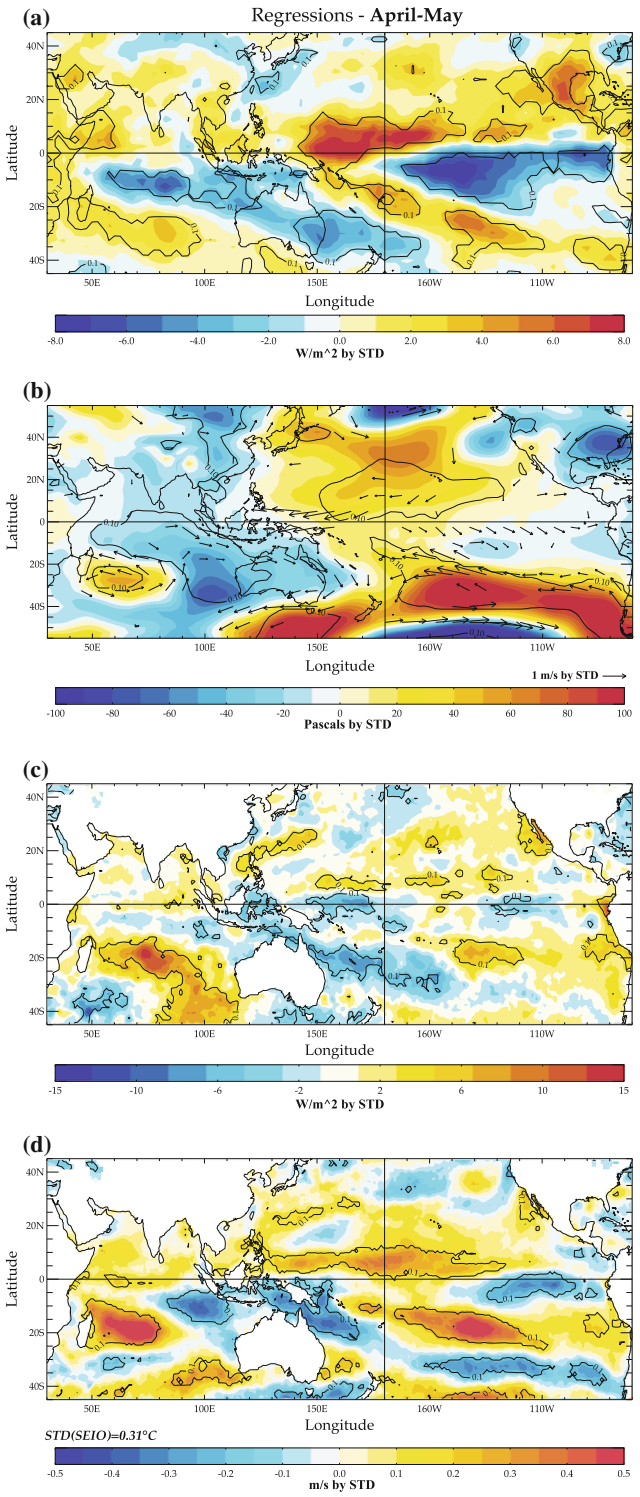

Fig. 10 Regression of SEIO index onto bimonthly **a** OLR anomalies, **b** SLP (*shading*) and 850 hPa wind anomalies (*arrows*), **c** upward latent heat flux anomalies and **d** wind speed anomalies, all in April–May (AM). Regressions that are above the 90% confidence level estimated with a phase-scrambling bootstrap test with 999 sampled are *encircled*. Only wind anomalies that are above the 90% confidence level are shown. The standard deviation of the SEIO index is given at the *bottom* of the panels

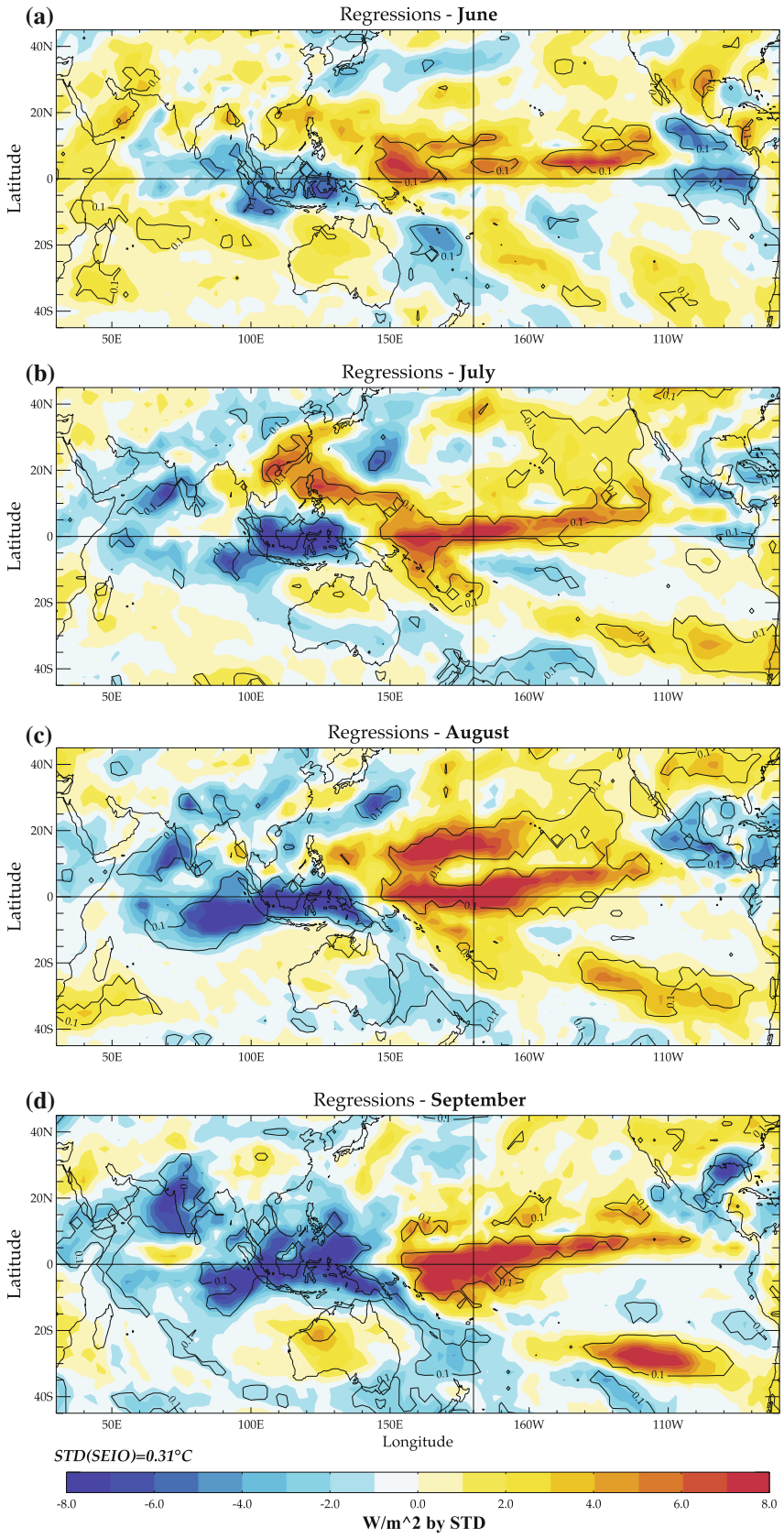

Fig. 11 Regression of SEIO index onto monthly OLR anomalies from June to September (**a**–**d**). Regressions that are above the 90% confidence level estimated with a phase-scrambling bootstrap test with 999 sampled are *encircled*. The standard deviation of the SEIO index is given at the *bottom* of the panels

dynamics may play a crucial role in the maintenance of warm anomalies at this particular time. Indeed, the northwesterly wind anomalies along the west coast of Sumatra can reduce the upwelling of cooler and deeper water, and subsequently lead to warmer SST and enhanced convection (Fischer et al. 2005; Terray et al. 2007). In line with Terray et al. (2007), our results thus suggest that a coastal upwelling feedback is triggered along the west coast of Sumatra in June, a process which could explain why both the SST and atmospheric anomalies then reinvigorate and gain large significance during summer (Fig. 11).

From July to September, the anomalous patterns associated with the SEIO index are consistent with the development of this coastal upwelling feedback. Indeed, while latent heat flux anomalies remain weakly significant (Fig. 12f–h), the negative wind speed anomalies are

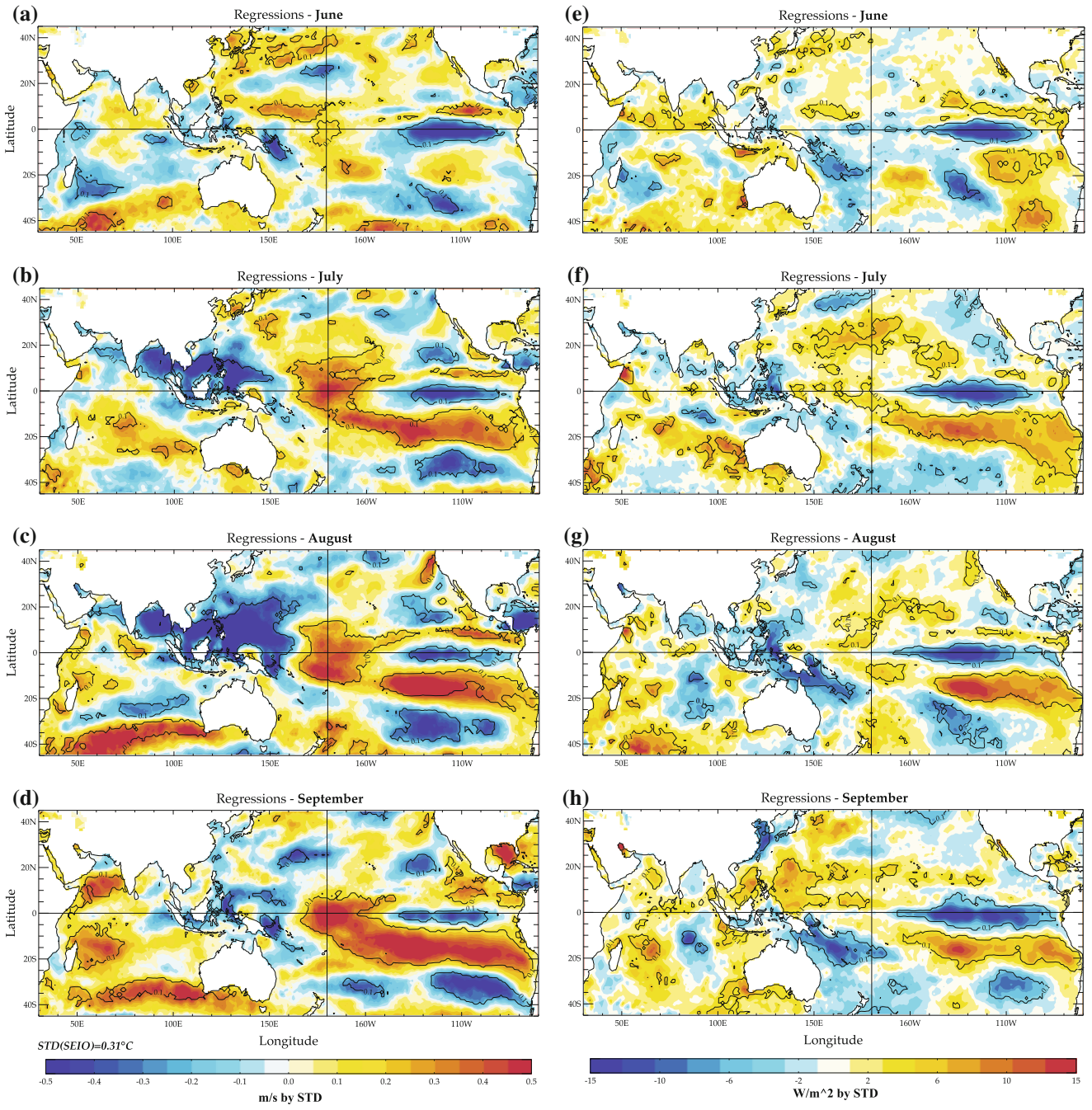

Fig. 12 Regression of SEIO index onto monthly wind speed (**a**–**d**) and upward latent heat flux anomalies (**e**–**h**) from June to September. Regressions that are above the 90% confidence level estimated with a phase-scrambling bootstrap test with 999 sampled are encircled. The standard deviation of the SEIO index is given at the *bottom* of the left panels

maintained (Fig. 12b–d) and anchor the positive SST anomalies along the west coast of Sumatra (Fig. 9g–h). The atmospheric response to these anomalies is characterized, from June onwards, by the persistence and amplification of convective anomalies over the Maritime Continent and the southeast equatorial Indian Ocean (Fig. 11). In parallel, significant negative OLR anomalies are also observed in July over the Arabian Sea, and these anomalies propagate northeastwards to reach the Indian subcontinent by the end of the summer: a low-frequency evolution that matches the gradual increase in correlation obtained between the ISMR and SEIO indices (Table 2). Note that this evolution of convective anomalies over the Arabian Sea is also reminiscent of previous observations with the Nino(−1) index (see Fig. 4), although we will show here that they stem from distinct dynamical processes.

Indeed, the regression analyses with the SEIO index suggest that convection over the Arabian Sea and the ensuing ISM rainfall response, are not directly linked to local processes in the north Indian Ocean, but may instead result from fluctuations in atmospheric moisture transport in the south Indian Ocean. To begin with, the anomalous patterns in July indicate that the positive WES feedback is reinvigorated in the central part of the south Indian Ocean. The increased wind speed over this region (Fig. 12b) is consistently collocated with upward latent heat flux (Fig. 12f) and a subsequent cooler SST anomaly (Fig. 9g). This enhances the amount of humidity available over the southern Indian Ocean, although the dynamical response to the SEIO index over the Arabian Sea is rather weak at this stage (Fig. 12b). Our results are thus consistent with Terray et al. (2007) and suggest that the appearance of negative OLR anomalies in the Arabian Sea in July (Fig. 11b) may result from the anomalous moisture transport from the south Indian Ocean via climatological winds.

From July onwards, the anomalous cyclone over the SEIO is amplified while it propagates northward (figure not shown). Once it reaches the equator in August, the northwesterly wind anomalies can trigger a Wind-Thermocline-SST feedback (Terray et al. 2007). This marks also the beginning of a dynamical response to the SEIO index in the north Indian Ocean, and the strengthening of interhemispheric winds (Fig. 12c). The ensuing feedback between the ISM circulation and the interhemispheric moisture transport may then eligibly account for the amplification of the OLR signal observed over the Arabian Sea and the increase in ISM rainfall during the late ISM season (Fig. 11c, d).

Note that the SEIO index is also significantly related to the variability in the Northwest Pacific region during the months of July and August (Figs. 11, 12). The observed patterns are remarkably similar to those associated with the Nino(−1) index, and are probably just a reflexion of the strong relationship between ENSO and SEIO indices. Indeed, the SEIO index used in this study is defined over a quite large geographical domain, which we suspect would embody both tropical (e.g. ENSO) and extra-tropical influences (e.g. subtropical Indian dipole) regarding ISM interannual variability.

5 Conclusions and discussion

This study has examined the variability and predictability of ISM rainfall at interannual timescales, by exploring its relationship with ENSO and various modes of Indian Ocean coupled variability. Several SST indices are computed using observational data over the 1979–2007 period, and their respective merits are compared through correlation and regression analyses with ISM rainfall.

Our first result is a deceptive one and points towards a generally weak relationship between most of the indices and seasonal mean ISM rainfall. However, correlation analysis on a shorter timescale shows that seasonal mean values are statistically biased as the ISM season is shaped by important subseasonal variability, linked, in particular, to the onset and withdrawal dates of the monsoon (in June and September). Surprisingly, the monthly correlation values increase steadily and significantly during the summer season, and give rise to prospects of higher ISM previsibility with ENSO, IOB and SEIO indices for both the onset of the monsoon and the amount of rainfall during the second half of the monsoon season. In contrast, the relationship between the IOD index and ISM rainfall remains weak throughout the season: this result depreciates the IOD's forecast skills for the 1979–2007 period in comparison with the other SST indices.

A regression analysis is then carried out with the four remaining indices [namely IOB, Nino(−1), SEIO and Nino(0) indices] in order to elucidate the physical processes responsible for these significant predictive relationships and understand their gradual increase during the boreal summer. Results show that distinct local processes occurring within the Indian Ocean can significantly impact the ISM rainfall and are responsible for the low-frequency evolution of the observed correlations.

First, the stepwise evolution of monthly SST, OLR and wind anomalies associated with the end of an El Niño event helps understand the steady increase in monthly correlations obtained between the ISMR and Nino(−1) or IOB indices documented in Table 2. The weak and negative correlation values in the early ISM season following an El Niño, can be due to a late ISM onset, followed by the development of convection in priority over a warmer south Arabian Sea. The gradual increase in correlation then

matches the low-frequency northeastward propagation of convection from the south Arabian Sea to the Indian subcontinent during the monsoon season. Several factors may contribute to the maintenance of convection over the south Arabian Sea from June to August and its subsequent northward propagation: such as local feedbacks or a possible interaction with wind anomalies originating from the Northwest Pacific region.

Secondly, the regression analyses with the SEIO and Nino(0) indices are very consistent with the model experiments of Terray et al. (2007). Altogether these results show that during boreal spring, SST anomalies in the SEIO are able to trigger local feedbacks which become responsible for the persistence and northward propagation of the SST anomalies, as well as their significant impact on ISM variability during the following summer. In June, anomalies are temporarily weakened due to the negative feedback of convective clouds, which suggests a weak impact of the SEIO index during the early ISM season. However, ocean dynamics are also suggested to play an important role at this time, in particular near the west coast of Sumatra where the interaction between SST anomalies and upwelling processes allows SST and convection to be maintained in this region during the whole summer. By July, the warm anomalies resulting from the reduced upwelling are further amplified by the uptake of the positive WES feedback in the south Indian Ocean. This process increases the amount of available humidity over the south Indian Ocean and thus modulates the moisture transport to the Arabian Sea. Once the upwelling feedback is sufficiently developed and the *SST-induced* cyclonic anomaly over the eastern Indian Ocean has reached a sufficient amplitude, a dynamical response is triggered over the north Indian Ocean. The enhanced ISM circulation strengthens the moisture transport from the south Indian Ocean and the ensuing ISM rainfall over the Indian subcontinent in the late summer season.

Moreover, the local processes described above are dynamically linked to different phases of ENSO in the Pacific Ocean. This last observation may have useful implications in terms of long-range seasonal prediction of the monsoon, as these local SST indices can offer relevant ISM forecasts as early as in late boreal winter [e.g. SEIO and Nino(−1) indices] or early spring (e.g. IOB index): the choice of the better forecasting index would then hinge on the concurrent phasing of the ENSO cycle in the Pacific Ocean.

Nevertheless, we need to bear in mind that the 1979–2007 period has been shaped by two particularly strong and long-lasting El Niño events, e.g. the 1982–1983 and 1997–1998 warm events. It thus becomes relevant to ask ourselves at this point if, and to what extent, these extreme events have influenced our statistical results. In order to test the robustness of the previous results, a composite analysis is carried out during the summer of developing and decaying years of four 'normal' (1986–1987, 1991–1992, 1994–1995 and 2002–2003) and two 'strong' (1982–1983 and 1997–1998) El Niño events (Figs. 13, 14). The composite anomalous OLR patterns show that the El Niño events have a considerable impact on convective activity over the Indian subcontinent and its adjacent oceans during summer. However, this impact is entirely different depending on the phasing and the strength of the El Niño events which are being considered.

For instance, during the developing summer of the two strong El Niño events, the equatorial Pacific is marked by a particularly strong convective dipole whereas OLR anomalies are weak and poorly significant over India and the north Indian Ocean (Fig. 13b). Although the development of convection in the Pacific is less intense during the summer of 'normal' El Niño events (Fig. 13a), the positive OLR signal has gained significance over India and the Arabian Sea in the late summer (e.g. AS), suggesting that, at this time, local feedbacks in the Indian Ocean may be affecting the ISM rainfall variability, a finding consistent with the possible role of the SEIO index. It is also worth noticing that during these 'normal' El Niño events, anomalous convection is developed in the central equatorial Pacific rather than in the east during the late summer season. These significant negative OLR anomalies are associated with a horseshoe pattern and flanked by opposite anomalies on both sides along the equator, an OLR distribution which is reminiscent of the El Niño 'Modoki' events (Ashok et al. 2007; Weng et al. 2007; Kug et al. 2009). These works have distinguished the El Niño 'Modoki' phenomenon from the canonical El Niño in terms of SST characteristics, teleconnections and a more frequent occurrence during recent decades. In a recent work, Kug et al. (2009) classify the two types of El Niño events depending on their spatial pattern of SST anomalies, in the Niño4 region for the 'Modoki' event and Niño3 region for the conventional El Niño. However, our observational results are quite insensitive to the choice of ENSO indices, as correlation values with Nino(0) and Nino(−1) in Tables 2 and 3 are unchanged by the use of the Niño3 or Niño4 indices instead of Niño3.4. This highlights again the importance of local interactions within the Indian Ocean for the ISM rainfall.

Nevertheless, it seems important to point out that the two 'strong' episodes have a significant but reversed impact during their decaying phase (Fig. 14). Indeed, OLR patterns in Fig. 14b are significant over the Indian region in the late summer of 1998 and 1983. In contrast, the OLR anomalies are weak and even of opposite sign during the decay of "normal" El Niño events (Fig. 14a). In other

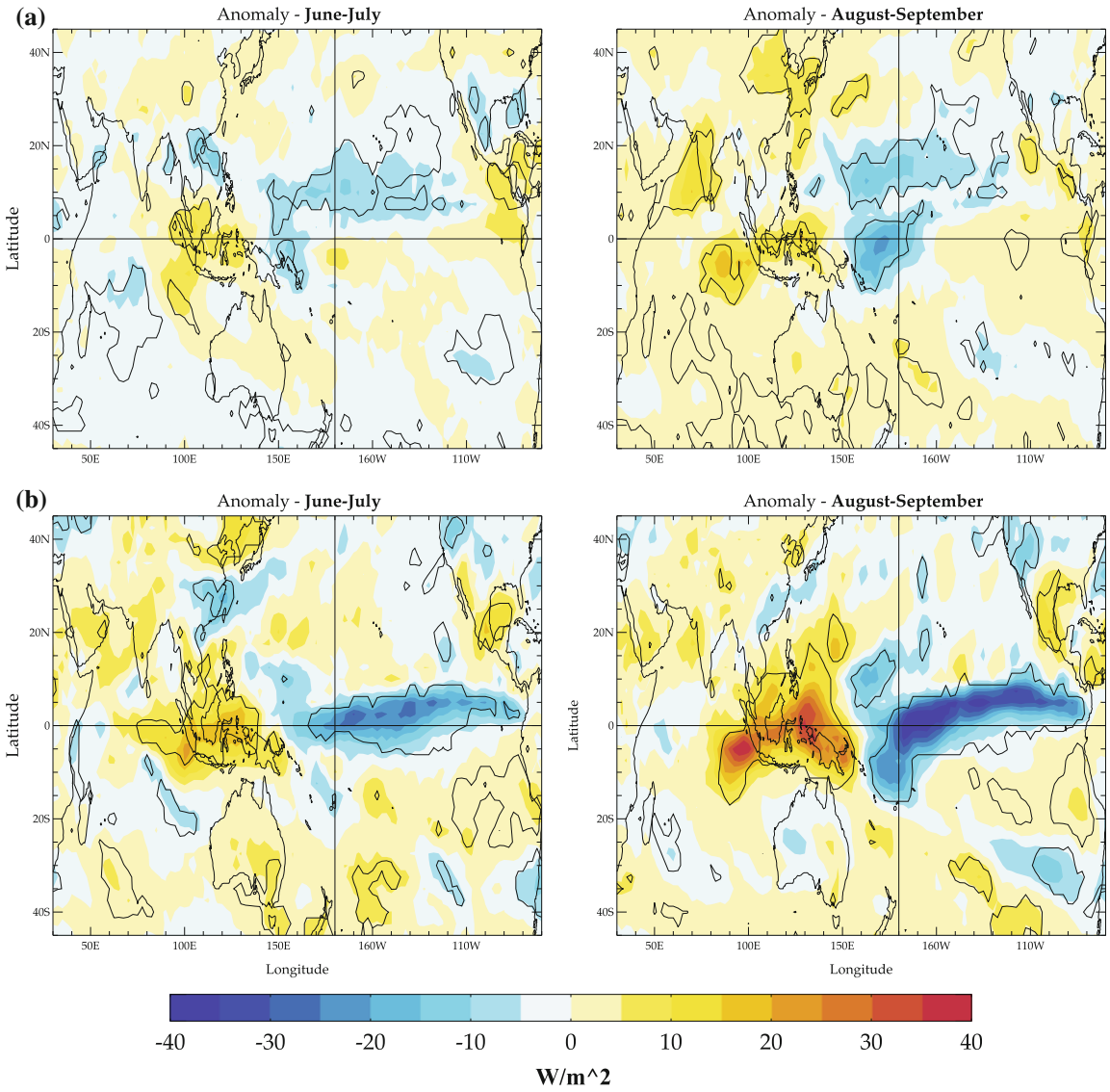

Fig. 13 OLR composites during the development of **a** "normal" El Nino events (1986–1987, 1991–1992, 1994–1995 and 2002–2003) and **b** "strong" El Nino events (1982–1983 and 1997–1998), in June–July (*left panels*) and August–September (*right panels*). Composite anomalies that are above the 90% confidence level using the Monte-Carlo procedure of Terray et al. (2003) are *encircled*

words, these composites suggest that the significant relationship which has been established between the Nino(−1) or IOB indices and ISM rainfall may be largely due to the occurrence of the two strongest El Niño events of the last century. This statistical bias thus sheds a doubt on the robustness and relevance of the IOB or Nino(−1) indices as ISM predictors. Moreover, it seems difficult to determine from this observational study which mechanisms are at play, and understand how the IOB index is able to affect ISM variability: whether it be directly via local processes in the Indian Ocean, or indirectly by accelerating the ENSO transition in the Pacific Ocean (Kug and Kang 2006; Ohba and Ueda 2007). Further work is needed in this direction, in particular to quantify the contribution of ENSO forcing on these interactions and reassess the merits of the IOB index as an intrinsic ISM predictor.

Likewise, our study and the recent work of Peings et al. (2009) have also highlighted the importance of variability in the Northwest Pacific Ocean for ISM prediction, as anomalies in this region are statistically significant during both the developing and decaying years of El Niño events. However, its contribution to ISM rainfall variability, regardless of ENSO, has also yet to be assessed. To this end, it would be interesting to use a fully coupled model and test its ability to simulate the Indian Ocean coupled interactions and their impact on ISM variability described in this paper. Numerical experiments may also be

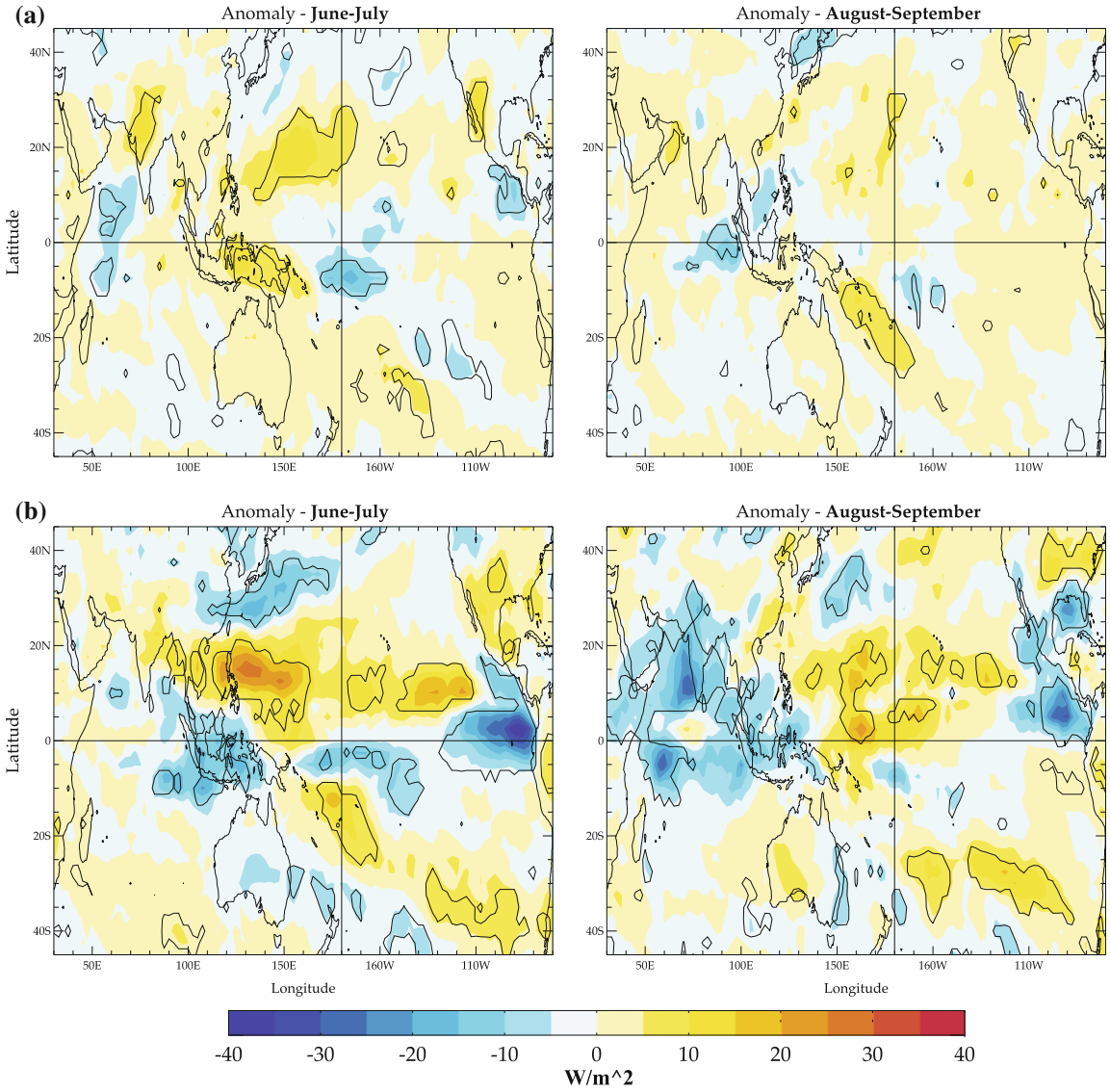

Fig. 14 OLR composites during the decaying phase of **a** "normal" El Nino events (in 1987, 1992, 1995 and 2003) and **b** "strong" El Nino events (in 1983 and 1998), in June–July (*left panels*) and August–September (*right panels*). Composite anomalies that are above the 90% confidence level using the Monte-Carlo procedure of Terray et al. (2003) are *encircled*

conducted as to unravel the relative contribution of each of these modes of variability and test their robustness as intrinsic ISM predictors, as already done for the SEIO index in Terray et al. (2007).

Finally, we would like to point out that our results regarding ISM interannual variability have shown an in-phase relationship between convective anomalies in the eastern equatorial Indian Ocean (just south of the equator) and over India. However, this OLR pattern seems to be in conflict with the OLR seesaw oscillation which has been observed on the intraseasonal timescales during boreal summer (Wang et al. 2005, 2006). Therefore, it will be of interest to analyze the links between these different timescales, with a particular focus on the interactions between the key SST indices from this study and subseasonal features associated with ISM variability.

Acknowledgments Financial support from the Indo-French CEFIPRA project (No. 3907/1) is acknowledged. We thank Prince Xavier for providing us the ISM onset and withdrawal dates. We also thank the anonymous reviewers for their comments that improved this paper. The Hadley SST, NCAR/NCEP2 reanalysis and NOAA OLR datasets were provided by the NOAA/OAR/ESRL PSD, Boulder, Colorado, USA, from their Web site at URL: http://www.cdc.noaa.gov/. The OAFLUX products are obtained from the Woods Hole Oceanographic Institute through ftp://ftp.whoi.edu/pub/science/oaflux/data. Graphics have been prepared using the SAXO package of Sébastien Masson.

References

Ailikun B, Yasunari T (2001) ENSO and Asian summer monsoon: persistence and transitivity in the seasonal March. J Meteorol Soc Jpn 79:145–159

Alexander MA, Bladé I, Newman M, Lanzante JR, Lau N-C, Scott JD (2002) The atmospheric bridge: the influence of ENSO teleconnections on air–sea interaction over the global oceans. J Clim 15:2205–2231

Alory G, Wijffels S, Meyers G (2007) Observed temperature trends in the Indian Ocean over 1960–1999 and associated mechanisms. Geophys Res Lett 34:L02606. doi:10.1029/2006GL028044

Annamalai H, Liu P, Xie S-P (2005) Southwest Indian Ocean SST variability: its local effect and remote influence on Asian monsoons. J Clim 18:4150–4167

Ashok K, Guan Z, Yamagata T (2001) Influence of the Indian Ocean Dipole on the relationship between the Indian monsoon rainfall and ENSO. Geophys Res Lett 28:4499–4502

Ashok K, Guan Z, Saji NH, Yamagata T (2004) Individual and combined influences of ENSO and the Indian Ocean Dipole on the Indian summer monsoon. J Clim 17:3141–3154

Ashok K, Behera S, Rao AS, Weng HY, Yamagata T (2007) El Nino Modoki and its teleconnection. J Geophys Res 112:C11007. doi:10.1029/2006JC003798

Behera SK, Yamagata T (2001) Subtropical SST dipole events in the southern Indian Ocean. Geophys Res Lett 28:327–330

Behera SK, Krishnan R, Yamagata T (1999) Unusual ocean-atmosphere conditions in the tropical Indian Ocean during 1994. Geophys Res Lett 26:3001–3004

Buermann W, Lintner BR, Bonfils C (2004) A wintertime Arctic oscillation influence on early season Indian Ocean monsoon intensity. J Clim 18(13):2247–2269. doi:10.1175/JCLI3377.1, 2005

Carton JA, Giese BS (2008) A reanalysis of ocean climate using Simple Ocean Data Assimilation (SODA). Mon Wea Rev 136:2999–3017

Chiang JCH, Sobel AH (2002) Tropical tropospheric temperature variations caused by ENSO and their influence on the remote tropical climate. J Climate 15:2616–2631

Chiodi AM, Harrison E (2007) Mechanisms of summertime subtropical Southern Indian Ocean sea surface temperature variability: on the importance of humidity anomalies and the meridional advection of water vapor. J Clim 20:4835–4852

Clark CO, Cole JE, Webster PJ (2000) Indian Ocean SST and Indian summer rainfall: predictive relationships and their decadal variability. J Clim 13:2503–2519

Cleveland RB, Cleveland WS, McRae JE, Terpenning I (1990) A seasonal-trend decomposition procedure based on Loess (with discussion). J Off Stat 6:3–73

Dominiak S, Terray P (2005) Improvement of ENSO prediction using a linear regression model with a Southern Indian Ocean Sea surface temperature predictor. Geophys Res Lett 32:L18702. doi:10.1029/2005GL023153

Du Y, Xie S-P, Huang G, Hu K-M (2009) Role of air–sea interaction in the long persistence of El Niño-induced North Indian Ocean warming. J Clim 22:2023–2038

Ebisuzaki W (1997) A method to estimate the statistical significance of a correlation when the data are serially correlated. J Clim 10:2147–2153

Findlater I (1969) A major low-level air current near the Indian Ocean during the northern summer. Q J Roy Meteorol Soc 95:362–380

Fischer AS, Terray P, Delecluse P, Gualdi S, Guilyardi E (2005) Two independent triggers for the Indian Ocean Dipole/Zonal Mode in a coupled GCM. J Clim 18:3428–3449

Gadgil S, Vinayachandran PN, Francis PA, Gadgil S (2004) Extremes of the Indian summer monsoon rainfall, ENSO and equatorial Indian Ocean oscillation. Geophys Res Lett 31:L12213. doi:10.1029/2004GL019733

Goswami BN, Xavier Prince K (2005) ENSO control on the South Asian Monsoon through the length of the rainy season. Geophys Res Lett 32:L18717. doi:10.1029/2005GL023216

Harzallah A, Sadourny R (1997) Observed lead-lag relationships between Indian summer monsoon and some meteorological variables. Clim Dyn 13:635–648

He H, Sui C-H, Jian M, Wen Z, Lan G (2003) The evolution of tropospheric temperature field and its relationship with the onset of Asian summer monsoon. J Meteorol Soc Jpn 81(5):1201–1223

Hermes JC, Reason CJC (2005) Ocean model diagnosis of interannual coevolving SST Variability in the South Indian and South Atlantic Oceans. J Clim 18:2864–2882

Huang B, Kinter JL III (2002) Interannual variability in the tropical Indian Ocean. J Geophys Res 107:3199. doi:10.1029/2001JC001278

Izumo T, De Boyer Montégut C, Luo J-J, Behera SK, Masson S, Yamagata T (2008) The role of the Western Arabian Sea upwelling in Indian monsoon rainfall variability. J Clim 21:5603–5623

Izumo T, Vialard J, Lengaigne M, De Boyer Montegut C, Behera SK, Luo J-J, Cravatte S, Masson S, Yamagata T (2010) Influence of the state of the Indian Ocean Dipole on the following year's El Niño. Nat Geosci 3:168–172. doi:10.1038/ngeo760

Joseph PV, Pillai PV (1984) Air-sea interaction on a seasonal scale over north Indian Ocean. Part I: interannual variations of sea surface temperature and Indian summer monsoon rainfall. Mausam 35:323–330

Joseph PV, Sijikumar S (2004) Intraseasonal variability of the low-level jet stream of the Asian summer monsoon. J Clim 17:1449–1458

Joseph PV, Eischeid JK, Pyle RJ (1994) Interannual variability of the onset of the Indian summer monsoon and its association with atmospheric features, El Nino, and sea surface temperature anomalies. J Clim 7:81–105

Joseph PV, Sooraj KP, Rajan CK (2003) Conditions leading to monsoon over Kerala and associated Hadley cell. Mausam 54(1):155–164

Kalnay et al (1996) The NCEP/NCAR 40-year reanalysis project. Bull Am Meteorol Soc 77:437–471

Kanamitsu M, Ebisuzaki W, Woolen J, Potter J, Yang SK, Hnilo JJ, Fiorino M, Potter GL (2002) NCEP-DEO AMIP-II Reanalysis (R-2). Bull Am Meteorol Soc 83:1631–1643

Kawamura R, Matsuura T, Iizuka S (2001) Role of equatorially asymmetric sea surface temperature anomalies in the Indian Ocean in the Asian summer monsoon and El Niño Southern oscillation coupling. J Geophys Res 106:4681–4693

Kinter JL, Miyakoda K, Yang S (2002) Recent change in the connection from the Asian monsoon to ENSO. J Clim 15:1203–1215

Klein SA, Soden BJ, Lau N-C (1999) Remote sea surface temperature variations during ENSO: evidence for a tropical atmospheric bridge. J Clim 12:917–932

Krishnamurti TN (1971) Tropical east–west circulations during northern summer. J Atmos Sci 28:1342–1347

Krishnan R, Swapna P (2009) Significance influence of the boreal summer monsoon flow on the Indian Ocean response during dipole events. J Clim 22:5611–5634

Krishnan R, Mujumdar M, Vaidya V, Ramesh KV, Satyan V (2003) The abnormal summer monsoon of 2000. J Clim 16:1177–1194

Kug J-S, Kang I-S (2006) Interactive feedback between ENSO and the Indian Ocean. J Clim 19:1784–1801

Kug J-S, Jin F-F, An S-I (2009) Two types of El Nino events: cold tongue El Nino and warm pool El Nino. J Clim 22:1499–1515

Lau NC, Nath MJ (2000) Impact of ENSO on the variability of the Asian–Australian monsoons as simulated in GCM experiments. J Clim 13:4287–4309

Lau NC, Nath MJ (2003) Atmosphere–ocean variations in the Indo-Pacific Sector during ENSO Episodes. J Clim 16:3–20

Lau NC, Nath MJ (2004) Coupled GCM simulation of atmosphere–ocean variability associated with zonally asymmetric SST changes in the tropical Indian Ocean. J Clim 17:245–265

Li T, Wang B, Chang CP, Zhang YS (2003) A theory for the Indian Ocean Dipole-Zonal Mode. J Atmos Sci 60:2119–2135

Li T, Liu P, Fu X, Wang B, Meehl GA (2006) Tempo-spatial structures and mechanisms of the tropospheric biennial oscillation in the Indo-Pacific warm ocean regions. J Clim 19: 3070–3087

Li SL, Lu J, Huang G, Hu K (2008) Tropical Indian Ocean basin warming and East Asian summer monsoon: a multiple AGCM study. J Clim 21:6080–6088

Liebmann B, Smith CA (1996) Description of a complete (interpolated) outgoing longwave radiation dataset. Bull Am Meteorol Soc 77:1275–1277

Loschnigg J, Meehl GA, Webster PJ, Arblaster JM, Compo GP (2003) The Asian monsoon, the tropospheric biennial oscillation and the Indian Ocean dipole in the NCAR CSM. J Clim 16:2138–2158

Meehl GA, Arblaster J (2002) The tropospheric biennial oscillation and the Asian–Australian monsoon rainfall. J Clim 15:722–744

Meehl GA, Arblaster JM, Loschnigg J (2003) Coupled ocean–atmosphere dynamical processes in the tropical Indian and Pacific Oceans and the TBO. J Clim 16:2138–2158

Nicholls N (1995) All-India summer monsoon rainfall and sea surface temperatures around northern Australia and Indonesia. J Clim 8:1463–1467

Nitta T, Yamada S (1989) Recent warming of tropical sea surface temperature and its relationship to the Northern Hemisphere circulation. J Meteorol Soc Jpn 67:375–383

Ohba M, Ueda H (2007) An impact of SST anomalies in the Indian Ocean in acceleration of the El Niño to La Niña transition. J Meteorol Soc Jpn 85:335–348

Pant GB, Rupa Kumar K (1997) Climates of South Asia. Wiley, Chichester. 320 pp. ISBN 0-471-94948-5

Park H-S, Chiang JCH, Lintner BR, Zhang JG (2010) The delayed effect of major El Nino events on Indian monsoon rainfall. J Clim 23:932–946

Parthasarathy B, Munot AA, Kothawale DR (1995) All India monthly and seasonal rainfall series: 1871–1993. Theor Appl Climatol 49:217–224

Peings Y, Douville H, Terray P (2009) Extended winter Pacific North America oscillation as a precursor of the Indian summer monsoon rainfall. Geophys Res Lett 36:L11710. doi:10.1029/2009GL038453

Ramesh Kumar MR, Sankar S, Reason C (2008) An investigation into the conditions leading to monsoon onset over Kerala. Theor Appl Climatol. doi:10.1007/s00704-008-0376-y

Rao KG, Goswami BN (1988) Interannual variations of sea surface temperature over the Arabian Sea and the Indian monsoon: A new perspective. Mon Wea Rev 116:558–568

Rayner NA, Parker DE, Horton EB, Folland CK, Alexander LV, Rowell DP, Kent EC, Kaplan A (2003) Global analyses of sea surface temperature, sea ice, and night marine air temperature since the late nineteenth century. J Geophys Res 108(D14):4407. doi:10.1029/2002JD002670

Reason CJC, Allan RJ, Lindesay JA, Ansell TJ (2000) ENSO and climatic signals across the Indian Ocean basin in the global context: part I. Interannual composite patterns. Int J Climatol 20:1285–1327

Reason CJC, Rouault M, Melice J-L, Jagadeesha D (2002) Winter rainfall variability in SW South Africa and large scale ocean-atmosphere interactions. Met Atmos Phys Spec Issue Atmos Surf Interact 80(1-4):19–29

Rupa Kumar K, Krishnakumar K, Ashrit RG, Patwardhan SK, Pant GB (2002) In: Shukla PR et al (eds) Climate change and India. Tata McGraw Hill, New Delhi, pp 24–75

Sahai AK, Grimm AM, Satyan V, Pant GB (2003) Long-lead prediction of Indian summer monsoon rainfall from global SST evolution. Clim Dyn 20:855–863

Saji NH, Goswami BN, Vinayachandran PN, Yamagata TA (1999) Dipole mode in the tropical Indian Ocean. Nature 401:360–363

Schott FA, Xie SP, McCreary Jr. JP (2009) Indian Ocean circulation and climate variability. Rev Geophys 47. doi:10.1029/2007RG000245

Shukla J (1987) Interannual variability of monsoons. In: Fein JS, Stephens PL (eds) Monsoons. Wiley, Chichester, pp 399–464

Shukla J, Misra BM (1977) Relationships between sea surface temperature and wind speed over the central Arabian Sea and monsoon rainfall over India. Mon Wea Rev 105:798–1002

Soman MK, Krishnakumar K (1993) Space time evolution of meteorological features associated with the onset Indian Summer monsoon. Mon Rev 121:1177–1194

Swapna P, Krishnan R (2008) Equatorial undercurrents associated with Indian Ocean Dipole events during contrasting summer monsoons. Geophys Res Lett 35:L14S04. doi:10.1029/2008GL033430

Terray P (1994) An evaluation of climatological data in the Indian Ocean area. J Meteorol Soc Jpn 72:359–386

Terray P (1995) Space/time structure of monsoons interannual variability. J Clim 8:2595–2619

Terray P (2010) Southern Hemisphere extra-tropical forcing: a new paradigm for El Niño-Southern Oscillation. Clim Dynam (Submitted)

Terray P, Dominiak S (2005) Indian Ocean sea surface temperature and El Niño-Southern oscillation: a new perspective. J Clim 18:1351–1368

Terray P, Delecluse P, Labattu S, Terray L (2003) Sea surface temperature associations with the late Indian summer monsoon. Clim Dyn 21:593–618

Terray P, Dominiak S, Delecluse P (2005) Role of the southern Indian Ocean in the transitions of the monsoon-ENSO system during recent decades. Clim Dyn 24:169–195. doi:10.1007/s00382-004-0480-3

Terray P, Chauvin F, Douville H (2007) Impact of southeast Indian Ocean Sea Surface temperature anomalies on monsoon-ENSO-dipole variability in a coupled ocean-atmosphere model. Clim Dynam 28:553–580. doi:10.1007/s00382-006-0192-y

Wang B, Wu R, Lau K-M (2001) Interannual variability of the Asian summer monsoon: contrasts between the Indian and the Western North Pacific-East Asian monsoons. J Clim 14:4073–4090

Wang B, Wu R, Li T (2003) Atmosphere-warm ocean interaction and its impacts on Asian–Australian monsoon variation. J Clim 16:1195–1211

Wang B, Webster PJ, Teng H (2005) Antecedents and selfinduction of active-break south Asian monsoon unraveled by satellites. Geophys Res Lett 32:L04704. doi:10.1029/2004GL020996

Wang B, Webster PJ, Kikuchi K, Yasunari T, Qi Y (2006) Boreal summer quasi-monthly oscillation in the global tropics. Clim Dyn 27:661–675

Weare B (1979) A statistical study of the relationships between ocean surface temperatures and the Indian monsoon. J Atmos Sci 36:2279–2291

Webster PJ, Hoyos C (2010) Beyond the spring barrier? Nat Geosci 3:152–153. doi:10.1038/ngeo760

Webster PJ, Magana VO, Palmer TN, Shukla J, Tomas RA, Yanai M, Yasunari T (1998) Monsoons: processes, predictability and the prospects for prediction. J Geophys Res 103(C7): 14451–14510

Webster PJ, Moore AM, Loschnigg JP, Leben RR (1999) Coupled ocean-atmosphere dynamics in the Indian Ocean during 1997–1998. Nature 401:356–360

Weng H, Ashok K, Behera SK, Rao SA, Yamagata T (2007) Impacts of El Nino Modoki on dry/wet conditions in the Pacific rim during boreal summer. Clim Dyn 29:113–125. doi:10.1007/s00382-007-0234-0

Wu R, Kirtman BP, Krishnamurthy V (2008) An asymmetric mode of tropical Indian Ocean rainfall variability in boreal spring. J Geophys Res 113:D05104. doi:10.1029/2007JD009316

Xavier PK, Marzin C, Goswami BN (2007) An objective definition of the Indian summer monsoon season and a new perspective on ENSO–monsoon relationship. Q J Meteorol Soc 133:749–764

Xie S-P, Annamalai H, Schott FA, McCreary JP (2002) Structure and mechanisms of south Indian Ocean climate variability. J Clim 15:864–878

Xie S-P, Hu K, Hafner J, Du Y, Huang G, Tokinaga H (2009) Indian Ocean capacitor effect on Indo-western Pacific climate during the summer following El Niño. J Clim 22:730–747

Yamagata T, Behera SK, Luo J-J, Masson S, Jury M, Rao S (2004) Coupled ocean-atmosphere variability in the tropical Indian Ocean. In: Wang C, Xie S-P, Carton JA (eds) Earth climate: the ocean–atmosphere interaction. Geophys Monogr Ser 147. AGU, Washington, DC, pp 189–212

Yang J, Liu Q, Xie S-P, Liu Z, Wu L (2007) Impact of the Indian Ocean SST basin mode on the Asian summer monsoon. Geophys Res Lett 34:L02708. doi:10.1029/2006GL028571

Yu L, Jin X, Weller RA (2008) Multidecade global flux datasets from the objectively analyzed air–sea fluxes (OAFlux) Project: Latent and sensible heat fluxes, ocean evaporation, and related surface meteorological variables. Woods Hole Oceanographic Institution, OAFlux Project Technical Report. OA-2008-01. Woods Hole. Massachusetts, 64 pp

II.3 Results

Results from this statistical analysis suggest only a weak relationship between the seasonal ISM rainfall (*i.e.* during JJAS) and most of the SST indices (*i.e.* during their respective peaking seasons, see Fig. II.1). However, if we consider these correlations on a 'monthly' timescale, we realize that this result is statistically biased as the ISM interannual variability is significantly influenced by the timing of rainfall onset and withdrawal (in June and September): this seriously questions the validity of the conventional *seasonal* ISM rainfall index. Besides, these monthly correlation values are much more promising as they give rise to prospects of **higher predictability for the ISM onset and the amount of rainfall during the 2^{nd} part of the season** (*e.g.* in August-September), with the **Nino(-1), IOB and SEIO** indices. Results with the IOD remain weak, which suggests this index may only play a secondary role for the ISM.

In a second part, regression analyses are carried out to explore the physical roots of these predictive relationships. A parallel is established between the IOB and Nino(-1) indices on one hand, and between the Nino(0) and SEIO on the other, suggesting that both the IOB and SEIO indices are associated with different phases of ENSO in the tropical Pacific. Besides, results show that these indices are linked to **distinct local processes, occurring within the IO** from late boreal winter or early spring onwards, and able to significantly impact ISM rainfall, particularly during the late summer season. The details of these mechanisms are given in Section 4 of the paper, and provide a possible explanation from the progressive increase of ISM predictability observed from June to September.

For instance, results obtained with the Nino(-1) or IOB index illustrate how the decaying phase of El Niño causes a 'weak' early ISM season, as it tends to delay the onset of the monsoon by favouring the development of convection in priority over the adjacent north Arabian Sea during May-June. This convection then slowly propagates towards the Indian subcontinent, which generates larger ISM rainfall anomalies during the following months of July-August-September.

The SEIO index is also linked to an enhancement of convection over India during the 2^{nd} part of the ISM season. However, the mechanism is this case is not related to local processes in the north IO, but stems from fluctuations in the atmospheric moisture transport from the *south IO* towards the Indian subcontinent.

Overall, these results have interesting implications for the predictability of ISM rainfall, since these local SST indices can offer relevant ISM forecasts as early as in late boreal winter (for the SEIO and Nino(-1) indices) and early spring (for the IOB index). The SEIO and Nino(-1) indices stand out as the most promising predictors for the recent period, although the effect of Nino(-1) seems largely due to the occurrence of the strong 1982-83 and 1997-98 El Niño events (see Figs. 13 and 14 in the paper).

II.4 Perspectives

An important outcome from this work is that **ISM predictability is significantly different for the early and late ISM season, and that both ENSO and local IO SST indices give rise to prospects of higher predictability for the rainfall in August-September**. However, we need to bear in mind that these results are based on the short recent 1979-2007 period, a time-period which has benefitted from satellite coverage and hence greater reliability in observational data. It thus seems legible to question the robustness of these predictive relationships, and their validity for other time periods, before 1979. Besides, this work is based on *pre-existing* SST indices, and does not exclude the existence of other relevant ISM SST predictors in regions outside of the tropical Indo-Pacific, such as the tropical Atlantic [*Kucharski et al.*, 2007, 2008, 2009].

Overall, these various limitations have required that we examine both the spatial and temporal robustness of the statistical associations and the physical linkages of ISM-SST relationships described in this work, in a more global framework. This has been one of the motivations of the following chapter in this thesis.

Chapter III

Robustness of ISM teleconnection and precursory patterns

Contents

III.1 Introduction

This chapter attempts to reconcile in a common and more comprehensive framework some of the various conflicting results found in the literature regarding ISM-SST teleconnections, with a particular focus here on the interdecadal changes in the relationship between ISM rainfall, ENSO and the IOD.

In the literature, there is extensive observational evidence that a sudden change occurred in the climate of the tropical and North Pacific Ocean in the mid-1970s (*e.g.* [*Nitta and Yamada*, 1989; *Terray*, 1994; *Graham*, 1994; *Wu and Wang*, 2002]), which has potentially significant bearings on the analysis of ISM teleconnections. This climate shift was accompanied by major changes in the Indo-Pacific sector: including an increase in IO SSTs after 1976-77, along with notable changes in the characteristics of ENSO evolution, and the lead-lag relationship between the two [*Terray and Dominiak*, 2005]. The ENSO-monsoon relationship has also been shown to weaken around this time [*Kinter et al.*, 2002], although the causes for such weakening are still today a largely debated matter (*e.g.* [*Gershunov et al.*, 2001]).

The purpose of this work is twofold:

(i) question the time-dependence and spatial robustness of ISM predictive relationships described in **Chapter 2** for the 1979-2007 period

(ii) examine probable causes for the weakening of the ENSO-monsoon relationship observed in recent decades.

To address the first question, we have extended the previous correlation analysis in [*Boschat et al.*, 2011a] to the period before the 1976-77 climate shift (*i.e.* during 1950-1976), and examined the relationship between ISM rainfall and *global* SST (and SLP) anomalies instead of pre-defined SST indices in the Indo-Pacific region (see Fig II.1). Results are analyzed in terms of the most robust teleconnections and precursory signals for the monsoon.

Besides, the correlation between ISM rainfall averaged from June to September (JJAS), and rainfall in June-July (JJ) and August-September (AS) suggests that there is rather weak coherency of monsoon rainfall inside the summer season (0.11 correlation between JJ and AS rainfall averages, in Fig III.1). As a result, the following analyses will be carried out separately for ISM rainfall in JJ and AS.

We will see that this distinction between the 'early' and 'late' monsoon season offers a new perspective in the analysis of ISM teleconnections. In particular, it will help us understand how the ENSO-monsoon relationship can be modulated during El Niño or La Niña years, and in turn, provide a possible explanation for the apparent weakening of this relationship in recent decades.

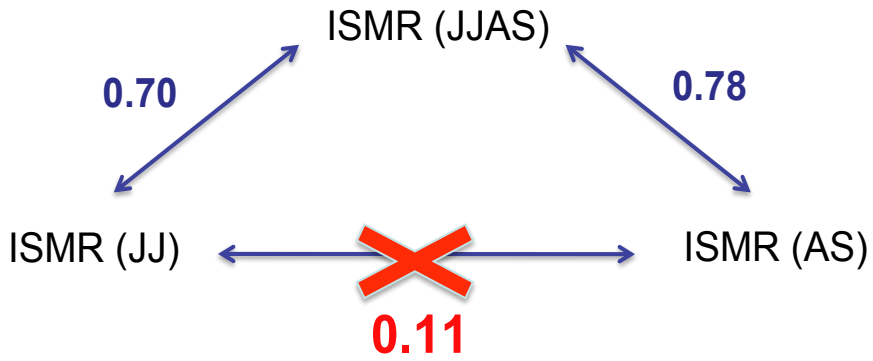

Figure III.1: Correlation between ISM rainfall in JJ, AS and JJAS over the 1871-2006 period in the HadISST1 dataset.

III.2 Article published in *Climate Dynamics*

Our results are based on statistical analyses of observations, over two periods before and after the 1976-77 climate shift (*i.e.* 1950-1976 and 1979-2007), and are detailed in the following article, published in Climate Dynamics in 2011.

Reference : Boschat G, Terray P, Masson S (2011b) Robustness of SST teleconnections and precursory patterns associated with the Indian summer monsoon *Climate Dynamics*, 1, 155, Doi 10.1007/s00382-011-1100-7.

Clim Dyn
DOI 10.1007/s00382-011-1100-7

Robustness of SST teleconnections and precursory patterns associated with the Indian summer monsoon

Ghyslaine Boschat · Pascal Terray · Sébastien Masson

Abstract This work attempts to reconcile in a common and comprehensive framework the various conflicting results found in the literature regarding Indian Summer Monsoon (ISM) rainfall-Sea Surface Temperature (SST) relationships, especially the links with El-Niño Southern Oscillation (ENSO) and the Indian Ocean Dipole (IOD). To do so, we first examine the linear relationships between ISM rainfall and global SST anomalies during 1950–1976 and 1979–2006 periods. Our results highlight the existence of significant modulations in SST teleconnections and precursory patterns between the first (June–July, JJ) and second part (August–September, AS) of the monsoon. This JJ–AS rainfall dichotomy is more pronounced after the 1976–1977 climate regime shift and tends to blur the global ISM-ENSO signal during the recent period, leading to an apparent weakening of this relationship *at the seasonal time scale*. Although ISM rainfall in JJ and AS is still strongly linked to ENSO over both periods, the lead-lag relationships between ENSO and AS Indian rainfall have changed during recent decades. Indeed, ENSO variability in the preceding boreal winter has now a significant impact on rainfall variability during the second half of ISM. To evaluate in more details the impact of this JJ-AS dichotomy on the ISM-ENSO-IOD relationships, ISM correlations are also examined separately during El Niño and La Niña years. Results indicate that the early onset of El Niño during boreal spring causes deficient monsoon rainfall in JJ. In response to weaker monsoon winds, warm SST anomalies appear in the west equatorial IO, generating favorable conditions for the development of a positive IOD in AS. Local air-sea processes triggered by the SST anomalies in the eastern node of IOD seem, in turn, to have a more active role on AS rainfall variability, as they may counteract the negative effect of El Niño on ISM rainfall via a modulation of the local Hadley circulation in the eastern IO. The JJ–AS rainfall dichotomy and its recent amplification may then result from an enhancement of these IO feedbacks during recent El Niño years. This explains why, although El Niño events are stronger, a weakening of the ISM-ENSO relationship is observed *at the seasonal scale* after 1979. Results during La Niña years are consistent with this hypothesis although local processes in the southeast IO now play a more prominent role and act to further modulate ISM rainfall in AS. Finally, our results highlight the existence of a biennal rhythm of the IOD-ENSO-ISM system during the recent period, according to which co-occurring El Niño and positive IOD events tend to be followed by a warming of the IO, a wet ISM during summer and, finally, a La Niña event during the following boreal winter.

Keywords Indian summer monsoon · Sea surface temperature · ENSO · Indian Ocean dipole

G. Boschat (✉)
LOCEAN/IPSL, Université Pierre et Marie Curie,
BP100—4 place Jussieu, 75252 Paris cedex 05, France
e-mail: gbolod@locean-ipsl.upmc.fr

P. Terray · S. Masson
LOCEAN/IPSL, CNRS/IRD/UPMC/MNHN,
Université Pierre et Marie Curie, BP100—4 place Jussieu,
75252 Paris cedex 05, France

1 Introduction

Interannual variability of the Indian Summer Monsoon (ISM) rainfall has a great impact on the economy of India and surrounding countries. Long-range forecasting of ISM rainfall is thus a matter of great concern for the people of South Asia, but is still a challenging scientific problem (Gadgil et al. 2005). To achieve this goal, a proper understanding of how

Published online: 28 May 2011

external slow boundary forcings modulate ISM variability is required. It is with this aim that many works have examined the links between ISM rainfall and various modes of variability in the Indo-Pacific region, since the seminal works of Blanford (1884) and Walker (1924).

In most of these past studies, a strong statistical relationship has been observed between ISM rainfall and El Niño-Southern Oscillation (ENSO) (Rasmusson and Carpenter 1983; Webster and Yang 1992; Shukla 1987; Webster et al. 1998; Wang 2006). Although ENSO accounts for only about 30% of ISM variability (see the correlations in Table 2 for further details), it has been shown that El Niño (La Niña) events tend to favor deficit (excess) ISM rainfall (Shukla and Paolino 1983; Ju and Slingo 1995). However, the relationship between ENSO and ISM is complex and not systematic (Krishna Kumar et al. 1999, 2006; Kinter et al. 2002; Annamalai and Liu 2005; Kucharski et al. 2007, 2008; Wang et al. 2008). As a notable example, the 1997–1998 El Niño event, despite its intensity, produced only marginal rainfall anomalies over India, while the much weaker 2002 El Niño was associated with a very severe drought (see Fig. 1; Slingo and Annamalai 2000; Gadgil et al. 2007). In addition, it has been noticed that ISM variability during recent decades may be more significantly influenced by the decaying phase of El Niño and the warming of the Indian Ocean (IO) which follows El Niño events in the late boreal winter and spring (Yang et al. 2007; Du et al. 2009; Park et al. 2010; Boschat et al. 2010). As an illustration, ISM rainfall was above normal in 1973, 1983 and 1988 following the El Niño events of 1972–1973, 1982–1983 and 1986–1987 (see Fig. 1). In other words, the links between ENSO and ISM are not yet properly understood, particularly in the context of global warming (Gershunov et al. 2000; Ashrit et al. 2003; Annamalai et al. 2007; Kucharski et al. 2007, 2008, 2009; Abram et al. 2008; Cai et al. 2009a).

Faced with observations of a recent weakening of the ISM–ENSO relationship, more and more studies have focused on the role played by the IO on ISM variability (Ashok et al. 2001, 2004; Gadgil et al. 2004, 2005, 2007; Krishnan et al. 2003; Krishnan and Swapna 2009; Clark et al. 2000; Terray et al. 2003, 2005, 2007; Yang et al. 2007; Izumo et al. 2008; Park et al. 2010; Boschat et al. 2010). Although Sea Surface Temperature (SST) anomalies over the equatorial IO are not statistically associated with ISM rainfall (Gadgil et al. 2004, 2005, 2007; Ihara et al. 2007), a lot of attention has been paid to the Indian Ocean Dipole (IOD) over the years, with debate regarding its existence as an intrinsic mode of IO variability, its dependence with ENSO (Chang et al. 2006), as well as its relationship with ISM (Ashok et al. 2001, 2004; Gadgil et al. 2004, 2005, 2007; Loschnigg et al. 2003; Terray et al. 2005; Kulkarni et al. 2007; Drbohlav et al. 2007; Hong et al. 2008). However, even the most recent studies have obtained quite contradictory results on this subject. Indeed, while some authors, like Ashok et al. (2004) or Krishnan and Swapna (2009) suggest the existence of a positive relationship between positive IOD events and strong ISMs (as in the years 1961 and 1994, see Fig. 1), others insist on the fact that the IOD-ISM relationship is closely tied with the Tropical Biennial Oscillation (TBO; Meehl and Arblaster 2002, Meehl et al. 2003; Loschnigg et al. 2003; Terray et al. 2005; Drbohlav et al. 2007; Webster and Hoyos 2010). In this scenario, positive IOD events are associated with a deficient monsoon during the current year, but the warm SST anomalies associated with these positive IOD events may contribute to the development of a stronger than normal monsoon during the next summer. The years 1982–1983 and 1987–1988 are good examples of this biennial rhythm (Fig. 1). However, as of today, the impact of IOD events, co-occurring with El Niño development in the Pacific, is still not well understood. For

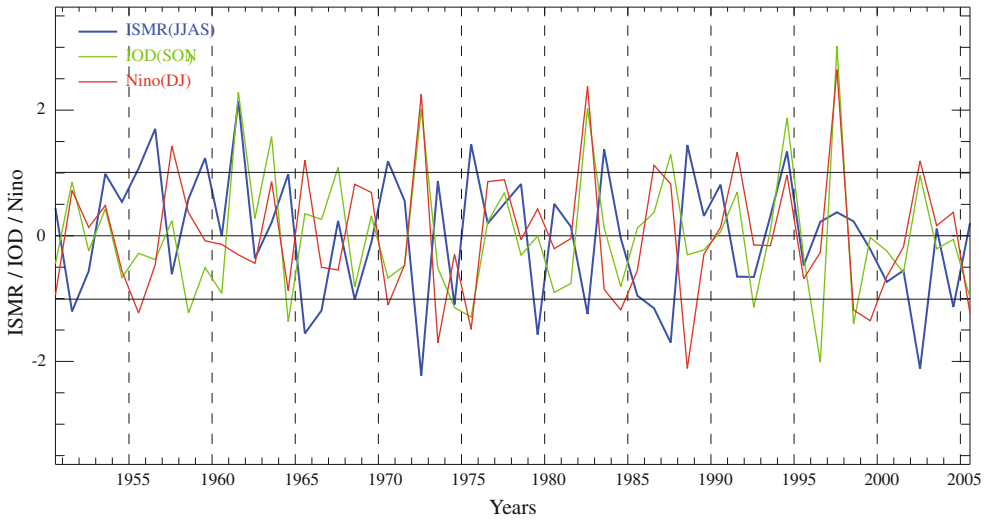

Fig. 1 Standardized time series of ISM rainfall in JJAS (*blue curve*), IOD in SON (*green curve*) and Niño 3.4 in DJ (*red curve*) during 1950–2006. The one standard deviation line (in *black*) is also added to this figure as it helps identify the extreme years

instance, the two strongest El Niño events of the last century, in 1982–1983 and 1997–1998, were both associated with IOD events, but ISM rainfall was deficient in 1982 and above normal in 1997 (Fig. 1). Therefore, an understanding of the role of IOD events on the ISM is also critical for improving ISM rainfall prediction (Gadgil et al. 2004, 2005, 2007).

Meanwhile, there have also been suggestions of significant extratropical influence on ISM variability, whether it be from the North Pacific (Peings et al. 2009), the North and South Atlantic (Srivastava et al. 2002; Kucharski et al. 2007, 2008 and 2009; Rajeevan and Sridhar 2008) or the South IO (Terray et al. 2003, 2005, 2007). As an illustration, the Indian Ocean Subtropical Dipole (IOSD) mode (Behera and Yamagata 2001) has been shown to play a significant role in influencing ISM, IOD and ENSO (Terray et al. 2005, 2007; Fischer et al. 2005; Terray 2010; Yoo et al. 2010), particularly after the so-called 1976–1977 climate shift (Terray and Dominiak 2005). This climate shift refers to the alteration of the North Pacific SSTs associated with a deepening of the Aleutian low pressure system after 1977 (Nitta and Yamada 1989). SSTs across the tropics have consistently risen since 1976–1977, particularly in the IO (Terray 1994), accompanied by notable changes in ENSO characteristics (Wang 1995). The ENSO-ISM relationship has also been shown to weaken around this time (Kinter et al. 2002), which calls to question the potential impact of this climate shift on the teleconnection between ISM and IO SSTs.

Altogether, these recent studies have thus suggested the existence of significant precursory SST signals in the tropical and extra-tropical regions before the ISM onset (Boschat et al. 2010). Nevertheless, we need to bear in mind that a majority of these works have focused on a recent time-period, e.g. the period from the late 1970s onwards, which has benefitted from satellite coverage, and, hence, greater reliability in observational data. Therefore, can we really be certain of the robustness of these precursory signals and their validity for other time periods? This question is particularly relevant since ENSO precursors have already been shown to change significantly following the 1976–1977 climate shift (Wang 1995; Terray and Dominiak 2005). In the context of a weakened ISM-ENSO relationship, it thus seems legitimate to ask ourselves whether ISM precursors have changed in a similar way during the recent period. Besides, a closer inspection of their mutual interaction could also eventually lead to a better ISM seasonal prediction. Note that these issues are particularly at stake, after the failure of the Indian Meteorological Department or international centres operational forecasts for the recent severe droughts of 2002, 2004 and 2009 (Gadgil et al. 2005; Rajeevan et al. 2006; Francis and Gadgil 2010).

Overall, the purpose of the present study is thus to question the time-dependence and spatial robustness of previous findings, as far as ISM is concerned. Besides, more emphasis must also be given to the association between global SST patterns and ISM rainfall inside of the set of El Niño (or La Niña) events in order to examine probable causes for the collapse of the ISM-ENSO relationship during recent decades.

The paper is organized as follows: the datasets used are described in Sect. 2. Section 3 examines statistical relationships with ISM over the 1950–1976 and 1979–2006 periods, based on correlation analyses between ISM rainfall and various SST indices. These correlation analyses are then extended in Sect. 4, in order to assess the robustness of global ISM teleconnection and precursory patterns, before and after the 1976–1977 climate shift. Finally, Sect. 5 aims to explore the association between these global SST patterns and ISM rainfall *within* the sets of El Niño and La Niña years. All the results are then summarized and discussed in Sect. 6.

2 Data and methods

In this study, we use the ISM rainfall data derived from the rain gauge in situ observations (Parthasarathy et al. 1995). This dataset is updated routinely by the Indian Institute of Tropical Meteorology and consists of an area-weighted average of 306 rain gauges distributed across India. The ISM rainfall time series is computed over the whole June to September (JJAS) season, as well as separately during the early part in June–July (JJ) and later part of the season in August–September (AS), following the results of Boschat et al. (2010).

To examine the SST anomalies associated with ISM variability, our analysis makes use of the Hadley Centre sea ice and sea surface temperature dataset (HadISST1.1) available from 1871 to 2007 (Rayner et al. 2003). To examine the associated atmospheric patterns, we also use Sea Level Pressure (SLP) time series from the monthly Hadley Center analyses, available from 1850 to 2005 (Allan and Ansell 2006). Note that we have intentionally not used any reanalysis product in our study, as data assimilation systems have their limits due to changes in the assimilated data stream in the reanalysis (i.e. with the introduction of satellite data after 1979). This would certainly introduce some biases in our comparison of the ISM precursory signals before and after the climate shift observed in the late 1970s (Kinter et al. 2004). Note, however, that the Hadley center SST and SLP datasets may also have problems and flaws, but the results shown here are reproducible with the other reanalyses currently available (Hurrell and Trenberth 1999).

Besides, the analysis of long-term SST time series has shown that the IO has undergone a significant secular variation associated with a 0.3° or 0.5°C shift to a warmer state during the 20th century (Nitta and Yamada 1989; Terray 1994; Clark et al. 2000; Alory et al. 2007). In order to remove this global warming effect from the SST and SLP timeseries, a preprocessing step is applied to the full period of each dataset. We use the STL additive scheme (Seasonal-Trend decomposition procedure based on Loess), developed by Cleveland et al. (1990) for this purpose, as it allows us to extract the interannual signal from the potentially noisy and non-stationary SST and SLP observations. Interannual anomalies are then defined as deviations from a (non-linear) long-term trend and a "local" annual cycle estimated by the STL scheme (for further detail see Terray 2010). Note that our results are robust and remain unchanged by the use of different parameters in the STL filtering procedure.

Once the preprocessing step completed, this study then focuses more specifically on two periods: 1950–1976 and 1979–2006. However, results shown here are not sensitive to the choice of this break point year around the 1976–1977 climate shift (not shown). Simple correlation and regression analyses are used to assess the associations between ISM rainfall and SST modes during the two periods. The significance of the cross-correlation coefficients is assessed by the phase-scrambling bootstrap test described in Ebisuzaki (1997).

3 Robustness of predictive relationships between ISM rainfall and key SST indices in the Indo-Pacific region

In this section, we wish to test the robustness of statistical relationships, which have been established in Boschat et al. (2010), between ISM rainfall and various modes of SST variability in the Indo-Pacific region during the recent decades (1979–2007). The aim is thus to extend this correlation anlaysis to the period before the 1976–1977 climate shift. Before doing so, the variability of ISM rainfall is examined and compared during 1950–1976 and 1979–2006, in order to justify the choice of these two time periods in the following analyses.

Table 1 summarizes the spatio-temporal definitions of the key-SST indices used here to represent various modes of variability over the Indo-Pacific region, as well as the references in the literature which have first proposed to use these "classical" time series. Note that these indices are computed from the detrended SST dataset over the two time periods. In light of previous findings, we have chosen to use the Niño 3.4 index to represent ENSO. Nevertheless, results in this section remain unchanged by the use of the Niño 3, Niño 4 or Niño 3.4 timeseries, which suggests that the spatial pattern of SST in the tropical Pacific does not significantly affect the ISM-ENSO teleconnection, in line with the results of Rajeevan and Pai (2007).

3.1 ISM rainfall time series during 1950–1976 and 1979–2006

In order to compare the variability of ISM rainfall during 1950–1976 and 1979–2006, standardized rainfall time series for the full ISM (JJAS), as well as the first (JJ) and second (AS) parts of ISM are shown in Figs. 2a and b. In these figures, the dashed horizontal lines designate the ± one standard deviation and help to identify anomalous ISM years during each period. The phase relationship with ENSO is also examined by simple comparison with the JJAS Niño 3.4 standardized SST time series (dashed black curve in Fig. 2).

Table 1 Description of the different indices used in this study as well as their first references in the literature

Index name	Reference	Geographical domain	Peaking season
Niño	Niño 3.4 index	170°W–120°W 5°N–5°S	December–January (DJ)
IOB	Indian Ocean basin mode (Yang et al. 2007)	40°–110°E 20°S–20°N	April–May (AM)
SEIO	South East Indian Ocean index (Terray and Dominiak 2005)	90°–122°E 5°–45°S	February–March (FM)
IOD	Indian Ocean dipole mode (Saji et al. 1999)	West box (60°E–80°E 10°N–10°S) 10°N–10°S) −East box (90°E–110°E 10°S–0°S)	September to November (SON)

Note that these key indices are computed from the detrended SST dataset separately over each time period (1950–1976 and 1979–2006)

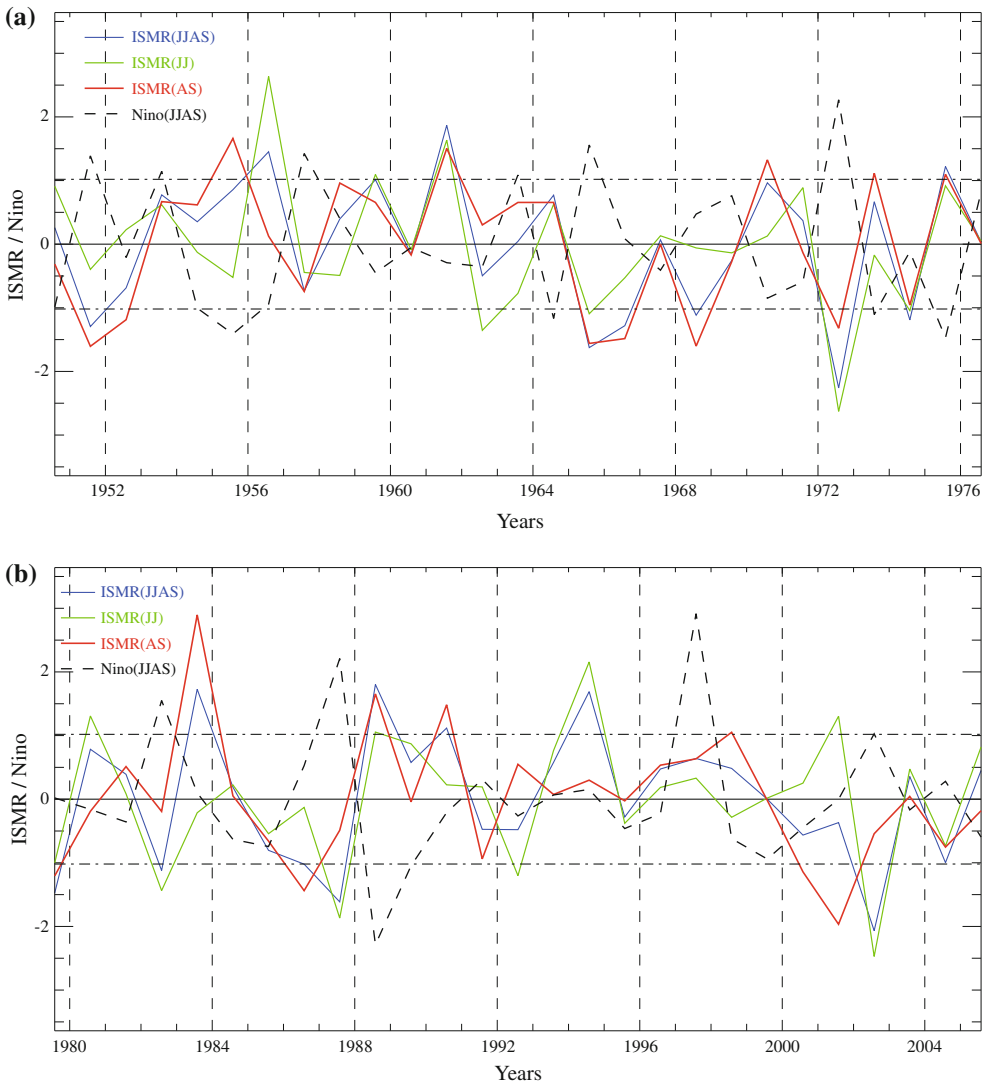

Fig. 2 Standardized time series of ISM rainfall in JJAS (*blue curve*), JJ (*green curve*) and AS (*red curve*) superimposed with the standardized Niño3.4 time series in JJAS (*black dotted curve*) during **a** 1950–1976 and **b** 1979–2006. The one standard deviation line (in *black*) is also added to this figure as it helps identify the extreme years

During 1950–1976, ISM rainfall anomalies show a rather strong coherency inside the monsoon season, and rainfall variability in JJAS, AS and JJ are highly correlated with a cross correlation of 0.78 between JJAS and JJ and of 0.88 between JJAS and AS rainfall time series (Fig. 2a). Indeed, during extreme monsoon years, the positive and negative rainfall peaks in JJAS coincide well with maxima and minima of rainfall in both JJ and AS and this is particularly true for the drought years (e.g. 1965, 1972 and 1974). Another remarkable characteristic of this period is the quite steady and out-of-phase relationship between ISM rainfall and the JJAS Niño3.4 SST time series with a correlation of −0.64 significant at the 99% confidence level. Many wet ISMs coincide with La Niña events in JJAS (e.g. 1956, 1975), and most dry ISMs with El Niño conditions (e.g. 1951, 1957, 1965, 1972) during this period. Note however that there are exceptions to this rule, as in 1961. This wet ISM year, which is the strongest monsoon on record for the full 1950–2006 period (see Fig. 1), is also identified as one of the strongest IOD episodes and more specifically one of the two positive IOD events (with 1967), which occurred in the absence of an El Niño before the 1976–1977 climate shift (see Fig. 1; Fischer et al. 2005). The 1967 IOD event, however, is not associated with any significant ISM rainfall anomalies in JJAS, JJ or AS (Figs. 1 and 2a).

The evolution of ISM rainfall seems to be substantially different during the 1979–2006 period, with both a stronger variability within the ISM season and a weaker synchronous relationship with ENSO (Fig. 2b). Unlike what is observed before 1976, extreme ISM years generally coincide with a peak in ISM rainfall either in JJ or AS, but rarely with both at the same time. Interestingly, severe droughts seem to be mostly associated with rainfall anomalies in JJ (e.g. 1982, 1987, 2002) whereas 3 of the 4 strong ISMs are due to highly positive rainfall anomalies during AS (e.g. 1983, 1988, 1990). Consistent with this weaker persistence of rainfall anomalies, the JJ and AS

rainfall time series are now generally decorrelated with an insignificant correlation of 0.11, as opposed to the higher significant value of 0.38 obtained from the earlier period. The rainfall evolution has sometimes even conflicting tendencies within the summer season as in 1992, 1998 and 2001: in these cases, JJAS ISM rainfall anomaly simply results from a compensation of opposite rainfall tendencies during JJ and AS.

In line with this apparent erratic behavior, the relationship between JJAS ISM rainfall and Niño 3.4 SST time series has also become quite ambiguous (correlation of −0.40) and although both time series remain out-of-phase during the beginning of the period, a more chaotic ISM-ENSO relationship seems to set in by the early 90s (Fig. 2b). Indeed, although many dry ISM events still coincide with El Niño conditions in JJAS (1982, 1987 and 2002), the 1997 El Niño, on the other hand, is associated with *slightly above normal* ISM rainfall, while other recent drought years like 2004 are not even characterized by any warming in the Pacific during summer (Fig. 2b). Similarly, the wet ISM years of 1983 and 1994 are not linked to La Niña episodes and it seems that wet ISMs are generally more associated with the decaying phase of El Niño events as in 1983, 1988 and 1998. Note that in these cases, the positive rainfall anomalies are also restricted to the second half of ISM (e.g AS).

Links with IOD events may also be suggested here, reflecting the complexity of recent ISM-ENSO-IOD relationships. Indeed, the 1994 ISM stands out both as one of the strongest wet ISM year of the recent decades and a strong positive IOD, which occurs independently from ENSO during boreal summer and fall (see Figs. 1 and 2b; Fischer et al. 2005; Drbohlav et al. 2007). However, this 1994 IOD event is associated with rainfall anomalies in JJ rather than AS as we would expect if IOD is influencing the monsoon. The positive rainfall anomalies observed in the boreal summer of the 1997 El Niño event have also been linked to the occurrence in fall of a positive IOD event (Slingo and Annamalai 2000; Ashok et al. 2001). However, El Niño and IOD events also co-occured in 1982, 1987 and 2002, but all of these years are marked by highly deficient rainfall over India (Fig. 2a).

Overall, the analysis of these ISM rainfall time series thus suggests a potentially different behavior of ISM rainfall during the two time periods,which can justify a separate examination of the pre-1976 and post-1976 periods in the following sections. It has also suggested a more erratic behavior of rainfall variability within the JJAS season during recent decades, which is consistent with a weaker ISM-ENSO relationship despite the fact that 1982–1983 and 1997–1998 were two of the strongest events in the 20th century. The possible causes for this recent collapse of the synchronous ISM-ENSO relationship will be discussed in Sect. 5.

3.2 Robustness of predictive relationships

In this section, we examine the epochal variations in the linear relationships of ISM rainfall with modes of inter-annual variability over the Indo-Pacific region. Table 2 shows results from a correlation analysis between ISM rainfall indices (in JJAS, JJ and AS) and key SST indices for the 1950–1976 and 1979–2006 periods. To facilitate the comparison with previous findings, we use the same spatio-temporal definitions as in Boschat et al. (2010) for the selected SST indices (see Table 1). Among these time

Table 2 Cross-correlations between the key SST indices (defined in Table 1) and the ISM rainfall (ISMR) averaged in seasonal (JJAS) and bimonthly mean (JJ and AS), for both the 1950–1976 (*blue values*) and 1979–2006 (*red values*) time periods

	ISMR (JJAS)		ISMR (JJ)		ISMR (AS)	
IOB	0.24	0.19	− 0.01	− 0.15	0.36*	0.45**
Niño(− 1)	0.20	0.18	− 0.03	− 0.20	0.32	0.50**
SEIO	0.41**	0.39**	0.16	0.06	0.49**	0.54***
Niño(0)	− 0.64***	− 0.40**	− 0.47**	− 0.30	− 0.59***	− 0.30
IOD(0)	− 0.22	− 0.16	− 0.24	− 0.16	− 0.14	− 0.07
IOD(0)—West box	− 0.45**	− 0.18	− 0.47**	− 0.34*	− 0.30	0.08
IOD(0)—East box	− 0.15	0.10	− 0.14	− 0.01	− 0.11	0.17
IOD(− 1)	− 0.04	0.24	− 0.15	− 0.02	0.06	0.38**
IOD(− 1)—West box	0.12	0.37*	0.02	0.06	0.16	0.51**
IOD(− 1)—East box	0.19	− 0.07	0.27	0.07	0.08	− 0.17

* $P < 0.1$; ** $P < 0.05$; *** $P < 0.005$

The coefficients exceeding the 10%, 5% and 5‰ confidence levels according to the phase-scrambling bootstrap test of Ebisuzaki (1997) with 999 samples are followed by one asterisks (*), two asterisks (**) and three asterisks (***), respectively

series, four precede ISM and may thus have a potential for ISM rainfall long-range forecasting: the IOD(−1) index defined during the previous fall in September–October–November (SON), the Niño(−1) during the previous winter in December–January (DJ), the SEIO in February–March (FM) and the IOB in April–May (AM). Two of these indices are also considered after the ISM in order to test the biennial nature of their relationships with ISM rainfall: the IOD(0) defined during the following fall (in SON), and the Niño(0) during the following winter (in DJ). These two time series are plotted in Fig. 1. The eastern and western nodes of IOD have also been taken into account in this analysis. This will provide a clearer understanding of the possible linkages, if any, between IOD and ISM variability in the framework of the TBO.

To begin with, results on a seasonal scale (e.g. JJAS) show that ISM rainfall is most significantly correlated with SEIO and Niño(0) time series during both time periods (Table 2). However, correlation values are generally weaker after 1979, and the most important decrease is recorded with the Niño(0) index, from −0.64 during 1950–1976 to −0.40 during 1979–2006: a result in line with recent studies (Kinter et al. 2002; Kucharski et al. 2007 among others). In contrast, the SEIO index is strongly correlated with ISM rainfall in the following summer during *both* periods. Note however that this significant SEIO-ISM relationship is exclusively restricted to the AS season, which is consistent with the higher predictability of the late ISM season already suggested by Terray et al. (2003), Park et al. (2010) and Boschat et al. (2010).

Meanwhile, our analysis also highlights the complexity of the ISM-ENSO relationship if we look more carefully at the relationships *within* the ISM (e.g. in JJ and AS). Before 1976–1977, ISM rainfall in JJAS, JJ or AS is strongly associated with Niño(0), but the relationships with Niño(−1) are always insignificant. This suggests that a weak (strong) ISM occurs during the developing year of El Niño (La Niña), but is not related to the previous ENSO state. After 1976–1977, the association of ISM rainfall in JJ or AS with Niño(0) becomes insignificant and the correlation with Niño(−1) reaches a significant maximum of 0.50 for the AS rainfall time series. These results thus suggest a 'phase shift' rather than a weakening of the ENSO-ISM relationship during recent decades, since AS rainfall is now significantly related to the state of the Pacific in the previous boreal winter. The statistical importance of the Niño(−1) index after 1979 was already noted by Boschat et al. (2010) and may reflect the influence of the strong 1982–1983 and 1997–1998 El Niño events on the recent ISM rainfall variability. Besides, our analysis also confirms the parallel evolution of the Niño(−1) and IOB indices evoked in previous studies (Yang et al. 2007; Du et al. 2009; Boschat et al. 2010), as both indices are marked by comparable correlation values with ISM rainfall in AS during both periods. Since the IOB SSTs act largely in response to ENSO, the IOB-ISM rainfall correlations in Table 2 are entirely consistent with the speculation of a phase shift rather than a weakening of the ENSO-ISM relationship after 1976.

On the other hand, results with the IOD index reflect rather well the conflicting theories found in the literature on this subject. Extreme IOD events occurred repeatedly in the more recent periods (see Fig. 1), and have been suggested as a major cause for the weakening of the "historical" ENSO-ISM relationship (Ashok et al. 2001, 2004, Abram et al. 2008). However, correlations with the IOD(0) index are systematically weak over the two periods, as much on a seasonal scale as within the season, and the values obtained are always negative. Indeed, it has been argued that when a positive IOD event occurs, both poles of the IOD contribute to the surplus rainfall over India (Ashok et al. 2001, 2004). But, the results in Table 2 suggest only a significant but reversed contribution from the western node of the IOD during early boreal summer (correlation of −0.47 with JJ rainfall before 1979 and −0.34 after), while correlation with the eastern node of IOD is near zero and insignificant for all the rainfall indices, and fails to reproduce a clear out-of-phase relationship with the western node. These results suggest that the ENSO signal dominates the SST variability over the IO, which is in line with previous analyses (Gadgil et al. 2004, 2005; Ihara et al. 2007). However, this does not rule out the possibility that the IOD contributes to neutralize the ENSO-induced anomalous subsidence over India when IOD and El Niño co-occur (see Sect. 5).

Meanwhile, results with the IOD(−1) index are in better agreement with its possible role in the framework of the TBO, but only for the recent period. The moderate, but significant, 0.38 correlation obtained between IOD(−1) and AS rainfall after 1979 is almost exclusively due to the western node of the IOD (0.51 correlation). However, no definite conclusion can be drawn at this point regarding the statistical robustness of this IOD(−1)-ISM relationship, nor its underlying causes. Indeed, correlation with the IOD(−1) index is weak before 1979, throughout the ISM season and with both nodes, implying again that statistics after 1979 may be biased and linked to the strong El Niño/IOD events of this period. As a result, we still need to investigate whether the western node of IOD actually plays a significant precursory role in the variability of the following ISM, or whether these anomalies are merely part of the slow IO warming which occurs after an El Niño and are thus intrinsically linked to the IOB and Niño(−1) indices (Drbohlav et al. 2007; Sooraj et al. 2009; Hong et al. 2010). The parallel evolution of the correlations of AS rainfall with the IOB, Niño(−1) and the western node of the IOD(−1) in Table 2 supports this last hypothesis. Note,

besides, that this strengthening of the ISM in the following year concerns essentially the second part of the season (e.g. AS, see Table 2), which once again points to a higher predictability of the AS rainfall. This is the case in 1973, 1983, 1988 and 1998, when AS rainfall is highly positive following the co-occurrence of IOD and El Niño events in 1972, 1982, 1987 and 1997 (see Figs. 1, 2).

Altogether, results from this section suggest a recent 'phase shift' in the ISM-ENSO relationship rather than a weakening, with an apparently stronger influence of the inter-related Niño(−1), IOB and IOD(−1) indices on the ISM after 1979, especially in AS. Table 2 also highlights the increasing significance of IO precursory signals after 1979, and in particular of the IOD(−1), IOB and SEIO indices.

4 Global teleconnections and precursory SST signals associated with ISM rainfall during 1950–1976 and 1979–2006

In an attempt to examine more objectively the statistical relationships with ISM rainfall, a correlation analysis is now carried out with *global* SST and SLP anomalies rather than *pre-defined* SST indices in the Indo-Pacific region. In light of previous results, these correlations are computed separately with ISM rainfall in JJ (Figs. 3 and 4) and AS (Figs. 5 and 6). The SST and SLP teleconnections and precursory patterns associated with each part of the monsoon season are then compared over the 1950–1976 and 1979–2006 periods.

4.1 Correlations with ISM rainfall in JJ

Overall, results for the JJ rainfall time series stress the importance of ENSO. Indeed, Figs. 3 and 4 indicate that, during both time periods, deficient (excess) JJ rainfall is significantly linked to the development of El Niño (La Niña) conditions in the tropical Pacific Ocean, where warm (cold) SST anomalies appear in boreal spring and consistently grow until the end of the year, in relation to a dry (wet) JJ season over India. Significant SLP anomalies are also observed over the tropical Indo-Pacific region during boreal summer, as part of the Southern Oscillation pattern, and illustrate the influence of El Niño (La Niña) on ISM through the eastward (westward) shift of the Walker circulation (Fig. 4). There are also suggestions that ISM rainfall in JJ may be linked to an *earlier* onset of ENSO during both periods, as significant SST anomalies appear as early as in FM in the tropical Pacific (Fig. 3).

Although this ISM-ENSO relationship in JJ seems quite robust over both time periods, the characteristics of the ENSO signal displayed in Figs. 3 and 4 seem to differ from one period to another. First, the ENSO-related SST and SLP anomalies are generally weaker during 1979–2006, in line with the theory of a weakening of the ISM-ENSO relationship in recent decades. Note also that the negative SLP anomalies over the north IO develop in JJ, one season after the positive SLP anomalies over the tropical Pacific Ocean during the recent period, whereas both poles of this tropical SLP oscillation appear simultaneously in AM during the earlier period. Finally, another noteworthy characteristic of the recent ISM-ENSO relationship, as far as JJ rainfall is concerned, is that SST anomalies appear in a rather central region of the tropical Pacific, recalling suggestions of a link between recent ISM rainfall variability and 'Modoki-type' El Niños (Ratnam et al. 2010). However, this cold central Pacific pattern is only flanked by warm anomalies on its western side. This central ENSO signal then propagates eastwards, in contrast with the more westward propagation observed during the 1950–1976 period (Fedorov and Philander 2000, 2001; Wang and An 2002; Trenberth et al. 2002; McPhaden and Zhang 2009).

In spite of these altered characteristics, the ISM-ENSO teleconnection stands out as a dominant feature during the first part of the ISM season for both periods. On the other hand, there are no hints of any IOD-related SST or SLP patterns in the boreal fall either preceding or following the ISM season during both periods (Figs. 3 and 4).

Focusing now on SST precursory patterns before ISM onset, there are suggestions of significant relationships with SST anomalies between northern Australia and Indonesia (Nicholls 1995) or with an anomalous SST dipole in the North Atlantic (Srivastava et al. 2002) persisting from ON to FM during 1950–1976 (Fig. 3). But, these ISM precursory SST signals are generally weak and scarcely significant after 1979. The implications of these results in terms of JJ rainfall predictability are thus rather pessimistic. However, a more robust SST signal is found in the North Pacific Ocean during boreal spring (Peings et al. 2009). These SST anomalies are collocated with significant SLP anomalies in the form of a North Pacific Oscillation (NPO) SLP pattern from DJ to AM during 1950–1976 and in AM after 1979 (Fig. 4). The NPO is a well-known precursor of ENSO, and may thus influence ISM rainfall variability via its forcing on ENSO. In Figs. 3 and 4, the anomalous SST and SLP patterns are consistent with the "seasonal footprinting mechanism" which was proposed to explain this NPO-ENSO teleconnection (Vimont et al. 2003, 2009; Alexander et al. 2010). In this scenario, the positive (negative) SLP anomalies forming the southern node of the NPO pattern (Fig. 4) are associated with an increase (reduction) of the trade winds in the subtropical North Pacific (not shown); this imparts a cold (warm) local SST 'footprint' (Fig. 3) which modulates the wind variability in the equatorial western Pacific, and leads to the

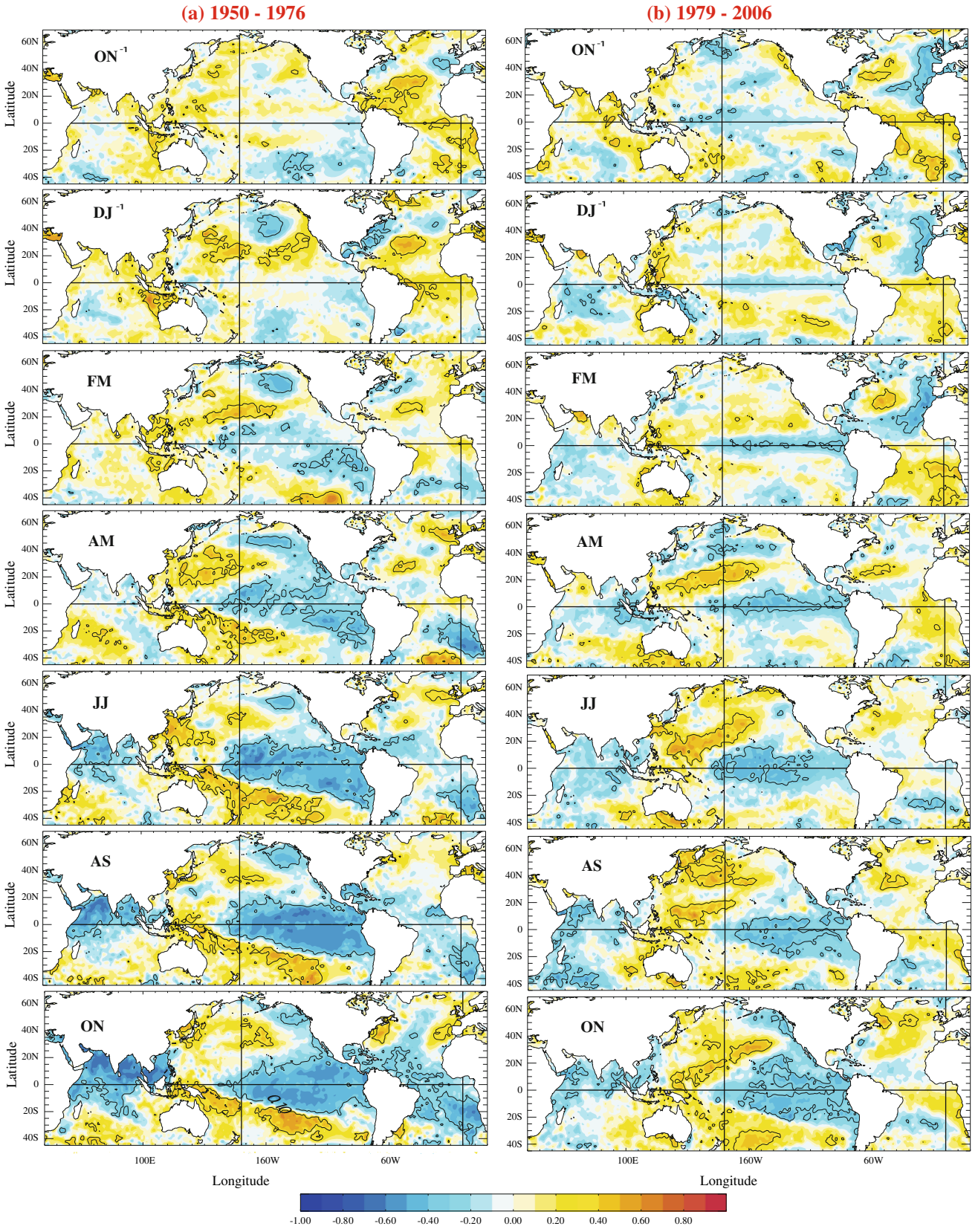

Fig. 3 Global correlation between **ISM rainfall in JJ** and bimonthly **SST** anomalies from the boreal fall preceding (ON^{-1}) to that following (ON) the ISM season during **a** 1950–1976 and **b** 1979–2006 time periods. Correlation coefficients that are above the 90% confidence level estimated with a phase-scrambling bootstrap test with 999 samples are encircled

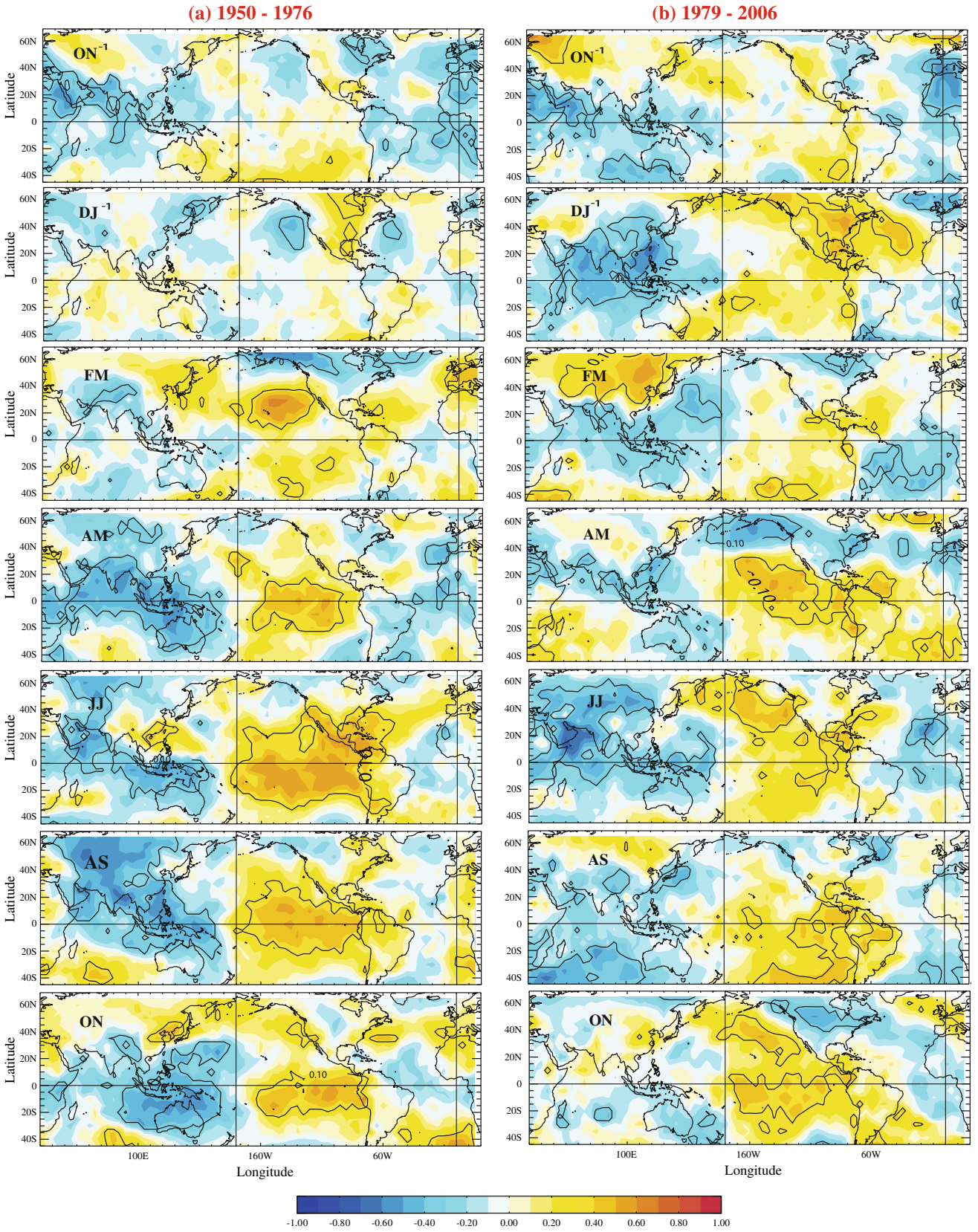

Fig. 4 Global correlation between **ISM rainfall in JJ** and bimonthly **SLP** anomalies from the boreal fall preceding (ON^{-1}) to that following (ON) the ISM season during **a** 1950–1976 and **b** 1979–2006 time periods. Correlation coefficients that are above the 90% confidence level estimated with a phase-scrambling bootstrap test with 999 samples are encircled

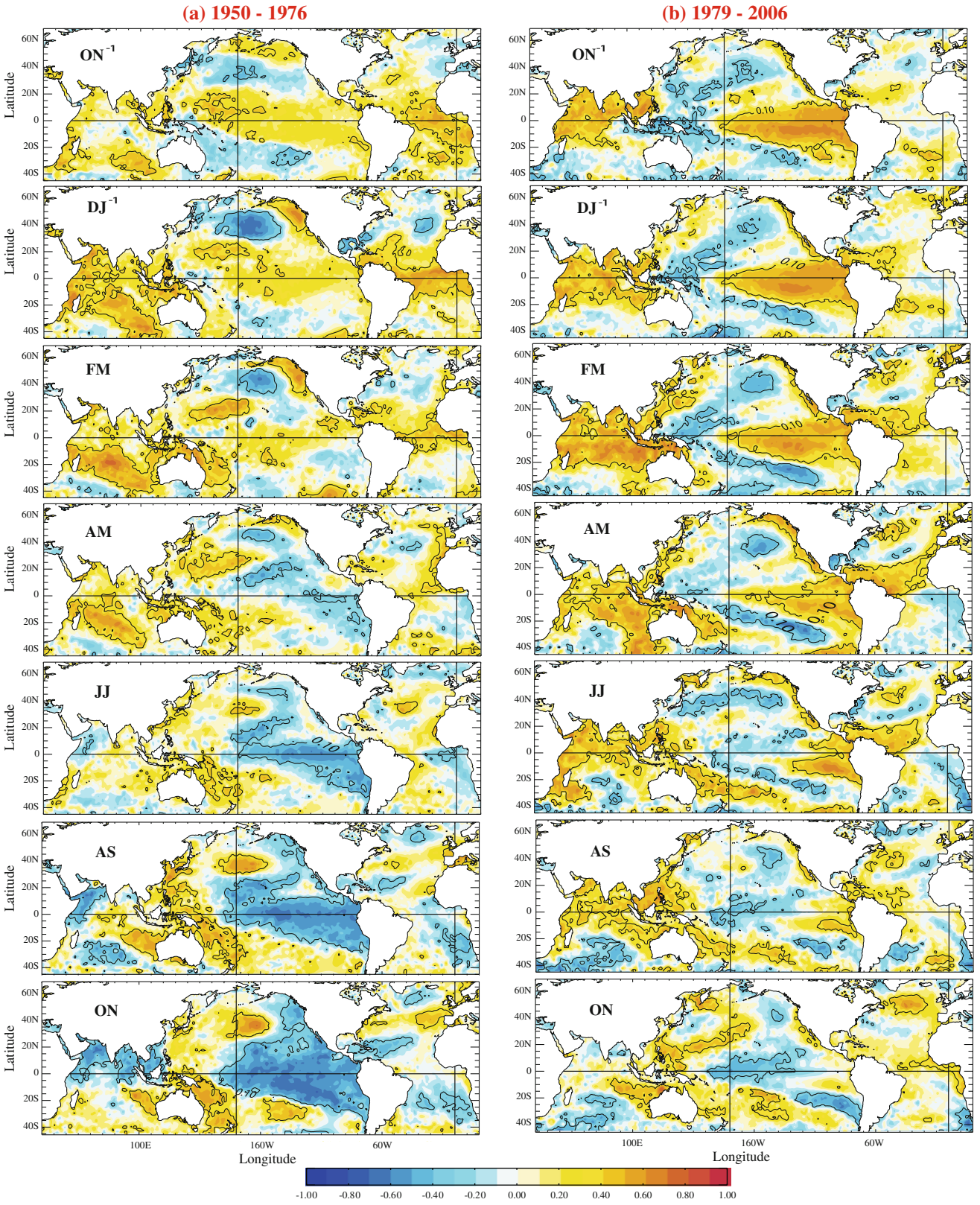

Fig. 5 Global correlation between **ISM rainfall in AS** and bimonthly **SST** anomalies from the boreal fall preceding (ON^{-1}) to that following (ON) the ISM season during **a** 1950–1976 and **b** 1979–2006 time periods. Correlation coefficients that are above the 90% confidence level estimated with a phase-scrambling bootstrap test with 999 samples are encircled

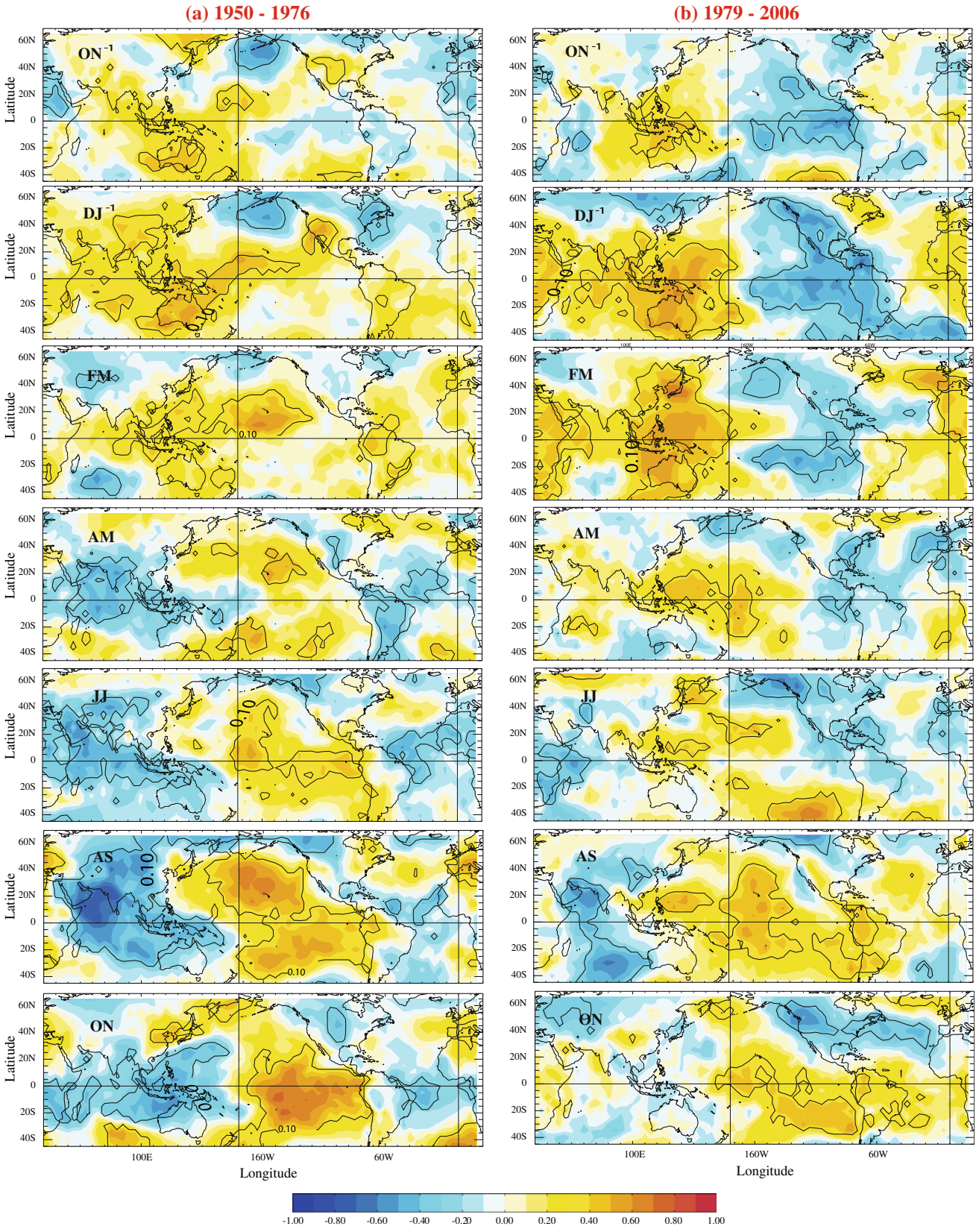

Fig. 6 Global correlation between **ISM rainfall in AS** and bimonthly **SLP** anomalies from the boreal fall preceding (ON^{-1}) to that following (ON) the ISM season during **a** 1950–1976 and **b** 1979–2006 time periods. Correlation coefficients that are above the 90% confidence level estimated with a phase-scrambling bootstrap test with 999 samples are encircled

development of a La Niña (El Niño) event through the generation of oceanic Kelvin waves.

4.2 Correlation with ISM rainfall in AS

Correlations of SST and SLP fields with AS rainfall timeseries yield results that are substantially different to those observed in JJ, and highlight the existence of a certain JJ–AS dichotomy in ISM-SST and ISM-SLP relationships, especially during the recent period (Figs. 5 and 6).

During the 1950–1976 period, results in AS show a robust ISM-ENSO relationship but point towards much more significant SLP and SST precursors for Indian rainfall in AS than JJ. Indeed, Figs. 5 and 6 (left panels) recapture a significant and very comparable ISM-ENSO relationship to that observed in JJ for the same period. This is consistent with the maximum correlation values obtained with Niño(0) before 1976–1977 in Table 2 (−0.47 in JJ and −0.59 in AS). However, significant SST anomalies in other regions seem to have gained importance for AS rainfall variability and predictability. This is the case in the tropical Atlantic Ocean, where warm (cold) SST anomalies persist from ON to FM in relation to a wet (dry) AS ISM season before 1976 (Fig. 5). However, this SST signal is opposite to the summer Atlantic-ISM relationship proposed by Kucharski et al. (2007, 2008, and 2009), and the lack of significant SLP anomalies in this region sheds a doubt on its potential impact on AS rainfall variability (Fig. 6). Meanwhile, an anomalous SST dipole is also observed from ON to AM in the South IO, associated with a significant modulation of the intensity of the Mascarene High during FM (Figs. 5 and 6). This is consistent with the occurrence of a subtropical dipole event in the South IO (Behera and Yamagata 2001). The persistent warm (cold) anomalies in the southeastern IO associated with these subtropical dipole events have been shown to play a significant role on ISM variability, via a modulation of the inter-hemispheric moisture transport or the position of the Mascarene High in the IO (Terray et al. 2003, 2007; Boschat et al. 2010). In Fig. 6, the northward propagation of negative (positive) SLP anomalies in the Indian sector from AM to AS is consistent with the dynamical processes detailed in these earlier studies. Note that these results are also in line with the increased influence of the SEIO index in AS in Table 2 (0.16 correlation in JJ and 0.49 in AS during 1950–1976). Besides, it seems important to point out that the anomalous SST and SLP dipoles associated with the NPO also prevail as highly significant and therefore robust precursors for AS rainfall during the 1950–1976 period (Figs. 5, 6). Altogether, the persistence *and* emergence of these significant precursory signals in both the North Pacific and Indian oceans thus reflect the higher predictability of AS rainfall, while also introducing a certain JJ-AS dichotomy in ISM-SST statistical relationships during the 1950–1976 period.

This JJ–AS dichotomy is even more pronounced during the 1979–2006 period, as this time, correlation patterns in AS (Figs. 5, 6, right panels) differ more substantially from results in JJ (Figs. 3, 4), as well as more generally from those observed during the same AS season of the 1950–1976 period (Figs. 5, 6, left panels). In line with the hypothesis of a 'phase-shift' of the ISM-ENSO relationship (see Table 2, in AS), Figs. 5 and 6 show that ISM rainfall in AS is now significantly linked to the decaying phase of ENSO rather than its development. This intense precursory signal in the tropical Pacific is a unique characteristic of the recent period and of the AS season *as it is not seen during the 1950–1976 period nor during JJ of the recent period*. Nevertheless, we must be careful about the implications of these results for ISM rainfall predictability, as composites of extreme ISM events during this period (not shown) indicate that this dominant signal in AS is largely due to the wet monsoons of 1983 and 1998, which followed the two strongest El Niño events of the 20th century (see Boschat et al. 2010). Based on results shown in Figs. 5 and 6, it thus seems that the most robust precursory signals for AS Indian rainfall stem from extratropical regions in the North Pacific and South IO, as these significant patterns are seen to persist during both periods, several months before the ISM onset, and concern both the weak and strong ISMs.

Correlation patterns in AS during 1979–2006 also illustrate a biennial rhythm of the IOD-ENSO-ISM system, according to which an El Niño event tends to be preceded by decreased AS rainfall during boreal summer, a positive IOD pattern during fall, and followed by a basin-wide warming of the tropical IO which persists until the next spring and, eventually, leads to enhanced AS rainfall and a La Niña event in the following year. The SST and SLP anomalies in Figs. 5 and 6 are consistent with these time and phase relationships, as well as the dynamical processes which have been shown to feed this biennial system, and influence the late ISM season (for further details see Yang et al. 2007; Sooraj et al. 2009; Boschat et al. 2010; Hong et al. 2010). Note that this biennial tendency is also consistent with the significant correlation values obtained with the IOD(-1), Niño(−1) and IOB indices in AS for the recent period in Table 2.

5 Modulation of ISM rainfall during El Niño and La Niña years (1950–2006)

Overall, our previous analyses have shed a light on the existence of significant modulations in ISM teleconnections and precursory signals between the first (JJ) and second part

(AS) of the monsoon season, and this especially after the 1976–1977 climate shift. ISM rainfall variability is strongly linked to ENSO during both 1950–1976 and 1979–2006 time periods as the relationship with ENSO is still highly significant for JJ and AS rainfall averages separately. However, the increased JJ–AS dichotomy observed after 1979 seems to blur the global ISM-ENSO signal, leading to an apparent weakening of these relationships at the seasonal time scale during the recent decades.

So far, this weakening has been attributed to a broad range of phenomena, ranging from changes in atmospheric fields due to global warming (Krishna Kumar et al. 1999), to changes in tropical Pacific SST patterns (Krishna Kumar et al. 2006) or tropical Atlantic during boreal summer (Kucharski et al. 2007, 2008, 2009), to the more frequent co-occurrence of positive IODs and El Niño events during recent decades (Ashok et al. 2001, 2004; Krishnan and Swapna 2009), possibly also due to global warming (Abram et al. 2008; Ihara et al. 2008, 2009; Cai et al. 2009b, c). Collectively, these studies suggest that more emphasis must be given to the association between global SST patterns and ISM rainfall *inside* of the set of El Niño (or La Niña) events, to examine probable causes for the failure of the ISM-ENSO relationship during the developing year of specific events. However, none of these works have drawn particular attention to the JJ–AS rainfall dichotomy observed during recent decades and evaluated its link to the recent modulation of the ISM-ENSO relationship.

In the following paragraphs, a correlation analysis is thus carried out between JJ and AS ISM rainfall and global SST and SLP fields inside of the sets of El Niño and La Niña years, in order to analyze what may cause a modulation *at the 2nd order* of ISM rainfall during each phase of ENSO. The El Niño (La Niña) years entering in this correlation analysis are selected over the entire 1950–2006 period, upon a 0.5 (−0.5) standard deviation of the Niño 3.4 index in DJ. These wider criteria and extended period allow us to gather a larger amount of years for the analysis and therefore obtain more robust results.

5.1 El Niño years

To begin with, the SST and SLP composites during JJ and AS computed from 16 selected El Niño years (1951, 1957, 1963, 1965, 1968, 1969, 1972, 1976, 1977, 1982, 1986, 1987, 1991, 1994, 1997 and 2002) display the development of well-known El Niño SST and SLP patterns in co-occurrence with a positive IOD pattern in the equatorial IO (Fig. 7a). Correlation analyses of ISM rainfall, separately in JJ and AS, with global SST and SLP anomalies are then carried out *during these El Niño years*.

Results show that ISM rainfall in JJ (Fig. 8a) is quite significantly influenced by the *early* development of El Niño conditions, compared to a "canonical" El Niño evolution (Fig. 7a), since correlations are significant and negative with SSTs over the central Pacific during the whole boreal summer. These correlations suggest that an earlier (later) El Niño onset causes deficient (excessive) ISM in JJ, associated with high (low) SLP anomalies and anomalous subsidence (ascent) over a large area extending from the Maritime Continent, to the North IO and the Asian continent (Fig. 8a). The correlation patterns between JJ rainfall and IO SSTs during these El Niño years then mainly reflect the warming of the equatorial western IO in response to reduced evaporative heat loss and upwelling associated with weaker monsoon winds: this suggests that IO SST anomalies play a passive role during the first part of the ISM season. However, these correlation patterns also reveal interesting features about the dynamics of the ENSO-ISM-IOD relationships since the mean SST gradient across the equatorial IO is anomalously positive to the west in AS following an early El Niño and a dry ISM in JJ. This may induce an anomalous zonal positive SLP gradient to the east and promote anomalous westward zonal wind stress across the equatorial IO. In other words, these changes provide very favorable conditions for a positive IOD to develop during the second half of ISM and following months as suggested by Loschnigg et al. (2003).

The same correlation analysis for the AS season (Fig. 8b) shows that the relationships of AS rainfall with SST and SLP anomalies are entirely different. IO SSTs have more influence on the monsoon than vice-a-versa during the second half of the season. Indeed, Fig. 8b indicates that, unlike results in JJ, the most significant anomalies associated with the second part of ISM are not located in the tropical Pacific, but in the southeast IO: a region where important air-sea feedbacks have been shown to operate during boreal summer (see Li et al. 2003). Indeed, the persistent cold anomalies along the coasts of Java and Sumatra are associated with positive SLP anomalies (Fig. 8b). Also, a significant anomalous cyclonic center is noted over the Arabian Sea and India during AS in relation to positive rainfall anomalies. This is consistent with a strengthening of the Bay of Bengal branch of ISM and a modulation of the local Hadley circulation over the eastern IO which can induce anomalous ascent and, hence, positive rainfall anomalies over the Indian subcontinent in AS. The positive correlations with SSTs in the south central IO are also consistent with an enhanced anticyclonic circulation over the eastern IO, as this circulation may reduce the intensity of the south-east trades in the Southern Hemisphere and, thus, decrease the evaporative heat loss (Terray et al. 2007). Put together, the SST and SLP patterns in Fig. 8b thus suggest that the anomalous anticyclone over the eastern node of the IOD may play a role in reducing the ENSO-induced subsidence over India during the second half of ISM.

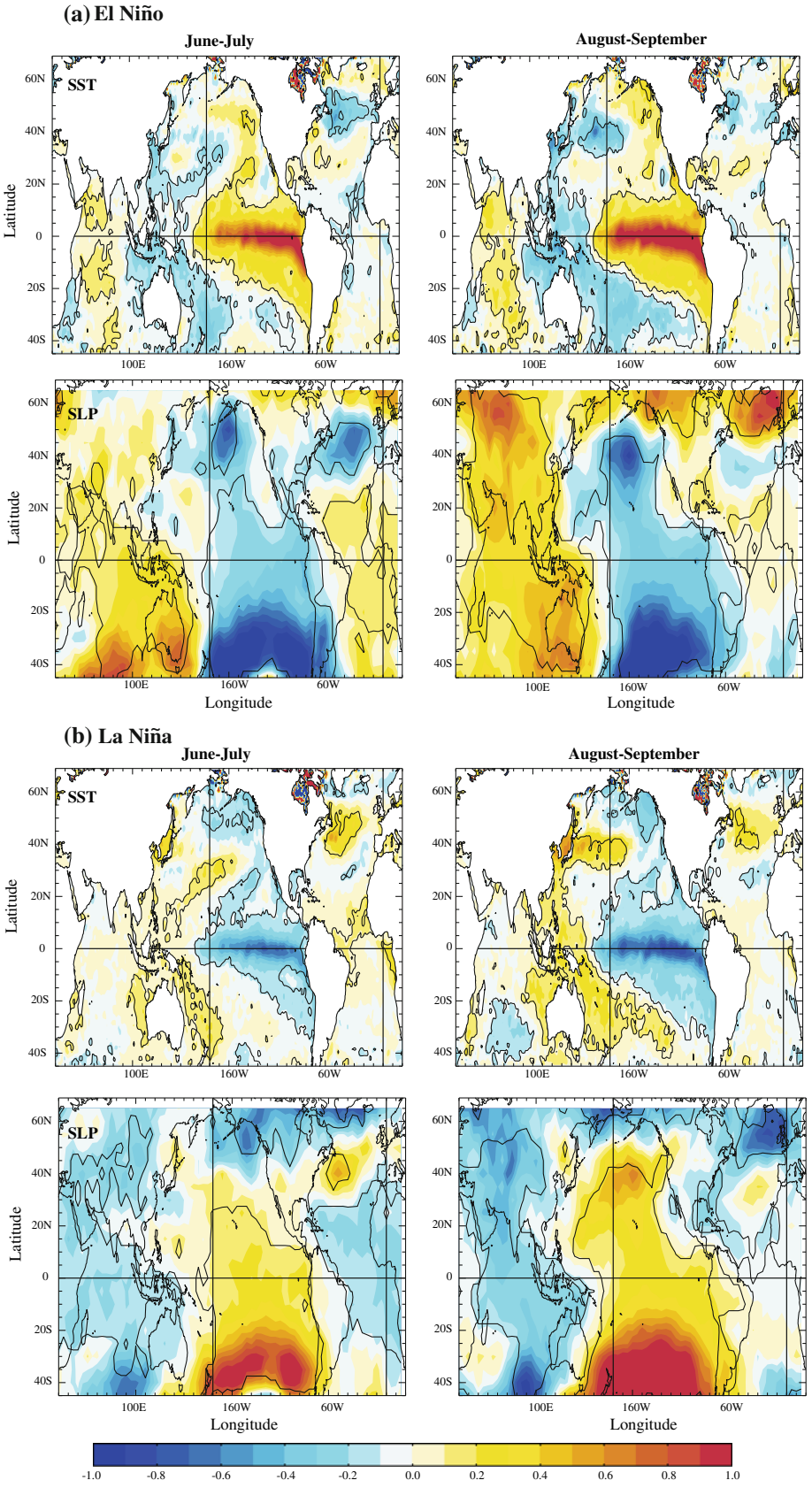

Fig. 7 Composite SST (*top panels*) and SLP (*bottom panels*) anomalies in JJ and AS during **a** the 16 El Niño years (*in 1951, 1957, 1963, 1965, 1968, 1969, 1972, 1976, 1977, 1982, 1986, 1987, 1991, 1994, 1997 and 2002)* and **b** 18 La Niña years *(in 1950, 1954, 1955, 1964, 1966, 1967, 1970, 1973, 1975, 1983, 1984, 1985, 1988, 1995, 1998, 1999, 2000 and 2005*). The composite anomalies significant at the 90% confidence level are encircled. The statistical significance has been determined by the method outlined in Terray et al. (2003)

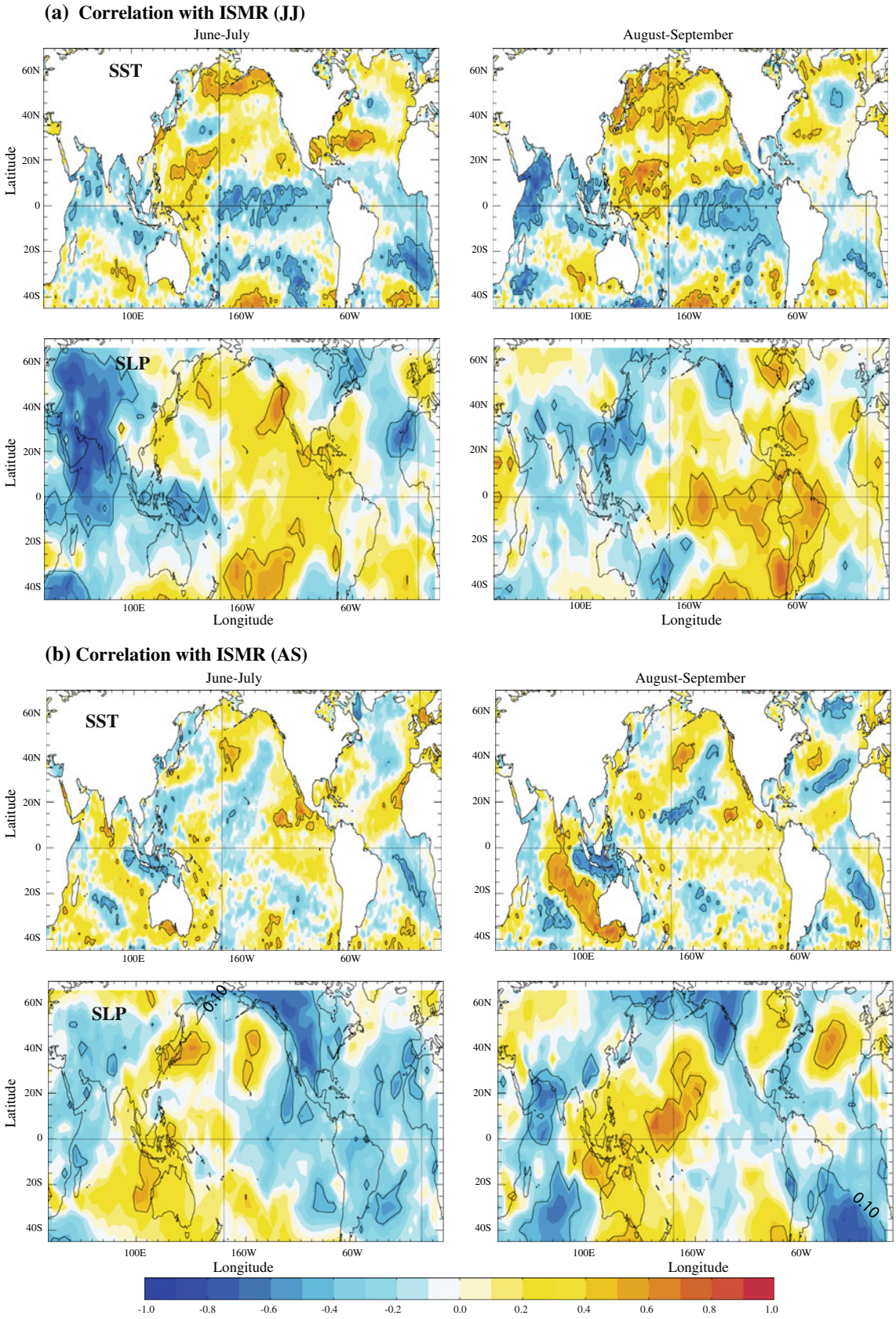
(a) Correlation with ISMR (JJ)
June-July
August-September
SST
SLP
Latitude
Longitude
60N
40N
20N
0
20S
40S
100E
160W
60W
(b) Correlation with ISMR (AS)
June-July
August-September
SST
SLP
0.10
0.10
Latitude
Longitude
-1.0
-0.8
-0.6
-0.4
-0.2
0.0
0.2
0.4
0.6
0.8
1.0

◀ **Fig. 8** Correlation of summer SST (*top panels*) and SLP anomalies (*bottom panels*) with **a** ISM rainfall in JJ and **b** ISM rainfall in AS, during the 16 El Niño years (*in 1951, 1957, 1963, 1965, 1968, 1969, 1972, 1976, 1977, 1982, 1986, 1987, 1991, 1994, 1997 and 2002*). Correlations significant at the the 90% confidence level according to a two-tailed student't test are encircled

In order to quantify the potential impact of these IOD-related anomalies in terms of ISM rainfall, a regression analysis between ISM rainfall and IOD-related time series in September–October-November is also carried out during the same El Niño years. Results in Table 3 confirm that the west (east) node of the IOD has a significant association with JJ (AS) ISM rainfall (−17 mm/month compared to a mean value of −12.06 mm/month in JJ and −11.9 mm/month compared to a mean value of −16.72 mm/month in AS, respectively). Altogether, the two IOD nodes are thus playing opposite roles (passive for the west and active for the east) with regards to ISM rainfall, while operating at different times. This can, at least partly, account for the JJ–AS dichotomy observed in ISM rainfall (consistent opposite values obtained in JJ and AS with the IOD time series in Table 3), as well as the rather conflicting results found in the literature on the IOD-ISM relationship (see Introduction of this paper).

Note, besides, that no significant correlations are observed over the tropical Atlantic Ocean during El Niño years (Fig. 8), even though the entire 1950–2006 period is considered: this result is not consistent with a possible contribution of Atlantic SSTs to the interdecadal modulation of the ENSO-ISM relationship (Kucharski et al. 2007, 2008, 2009).

5.2 La Niña years

Similar analyses are now carried out during the negative phase of ENSO. The SST and SLP composites computed from 18 selected La Niña years (in 1950, 1954, 1955, 1964, 1966, 1967, 1970, 1973, 1975, 1983, 1984, 1985, 1988, 1995, 1998, 1999, 2000 and 2005) are characterized by reversed SLP and SST patterns in the Pacific during summer: however, anomalies in the IO differ from El Niño conditions as they feature the development of a SST dipole in the south IO rather than an IOD pattern (Fig. 7b). Note also that among these 18 La Niña events, 9 follow the decaying phase of El Niño events while the 9 others correspond to lingering La Niña conditions in the Pacific.

The correlation with ISM rainfall in JJ and AS during these La Niña years (Fig. 9) shows patterns which are generally of the same sign as the SST and SLP composites in Fig. 7b. These correlations may thus be interpreted as a *global* modulation (i.e enhancement or damping) of La Niña conditions during boreal summer, without any significant spatial modification of the "canonical" patterns

Table 3 Regression between ISM rainfall in JJ, AS and JJAS, and the IOD, IOD-west node and IOD-east node time series in SON during the 16 El Niño years (*in 1951, 1957, 1963, 1965, 1968, 1969, 1972, 1976, 1977, 1982, 1986, 1987, 1991, 1994, 1997 and 2002*)

	ISMR (JJAS)	ISMR (JJ)	ISMR (AS)
IOD (SON)	2.97	−3.27	9.20
IOD—West node (SON)	−8.43	−17.00	0.15
IOD—East node (SON)	−10.83	−9.75	−11.90
Composite anomalies	−14.39	−12.06	−16.72

Regression coefficient are given in mm/month by standard deviation of the IOD time series. The last line shows the mean composite values (in mm/month) of ISM rainfall in JJ, AS and JJAS during the same El Niño years

(Fig. 7b). As during El Niño years, the first part of the ISM season seems to be mainly influenced by the state of the Pacific in JJ (Fig. 9a). Note however that, based on the years selected for this correlation analysis, this JJ ENSO signal may oppose years with an early onset of La Niña to those characterized by a late withdrawal of El Niño episodes.

On the other hand, results in AS highlight again the importance of IO anomalies and local coupled ocean–atmosphere processes during the second part of ISM, with the most significant SST anomalies observed in the north IO and in the form of a south IO dipole (Fig. 9b). Consistent with the existence of a JJ–AS dichotomy, the warming of the tropical IO in JJ enhances ISM rainfall in AS. In the south IO, the amplification from JJ to AS of negative SLP anomalies associated with the SST dipole is consistent with a strengthening of the trade-winds and an enhanced evaporation over the south central IO (Fig. 9b); both of which may enhance the interhemispheric moisture transport and, ultimately lead to positive ISM rainfall anomalies in AS (Terray et al. 2007; Boschat et al. 2010).

Altogether, the modulation of ISM rainfall during La Niña years (compared to a "canonical" La Niña) occurs again through distinct processes in JJ and AS, although both act to enhance rainfall activity over India. The first part of the ISM season is mostly influenced by the early appearance of La Niña conditions, whereas local processes, particularly in the southeast IO, are at play during the second part of the season and amplify AS rainfall. Note that this JJ–AS dichotomy in ISM rainfall has also been observed during the decaying phase of El Niño events during recent decades (Boschat et al. 2010).

In conclusion, the existence of a JJ–AS dichotomy is observed inside both the sets of El Niño and La Niña years. Local interactions in the IO are mainly responsible for the modulation of ISM response in AS, although these physical processes differ among El Niño (La Niña) years. In constrast, the extratropical regions and Atlantic Ocean seem to play only a secondary role.

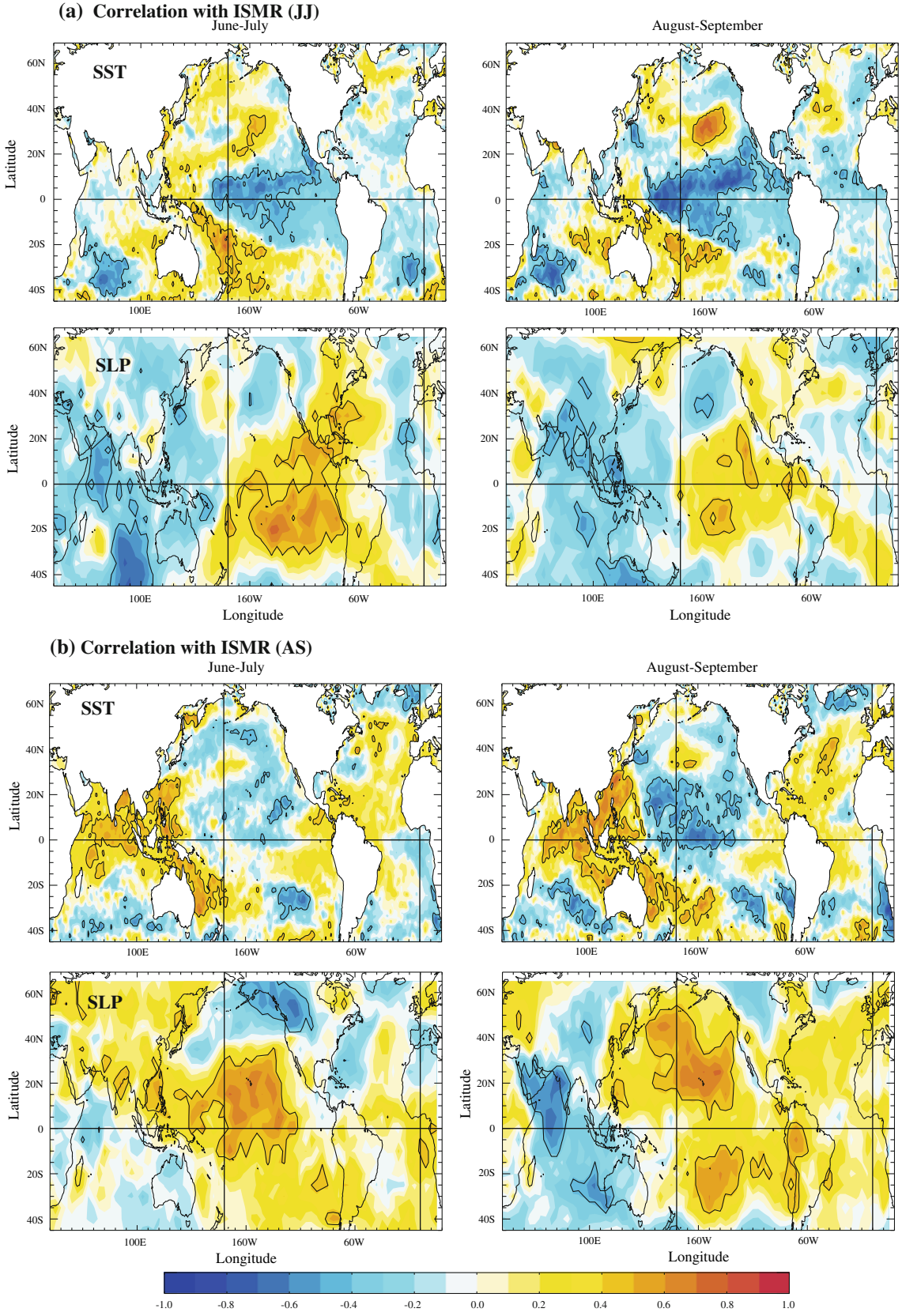
(a) Correlation with ISMR (JJ)
June-July
August-September
SST
SLP
Latitude
Longitude
60N
40N
20N
0
20S
40S
100E
160W
60W
(b) Correlation with ISMR (AS)
June-July
August-September
SST
SLP
Latitude
Longitude
-1.0
-0.8
-0.6
-0.4
-0.2
0.0
0.2
0.4
0.6
0.8
1.0

◀ **Fig. 9** Correlation of summer SST (top panels) and SLP anomalies (*bottom panels*) with **a** ISM rainfall in JJ and **b** ISM rainfall in AS, during the 18 La Niña years (*in 1950, 1954, 1955, 1964, 1966, 1967, 1970, 1973, 1975, 1983, 1984, 1985, 1988, 1995, 1998, 1999, 2000 and 2005*). Correlations significant at the the 90% confidence level according to a two-tailed student'*t* test are encircled

6 Conclusion and discussion

For years, many works have examined the links between ISM rainfall and various modes of interannual variability, such as ENSO or IOD (Webster et al. 1998; Wang 2006). However, so far, these studies have obtained quite different, and at times contradictory results. Besides, no general consensus has yet been reached, as to explain the weakening of the ISM-ENSO relationship observed during recent decades (Krishna Kumar et al. 1999, 2006; Gershunov et al. 2000; Kinter et al. 2002; Ashok et al. 2004; Kucharski et al. 2009). This work builds upon these earlier studies and attempts to reconcile in a common and comprehensive framework the various conflicting results found in the literature on ISM-SST relationships.

First, our results indicate the existence of a strong and steady ISM-ENSO relationship before the so-called 1976–1977 climate shift. However, tropical Pacific SSTs do not provide any significant precursory signal for ISM rainfall during this 1950–1976 period. Instead, anomalous SST and SLP dipoles are observed during the previous boreal winter and spring in the North Pacific and South IO. These significant extratropical patterns are identified as potential ISM precursors but essentially for the second part of the monsoon season (e.g. AS), which points to a certain dichotomy between the first and second parts of ISM as far as ISM predictability is concerned. Over the North Pacific, NPO-related SST and SLP patterns are detected before extreme ISM years. Further analysis suggests that this NPO-ISM predictive relationship is due to the apparent active role of the NPO in ENSO variability through the modulation of wind anomalies in the western Pacific (Vimont et al. 2003). These significant anomalies may thus be classified as "ENSO precursors" and signal the likely ENSO evolution during the following months. Local SST anomalies in the South IO during boreal winter and spring have also a significant relationship with ISM rainfall, but seem to evolve independently from ENSO during this period (Terray and Dominiak, 2005). Finally, it is important to stress that the Atlantic and equatorial IO (e.g. IOD) are devoid of any robust precursory SST signals during boreal fall and winter preceding ISM. Thus, they cannot provide any information on the type of ISM that may follow during this first epoch.

This distinction between the first (JJ) and second (AS) parts of the ISM season is even more pronounced after the 1976–1977 climate shift. The SST and SLP teleconnection patterns associated with rainfall anomalies in AS are also very different, in many aspects, from those observed in the first period. Moreover, our results strongly support the hypothesis that the recent weakening of the ISM-ENSO relationship at the seasonal time scale may be an artefact of this increased subseasonal rainfall variability, since the relationship with ENSO is still highly significant for JJ and AS rainfall averages separately. Indeed, correlation results in AS suggest a 'phase shift' rather than a weakening of this ISM-ENSO relationship after 1979, with the appearance of an intense precursory signal for AS Indian rainfall in the tropical Pacific (and IO) during the previous boreal winter and spring, linked in particular to the decaying phase of the two strong El Niño events of 1982–1983 and 1997–1998. Our analysis of the recent period also confirms the importance of extratropical forcing on the whole ENSO-monsoon system, with precursory signals stemming from the North Pacific and South IO for AS rainfall (Terray et al. 2005; Peings et al. 2009). Besides, results in AS also highlight a more biennial tendency in the ENSO-ISM-IOD system during recent decades, according to which co-occurring El Niño and positive IOD events are followed by a warming of the IO, a wet ISM in the next summer and, finally, a La Niña event during the following winter (Meehl et al. 2003; Hong et al. 2010). Note however that this TBO signal may be also largely influenced by the 1982–1983 and 1997–1998 El Niño events. On the other hand, changes in the date of El Niño/La Niña onsets are probably the main factor contributing to ISM rainfall variability during JJ.

Altogether, these analyses have thus shown that ISM is strongly linked to ENSO over both time periods. However, the increased JJ–AS dichotomy observed after 1979 tends to blur the ISM-ENSO signal, leading to an apparent weakening of this relationship at the seasonal time scale during the recent period. Note that this JJ–AS dichotomy may be linked to many factors, and may even be due to large intraseasonal variability which is being aliased by our bimonthly averaging. In order to gain a better understanding of this JJ–AS rainfall dichotomy and its link to the recent modulation of the ISM-ENSO relationship, we have finally examined the association between ISM rainfall and global SST and SLP fields, separately *inside* of the sets of El Niño and La Niña years.

The most notable features for the El Niño and La Niña years are (i) the sensitivity of ISM rainfall during JJ to the timing of ENSO onset and (ii) the importance of local air-sea feedbacks in the IO during the second half of boreal summer as key-factors for understanding the variability of ISM rainfall anomalies observed inside each set of events.

Our analysis suggests the following scenario as an important factor for modulating ISM response during El Niño events: an early onset of an El Niño causes a *more* deficient monsoon in JJ, which feeds back onto the IO by

inducing *warmer* SST anomalies in the western equatorial IO associated with the reduced monsoon winds and Somali jet. These SST changes over the western IO provide, however, a very favourable environment for positive IOD development during the second half of ISM (Loschnigg et al. 2003). The local air-sea feedbacks associated with the SST anomalies in the eastern node of the IOD seem, in turn, to have a more active role on the second half of the monsoon, as they may counteract the effect of El Niño on ISM rainfall through a modulation of the local Hadley circulation over the eastern IO. In other words, the IO seems to play a passive role during the first part of ISM, but a more active role during the second part. Interestingly, this scenario provides a plausible explanation for the existence of a JJ–AS rainfall dichotomy during the El Niño developing year, and may also justify why most dry ISM years are associated with a *dry JJ season* during the recent period (see Fig. 2b).

Our results are thus partly consistent with the mechanism proposed by (Ashok et al. 2001, 2004) whereby the IOD is able to counteract the effect of El Niño on ISM rainfall—bearing in mind that the modulations we have described occur only at a *second level* during El Niño years. These authors argued that the anomalous convergence over the western pole of IOD induced by a positive IOD, enhanced the atmospheric circulation towards India and led to increased ISM rainfall; while the anomalous divergence over the eastern pole decreased the effect of El Niño-induced subsidence over India, by strengthening the meridional circulation over the eastern IO. However, we here suggest that only the *eastern* node of the IOD plays an active role in the modulation of ISM rainfall and, only, during the second half of ISM, whereas SST anomalies in the *western* node may be interpreted as a passive response to the atmospheric signal of an early developing El Niño and ensuing weak monsoon in JJ. We suspect that Ashok et al. (2001, 2004) were unable to reproduce this atmospheric forcing in the IO, as their results are derived from an atmospheric circulation model forced by observed SSTs (Krishna Kumar et al. 2005; Wang et al. 2005).

Yet, our results stress the key-importance of local ocean–atmosphere interactions for enhancing or counteracting the effect of El Niño on ISM rainfall, consistent with the second mechanism proposed by Ashok et al. (2004). The JJ–AS dichotomy observed more distinctively in recent El Niño events may then result from an enhancement of these IO feedbacks, with a more frequent occurrence of positive IODs. This, in turn, may explain why, although El Niño events are stronger, a global weakening of the ISM-ENSO relationship may be observed *at the seasonal scale* during recent decades.

A similar analysis for the La Niña years illustrates again the combined effects of ENSO and IO anomalies on wet ISMs. Indeed, results suggest that ISM rainfall anomalies in JJ are also influenced by the early onset of La Niña conditions in the Pacific, while local IO processes, particularly in the southeast, play an important role in the enhancement of ISM rainfall in AS (Terray et al. 2007; Park et al. 2010; Boschat et al. 2010). Note that these processes are consistent with recent results from Boschat et al. (2010), where the decaying phase of El Niño is considered. Indeed, they show that, during the 1979–2007 period, the mature phase of El Niño causes a delayed ISM onset and an anomalously deficient ISM in JJ, whereas local feedbacks particularly in the South IO enhance ISM rainfall activity in AS. In other words, the ocean–atmosphere interactions in the IO may also be responsible for a JJ-AS dichotomy in the set of the La Niña years *or* decaying El Niño years. This scenario also explains why most wet ISM events are associated with anomalously *wet AS season* during the recent period (Fig. 2b).

Altogether, our results thus highlight the importance of local processes for understanding the changes in the ISM-ENSO relationship during the recent period. But why are the IO ocean–atmosphere interactions stronger in recent decades? Terray and Dominiak (2005) argued that this may be related to the sustained warming of the IO. Besides, several works have suggested a more frequent occurrence of extreme IOD events, possibly due to global warming (Abram et al. 2008; Ihara et al. 2008, 2009; Cai et al. 2009b, c) or a natural decadal fluctuation of the tropical system (Zheng et al. 2010), developing in association with strong El Niño events. The causes for such changes in ENSO and IOD properties, cannot obviously be detected by our simple statistical analyses. The mechanims proposed in this work regarding the modulation of ISM rainfall variability, as well as the possible causes of these decadal fluctuations, need to be tested and validated through numerical experiments with coupled ocean–atmosphere models.

Acknowledgments Financial support from the Indo-French CEFIPRA project (N° 3907/1) is acknowledged. The Hadley SST and SLP datasets were provided by the NOAA/OAR/ESRL PSD, Boulder, Colorado, USA, from their Web site at URL: http://www.cdc.noaa.gov/. Graphics have been prepared using the SAXO package of Sébastien Masson. We also thank the anonymous reviewers for their comments that improved this paper.

References

Abram NJ, Gagan MK, Cole JE, Hantoro WS, Mudelsee M (2008) Recent intensification of tropical climate variability in the Indian Ocean. Nat Geosci 1:849–853

Alexander MA, Vimont DJ, Chang P, Scott JD (2010) The impact of extra tropical atmospheric variability on ENSO: testing the seasonal foot printing mechanism using coupled model experiments. J Clim 23:2885–2901

Allan R, Ansell T (2006) A new globally complete monthly historical gridded mean sea level pressure dataset (HadSLP2): 1850–2004. J Clim 19:5816–5842

Alory G, Wijffels S, Meyers G (2007) Observed temperature trends in the Indian Ocean over 1960–1999 and associated mechanisms. Geophys Res Lett 34:L02606. doi:10.1029/2006GL028044

Annamalai H, Liu P (2005) Response of the Asian summer monsoon to changes in El Niño properties. Q J R Meteorol Soc 131:805–831

Annamalai H, Hamilton K, Sperber KR (2007) The South Asian summer monsoon and its relationship with ENSO in the IPCC AR4 simulations. J Clim 20:1071–1092

Ashok K, Guan Z, Yamagata T (2001) Influence of the Indian Ocean dipole on the relationship between the Indian monsoon rainfall and ENSO. Geophys Res Lett 28:4499–4502

Ashok K, Guan Z, Saji NH, Yamagata T (2004) Individual and combined influences of ENSO and the Indian Ocean dipole on the Indian summer monsoon. J Clim 17:3141–3154

Ashrit RG, Douville H, Rupa Kumar K (2003) Response of the Indian monsoon and ENSO-monsoon teleconnection to enhanced greenhouse effect in the CNRM coupled model. J Meteor Soc Jpn 81:779–803

Behera SK, Yamagata T (2001) Subtropical SST dipole events in the southern Indian Ocean. Geophys Res Lett 28:327–330

Blanford HF (1884) On the connexion of Himalaya snowfall and seasons of drought in India. Proc R Soc Lond 37:3–22

Boschat G, Terray P, Masson S (2010) Interannual relationships between Indian summer monsoon and Indo-Pacific coupled modes of variability during recent decades. Clim Dyn. doi:10.1007/s00382-010-0887-y

Cai W, Sullivan A, Cowan T (2009a) Rainfall teleconnections with Indo-Pacific variability in the WCRP CMIP3. Model J Clim 22:5046–5071

Cai W, Cowan T, Sullivan A (2009b) Recent unprecedented skewness towards positive Indian Ocean dipole occurrences and its impact on Australian rainfall. Geophys Res Lett 36:L11705. doi:10.1029/2009GL037604

Cai W, Sullivan A, Cowan T (2009c) Climate change contributes to more frequent consecutive positive Indian Ocean dipole events. Geophys Res Lett 36:L23704. doi:10.1029/2009GL040163

Chang P et al (2006) Climate fluctuations of tropical coupled systems—the role of ocean dynamics. J Clim 19:5122–5174

Clark CO, Cole JE, Webster PJ (2000) Indian Ocean SST and Indian summer rainfall: predictive relationships and their decadal variability. J Clim 13:2503–2519

Cleveland RB, Cleveland WS, McRae JE, Terpenning I (1990) A seasonal-trend decomposition procedure based on loess (with discussion). J Off Stat 6:3–73

Drbohlav HKL, Gualdi S, Navarra A (2007) A diagnostic study of the Indian Ocean dipole mode in El Niño and non-El Niño years. J Clim 20:2961–2977

Du Y, Xie S-P, Huang G, Hu K-M (2009) Role of air–sea interaction in the long persistence of El Niño -induced North Indian Ocean warming. J Clim 22:2023–2038

Ebisuzaki W (1997) A method to estimate the statistical significance of a correlation when the data are serially correlated. J Clim 10:2147–2153

Fedorov AV, Philander SG (2000) Is El Niño changing? Science 288:1997–2002. doi:10.1126/science.288.5473.1997

Fedorov AV, Philander SG (2001) A stability analysis of tropical ocean-atmosphere interactions: bridging measurements and theory for El Niño. J Clim 14:3086–3101

Fischer AS, Terray P, Delecluse P, Gualdi S, Guilyardi E (2005) Two independent triggers for the Indian Ocean dipole/zonal mode in a coupled GCM. J Clim 18:3428–3449

Francis PA, Gadgil S (2010) Towards understanding the unusual Indian monsoon in 2009. J Earth Syst Sci 119:397–415

Gadgil S, Vinayachandran PN, Francis PA, Gadgil S (2004) Extremes of the Indian summer monsoon rainfall, ENSO and equatorial Indian Ocean oscillation. Geophys Res Lett 31:L12213. doi:10.1029/2004GL019733

Gadgil S, Rajeevan M, Nanjundiah R (2005) Monsoon prediction—why yet another failure? Curr Sci 84:1713–1719

Gadgil S, Rajeevan M, Francis PA (2007) Monsoon variability: links to major oscillations over the equatorial Pacific and Indian oceans. Curr Sci 93:182–194

Gershunov A, Schneider N, Barnett T (2000) Low-frequency modulation of the ENSO-Indian monsoon rainfall relationship: signal or noise? J Clim 14:2486–2492

Hong CC, Lu MM, Kanamitsu M (2008) Temporal and spatial characteristics of positive and negative Indian Ocean dipole with and without ENSO. J Geophys Res 113:DO8107. doi:10.1029/2007JD009151

Hong CC, Li T, Lin HO, Chen YC (2010) Asymmetry of the Indian Ocean basin wide SST anomalies: roles of ENSO and IOD. J Clim 23:3563–3576

Hurrell JW, Trenberth KE (1999) Global sea surface temperature analyses: multiple problems and their implications for climate analysis, modeling and reanalysis. Bull Amer Met Soc 80:2661–2678

Ihara C, Kushnir Y, Cane MA, de la Pena V (2007) Indian summer monsoon rainfall and its link with ENSO and the Indian Ocean climate indices. Int J Clim 27:179–187

Ihara C, Kushnir Y, Cane MA (2008) Warming trend of the Indian Ocean SST and Indian Ocean dipole from 1880 to 2004. J Clim 21:2035–2046

Ihara C, Kushnir Y, Cane MA, Victor HP (2009) Climate change over the equatorial Indo-Pacific in global warming. J Clim 22:2678–2693

Izumo T, De Boyer Montégut C, Luo J-J, Behera SK, Masson S, Yamagata T (2008) The role of the Western Arabian Sea upwelling in Indian monsoon rainfall variability. J Clim 21:5603–5623

Ju J, Slingo JM (1995) The Asian summer monsoon and ENSO. Quart J Roy Meteor Soc 121:1133–1168

Kinter JL, Miyakoda K, Yang S (2002) Recent change in the connection from the Asian monsoon to ENSO. J Clim 15:1203–1215

Kinter J, Fennessy M, Krishnamurthy V, Marx L (2004) An evaluation of the apparent interdecadal shift in the tropical divergent circulation in the NCEP-NCAR reanalysis. J Clim 17:349–361

Krishna Kumar K, Rajagopalan B, Cane M (1999) On the weakening relationship between the Indian monsoon and ENSO. Science 284:2156–2159

Krishna Kumar K, Hoerling M, Rajagopalan B (2005) Advancing dynamical prediction of Indian monsoon rainfall. Geophys Res Lett 32:L08704. doi:10.1029/2004GL021979

Krishna Kumar K, Rajagopalan B, Hoerling H, Bates G, Cane M (2006) Unraveling the mystery of Indian monsoon failure during El Niño. Science 314:115–119. doi:10.1126/science.1131152

Krishnan R, Swapna P (2009) Significance influence of the boreal summer monsoon flow on the Indian Ocean response during dipole events. J Clim 22:5611–5634

Krishnan R, Mujumdar M, Vaidya V, Ramesh KV, Satyan V (2003) The abnormal summer monsoon of 2000. J Clim 16:1177–1194

Kucharski F, Bracco A, Yoo JH, Molteni F (2007) Low-frequency variability of the Indian monsoon-ENSO relation and the Tropical Atlantic; the 'weakening' of the 1980s and 1990s. J Clim 20:4255–4266

Kucharski F, Bracco A, Yoo JH, Molteni F (2008) Atlantic forced component of the Indian monsoon interannual variability. Geophys Res Lett 35:L04706. doi:10.1029/2007GL033037

Kucharski F, Bracco A, Yoo JH, Tompkins A, Feudale L, Ruti P, Dell'Aquila A (2009) A Gill-Matsuno-type mechanism explains the tropical Atlantic influence on African and Indian monsoon rainfall. Quart J Roy Meteor Soc 135:569–579. doi:10.1002/qj.406

Kulkarni A, Sabade SS, Kripalani RH (2007) Association between extreme monsoons and the dipole mode over the Indian subcontinent. Meteorol Atmos Phys 95:255–268

Li T, Wang B, Chang CP, Zhang YS (2003) A theory for the Indian Ocean dipole-zonal mode. J Atmos Sci 60:2119–2135

Loschnigg J, Meehl GA, Arblaster JM, Compo GP, Webster PJ (2003) The Asian monsoon, the tropospheric biennial oscillation, and the Indian Ocean dipole in the NCAR CSM. J Clim 16:1617–1642

McPhaden MJ, Zhang X (2009) Asymmetry in zonal phase propagation of ENSO sea surface temperature anomalies. Geophys Res Lett 36:L13703. doi:10.1029/2009GL038774

Meehl GA, Arblaster J (2002) The tropospheric biennial oscillation and the Asian-Australian monsoon rainfall. J Climate 15:722–744

Meehl GA, Arblaster JM, Loschnigg J (2003) Coupled Ocean-atmosphere dynamical processes in the tropical Indian and Pacific Oceans and the TBO. J Clim 16:2138–2158

Nicholls N (1995) All-India summer monsoon rainfall and sea surface temperatures around northern Australia and Indonesia. J Clim 8:1463–1467

Nitta T, Yamada S (1989) Recent warming of tropical sea surface temperature and its relationship to the Northern Hemisphere circulation. J Meteor Soc Jpn 67:375–383

Park H-S, Chiang JCH, Lintner BR, Zhang JG (2010) The delayed effect of major El Niño events on Indian monsoon rainfall. J Clim 23:932–946

Parthasarathy B, Munot AA, Kothawale DR (1995) All India monthly and seasonal rainfall series: 1871–1993. Theor Appl Climatol 49:217–224

Peings Y, Douville H, Terray P (2009) Extended winter Pacific North America oscillation as a precursor of the Indian summer monsoon rainfall. Geophys Res Lett 36:L11710. doi:10.1029/2009GL038453

Rajeevan M, Pai DS (2007) On the El Niño-Indian monsoon predictive relationships. Geophys Res Lett 34:L04704. doi:10.1029/2006GL028916

Rajeevan M, Sridhar L (2008) Inter-annual relationship between Atlantic sea surface temperature anomalies and Indian summer monsoon. Geophys Res Lett 35:L21704. doi:10.1029/2008GL036025

Rajeevan M, Pai DS, Anil Kumar R, Lal B (2006) New statistical models for long-range forecasting of southwest monsoon rainfall over India. Clim Dyn. doi:10.1007/s00382-006-0197-6

Rasmusson EM, Carpenter TH (1983) The relationship between the eastern Pacific sea surface temperature and rainfall over India and Sri Lanka. Mon Weather Rev 111:517–528

Ratnam JV, Behera SK, Masumoto Y, Takajashi K, Yamagata T (2010) Pacific Ocean origin for the 2009 Indian summer monsoon failure. Geophys Res Lett 37:L07807. doi:10.1029/2010GL042798

Rayner NA, Parker DE, Horton EB, Folland CK, Alexander LV, Rowell DP, Kent EC, Kaplan A (2003) Global analyses of sea surface temperature, sea ice, and night marine air temperature since the late nineteenth century. J Geophys Res 108(D14):4407. doi:10.1029/2002JD002670

Saji NH, Goswami BN, Vinayachandran PN, Yamagata TA (1999) Dipole mode in the tropical Indian Ocean. Nature 401:360–363

Shukla J (1987) Interannual variability of monsoons in *Monsoons*. In: Fein JS, Stephens PL (eds), Wiley, Hoboken, pp 399–464

Shukla J, Paolino DA (1983) The southern oscillation and long-range forecasting of the summer monsoon rainfall over India. Mon Wea Rev 111:1830–1837

Slingo JM, Annamalai H (2000) [1997]: The El Niño of the century and the response of the Indian summer monsoon. Mon Wea Rev 128:1778–1797

Sooraj KP, Kug J-S, Li Y, Kang I-S (2009) Impact of El Nino onset timing on the Indian Ocean: Pacific coupling and subsequent El Nino evolution. Theor Appl Climatol 97(1–2):17–27

Srivastava AK, Rajeevan M, Kulkarni R (2002) Teleconnection of OLR and SST anomalies over Atlantic Ocean with Indian summer monsoon. Geophys Res Lett 29:1284. doi:10.1029/2001GL013837

Terray P (1994) An evaluation of climatological data in the Indian Ocean area. J Meteor Soc Japan 72:359–386

Terray P (2010) Southern hemisphere extra-tropical forcing: a new paradigm for El Niño-southern oscillation. Clim Dyn. doi:10.1007/s00382-010-0825-z

Terray P, Dominiak S (2005) Indian Ocean sea surface temperature and El Niño-Southern Oscillation: a new perspective. J Clim 18:1351–1368

Terray P, Delecluse P, Labattu S, Terray L (2003) Sea surface temperature associations with the late Indian summer monsoon. Clim Dyn 21:593–618

Terray P, Dominiak S, Delecluse P (2005) Role of the southern Indian Ocean in the transitions of the monsoon-ENSO system during recent decades. Clim Dyn 24:169–195. doi:10.1007/s00382-004-0480-3

Terray P, Chauvin F, Douville H (2007) Impact of southeast Indian Ocean sea surface temperature anomalies on monsoon-ENSO-dipole variability in a coupled ocean-atmosphere model. Clim Dyn 28:553–580. doi:10.1007/s00382-006-0192-y

Trenberth KE, Caron JM, Stepaniak DP, Worley S (2002) The evolution of ENSO and global atmospheric surface temperatures. J Geophys Res 107(D8). doi:10.1029/2000JD000298

Vimont DJ, Wallace JM, Battisti DS (2003) The seasonal footprinting mechanism in the Pacific: implications for ENSO. J Clim 16:2668–2675

Vimont DJ, Alexander M, Fontaine A (2009) Mid latitude excitation of tropical variability in the pacific: the role of thermodynamic coupling and seasonality. J Clim 22:518–534

Walker GT (1924) Correlation in seasonal variations of weather, IV: a further study of world weather. Mem Ind Meteorol Dep 24:275–332

Wang B (1995) Interdecadal changes in El Niño onset in the last four decades. J Clim 8:267–285

Wang B (2006) The Asian monsoon. Springer/Praxis Publishing, New York, p 787

Wang B, An S-I (2002) A mechanism for decadal changes of ENSO behavior: roles of background wind changes. Clim Dyn 18:475–486

Wang B, Ding Q, Fu X, Kang I-S, Jin K, Shukla J, Doblas-Reyes F (2005) Fundamental challenge in simulation and prediction of summer monsoon rainfall. Geophys Res Lett 32:L15711. doi:10.1029/2005GL022734

Wang B, Yang J, Zhou T (2008) Interdecadal changes in the major modes of Asian–Australian Monsoon variability: strengthening relationship with ENSO since the Late 1970 s. J Clim 21:1771–1788

Webster PJ, Hoyos C (2010) Beyond the spring barrier? Nat Geosci 3:152–153. doi:10.1038/ngeo760

Webster PJ, Yang S (1992) Monsoon and ENSO: selectively interactive systems. Quart J Roy Meteor Soc 118:877–926

Webster PJ, Magana VO, Palmer TN, Shukla J, Tomas RA, Yanai M, Yasunari T (1998) Monsoons: processes, predictability and the prospects for prediction. J Geophys Res 103(C7):14451–14510

Yang J, Liu Q, Xie S-P, Liu Z, Wu L (2007) Impact of the Indian Ocean SST basin mode on the Asian summer monsoon. Geophys Res Lett 34:L02708. doi:10.1029/2006GL028571

Yoo SH, Fasullo J, Yang S, Ho CH (2010) On the relationship between Indian Ocean sea surface temperature and the transition from El Niño to La Niña. J Geophys Res 115:D15114. doi: 10.1029/2009JD012978

Zheng X-T, Xie S, Vecchi AG, Liu Q, Hafner J (2010) Indian Ocean dipole response to global warming: analysis of ocean–atmospheric feedbacks in a coupled model. J Clim 23(5). doi: 10.1175/2009JCLI3326.1

III.3 Results

Overall, our results highlight the existence of **significant modulations in SST teleconnections and precursory patterns between the 1^{st} and 2^{nd} part of the monsoon** (see Table III.1). This JJ-AS rainfall dichotomy, observed during 1950-1976 and 1979-2006, is first illustrated in terms of ISM precursors, since the most significant precursory signals in this analysis are essentially linked to *AS* rainfall, in line with a higher predictability of the 'late' monsoon season suggested in [*Boschat et al.*, 2011a]. The **most robust precursors** are detected in extratropical regions of the **North Pacific and South IO** during the previous boreal winter and spring, and recognized as common precursors of both ENSO and AS Indian rainfall.

This distinction between the 1^{st} and 2^{nd} part of the ISM season is also reflected in the ISM-ENSO relationship. Although ISM rainfall in JJ and AS is still strongly linked to ENSO over both periods, the lead-lag relationships between ENSO and AS Indian rainfall has changed during recent decades (see Table III.1). Indeed, ISM rainfall in AS is shown to be more significantly linked to the decaying phase of ENSO (*i.e.* Nino(-1)), and no longer to its development (*i.e* Nino(0)). This **AS 'phase-shift' of the ENSO-monsoon relationship** thus tends to amplify the JJ-AS dichotomy during the 1979-2006 period.

	1950-1976	**1979-2006**
ISM rainfall in JJ	linked to Nino(0)	linked to Nino(0)
ISM rainfall in AS	linked to Nino(0) **+** extratropical precursors	linked to **Nino(-1) !** **+** extratropical precursors

Table III.1: Main ISM teleconnections and precursors identified during 1950-1976 and 1979-2006. (see Figs 3 to 6 in Article).

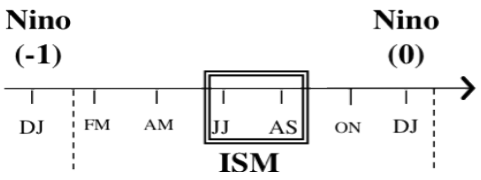

Figure III.2: Temporal definition of Nino(0) and Nino(-1) indices in Table III.1.

In order to understand and possibly explain this AS 'phase-shift' in the ENSO-monsoon relationship, we have set up a methodology which consists in a dual decomposition of ISM-SST teleconnections:

(i) within the ISM season (*i.e* in JJ and AS)

(ii) within the interannual variability of ENSO (*i.e* during El Niño and La Niña years).

Results suggest that, during both El Niño and La Niña years, different processes may be occurring during the 1^{st} and 2^{nd} part of the monsoon season, with potentially opposite impacts on ISM rainfall.

We will here illustrate by a simple diagram the two-step scenario proposed for El Niño years (see Fig III.3). Our results indicate that the early onset of El Niño conditions in the Pacific causes a deficient monsoon in JJ. In response to weaker monsoon winds, warm SST anomalies appear in the west equatorial IO (Fig III.3a), generating favourable conditions for the development of a positive IOD in AS. By triggering air-sea feedbacks in the southeast IO, the cold SST anomalies induced in the eastern IOD node can then have a more active role on the monsoon, and even counteract the negative effect of El Niño on AS rainfall through a modulation of the local Hadley Cell in the east IO (Fig III.3b).

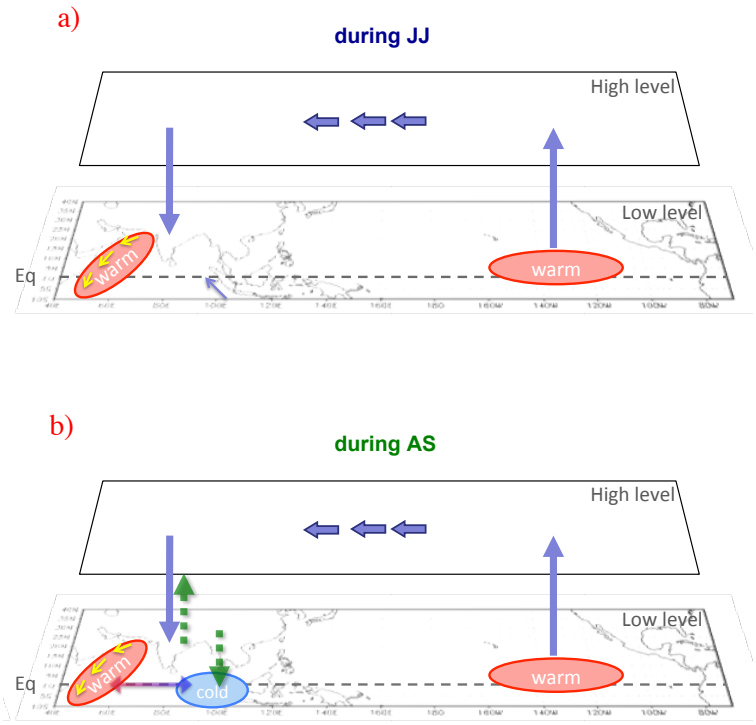

Figure III.3: Diagram showing the modulation of ISM rainfall in **(a)** JJ and **(b)** AS during El Niño years.

The mechanism, built partly on previous works, here reconciles two apparently conflicting theories on the variability of the ISM-ENSO-IOD system, by suggesting the predominance of:

$\surd$ a **biennial tendency** of the ENSO-ISM-IOD system in **JJ** (consistent with the Tropical Biennial Oscillation theory, [*Loschnigg et al.*, 2003])

$\surd$ **local IO processes** in **AS**, where the IOD and ENSO may have a combined effect on ISM rainfall (consistent with [*Ashok et al.*, 2001, 2004]; although only the eastern pole of the IOD in our case plays an active role and only during AS).

Our analysis stresses the importance of these local IO processes in AS. Indeed, the JJ-AS dichotomy observed during El Niño years is mainly linked to these local air-sea interactions in the IO, and may lead to an *apparent* weakening of the global ISM-ENSO signal when these feedbacks are particularly active.

The distinction between the 1^{st} and 2^{nd} part of the monsoon in observations has thus shed a light on:

- the importance of local IO processes for understanding the changes in the ISM-ENSO relationship during the recent period
- the importance of extratropical forcing on the whole ENSO-monsoon system, with significant precursory signals for AS rainfall stemming from the North Pacific and South IO.

III.4 Perspectives

Our results suggest that the ENSO-monsoon relationship may appear weaker due to an enhancement of local IO processes during AS. But why would these feedbacks be stronger in recent decades? Several hypotheses have been proposed in the literature - such as a more frequent occurrence of extreme IOD events [*Cai et al.*, 2009b; *Ihara et al.*, 2008, 2009], or general changes in ENSO and IOD properties due to global warming - but the causes for such decadal modulations are still to be tested and validated through numerical experiments.

It is faced with this issue that we first decided to confront our results to outputs from a coupled model (the SINTEX-F model described in Appendix A), with the hope of testing our hypothesis on the causes for the weakening of the ISM-ENSO relationship. To do so, we started by examining the ability of the model to reproduce some of our main results regarding ISM teleconnections. Results

from these analyses are shown in Appendix A, and illustrate the existence of a realistic ISM - ENSO relationship in the model's control run, and this during both parts of the monsoon season (*i.e.* in JJ and AS). The model also captures the importance of extratropical sources of forcing for both ENSO and the monsoon, but fails to reproduce the key role played by local processes (in the eastern IO) in the modulation of AS rainfall during El Niño years (*i.e.* the supposed cause for the JJ-AS dichotomy observed during El Niño years, and the key element to our hypothesis of a weakened ENSO-monsoon relationship in recent decades).

Due to the importance of ENSO and of these common extratropical precursors for the monsoon, and based on the model's higher skill in representing the behavior of ENSO (rather than the ISM, see Appendix A), we have decided to examine the importance and robustness of this extratropical forcing on the monsoon-ENSO system *through the window of ENSO variability*.

Chapter 4 of this thesis will thus be focusing more of the interannual variability and predictability of ENSO in both observations and the SINTEX-F coupled model.

Chapter IV

ENSO representation and predictability in observations and in the SINTEX-F coupled model

INTRODUCTION

The ENSO cycle has been at the core of a great deal of studies over the past decades (*e.g.* [*Neelin et al.*, 1998; *Wang and Picaut*, 2004; *Guilyardi et al.*, 2009; *Collins*, 2010] for reviews) and there has been significant progress in understanding, modelling, and predicting El Niño and La Niña events [*Delecluse et al.*, 1998; *AchutaRao and Sperber*, 2002; *Guilyardi*, 2006; *Randall et al.*, 2007]. However, if dynamical and statistical models are generally successful in predicting the peaking and decaying phase of ENSO [*Luo et al.*, 2005c, 2008], their skills are often degraded during the ENSO onset period [*Webster and Yang*, 1992; *Clarke and Van Gorder*, 2003]: this is related to the so-called 'spring predictability barrier'. As an example, most El Niño prediction models failed to predict the excessive growth of the largest 1997-98 El Niño when forecasted from the point prior to its onset in early 1997 [*Barnston et al.*, 1999].

In order to overcome this challenge and bridge this spring prediction barrier, key factors and processes have been identified to have a close relationship with the onset of ENSO events. Among these, two have been quite extensively studied and are now widely recognized as important ENSO predictors during boreal spring: the upper ocean heat content in the tropical Pacific [*Zebiak and Cane*, 1987; *Jin*, 1997; *Meinen and McPhaden*, 2000; *Hasegawa and Hanawa*, 2003; *McPhaden*, 2003], and wind anomalies over the western Pacific and the Indian Ocean warm pool region [*Clarke and Van Gorder*, 2003]. However, the forcing of this low-frequency wind variability is still a matter of debate. Indeed, while some studies seem to emphasize the role of *local air-sea feedbacks* [*Wang and Zhang*, 2002], other works suggest a closer link with *tropical SST anomalies* in the Indian Ocean [*Annamalai and Liu*, 2005; *Kug et al.*, 2005; *Kug and Kang*, 2006; *Luo et al.*, 2010; *Izumo et al.*, 2010] or Atlantic Ocean [*Dommenget et al.*, 2006; *Wang*, 2006b; *Rodriguez-Fonseca et al.*, 2009]. Recently, there have also been suggestions that these western Pacific winds may result from *midlatitude* atmospheric variabilities, in the North Pacific [*Vimont et al.*, 2001, 2003a, 2009], or in the South Atlantic or Indian Oceans [*Terray*, 2011]. Finally, interactions with other time scales have also been suggested, such as a possible influence from intraseasonal westerly wind bursts or the Madden Julian Oscillation over the western Pacific [*McPhaden*, 1999; *Lengaigne et al.*, 2004; *Kug et al.*, 2008, 2010].

Altogether, these various studies give rise to prospects of higher predictability of ENSO events. However, so far it is not clear how all these precursors are related to each other and how effectively each of them may impact ENSO *independently of the others*. The aim of this work is to attempt to *unite* these different precursors in a single conceptual framework, as to assess their role in ENSO onset and development.

In Part I, we will assess if a fully global coupled model is able to properly simulate these remote teleconnections and their potential impacts on ENSO variability. To this end, the Singular Value Decomposition (SVD) method will be used to identify and compare leading modes of covariance, which may carry important information relevant to ENSO in both observations and the SINTEX-F coupled model[1]. The description of the model used in this work is given in Appendix A, and the SVD methodology is briefly detailed in Appendix B.

Our results will be analyzed in terms of:

- the capacity of the model to reproduce observed behaviour
- and the implication of these determined covariabilities for the potential long-range predictability of ENSO.

Note that an article has been written in relation to these results, and submitted to the Geophysical Research Letters journal (see Appendix C).

Finally, in Part II of this chapter, numerical experiments will be carried out with the SINTEX-F model, in order to examine the respective role of these precursors, and test their robustness as ENSO predictors.

[1] As a reminder, these covariabilities are examined at the *interannual* timescale, *i.e.* with anomalous fields which have been pre-filtered with the STL methodology (see Appendix B or [*Boschat et al.*, 2011a] for further detail)

PART I

ENSO predictability in observations and the SINTEX-F coupled model

IV.1 Introduction

According to many studies, the crucial set of information for ENSO forecasts is the spatial variation of the thermocline depth (or heat content), and the structure of low-frequency wind variability in the tropical Pacific Ocean. The aim of this section is first to test the representation of ENSO in the SINTEX-F model, by examining these conventional predictors (heat content and low-frequency wind) and comparing their relationship with Pacific SSTs several months after, in the model and in observations (step ① in Fig IV.1).

The question of what may modulate this low-frequency wind variability during boreal spring will then be addressed in a second part, by exploring the possible role of precursory SST signals in tropical and extratropical regions (step ② , Fig IV.1).

Finally, in a last part we will examine the performance of these selected SST modes in predicting ENSO via wind modulation or other physical processes. More precisely, we will try to compare the relative role of these SST precursors and determine whether they provide additional or more efficient information than the conventional heat content or wind predictors for the forecast of ENSO events. This may suggest the existence of other predictability sources, not restricted to the wind variability over the western Pacific. This last part is a focal point in the larger issue of ENSO predictability (step ③ , Fig IV.1).

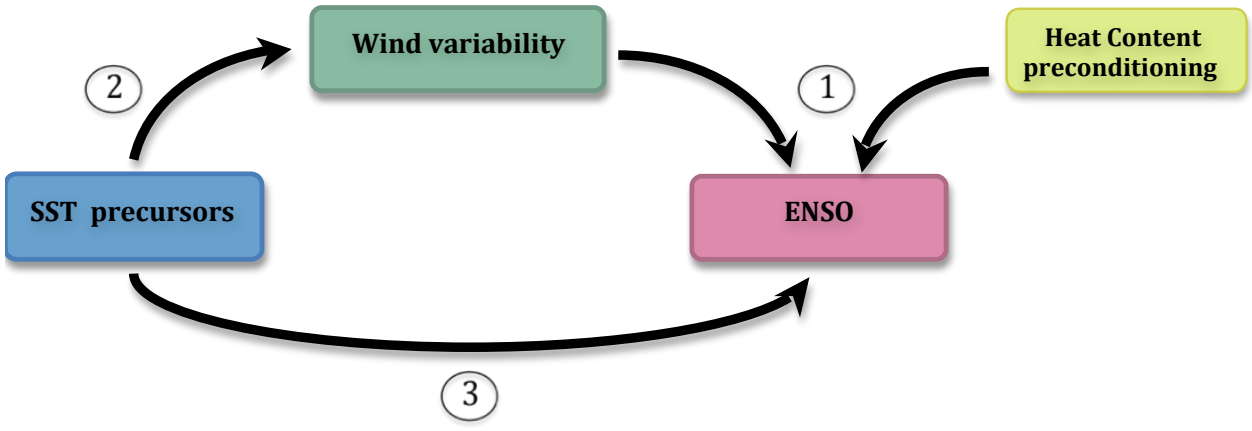

Figure IV.1: Schematic view of the analysis of ENSO predictability in this section.

IV.2 Conventional ENSO predictors

IV.2.1 Heat content preconditioning in the tropical Pacific

The role of the tropical Pacific heat content, initially suggested by [*Wyrtki*, 1985] is now widely recognized under the framework of the recharge oscillator [*Jin*, 1997]. Although disputed by *Kessler* [2002] among others, this oscillatory paradigm of ENSO stipulates that the build up of warm waters in the western Pacific is a necessary precondition for the development of an El Niño event. At the simplest level, warm surface water is accumulated in the western Pacific prior to the onset of an El Niño, and then propagates eastward along the equator first in the form of Kelvin waves to give birth to an El Niño event. Once this El Niño approaches maturity, the excess of equatorial warm waters is redistributed or "discharged" towards higher latitudes, leading to the end of the event and a transition to an opposite La Niña phase. The resulting cooler area then has to "recharge" warmth from the subtropics for several years before another El Niño event can take place.

The depth of the 20°C isotherm (Z20) is used here as a proxy of the thermocline depth or heat content in the tropical Pacific. In order to examine the relationship between ENSO and heat content at the interannual timescale, a SVD analysis is performed between spring Z20 anomalies (from January to March, JFM) and winter SST anomalies 7 months later (from October to the following February, ONDJF hereafter), in the whole tropical Pacific. These two seasons have been selected since *(i)* El Niño and La Niña events typically start in boreal spring and peak in boreal winter [*Rasmusson and Carpenter*, 1982], *(ii)* there is no spring persistence barrier for upper ocean heat content (see Fig. 2 of [*McPhaden*, 2003]). This strong phase-locking feature of Pacific SSTs is well illustrated in Fig IV.2, which shows the evolution of the Niño3.4 SST monthly standard deviations over the 1870-2007 period.

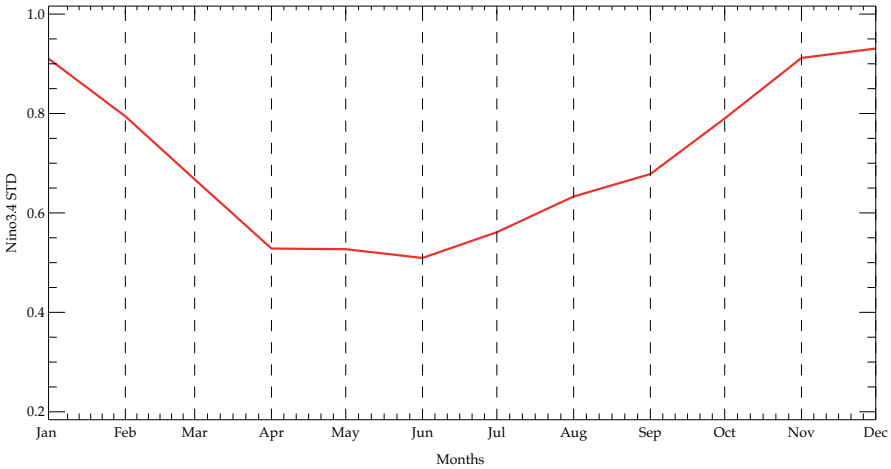

Figure IV.2: Evolution of Niño3.4 monthly standard deviation values in observations (1870-2007).

In the SVD analysis, the comparison with observations is made over the 1989-2007 period, using SST anomalies from the HadISST dataset [*Rayner et al.*, 2003], and Z20 anomalies from a DRAKKAR forced simulation (ORCA oceanic model at $\frac{1}{4}$°horizontal resolution, forced by ERA-interim winds during the 1989-2009 period). This ocean forced simulation will be frequently referred to as 'observations' in the text of this thesis. Note however that similar results are obtained with oceanic reanalyses such as SODA and ECMWF (ORA-S3 product).

Results from this analysis are shown in Fig IV.3, respectively, for the model (a-b) and observations (c-d), in terms of the spatial structures (or homogeneous maps) associated with the first leading SVD mode: in both cases, this mode accounts for most of the covariability between the two fields (see Appendix B). The statistics for these SVDs are also summarized in Table IV.1 for the first two leading modes, as useful tools for assessing and comparing the strength of the relationship in the model (blue values) and in observations (red values). Shown here are the squared covariance fraction (SCF) for each mode, and the correlation coefficient (r) between the expansion coefficient time series of both fields. The SCF is a first simple measure of the relative importance of each mode in the relationship between the two fields, while r values indicate how strongly related the coupled patterns are [*Zhang et al.*, 1998]. The two following columns indicate how much of the Z20 or SST field variance each SVD mode is able to explain. Finally, the correlation between each mode's expansion coefficient time series and the Niño3.4 SST index averaged in the following December-January season is given in the last column, as an indication of the potential predicting skill of these SVD modes for the following ENSO event. We will be particularly interested in these two last columns (%SSTvar and Cor Niño3.4) for our study of ENSO predictability.

SVD		SCF (%)		r		Z20 var (%)		SST var (%)		Cor Niño 3.4	
Z20 (JFM)	m1	87.1	95.5	0.57	0.91	25	42.6	63.8	80.6	**0.56*** **	**0.90*** **
	m2	10	3.6	0.52	0.86	20.9	15.4	10.8	9.5	0.01	-0.21

* **P**<0.1, ****P**<0.05, *****P**<0.005

Table IV.1: Results from SVD analysis between 20°C isotherm depth (Z20) anomalies in JFM and SST anomalies in ONDJF (7 months later) in the tropical Pacific Ocean ([140°E-80°W,20°S-20°N] for Z20 and [120°E-80°W,15°S-15°N] for SST). The statistics are given for the first 2 leading modes of the SVD computed separately for SINTEX-F control run (in blue) and observations (in red).

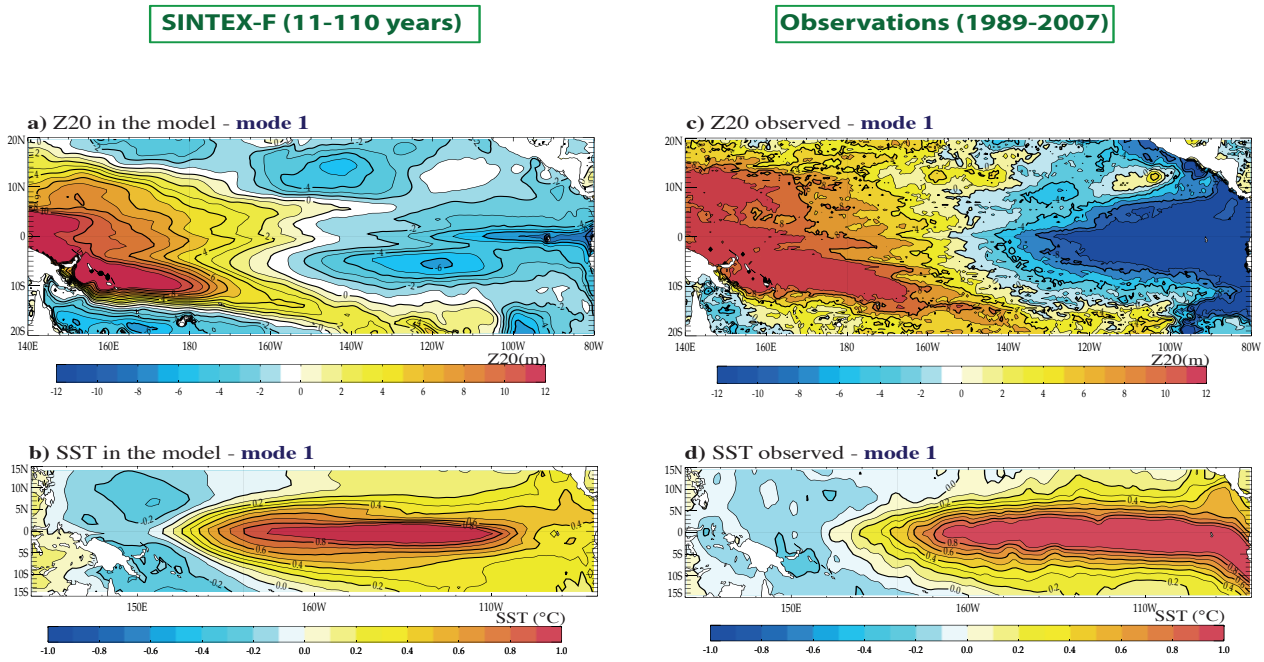

Figure IV.3: Z20 and SST homogeneous maps (**a-b** respectively in the model, and **c-d** in observations) associated with the 1^{st} SVD mode between Z20 anomalies in JFM and SST anomalies in ONDJF (7 months later) in the tropical Pacific Ocean ([110°E-70°W,20°S-20°N] for Z20 and [140°E-80°W,15°S-15°N] for SST).

A first interesting result is that, overall, the model seems to reproduce reasonably well the phase relationship observed between the two fields, as the various statistics in Table IV.1 are consistent, and both the simulated SST and Z20 spatial patterns are very similar to observations (Fig IV.3). Indeed, the Z20 pattern both in the model (Fig IV.3a) and in observations (Fig IV.3c) represents an East-West tilting mode with the axis near 16O°W, very close to that described in previous observational studies [*Meinen and McPhaden*, 2000]. This pattern is marked by positive Z20 anomalies in the west tropical Pacific in spring, while the corresponding SST pattern illustrates a typical El Niño peak phase during the following winter (Fig IV.3b and d), with warm SST anomalies prevailing in the central Pacific (slightly shifted west compared to observations), and flanked by cold anomalies in the far west. The Hovmöller time-longitude plot of Z20 anomalies regressed onto this 1^{st} SVD mode, displayed in Fig IV.4, illustrates the eastward propagation of warm surface water along the equatorial Pacific, from JFM to the following winter, with a slightly slower propagation speed in the model (approximately 46 cm/s in Fig IV.4a) compared to observations (48 cm/s in Fig IV.4b). These elements captured by the 1^{st} SVD mode are thus consistent with the recharge oscillator theory, or, at least, with the predicting potential of heat content in the context of ENSO forecasting.

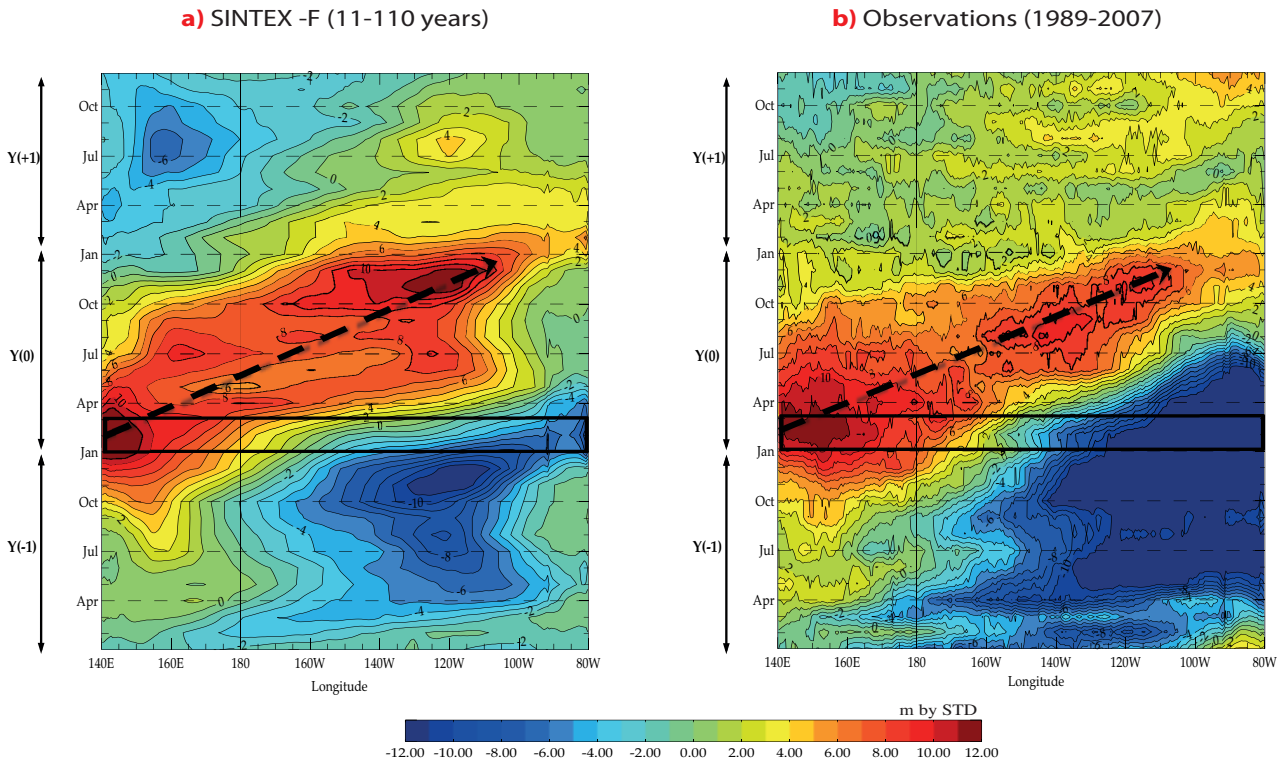

Figure IV.4: Time-Longitude Hovmöller plot of 20°C isotherm depth (Z20) anomalies in the equatorial Pacific, regressed onto the Z20 expansion coefficient time series of the 1^{st} SVD mode between (Z20-SST), from the previous to the following year, in the model **(a)** and in observations **(b)**.

Moreover, results from Table IV.1 also confirm that Z20 anomalies during boreal spring are strongly correlated with SST anomalies in the tropical Pacific during the following winter (r=0.57 and 0.91 for mode 1 in the model and in observations, respectively), and that the 1^{st} mode is able to recover a significant fraction of the Z20-SST covariance matrix (87.1% for the model and up to 95.5% for observations). This 1^{st} SVD mode also accounts for a significant 63.8% of tropical Pacific SST variance during winter in the model (against 80.6% in observations). Consistently, the Z20 expansion coefficients are strongly correlated with the Niño3.4 SST time series in December-January, although this correlation value is substantially higher in observations, with a significant correlation of 0.56 in the model and 0.90 in observations (see Table IV.1). This very high value in the observations may be linked to the very short period used for computing the SVD from observations and the occurrence of the intense 1997-98 El Niño event *in* this short time period.

Altogether, these SVD results confirm, without any ambiguity, the existence of a significant link between Z20 anomalies in spring and SST anomalies during the following winter in the tropical Pacific, and thus highlight the importance of a local heat content preconditioning for ENSO in both observations and the model.

SVD results obtained with the 2^{nd} mode will not be detailed here, as this mode accounts for a much weaker portion of the Z20-SST covariability (only 10% in the model, and 3.6% in observations), and most importantly, the weak correlation obtained with the Niño3.4 SST index in both the model and observations suggests that this 2^{nd} mode has no significant predicting skills for the following ENSO variability (see Table IV.1).

IV.2.2 Zonal wind stress anomalies in the western Pacific

To examine the impact of low-frequency wind variability on ENSO, we perform a similar type of SVD analysis between zonal wind stress (USTR) anomalies during boreal spring (from February to April, FMA), before ENSO onset, and SST anomalies during the following winter (in ONDJF) in the tropical Pacific domain. Sensitivity analyses have been performed with the precursors taken successively in JFM, FMA or from March to April and for each case, we have chosen the season which offers the best predicting skill for the following ENSO (*e.g.* the FMA season in the case of the USTR precursor). The comparison with observations is made using the ERA-40 wind stress from 1979 to 2001 [*Uppala et al.*, 2005]. Results are shown in terms of homogeneous maps for each field (Fig IV.5), and SVD statistics are summarized in Table IV.2 for the first two leading modes of covariability, separately for the model, and observations.

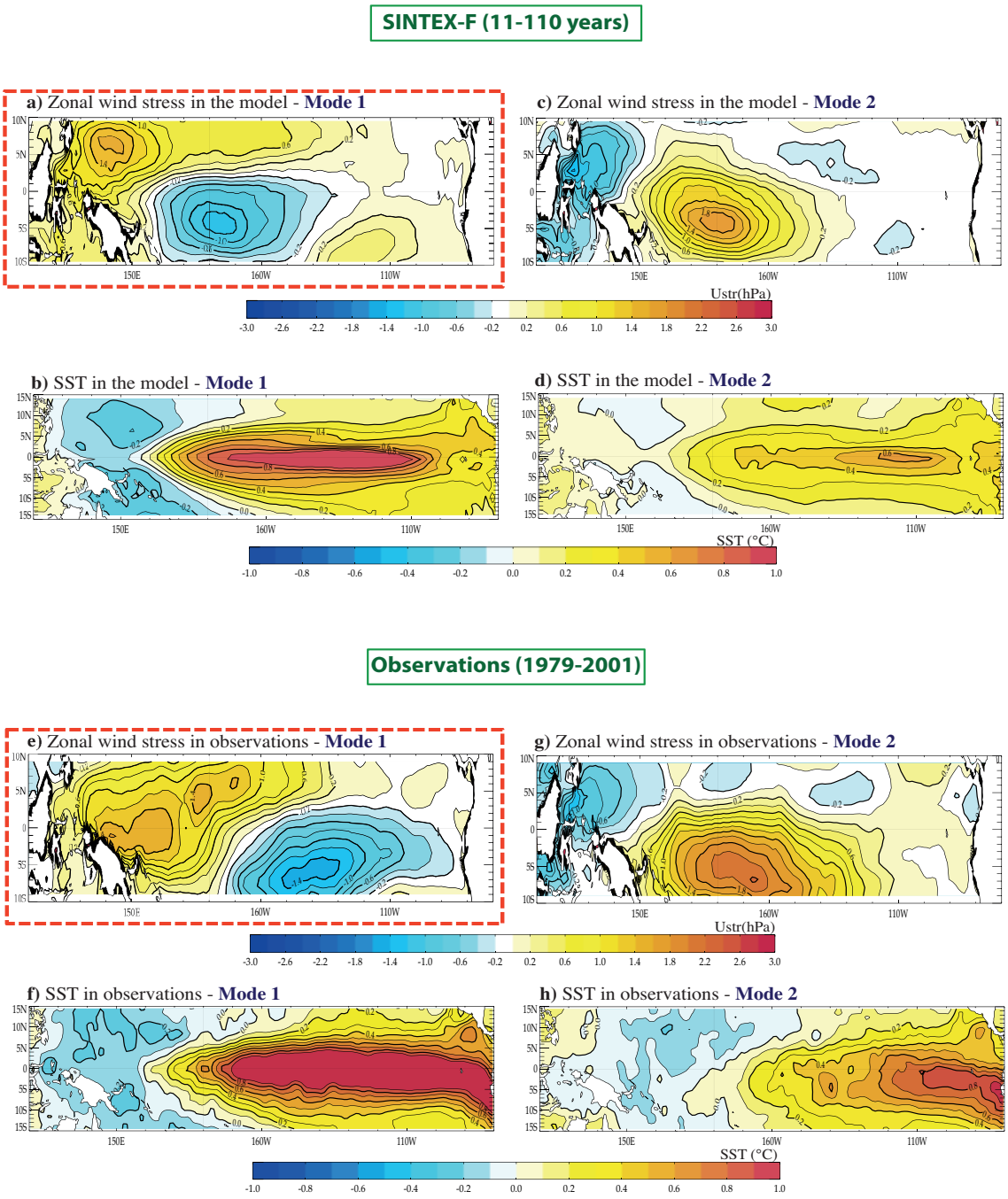

Figure IV.5: Zonal Wind Stress (USTR) and SST homogeneous maps associated with the 1^{st} *(left panels)* and 2^{nd} *(right panels)* SVD modes between USTR anomalies in FMA and SST anomalies in ONDJF in the tropical Pacific Ocean ([110°E-70°W,10°S-10°N] for USTR and [120°E-80°W,15°S-15°N] for SST), separately in the model **(a-d)** and in observations **(e-h)**.

SVD		SCF (%)		r		Ustr var (%)		SST var (%)		Cor Niño 3.4	
Ustr (FMA)	m1	84.9	91.9	0.53	0.67	21.5	32.9	67.1	75.9	0.54***	0.72***
	m2	11.6	6.2	0.60	0.60	20.8	34.8	7.3	5.9	0.03	0.07

* P<0.1, **P<0.05, ***P<0.005

Table IV.2: Results from SVD analysis between Zonal Wind Stress (USTR) anomalies in FMA and SST anomalies in ONDJF (6 months later) in the tropical Pacific Ocean ([110°E-70°W,10°S-10°N] for USTR and [120°E-80°W,15°S-15°N] for SST). The statistics are given for the first 2 leading modes of the SVD computed separately for SINTEX-F control run (in blue) and observations (in red).

Altogether, results show that SST variability during boreal winter in the tropical Pacific is also closely related to the spatial structure of zonal wind anomalies over the western and central tropical Pacific during the previous boreal spring, and that the model is able to reproduce very well the lagged relationship observed between the two fields. Indeed, in Table IV.2, the coupling between the two fields is strong for both of the leading SVD modes (with r>0.53 in the model and observations), although the 1^{st} mode captures most of this wind-SST covariability (with over 84% of SCF in the model and observations) and is able to explain most of the tropical Pacific SST variance during winter (see the SSTvar column in Table IV.2).

In Fig IV.5, this 1^{st} SVD mode is characterized by a dipole structure of zonal wind stress anomalies reflecting a convergence of zonal wind in the western part of the basin, with the strongest positive anomalies in the far west between 0°-10°N and negative anomalies near the dateline and just south of the equator (note that the centre of this dipole is shifted slightly west in the model (a) compared to observations (e)). This positive westerly wind signal has been suggested as a possible trigger of El Niño onset, as it can induce eastward-propagating equatorial downwelling Kelvin waves along the thermocline (see Fig IV.4), leading to a significant surface warming in the central and eastern equatorial Pacific several months later [*Chang et al.*, 2006]. The time-longitude evolution of SST anomalies regressed onto this 1^{st} mode, shown in Fig IV.6a, illustrates this surface warming along the equatorial Pacific, with positive SST anomalies appearing 3 to 4 months after the zonal wind forcing in FMA (marked by the black box in Fig IV.6). In line with these previous findings, our SVD analysis shows that these westerly wind anomalies in spring are well associated with an ENSO-like pattern of variability during the following winter (Fig IV.5b and f). This winter pattern also closely resembles the SST pattern in Fig IV.3b and d, which adds to the physical coherence of the SST homogenous maps, and more generally illustrates the close relationship between heat content, wind and SST variability usually observed in this region at the interannual timescale. In the model, this 1^{st} SVD mode accounts for a significant 67.1% fraction of the SST variance in winter (75.9% in observations), in line with the high 0.54 correlation obtained with the Niño3.4 index (0.72

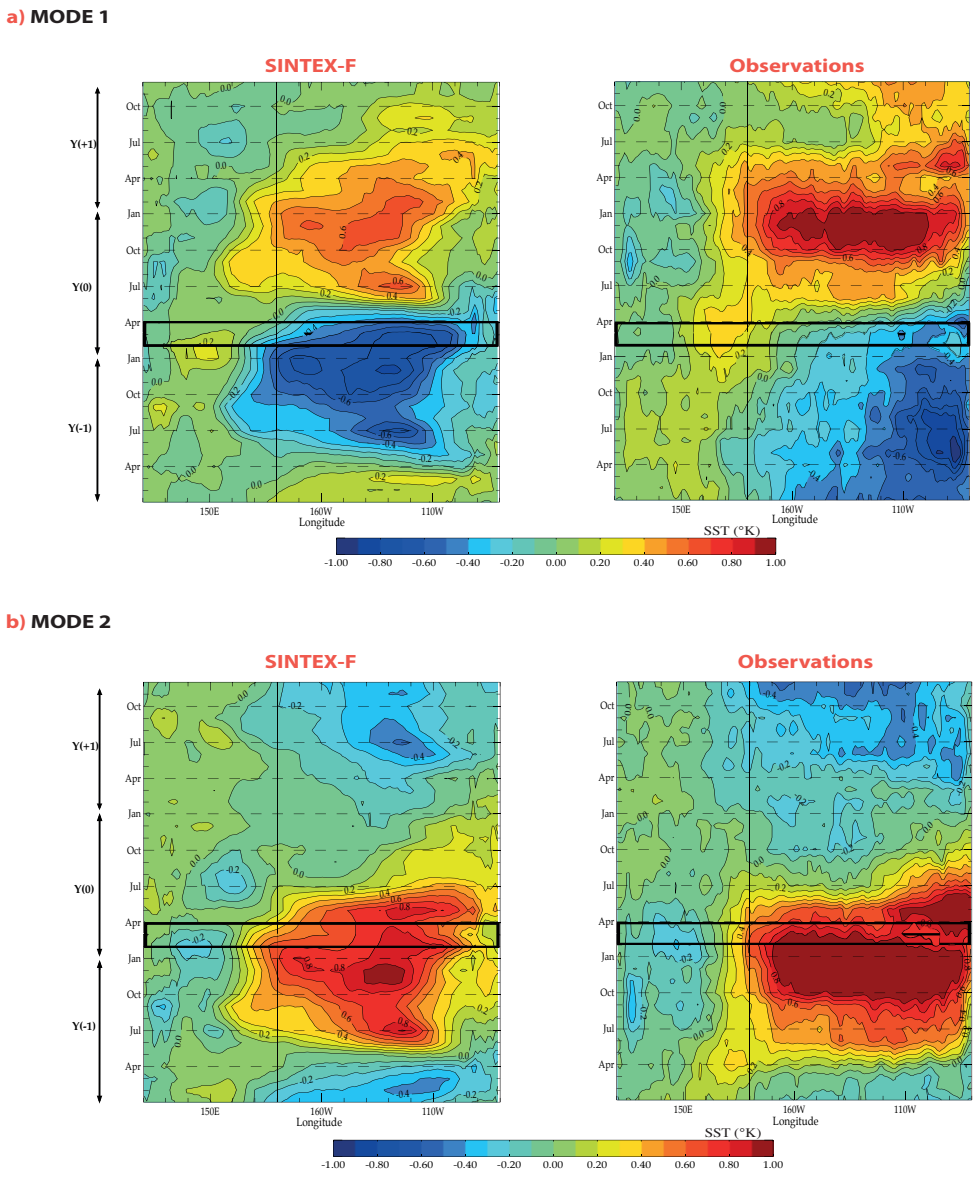

Figure IV.6: Time-Longitude Hovmöller plot of SST anomalies in the equatorial Pacific, regressed onto the USTR expansion coefficient time series of the 1^{st} **(a)** and 2^{nd} **(b)** SVD modes between (USTR-SST), from the previous to the following year, in the model *(left panels)* and in observations *(right panels)*. The black box in these plots represents the 0 lag between SST anomalies and the zonal wind stress pattern (in FMA, see Fig IV.5)

in observations, see Table IV.2). These statistics for the 1^{st} mode in the model are comparable to results in Table IV.1, suggesting an equivalent role in terms of ENSO predictability for heat content and wind variability during spring. However, in observations, the predicting scores obtained with Z20 are substantially higher than those associated with zonal wind anomalies.

The 2^{nd} SVD mode from this analysis accounts for a lower 11.6% of SCF in the model (only 6.2% in observations), and yields no significant predicting skill for the following ENSO (weak correlation with the Niño3.4 index in Table IV.2). Nevertheless, it seems interesting to note that the correlation between the wind and SST expansion coefficients time series for this 2^{nd} SVD mode is slightly stronger than for the 1^{st} mode (r=0.60 compared to 0.53 in Table IV.2).

Another intriguing feature is that, in both the model and observations (Fig IV.5c-d and g-h), this 2^{nd} mode is also related to an El Niño-like SST pattern (although weaker), but preceded this time in spring by *positive* wind stress anomalies below the equator and *negative* in the far west Pacific: this relationship is thus opposite to the 1^{st} SVD mode! In order to understand the physical meaning of this mode and compare the coupled processes linked to these two wind patterns (*i.e* modes 1 and 2), we have examined carefully the SST anomalies associated with each mode through regression analyses. Fig IV.6 shows the evolution of SST anomalies regressed onto the 1^{st} (a) and 2^{nd} modes (b) in the form of time-longitude Hovmöller plots from the year preceding to that following the wind forcing in FMA, separately for the model and observations. Overall, this figure shows distinct SST patterns for modes 1 and 2, in both the model and observations, which suggest that the two previous wind patterns are linked to very different SST evolutions in the equatorial Pacific. Indeed, if we start by focusing on the synchronous FMA period (see black box in Fig IV.6a-b), we can notice that the wind patterns are associated with opposite SST conditions east of the dateline for modes 1 and 2. The 1^{st} mode in Fig IV.6a illustrates a potential *forcing* of wind variability during spring on the onset of an El Niño event in June, as well as the transition from previous La Niña to El Niño conditions (or vice versa for an opposite wind anomaly pattern). However, for the 2^{nd} mode, the ENSO phase transition is less evident and the wind pattern seems to be more significantly linked to the decaying phase of an El Niño event (Fig IV.6b). This is further demonstrated in Fig IV.7, which shows Indo-Pacific SSTs regressed onto the USTR expansion coefficient time series of this same 2^{nd} mode. The remnant warm SST signal here persists until the following summer (season not shown), and evokes the occurrence of long-lasting El Niño episodes in both observations and the model: the wind pattern in this case may thus appear as a *result* of the previous ENSO phase. This hypothesis is consistent with the weak predictability associated with the 2^{nd} mode in Table IV.2 (last column).

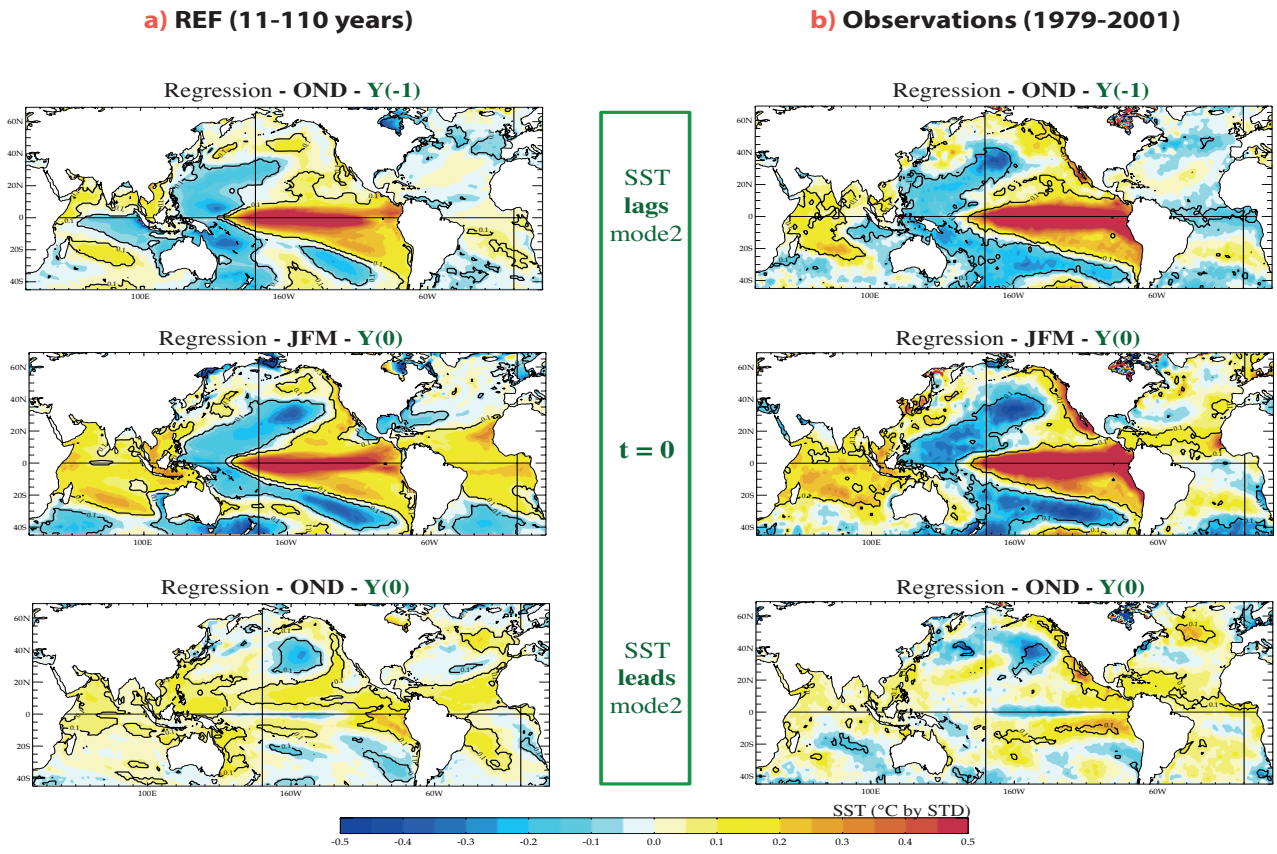

Figure IV.7: Lagged regression of Indo-Pacific SST anomalies onto the USTR expansion coefficient time series of the 2^{nd} SVD mode between (USTR-SST), from the previous to the following boreal fall, in the model **(a)** and in observations **(b)**.

Overall, this analysis thus highlights the importance of the wind pattern associated with the 1^{st} mode for ENSO predictability (framed in red in Fig IV.5a and e). This 1^{st} mode reflects a rather biennial tendency of ENSO in both the model and observations, although it has been noted in the literature that El Niño events tend to be more often followed by La Niña events than the opposite. We will need to bear in mind this assymetric tendency of ENSO variability (*i.e.* that ENSO variability does not operate in a symmetrical way), and the predicting paths we are exploring will need to be examined separately for El Niño and/or La Niña events. This will be done in Section 3.

IV.2.3 Conclusion

Altogether, the two SVD analyses presented in this section have shown that

- both heat content preconditioning and low-frequency wind variability in the western Pacific in boreal spring are key elements related to the onset and development of ENSO, as they appear as leading modes of covariability between the two fields
- and that the model is overall successful in reproducing the space and time covariability between ENSO and these *conventional* precursors.

Our results suggest that these two factors are both *statistically* important for ENSO prediction in the model, although maximum predicting score is obtained with heat content (especially in observations). However we need to bear in mind that they may come into play at different (time and spatial) scales. Indeed, the positive Bjerknes feedback between westerly wind anomalies in the western Pacific and warm SST anomalies in the tropical Pacific can provide the necessary instability for an El Niño to develop. However, favourable grounds are also needed for this coupled feedback to result in an El Niño event several months later: hence the key importance of heat content preconditioning in the tropical Pacific region. Each precursor by itself is a *necessary* but not sufficient condition for El Niño onset.

Assuming that the necessary heat content background conditions are met, the next question that we need to address now is: what exactly *forces* this low-frequency wind variability from boreal fall to spring over the western-central Pacific?

IV.3 Interannual forcing of zonal wind anomalies in the tropical Pacific

In the following subsection, we will be focusing on low-frequency wind variability in the western Pacific [*Clarke and Van Gorder*, 2003; *Kug and Kang*, 2006], and comparing the impact of different forcing sources which have been identified in tropical and extratropical regions.

IV.3.1 A potential set of new ENSO precursors

For many years, studies on ENSO predictability focused on the role played by air-sea interactions occurring *within* the tropical Pacific basin itself, before ENSO onset. As an illustration, *Weisberg and Wang* [1997] argued that the western Pacific wind variability during boreal spring was mainly driven by local SST directly related to ENSO, thereby according the most predicting power to the **previous state of the tropical Pacific** and the biennial tendency of ENSO.

However, there has been growing evidence in the literature, that other tropical and extratropical regions may also influence this wind variability in the western Pacific, and therefore may also be playing an important role in ENSO onset and development. A few of these potential forcings, those operating at the interannual timescale, are described here, along with the mechanisms which have been proposed to explain their influence on ENSO.

A large number of studies have focused on the remote impact of the tropical IO on ENSO. *Yu et al.* [2002] and *Wu and Kirtman* [2004] found that tropical IO SSTs affect ENSO through the modulation of the Pacific and IO Walker circulations in their coupled simulations. *Kug et al.* [2005] and *Kug and Kang* [2006] also found indications in observations that IO SST anomalies shorten the duration of El Niño events, and lead to faster ENSO transitions. Their results rely on the existence of a strong interactive feedback between the IO and ENSO, and highlight the importance of the IO warming which follows most El Niño events **during boreal spring**, otherwise known as the Indian Ocean Basin (**IOB**) mode. This IO warming persists, and produces easterly wind stress anomalies, which propagate eastward into the western Pacific region during the decaying phase of El Niño. The wind anomalies then generate oceanic upwelling Kelvin waves, which tend to accelerate the decay of warm SST in the eastern Pacific and thus fasten the transition to opposite La Niña conditions.

More recently, *Luo et al.* [2010] and *Izumo et al.* [2010] stressed the importance of the Indian Ocean Dipole (**IOD**) mode **during boreal fall**, and its potential skill in predicting ENSO 14 months before its peak. The mechanism proposed by *Izumo et al.* [2010] to explain the impact of the IOD on the Pacific is summarized in Fig IV.8 below.

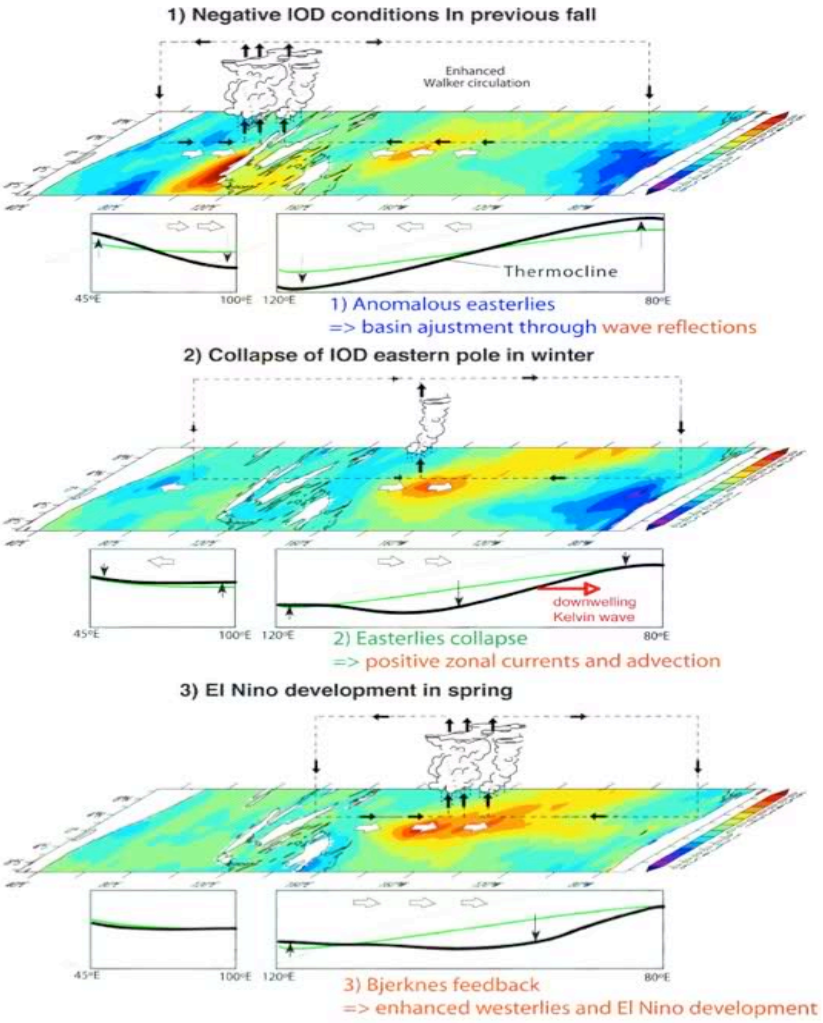

Figure IV.8: Schematic illustration of how the previous year IOD conditions can trigger ENSO, from [*Izumo et al.*, 2010].

Meanwhile, there has also been growing interest in the importance of extratropical climate modes for ENSO.

In recent works, *Terray et al.* [2005a], *Terray and Dominiak* [2005] and *Terray* [2011] emphasized the role of mid-latitude coupled variability in the Southern Hemisphere, particularly in the South IO (**SIO**) during **late boreal winter**. This subtropical forcing is shown to operate through various coupled feedbacks involving the propagation of subtropical SST anomalies into the tropics from boreal winter to spring, following the occurrence of subtropical dipole events in the southern Indian Ocean [*Behera and Yamagata*, 2001]. The weakened InterTropical Convergence Zone (ITCZ) induced by these SST anomalies, can force an equatorial cold Kelvin wave response over the equatorial Indo-Pacific region in the upper atmosphere. These cold upper anomalies then rapidly spread to the western Pacific and destabilize the local atmospheric column. This gives very favourable large-scale conditions to trigger local convection and promote westerly wind anomalies at the surface, and, subsequently, El Niño onset a few months later.

Finally, it has also been suggested that the extratropical North Pacific region may have a significant influence on ENSO [*Vimont et al.*, 2001, 2003a, 2009; *Chang et al.*, 2007; *Alexander et al.*, 2010]. These studies imply a connection between the mid-latitude and tropical Pacific, whereby the **winter** atmospheric variability in the North Pacific (**NPO**) impacts tropical zonal wind anomalies during boreal spring. Fig IV.9 below illustrates the "Seasonal Footprinting Mechanism" which was proposed to explain the potential forcing of the North Pacific Ocean on ENSO. In this scenario, the mid-latitude atmospheric variability during boreal winter can impart a SST "footprint" onto the ocean via changes in the net surface heat flux (Step A). The subtropical portion of this SST footprint is able to persist into late boreal spring and summer by various feedbacks, and forces an atmospheric circulation that includes zonal wind stress anomalies in the equatorial western Pacific, which may be responsible for exciting subsequent El Niño events (Step B).

Altogether, these studies thus suggest that potential sources of ENSO forcing may exist outside of the tropical Pacific ocean, in various regions of the globe and with an influence spanning over a large time frame: from the previous boreal fall to a few months before ENSO onset in boreal spring. However, these possible predicting paths have never really been compared in detail in the literature, and several open questions remain regarding the robustness and relative importance of each of the mechanisms involved in these forcings.

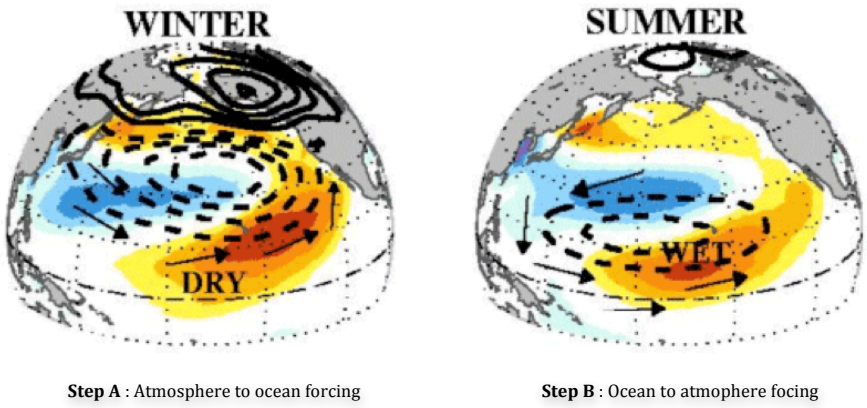

Figure IV.9: Schematic illustration of the 'Seasonal Footprinting Mechanism'. Contours denote SLP anomalies, red (blue) shadings denote positive (negative) SST anomalies, vectors denote wind stress anomalies, and text indicates anomalous precipitation, from [*Vimont et al.*, 2001].

(i) *First of all, does the extratropical forcing occur in each case through a modulation of tropical wind variability in the western Pacific? If so, what is the spatial structure and the amplitude of wind anomalies that are produced by each source of forcing during boreal spring?*

(ii) *The next question, which we need to address, is whether these various teleconnections are* independent *means of forcing the local wind variability over the western Pacific?* Indeed, the interannual climate modes mentioned here interact in a quite complicated manner with ENSO and with one another, particularly in the tropical IO. Therefore, it seems important to discern the specific effects of each potential precursor. For instance, are the wind anomalies observed in spring generated only a few months earlier by basinwide IO SST anomalies (*i.e.* IOB mode) or is this signal essentially due to the occurrence of an IOD event during the previous boreal fall? Are these two effects complementary? Or does this forcing simply result from the interaction of various tropical and extratropical modes?

(iii) *And finally, what are the implications in terms of ENSO prediction for each of these modes?*

In an attempt to answer these various questions, we have here gathered in a single conceptual framework, some of the main sources of ENSO forcing proposed in the recent literature, in the tropical IO (*e.g.* IOB or IOD modes) and in extratropical regions of the South IO (SIO mode) or North Pacific Ocean (NPO mode). The spatial domains and peaking seasons used to define these potential precursors are detailed in Table IV.3. Our aim is to evaluate the efficiency of the climate anomalies observed in these key regions in predicting ENSO onset, first through a forcing of zonal wind variability, particularly in the western tropical Pacific during late boreal winter and early spring

(*i.e* FMA), e.g. before or at El Niño onset.

Precursor (name and reference)		SST spatial domain	SLP spatial domain	Temporal definition
ENSO(-1)		120°E-280°E, 15°S-15°N	same as SST	ONDJF (Y-1)
IOD (Saji et al., 1999)	*Full region*	50°E-110°E, 10°S-10°N	same as SST	SON (Y-1)
	West pole	50°E-70°E, 10°S-10°N	same as SST	
	East pole	90°E-110°E, 10°S-0°	same as SST	
IOB (Yang et al., 2007)		40°E-110°E, 20°S-20°N	same as SST	JFM
SIO (Terray 2011)		25°E-150°E, 0°-50°S	25°E-150°E,10°S-50°S	JFM
NPO (Vimont et al., 2003)		110°E-270°E, 0°-50°N	110°E-270°E, 0°-90°N	JFM

Table IV.3: Spatial and temporal definitions of the various SST and SLP indices, which have been suggested to play a significant role in the onset of ENSO.

Finally, we need to bear in mind that ENSO also affects climate anomalies in each of the regions defined above, through the atmospheric bridge mechanism [*Lau and Nath*, 2000; *Alexander et al.*, 2002; *Lau and Nath*, 2003] or by inducing westward-propagating oceanic Rossby waves (*e.g.* in the South IO, see [*Xie et al.*, 2002]). Therefore, the SST signal observed in these key regions may combine SST anomalies *resulting* from the previous ENSO state as well as SST anomalies produced by other phenomena, particularly in the extratropics. We are particularly interested in extracting this second part of the signal as this contribution represents an effective and independent *forcing* on the following ENSO event. In order to ensure that the seasonal relationships are independent from the ENSO variability that may have occurred during the preceding winter, most studies removed or 'filtered' the previous ENSO signal from their initial data, by using simple linear statistical methods such as partial regression analysis. However, important climate modes such as IOD events have a tendency to co-occur with ENSO. Therefore, by simply removing this ENSO signal by statistical methods on short periods, we take the risk of losing portions of climatic signals correlated to ENSO, but not physically linked to it, and which may carry significant weight for ENSO predictability. In order to sidestep these statistical limitations and avoid any loss of information for ENSO predictability, we have decided to keep the entire ENSO signal in our data, and have tried instead to separate these mixed SST signals 'more objectively' by considering systematically different SVD modes (and testing different domains) in our analysis. This strategic choice has proved to be quite successful in extratropical regions (SIO and NPO modes), where we tested various spatial domains for our SVD computations, and finally managed to separate in two different SVD modes: the SST signal forced by ENSO, from a signal reflecting a more intrinsic source of SST variability in these regions. However,

this separation was more difficult in the tropical IO, as we will see.

Finally, to account for the effect of the previous ENSO state still present in our SST signals and to further test the robustness of the proposed precursors, we have decided to consider ENSO as an independent source of forcing during the preceding boreal winter (ENSO(-1) precursor in Table IV.3) and examined its impact on wind variability during the next boreal spring, and its predicting skill for the following ENSO event. This ENSO(-1) mode will serve as a ***benchmark*** for our entire study of ENSO predictability, as the relevance of the other ENSO precursors will always be evaluated in comparison with ENSO(-1).

IV.3.2 Impact of these SST precursors on Zonal Wind Stress

In the following section, SVD analyses are performed between each SST and SLP precursor (during its peaking season, defined in Table IV.3) and zonal wind stress anomalies during the following boreal spring in FMA, in order to compare the relative impact of each precursor on tropical wind variability and assess its respective weight in ENSO forecasting.

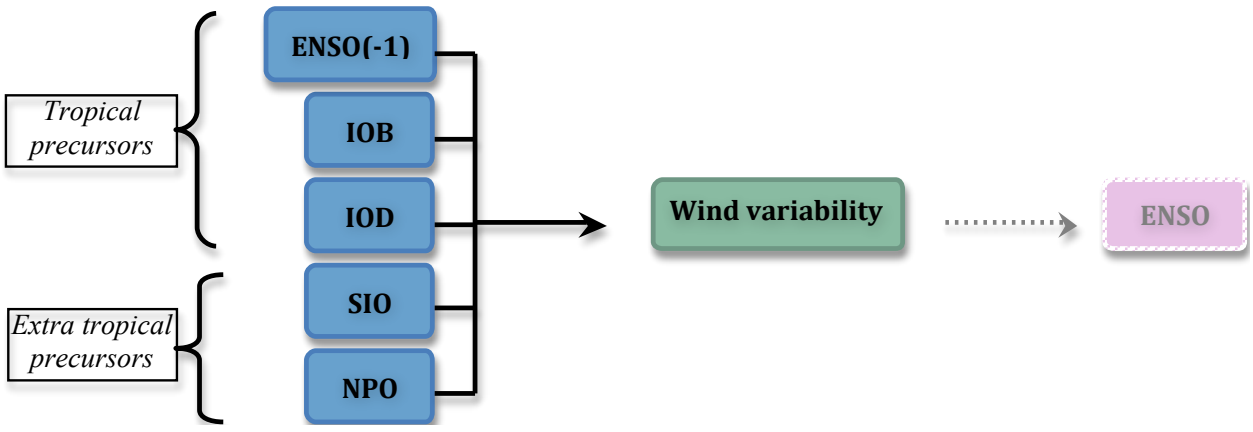

Figure IV.10: Relative impact of the selected precursors on wind variability in the tropical Pacific.

These analyses are conducted in parallel for the model and observations, and results are shown here for SST precursors and for the most dominant SVD modes, in terms of the spatial patterns for each field (SST and zonal wind) and corresponding statistics in Table IV.4.

a - A first overview of the SVD statistics

Overall, results in the model and in observations show that all the SST precursors considered here are significantly coupled with zonal wind stress anomalies in FMA in the tropical Pacific (with a correlation of r>0.5 between the leading SVD modes of the two fields in most cases). The 1^{st} SVD mode captures most of this SST-wind covariability and explains in each case a significant and quite comparable portion of zonal wind stress variance during boreal spring (approximately 30% in the model, and near 35% in observations). However, the last column in Table IV.4 shows that this 1^{st} mode is not always strongly correlated with the following Niño3.4 SST index (e.g. NPO mode), which incites us to also examine the predictability offered by the higher modes, especially the 2^{nd} SVD mode. In many cases, this 2^{nd} SVD mode, while describing less zonal wind stress variance over the equatorial Pacific (see Table IV.4), also obtains very promising correlation scores with the Niño3.4 SST index (up to 0.69 for observations and 0.53 for the model), similar to those obtained directly between zonal wind stress during FMA and tropical Pacific SSTs during ONDJF (0.72 and 0.54 for observations and model, respectively; see Table IV.2).

SVD		SCF (%)		r		SST var (%)		Zonal wind Stress var (%)		Cor Niño 3.4	
ENSO(-1)	m1	97.6	91.9	0.88	0.88	69.5	79.7	30.1	37.9	0.27*	0.25
	m2	0.7	7.4	0.70	0.76	3.1	9.7	7.9	32.8	-0.02	0.53**
IOB	m1	92.3	92.2	0.75	0.77	42.8	61	30	37.6	0.39**	0.39
	m2	3.7	4.9	0.49	0.61	10.3	6.2	12	31.7	0.01	0.49**
IOD	m1	92.9	83.3	0.53	0.76	57.8	49.3	29	36.6	0.21*	0.64***
	m2	2.7	13.5	0.37	0.51	12.2	22.5	8	28.7	0.32**	0.36
IOD-West	m1	79.8	96.1	0.52	0.77	33	71.3	29.5	36.4	0.09	**0.69***
	m2	13.2	2	0.40	0.53	36.8	3.6	7.5	31.4	0.35***	0.31
IOD-East	m1	98.1	94.8	0.50	0.63	87.1	82.6	28.7	34.5	0.24*	0.20
	m2	0.8	3.3	0.53	0.64	2.4	3.1	7.9	31.6	0.22*	0.41**
SIO	m1	87.4	73.3	0.75	0.82	24.7	29.2	30	37.7	0.32**	0.56**
	m2	3.7	18.6	0.50	0.69	7	12.2	10.3	32.5	0.32 ***	**0.69****
NPO	m1	83.9	79.2	0.91	0.92	25.4	43.1	30.3	37.7	0.29*	0.10
	m2	8.7	17.1	0.66	0.80	11.5	14	13.3	33.7	**0.53*****	0.67***

* **P**<0.1, ****P**<0.05, *****P**<0.005

Table IV.4: Results from SVD analysis between the various SST indices (see Table IV.3 for definition) and Zonal Wind Stress anomalies in FMA in the tropical Pacific Ocean [110°E-70°W,10°S-10°N]. The statistics are given for the first 2 modes of the SVD computed separately for SINTEX-F control run (in blue) and observations (in red).

b - Comparative analysis of the new precursors

In the following section, we will be showing, for each precursor, the SST and zonal wind stress homogeneous maps associated with the SVD mode which offers most promise for ENSO's predictability (*i.e.* with maximum correlation with the Niño3.4 SST index). Note also that the results remain unchanged if we consider SLP instead of SST anomalies for each precursor (in Table IV.3).

What we will be interested in here, is to compare the structure and amplitude of the wind response associated with each precursor, and its physical link with ENSO (with the help of the previous SVD analyses). The statistics will provide a more quantitative approach, allowing us to compare *how much* zonal wind stress variance each precursor is able to explain, and to *evaluate* its connection and predicting score for the following ENSO event (last two columns in Table IV.4).

○ ENSO(-1)

Results from the SVD analysis between ENSO(-1) and wind are displayed in Fig IV.11 in terms of homogeneous SST and zonal wind stress maps associated with the two first leading modes, for the model (a-d) and observations (e-h), respectively. The spatial patterns associated with the 1^{st} mode show a mature La Niña phase during boreal winter related to an anomalous dipole of zonal wind stress in the western Pacific during the following spring: a structure which closely resembles the wind pattern in Figs IV.5a and e, and is consistent with a *La Niña-induced* modulation of the Walker circulation and enhanced convection over the western Pacific. This 1^{st} mode reflects a biennial tendency of ENSO, but has only a weak predicting skill for the following ENSO in both the model and observations (correlation with Niño3.4 SSTs during the following winter of 0.25 in observations and 0.27 in the model).

The predicting score is substantially higher for the 2^{nd} SVD mode, but only in observations (0.53 correlation in observations and near 0 in the model, see Table IV.4). The spatial patterns associated with this mode illustrate how warm SST anomalies in the central Pacific are associated with a local convergence of zonal wind anomalies and enhanced convection during boreal spring in observations (Fig IV.11g-h), while these patterns are weaker and scarcely significant in the model (Fig IV.11e-d). This 2^{nd} mode thus highlights the importance of local SST-wind coupling in the central Pacific, for triggering the following ENSO event. This **0.53 predicting score** may be interpreted as the portion of ENSO predictability, which is produced by local air-sea interactions (*i.e.* resulting from the previous ENSO event) or, simply, stems from the transition from El Niño to La Niña events in observations. This score will now stand as a **benchmark value** for evaluating and comparing the potential predicting power offered by precursors in regions outside of the tropical Pacific. Since these precursors are considered within the same ONDJF time frame as ENSO(-1) (see Table IV.3), they will need to "achieve" higher predicting scores than 0.53 in order to be considered as relevant and

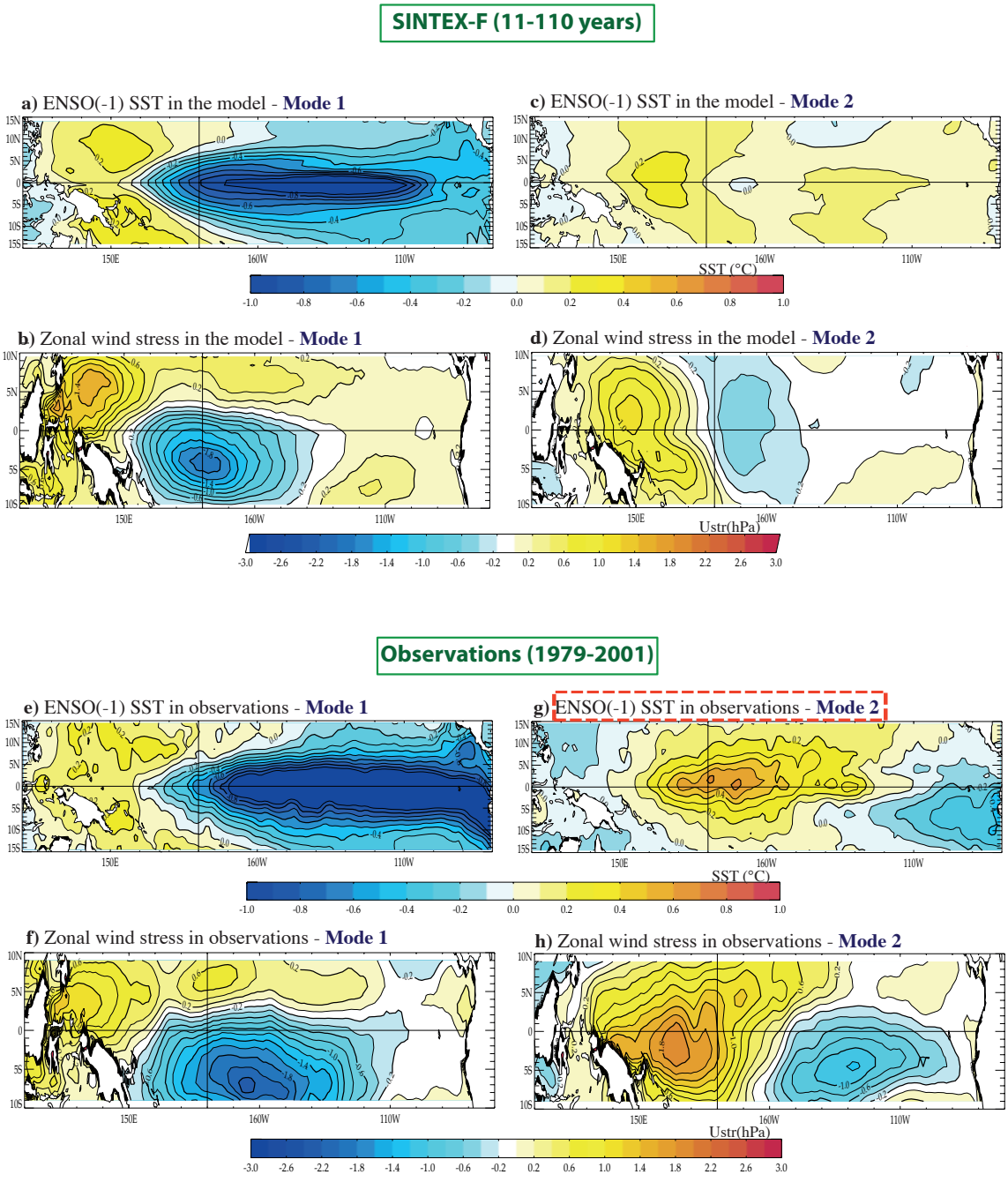

Figure IV.11: SST and Zonal Wind Stress (USTR) homogeneous maps associated with the 1^{st} *(left panels)* and 2^{nd} *(right panels)* SVD modes between **ENSO(-1)** SST in ONDJF — USTR anomalies during the next FMA in the tropical Pacific Ocean ([120°E-80°W,15°S-15°N] for SST and [110°E-70°W,10°S-10°N] for USTR), separately in the model **(a-d)** and in observations **(e-h)**.

useful predictors for ENSO.

○ Tropical IO modes

We will now examine the relationship between tropical IO SST modes and zonal wind variability over the tropical Pacific during boreal spring, as well as the potential for ENSO predictability lying in the Indian tropical region. Fig IV.12 shows the SST and zonal wind patterns associated with the 1^{st} SVD mode, separately for the IOB (left) and IOD (right) domains, in the model (a-d) and observations (e-h), respectively. Although slightly higher correlation values with the Niño3.4 SST index are sometimes obtained with the 2^{nd} SVD mode (*e.g.* for the IOB in observations, and IOD in the model, see Table IV.4), we have decided here to only focus on the 1^{st} SVD mode. Indeed, in both cases, these correlation values obtained from the 2^{nd} SVD mode remain below the threshold value obtained with ENSO(-1), and the associated spatial SST patterns are physically incoherent or at least do not capture the occurrence of an expected IO basin warming (IOB) or dipole event (IOD).

In Figs IV.12a-b and e-f, the SST and wind patterns are consistent with the influence of basin-wide tropical IO (IOB) SST anomalies on zonal wind variability in the western tropical Pacific during boreal spring. In line with previous works, cold (warm) SST anomalies in JFM are associated with westerly (easterly) wind anomalies in the western Pacific in FMA, which then tend to accelerate the transition from La Niña to El Niño (El Niño to La Niña) events [see *Kug and Kang*, 2006]. However, correlation with the following Niño3.4 SST index is weak (0.39 for observations and model in Table IV.4), or at least below the observed ENSO(-1) benchmark value (of 0.53), which suggests that the IOB mode in JFM provides no added value to the skill offered even earlier by the ENSO(-1) mode during the ONDJF season in observations. Interestingly, this result echoes the parallel which was established between the IOB and ENSO(-1) indices in the framework of monsoon predictability ([*Boschat et al.*, 2011a], see **Chapters 2**).

For the IOD domain, the 1^{st} SVD mode is characterized, as expected, by an anomalous SST gradient in the equatorial IO (negative IOD pattern) during boreal fall, related to westerly wind anomalies over the western Pacific during the following boreal spring (Figs IV.12c-d and g-h, in line with [*Izumo et al.*, 2010]). In both the model (Fig IV.12d) and observations (Fig IV.12h), this wind pattern is strikingly similar to the wind structures observed for the 1^{st} mode of ENSO(-1) (Figs IV.11b and f) and IOB precursors (Fig IV.12b and f), thereby suggesting a similar type of wind response for the 1^{st} modes of all tropical precursors considered here. However, in spite of these similarities, the results obtained with the IOD mode in observations are much more promising in terms of ENSO predictability, since correlation values are substantially higher (0.64), and above the ENSO(-1) threshold value in the observations. Interestingly, maximum correlation

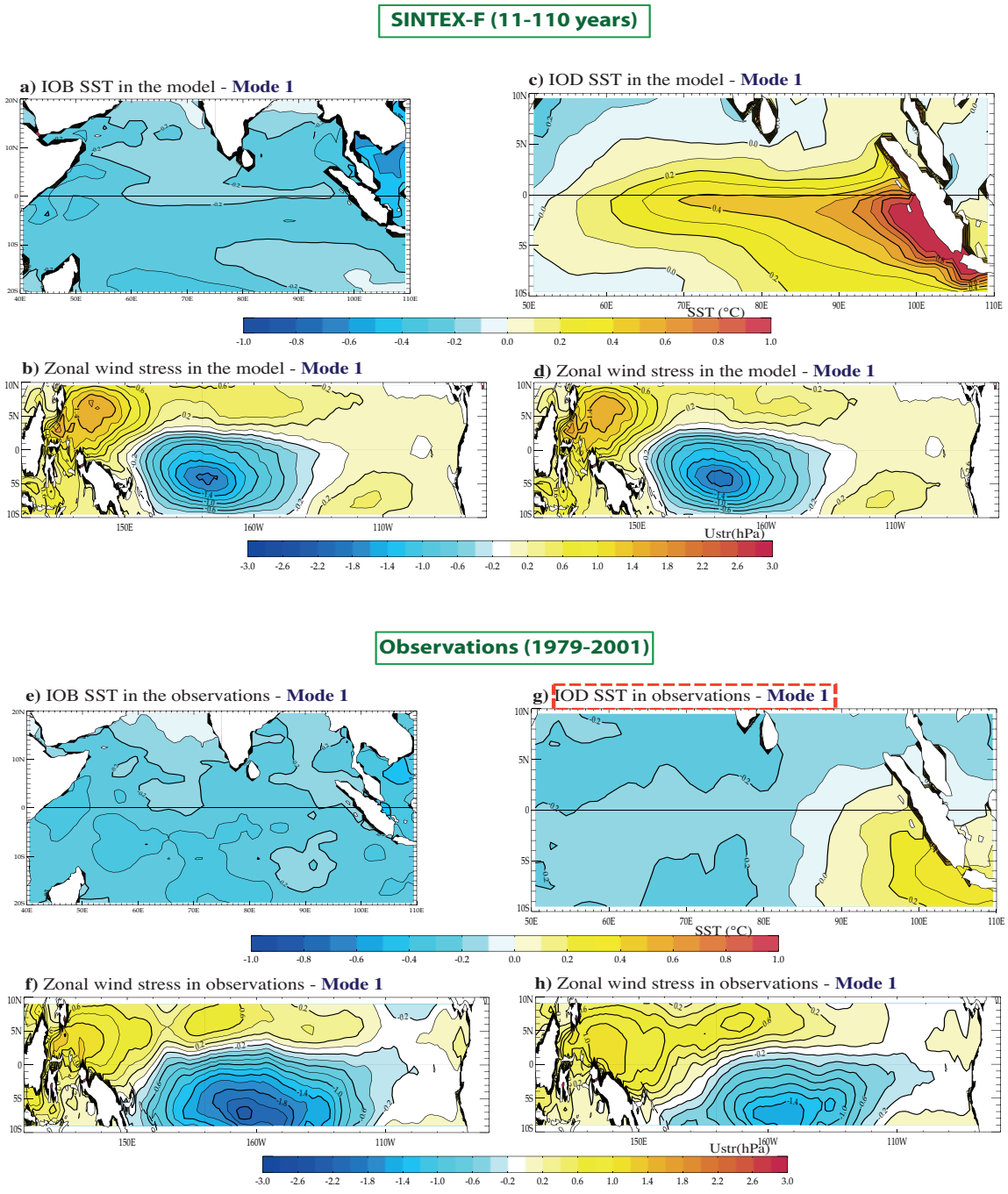

Figure IV.12: SST and Zonal Wind Stress (USTR) homogeneous maps associated with the 1^{st} SVD modes between **IOD** SST in OND *(right panels)* or **IOB** SST in JFM *(left panels)* — USTR anomalies during the next FMA in the tropical Pacific Ocean ([110°E-70°W,10°S-10°N] for USTR, see Table IV.3 for SST spatial definitions), separately in the model **(a-d)** and in observations **(e-h)**.

(again in observations) is obtained from the SVD analysis restricted to the west pole of the IOD mode (0.69 correlation in Table IV.4), suggesting a major contribution from SST anomalies in the *western region of the IO*. Furthermore, these western IO SST anomalies have the earliest significant predicting skill in this analysis, as these SST anomalies are defined during the previous boreal fall, more than 1 year before the ENSO event we wish to predict. It seems important to note that our result is here inconsistent with the triggering mechanism proposed by *Izumo et al.* [2010] to explain the influence of a negative IOD on the following El Niño event. Indeed, their mechanism essentially relies on the existence of convective anomalies over the eastern IOD pole during boreal fall (see Fig IV.8), whereas our analysis highlights the importance of SST anomalies over the *western* pole for impacting zonal wind anomalies over the west Pacific during boreal spring, and for predicting the following ENSO event. The processes involved in our case may thus be different.

Besides, it seems worth noting that in the model, the spatial structure of SST anomalies in the IOD region differs quite substantially from observations, as the warm anomalies in the east pole extend too westward, inducing a significant warm bias in the central equatorial IO (Fig IV.12c; see [*Fischer et al.*, 2005]). Although the model is able to reproduce the similarity in the wind response between the IOD and IOB modes, this SST discrepancy in the equatorial region may be seriously hampering the predicting skill of the IOD in the model.

In the following subsections, we will be examining the importance of *extratropical* climate modes for ENSO, by focusing on subtropical SST dipole modes observed during boreal winter in the South IO and North Pacific Ocean. Can these subtropical modes provide a more efficient prediction of ENSO than tropical IO modes?

◦ Subtropical SIO modes

We first examine the relationship between subtropical SST anomalies in the South IO in JFM and zonal wind variability in FMA in the tropical Pacific, in observations and the model. SVD results in Table IV.4 show that, this time, both the 1^{st} and 2^{nd} leading SVD modes have significant predicting skills for the following ENSO, with correlation values above the ENSO(-1) threshold and even comparable to the IOD score ! (0.56 correlation for the 1^{st} mode and 0.69 for the 2^{nd} mode in observations, and a constant 0.32 value for both modes in the model). In light of these promising results, we have decided to show SST and wind patterns associated with the SIO region for these *two* first SVD modes, in the model (Figs IV.13a-d) and in observations (Figs IV.13e-h).

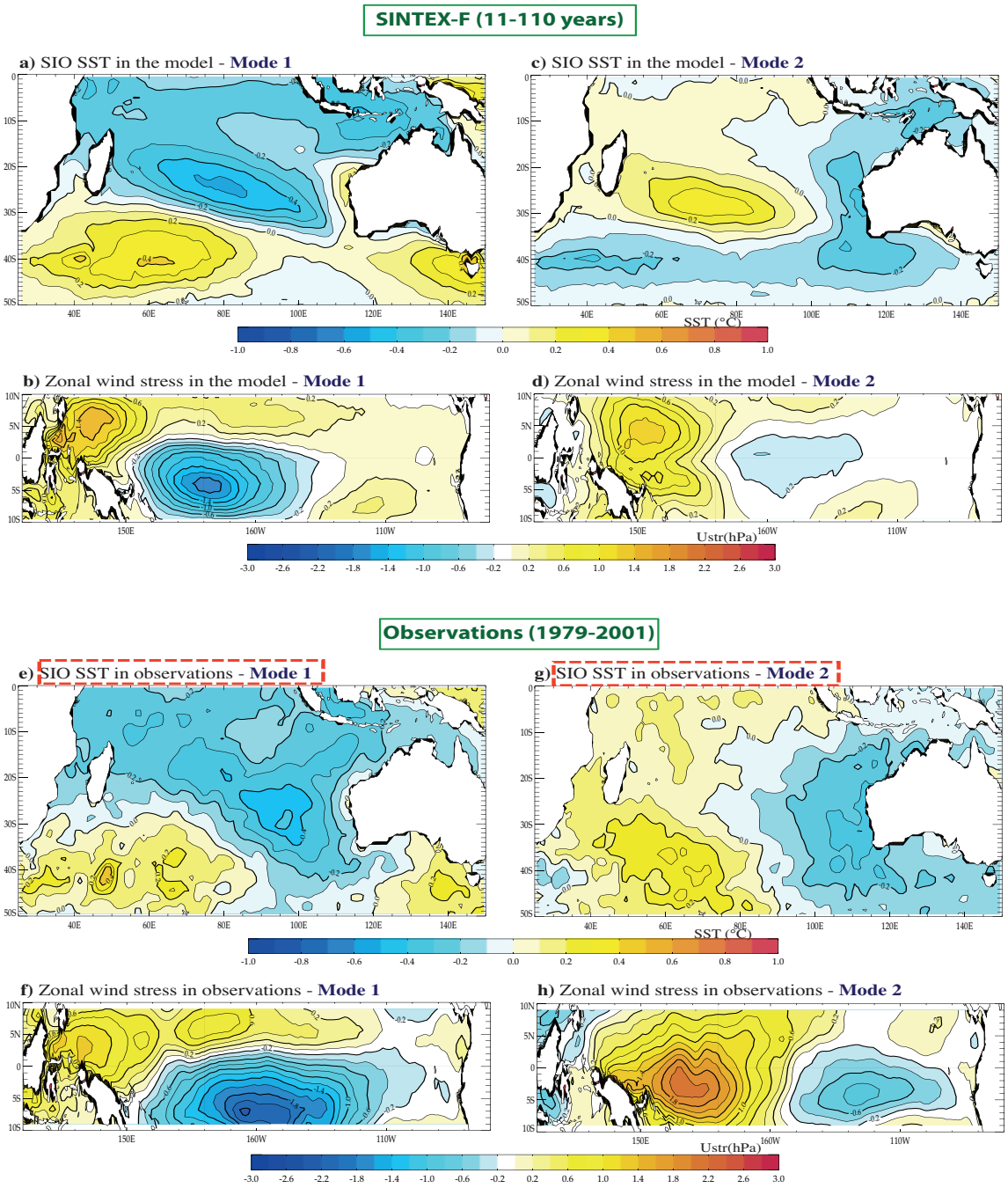

Figure IV.13: SST and Zonal Wind Stress (USTR) homogeneous maps associated with the 1^{st} *(left panels)* and 2^{nd} *(right panels)* SVD modes between **SIO** SST in JFM – USTR anomalies during the next FMA in the tropical Pacific Ocean ([110°E-70°W,10°S-10°N] for USTR, and [25°E-150°E,0°-50°S] for SST), separately in the model **(a-d)** and in observations **(e-h)**.

Overall, Fig IV.13 shows a close correspondence between observations and the model in terms of spatial patterns for each mode. The SST patterns are marked by anomalous SST dipoles in the subtropical IO, which are reminiscent of subtropical dipole events studied by *Behera and Yamagata* [2001] or *Chiodi and Harrison* [2007]: for the 1^{st} mode, this SST dipole has a northeastward tilt, and a negative pole which extends to the equator (Figs IV.13a and e), whereas the SST dipole associated with the 2^{nd} mode has a more zonal structure with a negative pole mostly confined below 15°S, and with the mid-latitude parts somewhat different between the observations and the model (Figs IV.13c and g). Both SST patterns are linked to westerly wind anomalies in the western tropical Pacific. The 1^{st} mode reflects the convergence of zonal wind anomalies in the western tropical Pacific (close to the wind patterns observed with the previous SST precursors). For the 2^{nd} mode, on the other hand, the SST dipole is more significantly linked to an enhancement of westerly wind anomalies over the whole western equatorial Pacific both in observations and model (Figs IV.13d and h).

Both of these modes seem important for ENSO prediction (see Table IV.4). However based on these statistical values alone we cannot assess which part of the prediction comes from the previous ENSO (*i.e.* the biennial tendency of ENSO), and which part may result from an intrinsic source of forcing in the South IO. In order to understand the physical origins and potential differences between these two SVD modes, we have examined the atmospheric circulation anomalies associated with each SST signal in Fig IV.13 . Figure IV.14 displays maps of global SLP anomalies regressed separately onto the 1^{st} (a) and 2^{nd} (b) SVD modes, and this during the same period as the SST patterns in JFM, and 3 months earlier in OND.

The SLP patterns obtained for the 1^{st} mode are remarkably similar in the model and in observations, and are characteristic of the peak phase of a La Niña event (Fig IV.14a), with large SLP anomalies of opposite polarity between the eastern and central Pacific and the rest of the Indo-Pacific domain (recalling the Southern Oscillation). This modulated Walker cell has been shown to induce SST anomalies in the South IO [*Lau and Nath*, 2000, 2003], which suggests the SST dipole associated with the 1^{st} mode in the model and in observations may result from the previous ENSO event, and hence the predictability offered by this 1^{st} SVD mode may be linked to the biennial tendency of ENSO. Nevertheless, the SIO precursor in JFM may still provide added value to this ENSO prediction, since its predicting score is slightly higher than the ENSO(-1) benchmark value (0.56 correlation compared to 0.53 in observations, see Table IV.4).

For the 2^{nd} SVD mode, however, the SLP patterns in Fig IV.14b are substantially different, as they are devoid of any significant signal in the tropical regions in OND. The predominance of significant SLP anomalies over higher latitudes of the southern hemisphere here points towards a potential influence from extratropical atmospheric variability.

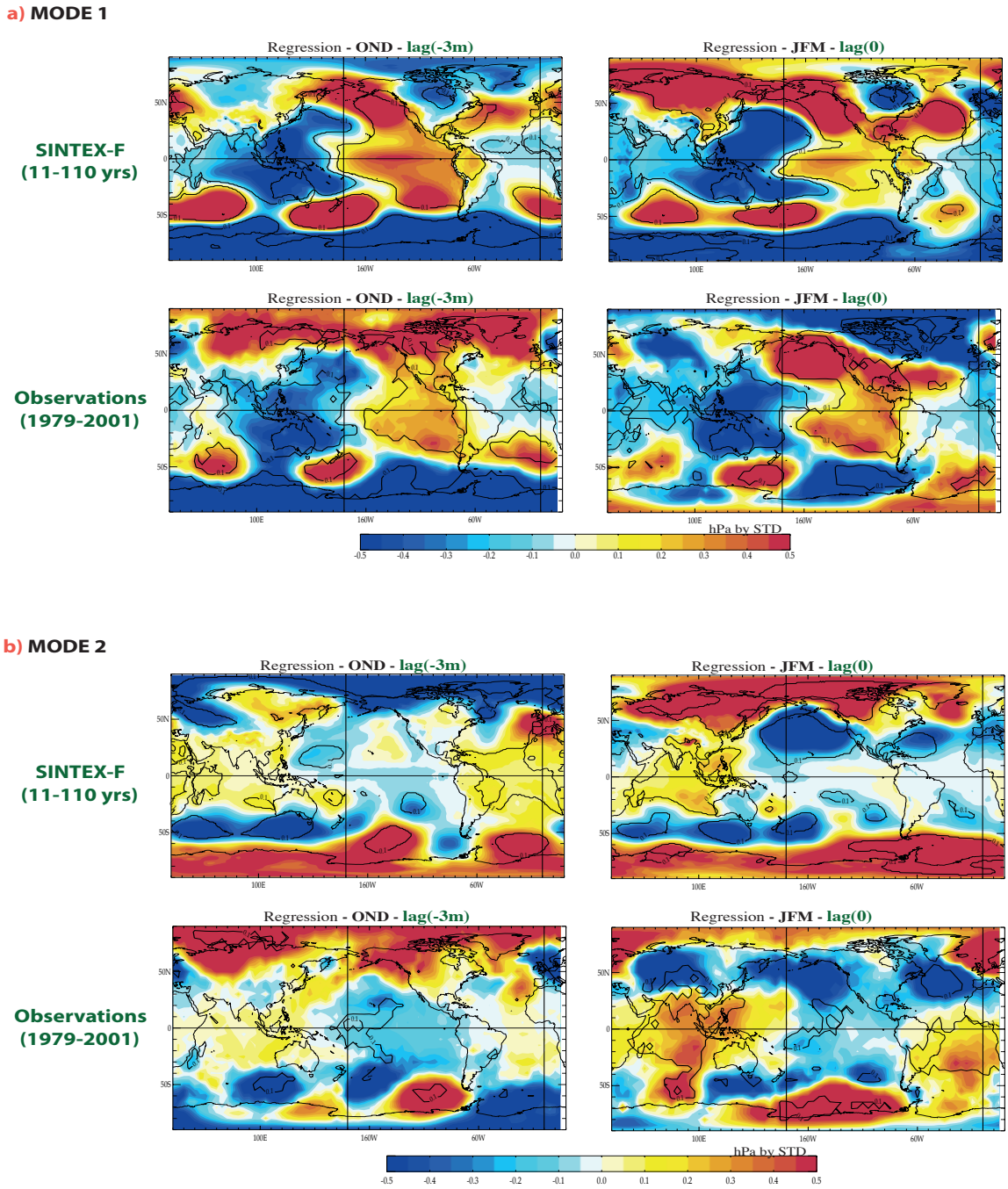

Figure IV.14: Lagged SLP anomalies regressed onto the SST expansion coefficient time series of the 1^{st} **(a)** and 2^{nd} **(b)** SVD mode between **SIO** SST in JFM and USTR anomalies in FMA, during the previous boreal fall in OND and synchronous JFM season, in the model *(top panels)* and observations *(bottom panels)*.

In observations, the positive SLP pulsations near 80°E-50°S in JFM are associated with a strengthening of the subtropical anticyclone, usually dominant in this region during austral summer [*Behera and Yamagata*, 2001], and reflect the occurrence of a blocking event. This strengthened anticyclone episode has been shown to play an important role in ENSO variability as it is able to force ENSO through various coupled feedbacks, involving, in particular, a modulation of zonal wind anomalies in the western Pacific (see Fig IV.13h and [*Terray*, 2011]). The positive SLP anomalies in JFM in observations are thus consistent with these previous findings (Fig IV.14b). Since this 2^{nd} SVD mode acquires a maximum correlation of 0.69 in observations with winter Niño34 SSTs, well above the ENSO(-1) threshold value and equivalent to the tropical west IO SST during the previous boreal fall (IOD-West pole), it illustrates that the South IO may also provide substantial skills for predicting the following ENSO variability and overcome the spring predictability barrier.

Nevertheless, it seems important to note that the model fails to reproduce in its 2^{nd} mode the occurrence of these blocking events in the southern IO. Indeed, the mid-latitude SLP signal in Fig IV.14b is marked by a rather zonal fluctuation of SLP anomalies in the South IO from OND to JFM, instead of the observed positive and negative pulsations reflecting the occurrence of blocking events. Thus, although the SST or SLP patterns obtained in JFM in the model are very close to observations, they may not have been induced by similar processes or mechanisms and may not have the same impact on zonal wind and ENSO onset, as it was proposed in [*Terray*, 2011]. This analysis raises the issue of validating models by simply examining SST signals, and questions the portion of ENSO predictability in the model, which may be inherent to the SST subtropical variability in the SIO.

○ Subtropical NPO modes

By following a similar methodology as for the SIO domain (*i.e.* considering the first 2 leading SVD modes), and by expanding the spatial domain of the NPO precursor to the lower tropical region of the Pacific ocean (as it was done for the SIO region, see Table IV.3), we have managed to separate the NPO subtropical SST signal resulting from the previous ENSO, from the signal which may emerge as an intrinsic source of forcing in the North Pacific ocean. However, unlike the SIO precursor, only the 2^{nd} SVD mode related to this NPO precursor carries potential for ENSO prediction (with high 0.67 correlation in observations, and 0.53 in the model, see Table IV.4)! This is the strongest predicting score obtained in the model, and the 2^{nd} highest score in observations (after the IOD-West pole and SIO precursors). Although we are mostly interested in this 2^{nd} SVD mode, we have decided to show again results from *both* of the leading SVD modes, in order to illustrate this 'separation' of the SST signal in the North Pacific Ocean. These results are displayed in Fig IV.15, in terms of SST and wind patterns associated with the NPO precursor, in the model (panels a-d) and observations (panels e-h).

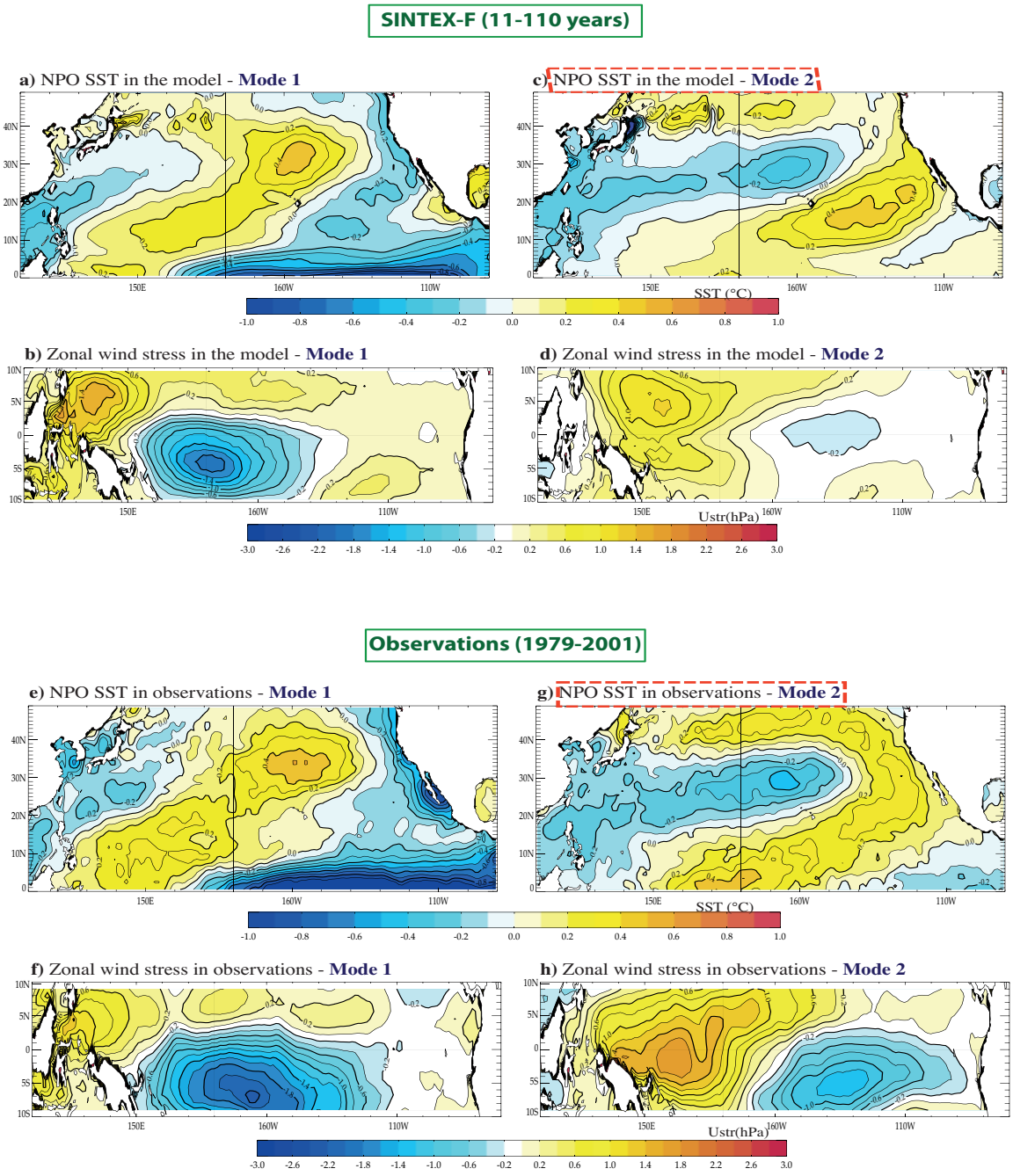

Figure IV.15: SST and Zonal Wind Stress (USTR) homogeneous maps associated with the 1^{st} *(left panels)* and 2^{nd} *(right panels)* SVD modes between **NPO** SST in JFM – USTR anomalies during the next FMA in the tropical Pacific Ocean ([110°E-70°W,10°S-10°N] for USTR, and [110°E-270°E,0°-50°N] for SST), separately in the model **(a-d)** and in observations **(e-h)**.

In Fig IV.15, the SST patterns display a dipole structure of SST anomalies in the North Pacific Ocean, with a similar northwestward tilt, but a reversed polarity between modes 1 and 2. Most importantly, the 1^{st} mode is characterized by a strong La Niña-like pattern along the equator which has completely disappeared in the 2^{nd} mode (Figs IV.15a and e): this equatorial pattern illustrates the possible influence from the previous ENSO on the extratropical SST signal during JFM, and marks a clear visual separation between the two first SVD modes, in both observations and the model. This separation is less discernable in the wind signal in Fig IV.15, which, incidentally, is very similar to the wind patterns associated with the previous SST precursors.

In order to confirm this separation between the two SVD modes, we have applied the same methodology as for the SIO precursor, and examined the atmospheric circulation anomalies related to each SST pattern. The global SLP anomalies regressed onto the 1^{st} and 2^{nd} modes are shown in Fig IV.16a and b hereafter.

The SLP patterns in Fig IV.16a indicate that the 1^{st} SVD mode is significantly linked to the peaking phase of a La Niña event during winter, suggesting this mode mainly reflects the influence from the previous ENSO phase onto the North Pacific variability [*Trenberth et al.*, 1998]. However, unlike the SIO precursor, this 1^{st} SVD has no significant predicting skill for the following ENSO (weak correlation with the winter Niño3.4 index in both the model and observations in Table IV.4).

The 2^{nd} SVD mode is much more important for ENSO predictability, as it has a substantially higher predicting score (0.67 compared to 0.10 for the 1^{st} mode in observations), and for the first time this score is also very important in the model (0.53 compared to 0.29 for the 1^{st} mode in model). Consistent with a forcing from the North Pacific onto the tropical Pacific, the SLP signal in Fig IV.16b associated with the 2^{nd} mode is weak over the tropical regions, and most significant in the form of an anomalous dipole in the North Pacific region from OND to JFM (Fig IV.16b). The southern negative lobe of this SLP dipole has been shown to play an important role in ENSO forcing, as it is associated with a weakening of the trade winds, which can impart a warm SST footprint onto the ocean. The warm horseshoe SST signal in Figs IV.15e and g and the westerly wind anomalies observed along the equatorial western Pacific in Figs IV.15d and h are both consistent with the 'Seasonal Footprinting Mechanism' proposed by *Vimont et al.* [2001, 2003a] to explain the potential forcing of North Pacific climate anomalies on ENSO (see Fig IV.9). Furthermore, this forcing is well reproduced by the model.

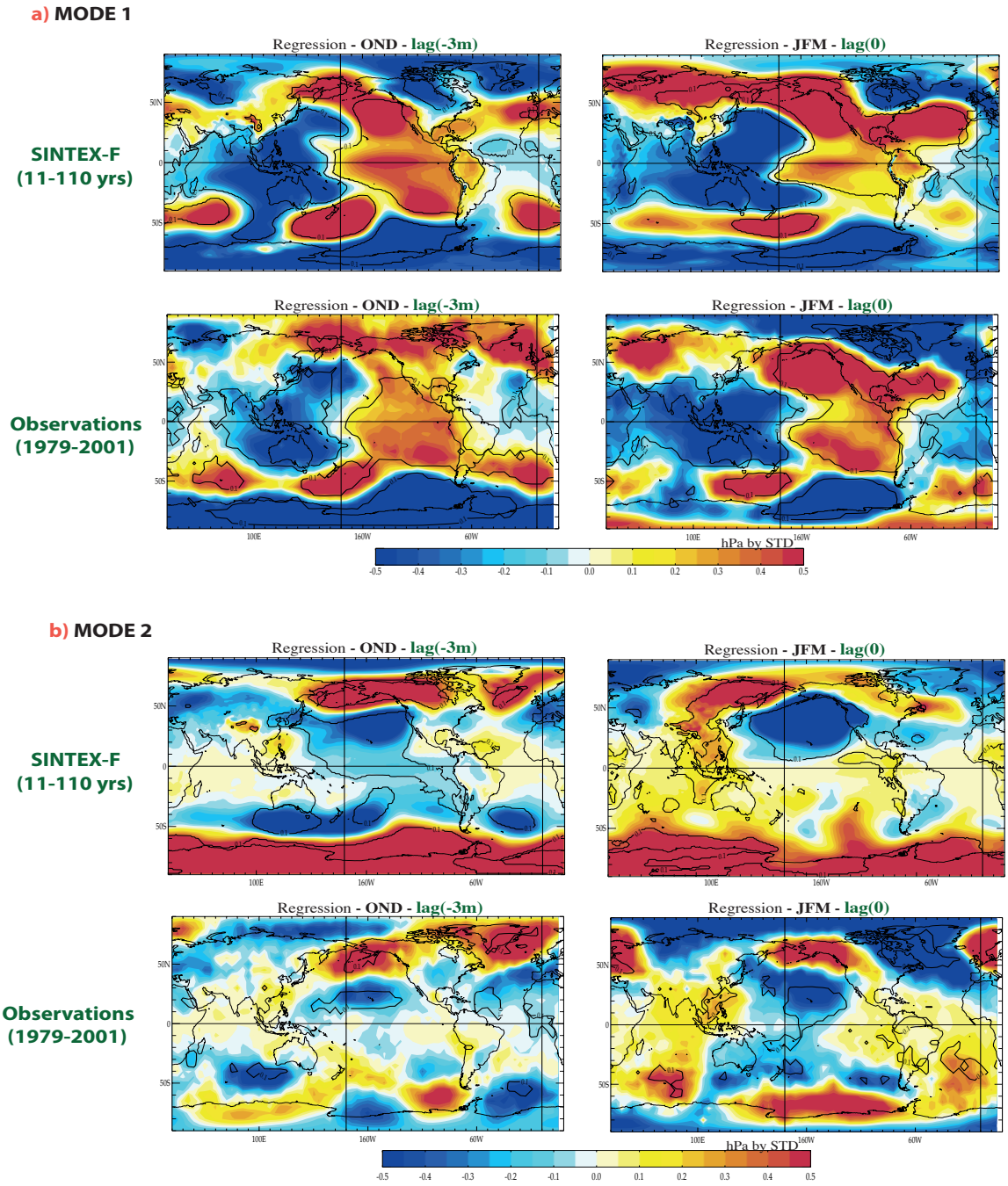

Figure IV.16: Lagged SLP anomalies regressed onto the SST expansion coefficient time series of the 1^{st} **(a)** and 2^{nd} **(b)** SVD mode between **NPO** SST in JFM and USTR anomalies in FMA, during the previous boreal fall in OND and synchronous JFM season, in the model *(top panels)* and observations *(bottom panels)*.

However, it seems interesting to point out here that this SLP anomalous dipole in the NPO has a slightly different position and orientation in observations and the model (Fig IV.16b). In the model, it is shifted northward in OND (with a centre near 50°N compared to 40°N in observations), and then tilted northwestwards in JFM while this dipole remains meridional in observations. The southern SLP pole is also stronger in the model, which suggests it may be associated with an intense anomalous Aleutian low, able to affect *more directly* the wind variability in the western tropical Pacific. The warm SST footprint in Fig IV.15c and the westerly wind anomalies in Fig IV.15d are also consistently shifted northward, whereas these anomalies remain along the equator in observations. These elements suggest again that a slightly different mechanism may be at play in the model.

c - Discussion

Overall, results from the previous SVD analyses in observations highlight the importance of IO SST and their coupling with zonal wind anomalies in the western Pacific in FMA for ENSO predictability. SST anomalies in the North Pacific ocean also seem to play an important role in JFM, although the most significant predicting skills are obtained in the IO, with the **IOD** (mode 1) during the previous boreal fall and with the **SIO precursor** (mode 1 *and* 2) during boreal spring (for observations).

The IOD mode offers the earliest prediction for ENSO events in observations: this effect is largely due to the SST variability in the west IO. However, we suspect that a significant part of this prediction may also arise from ENSO itself (*i.e.* its biennial behaviour), and from the close interaction with tropical (*e.g.* IOB) and subtropical (*e.g.* SIO) SST modes in the IO (correlation above 0.8 between these three IO modes in observations). Unfortunately, we were not able to separate these different contributions for the tropical precursors in our analysis: as a result the **predictability captured by the 1^{st} SVD mode in each case may essentially stem from this biennial tendency of ENSO**. As an illustration, Fig IV.17 here shows the evolution of SST anomalies regressed onto the expansion coefficients of the West-IOD mode during boreal fall in observations (1^{st} SVD mode in Fig IV.12).

In this figure, the cold SST anomalies observed in the west IO during boreal fall are well associated with the onset of El Niño conditions during the following summer, which is consistent with a potential prediction of ENSO onset by this West-IOD mode. However, these cold anomalies are also collocated with a strong La Niña signal from boreal fall to spring, as well as a basin-wide cooling in FM, and the development of anomalous SST dipoles in the South Atlantic and IO, and in the North Pacific Ocean (Fig IV.17). This prediction is thus significantly influenced by the previous ENSO event, and by a combination of interrelated SST modes in the IO (IOD-West-IOB-SIO modes), in the North Pacific, and perhaps even in the South Atlantic Ocean (although this region has not been discussed

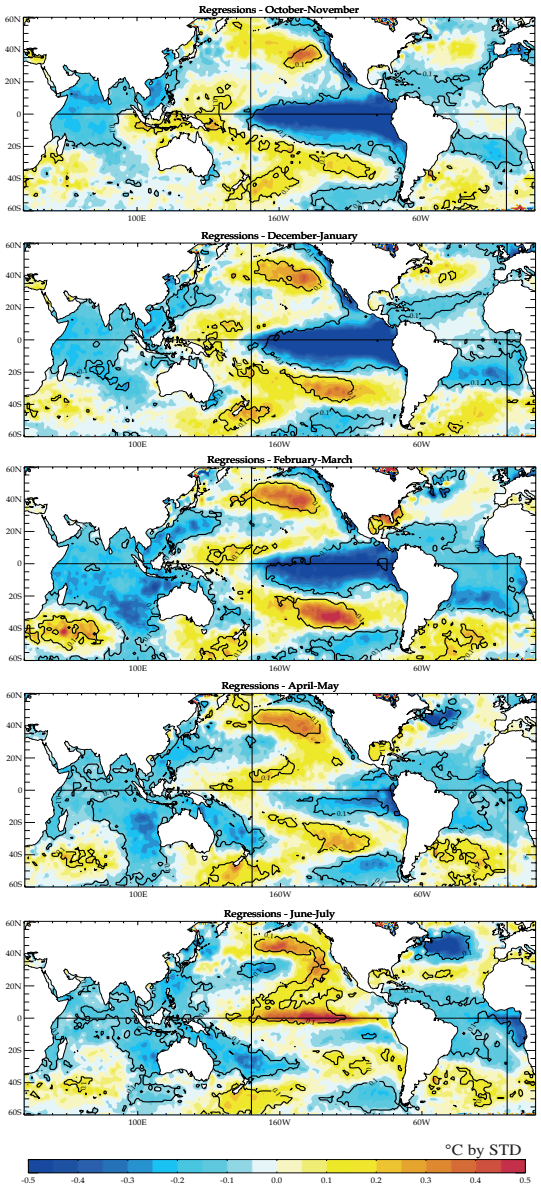

Figure IV.17: Bimonthly SST anomalies regressed onto the SST expansion coefficient time series of the 1^{st} SVD mode between West-IOD SST in SON and USTR anomalies in FMA ([110°E-70°W,10°S-10°N] for USTR, and [50°E-70°E,10°S-10°N] for SST), from the boreal fall (lag 0) to the following boreal summer, in observations. A similar figure is obtained with the model.

in Section 2). The strong correlation between the 1^{st} SIO, IOD-West, IOB modes and the ENSO(-1) mode in Table IV.5a is consistent with this predominance of ENSO bienniality, and may also explain why we have obtained very similar wind responses for the 1^{st} mode of each of these precursors.

a)

	IOD-West (mode1)	SIO (mode1)	IOB (mode1)
ENSO(-1) mode	0.54*** 0.66***	0.83*** 0.89***	0.82*** 0.86***

b)

	SIO		NPO	
	mode 1	**mode 2**	**mode 1**	**mode 2**
ENSO(-1) mode	0.83*** 0.89***	-0.11 0.24	0.94*** 0.97***	-0.11 -0.24

* **P**<0.1, **P**<0.05, ***P**<0.005

Table IV.5: Cross correlation between the ENSO(-1) mode in ONDJF and **a)** the 1st IOD-West mode in SON, the 1^{st} SIO and IOB modes during the next JFM, **b)** the 1^{st} and 2^{nd} SIO and NPO modes during the next JFM. These modes have been obtained from the SVD analysis between the SST precursors (defined in Table IV.3) and zonal wind stress anomalies in the tropical Pacific in FMA and the expansion coefficient time series associated with the SST fields have been used in the correlation analysis. The coefficients exceeding the 95% confidence levels according to the phase-scrambling bootstrap test of *Ebisuzaki* [1997] with 999 samples are followed by three asterisks (***), and are given for SINTEX-F in blue, and observations in red.

However, results from Section 2 also indicate that predictability for ENSO exists *outside* of this biennial tendency, in the form of **subtropical (dipolar) SST variability in the South IO and North Pacific ocean**. In these regions, we were able to distinguish in two separate SVD modes: the SST signal resulting from the previous ENSO state, from the signal emerging as an intrinsic local source of ENSO forcing. The 2^{nd} mode related to these extratropical precursors thus provides an important source of predictability which is no longer correlated with the ENSO(-1) mode (see Table IV.5b). Interestingly, the SIO precursor offers predictability with its *two* first modes (linked to the effect of the previous ENSO event *and* to a local source of forcing in the South IO) whereas *only* the SST variability independent from ENSO offers predictability in the North Pacific (*i.e.* its 2^{nd} mode). Note that our analysis does not preclude the existence of such intrinsic source of predictability in the tropical IO, but we were not able to discern this signal from the effect of the previous ENSO within our SVD framework.

Besides, we need to bear in mind that in this section, ENSO predictability has been explored through the window of FMA wind forcing in the tropical Pacific. Therefore it seems legitimate to ask ourselves at this point: would we have obtained different predicting scores if we had considered this wind variability earlier during the year, or a few months later in spring? Would these new scores be stressing the importance of *other* precursors for ENSO or even changing the order of importance of these precursors?

In the following section, direct SVD analyses are thus performed between each precursor and the following ENSO state. The purpose of this last analysis is first to assess the robustness of these previous results, by testing whether they are dependent on the choice of this time frame for tropical wind variability. These direct SVD analyses will also reveal if different or additional factors may be impacting ENSO, without necessarily influencing wind variability in the tropical Pacific during boreal spring. Can higher predicting scores be achieved this way?

IV.4 Comparison of the various SST indices and their predicting skills for ENSO

This section is the last step in our study of potential ENSO predictability in observations and the SINTEX-F model. The aim here is to come to a more direct comparison of the various precursors in their predicting skills for ENSO, without necessarily considering the intermediate step of their possible impact on zonal wind variability in the tropical Pacific during boreal spring.

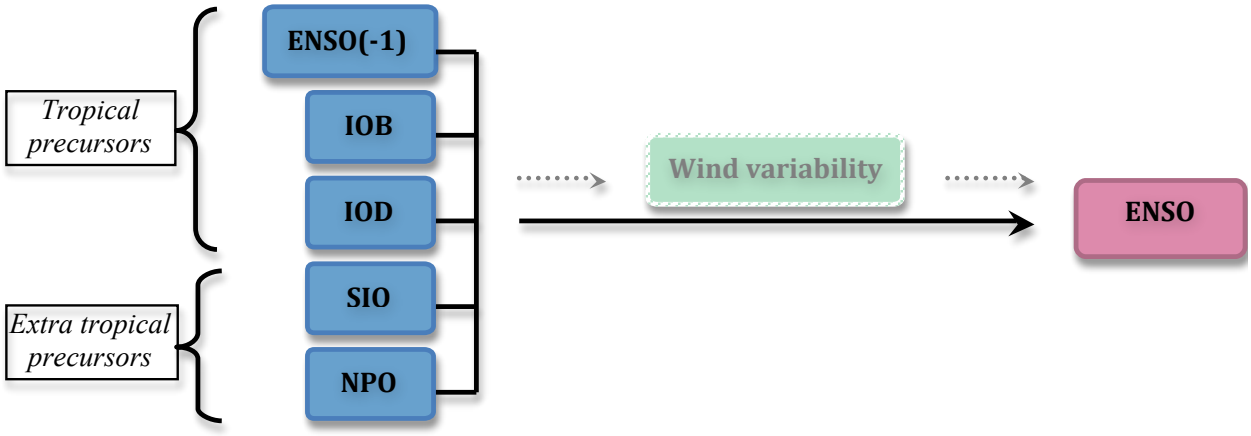

Figure IV.18: Relative role of each selected precursor for ENSO.

This time, both SST and SLP indices are considered (see definitions in Table IV.3), and a similar set of SVD analyses is carried out between each of these precursors and SST anomalies during the following winter (in ONDJF) over the whole tropical Pacific domain. Results are shown in terms of statistics, for SST precursors in Table IV.6 and SLP precursors in Table IV.7. Note that we have decided not to show the corresponding spatial patterns as they are generally very close to the SST patterns associated with each precursor in Section 2, and to the ENSO-like SST pattern associated with the Z20 or USTR precursors in Section 1 (even though the order of the first two leading modes may change between this set of SVD analyses and the SVD analyses discussed in Section 2).

IV.4.1 Comparison of SST and SLP predictors

In order to examine the potential predicting skills of these precursors, we will once again be focusing on the two last columns in Tables IV.6 and IV.7, which indicate how much of SST variance during winter (*i.e.* ENSO) each SVD mode is able to explain, and how well each mode is correlated with the Niño3.4 index during the following winter.

SVD		SCF		r		SST var		ENSO SST var		Cor Niño 3.4	
ENSO(-1)	m1	93.5	81.3	0.37	0.40	65.3	60.4	47.1	39.2	0.30*	0.36
	m2	4.8	16.8	0.33	0.27	7.7	24.9	26.6	44.7	0.06	0.05
IOB	m1	95	90.7	0.43	0.43	40.8	48.7	58.9	65.7	0.40**	0.46**
	m2	1.6	6.8	0.36	0.35	4.1	17.1	14.3	21	0.02	-0.03
IOD	m1	90.6	95.8	0.34	0.60	34.4	49	62.4	74.5	0.35**	0.63***
	m2	5.8	1.9	0.23	0.56	34.2	14.6	8.5	5.7	-0.01	0.02
IOD-West	m1	92.6	99	0.39	0.59	34.1	69.6	65.5	75.4	0.38***	0.63***
	m2	4.8	0.4	0.35	0.52	32.7	9.7	4.3	2.8	0.02	-0.03
IOD-East	m1	98	90.5	0.24	0.26	83.2	73.3	59.3	57.3	0.25**	0.25
	m2	1.2	5.5	0.19	0.53	8.2	9.6	12.1	6.3	-0.01	-0.03
SIO	m1	85	92.8	0.49	0.75	18.9	23.3	63.7	78.3	0.48**	**0.78***
	m2	9.9	4.9	0.46	0.61	14.9	15.1	10.5	9.7	0.01	-0.12
NPO	m1	83.3	74.9	0.65	0.62	14.4	13	67.6	77.3	**0.66***	0.65***
	m2	12.5	20.4	0.63	0.58	23.4	40.1	6.6	7.8	-0.02	-0.11

* **P**<0.1, ****P**<0.05, *****P**<0.005

Table IV.6: Results from SVD analysis between SST precursors (see definition Table IV.3) and SST anomalies in the tropical Pacific [120°E-80°W,15°S-15°N] during ONDJF. The statistics are given for the first 2 modes of the SVD computed separately for SINTEX-F (in blue) and observations (in red).

SVD		SCF		r		SST var		ENSO SST var		Cor Niño 3.4	
ENSO(-1)	m1	94.8	76.4	0.40	0.37	61.9	54.9	50.9	42.1	0.35**	0.33
	m2	3.6	21.1	0.30	0.29	9.2	25.5	22.4	40.9	0.06	0.04
IOB	m1	81.5	95.1	0.25	0.37	57.4	71	43.6	66.7	0.20	0.24
	m2	14.1	2.7	0.27	0.41	13	6.5	29.5	16.5	0.05	0.19
IOD	m1	94.7	95.3	0.26	0.31	84	73	40.4	63	0.19	0.34
	m2	4.8	2.8	0.18	0.30	12	6.8	30	21.7	0.05	-0.03
IOD-West	m1	86.9	69.7	0.41	0.23	92	30.8	5.3	71.3	0.05	0.23
	m2	12	21.3	0.20	0.29	4.8	42.1	60.3	9.7	0.17	-0.06
IOD-East	m1	99.8	98.8	0.27	0.32	97.7	91.7	47	60.5	0.23*	0.32
	m2	0.1	0.6	0.22	0.25	0.4	2.2	24.9	24.2	0.04	-0.04
SIO	m1	77	86	0.34	0.61	17.8	26.1	53.8	78.4	0.31**	**0.56**
	m2	10.4	10.4	0.27	0.65	13.9	25	14.7	8.7	0.01	0.18
NPO	m1	87.5	73.9	0.46	0.36	26.9	27.9	67.7	61.8	**0.43***	0.41**
	m2	9.4	20.1	0.57	0.34	24	24.6	5.3	22	0.06	-0.05

* **P**<0.1, ****P**<0.05, *****P**<0.005

Table IV.7: Same as Table 6 but for SLP precursors (see definition in Table IV.3).

Overall, results suggest that higher predictability for ENSO is obtained with the $\mathbf{1}^{st}$ leading SVD modes related to **SST precursors** rather than SLP precursors, in both observations and the model. Indeed, winter SST explained variance and correlation values with the Niño3.4 SST index are significantly larger for SST modes in Table IV.6 compared to Table IV.7 (with the exception perhaps of ENSO(-1)).

These results also highlight the importance of **extratropical modes** for ENSO predictability, as maximum predicting scores are obtained with the **NPO and SIO precursors in JFM**, whether in terms of SST (Table IV.6) or SLP anomalies (Table IV.7). In observations, correlation with the winter Niño3.4 index is maximum for the SIO precursor (0.78 correlation for the SST mode, 0.56 for the SLP mode), although significant values are also obtained for the NPO (0.65) and West-IOD SST modes (0.63 correlation; see Table IV.6). In the model, the NPO mode exceeds the SIO score and offers maximum predicting skills (0.66 correlation for the SST mode, 0.43 for the SLP mode). Interestingly, this NPO SST score in the model is even higher than the one obtained with the conventional ENSO predictors of Z20 (correlation of 0.56, in Table IV.1) and zonal wind stress (correlation of 0.54, in Table IV.2). This is also true for the SIO SST mode in observations (0.78 compared to 0.72 correlation for zonal wind stress, in Table IV.2), although maximum predicting score in this case is still achieved by the Z20 predictor (correlation of 0.90, in Table IV.1). Can these extratropical precursors provide more efficient information for the predictability of ENSO events? Do they mainly impact ENSO variability through tropical zonal wind variability during boreal spring? The robustness of these extratropical precursors for ENSO will be tested in more detail in Part II of this chapter.

IV.4.2 Are these indices better predictors for El Niño or La Niña events?

The final question we need to address is whether these ENSO precursors are equivalent in their prediction of El Niño and/or La Niña events. To answer this question, we have compared the time expansion coefficients of the leading SVD mode associated with each SST precursor in Table IV.6, and superimposed each of these standardized time series during their peaking season (see Table IV.3) with the Niño3.4 SST standardized time series in DJ (Fig IV.19 to IV.23). The correspondence between these two curves will help us assess how well each SST precursor is able to anticipate/reproduce ENSO variability and therefore predict the occurrence of extreme El Niño or La Niña events. To facilitate this comparison of SST precursors, we have added in each figure the correlation value obtained between the two time series (already given in the last column of Table IV.6). Furthermore, we have also counted the number of El Niño and La Niña events predicted by each SST precursor; a successful forecast occurring when *both* time series exceed a 0.75 standard deviation threshold. We have tested the sensitivity of our results to the choice of this threshold value, and the general

classification of the SST precursors remains unchanged if we consider a 0.5 or 1 standard deviation value.

Overall, this analysis supports our previous results and shows that the NPO and SIO precursors in JFM have the most promising predicting skills for the forecast of both El Niño and La Niña events. The following paragraphs detail how we have compared and classified the performance of the ENSO(-1), IOB, West-IOD, SIO and NPO SST precursors.

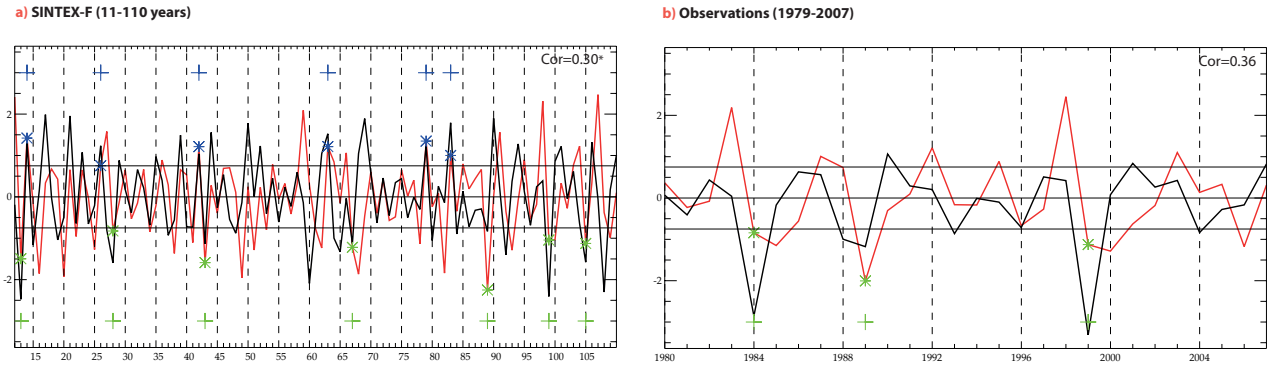

Figure IV.19: **ENSO(-1)** SST expansion coefficient time series in ONDJF (reversed, in black) and Niño3.4 SST standardized time series during the next DJ season (in red), in **a)** the model and **b)** observations The blue (green) crosses indicate the number of predicted El Niño (La Niña) events.

In Fig IV.19, we have represented the reversed ENSO(-1) time series, and in both observations and the model, this time series in ONDJ exhibits only a weak linear relationship with the Niño3.4 SST time series during the following winter, in line with the weak correlation obtained in Table IV.6 (0.36 in observations, 0.30 in the model). In Fig IV.19b, this ENSO(-1) precursor fails to predict any of the El Niño events observed during 1979-2007, but is able to predict 3 out of the 6 La Niña events (marked by a green cross): in particular those following the strongest El Niño events of the past decades in 1982-83, 1986-87 and 1997-98. This suggests that the ENSO(-1) precursor anticipates only the transition from El Niño to La Niña events in observations. On the other hand, the model allows us to explore this predictability over a larger number of ENSO events. In Fig IV.19a, the ENSO(-1) time series predicts only a weak percentage of these events in the model (6 El Niños out of 20 marked by blue crosses, and 7 La Niñas out of 25), but the number of positive and negative events is nearly equivalent here, which points towards a near zero skewness of ENSO in the model.

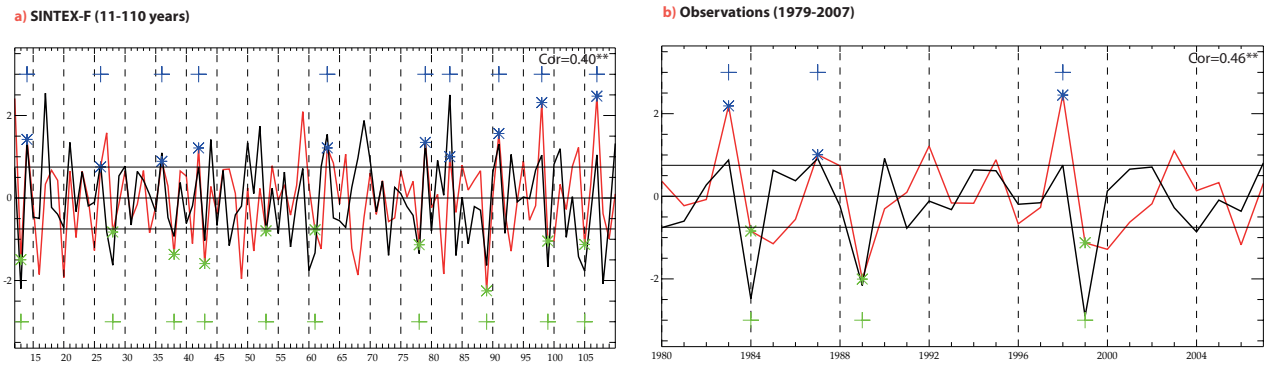

Figure IV.20: **IOB** SST expansion coefficient time series in JFM (black) and Niño3.4 SST standardized time series during the next DJ season (red), in **a)** the model and **b)** observations The blue (green) crosses indicate the number of predicted El Niño (La Niña) events.

The evolution of the IOB time series in Fig IV.20 is very similar to the ENSO(-1) time series, and this is particularly noticeable in observations. Indeed, the red and black curves in Fig IV.20b mostly coincide in their transition from positive to negative peaks, which suggests the IOB is also able to anticipate the phase transition from El Niño to La Niña events (in line with *Kug and Kang* [2006]). In Section 2, our results have suggested that the IOB offers no added value to the prediction of ENSO, compared to the ENSO(-1) precursor. However, in Fig IV.20, correlation between the IOB and Niño3.4 time series is higher than in Fig IV.19 (0.46 in observations and 0.40 in the model), and the IOB manages to predict 3 of the observed El Niño events *(although this forecast is dependent on the 0.75 threshold value used to define the occurrence of ENSO events)*. In the model, the IOB is also able to forecast a higher ratio of both El Niño and La Niña events.

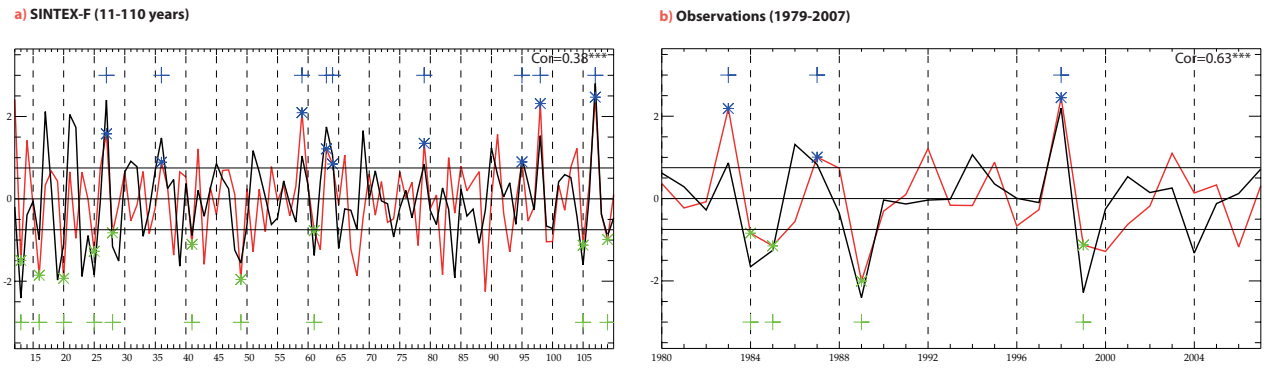

Figure IV.21: **IOD-West** SST expansion coefficient time series in JFM (black) and Niño3.4 SST standardized time series during the next DJ season (red), in **a)** the model and **b)** observations The blue (green) crosses indicate the number of predicted El Niño (La Niña) events.

In line with the high predicting potential of the West-IOD mode (see Section 2), Fig IV.21b shows a very close correspondence between the West-IOD time series during boreal fall and the Niño3.4

time series during the following winter in observations (with a significant 0.63 correlation). This West-IOD time series predicts the same number of El Niño events as the IOB (in 1982-83, 1986-87 and 1997-98), but with closer amplitude (especially for the 1997-98 episode), and an additional La Niña in 1984-85. The model tends to reproduce this higher performance of the West-IOD for predicting La Niña events (Fig IV.21a), but the distinction between the West-IOD and IOB predicting skills is less clear in this case, probably due to the strong SST bias dominating the IOD region in the model. Interestingly, in both the model and observations, the IOD time series closely follows this West-IOD curve (significant 0.47 correlation between the two in the model, 0.96 in observations!), but is less successful in predicting El Niño events (not shown). The East-IOD mode, on the other hand, evolves quite independently from these two time series (*e.g.* 0.19 correlation between the west and east pole of the IOD in the model, and a lower 0.47 in observations), and is globally ineffective in predicting any type of ENSO event (not shown), which seems once again inconsistent with the work of *Izumo et al.* [2010].

The last figures (Figs IV.22 and IV.23) are marked by a near perfect similarity between the SIO or NPO time series in JFM and the Niño3.4 SST time series during the following DJ, and thus highlight the importance of both extratropical precursors for the forecast of ENSO events.

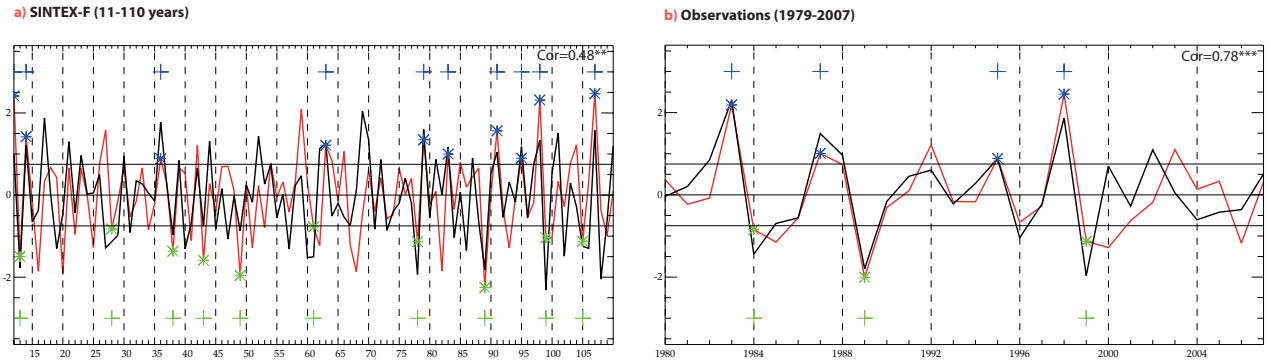

Figure IV.22: **SIO** SST expansion coefficient time series in JFM (black) and Niño3.4 SST standardized time series during the next DJ season (red), in **a)** the model and **b)** observations. The blue (green) crosses indicate the number of predicted El Niño (La Niña) events.

This correspondence between SIO and Niño3.4 SST time series is particularly noticeable in observations (Fig IV.22b), and consistent with the maximum 0.78 correlation obtained in Table IV.22. In this figure, the SIO precursor provides valuable information in terms of *timing* and *amplitude* for the forecast of ENSO events, with the greatest skill for predicting El Niño events amongst the different SST precursors. Although the performance of the SIO precursor in the model equals the IOB in terms of predicted ENSO events, the correlation with the Niño3.4 SST time series is higher (0.48 compared to 0.40 for the IOB), and the SIO seems to better anticipate the *amplitude* of the El

Niño events during the following winter (Fig IV.22a).

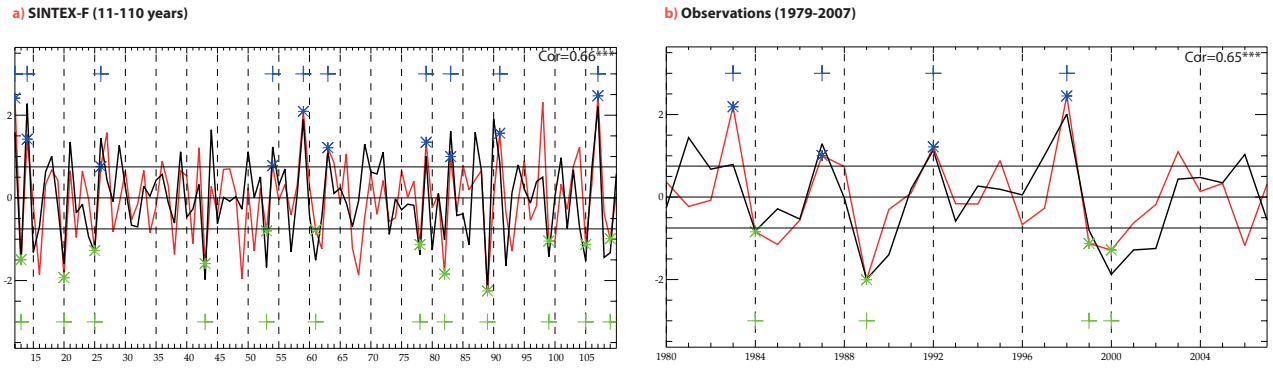

Figure IV.23: **NPO** SST expansion coefficient time series in JFM (black) and Niño3.4 SST standardized time series during the next DJ season (red), in **a)** the model and **b)** observations. The blue (green) crosses indicate the number of predicted El Niño (La Niña) events.

Finally, although correlation with the Niño3.4 SST time series in observations is slightly weaker for the NPO than SIO time series (0.65 compared to 0.78 correlation), the NPO time series here seems able to forecast as many El Niño events as the SIO precursor (*i.e.* so far the best El Niño predictor), and even excels in the prediction of La Niña events (with a maximum of 4 predicted La Niñas out of 6). This highest predictability of La Niña events is well reproduced in the model (with a maximum of 12 predicted La Niñas out of 25, see Fig IV.23a). Besides, the NPO and Niño3.4 time series are strongly correlated in the model (maximum 0.66 correlation, see Table IV.6), and the NPO precursor here seems to anticipate the amplitude of both El Niño and la Niña events, which would overall suggest that ENSO has a nearly fully discernible signal several months in advance in the North Pacific ocean.

Overall, these results support the existence of promising predictors for ENSO in the South IO and North Pacific ocean. In spite of a limited time record in observations, the ratio of predicted El Niño and La Niña events highlights the importance of the NPO predictor for the forecast of both type of events, followed by the SIO precursor for El Niño events, and the West-IOD precursor for La Niña events. These results are generally confirmed by the model, where the NPO retains the best predicting skills, but the IOB and SIO are equally efficient for the forecast of El Niño events.

IV.5 Conclusion

The purpose of this first part was to examine the potential long-range predictability of ENSO, in observations and in the SINTEX-F model. The SVD methodology has allowed us to gather in a *single* conceptual framework, some of the main sources of ENSO forcing proposed in the literature, and compare the efficiency of climate anomalies observed in these key regions for predicting El Niño and La Niña events.

To begin with, the SVD analyses carried out in Section 1, show that the SINTEX-F model is quite realistic in its representation of ENSO and its relationship with conventional precursors during the previous boreal spring, such as heat content or low-frequency wind variability in the tropical Pacific.

In Section 2, we have examined what may force this wind variability during boreal spring, and explored potential sources of forcing in the tropical and extratropical regions of the Indo-Pacific domain. SVD analyses have been performed between precursory SST signals in these key areas and zonal wind variability in the tropical Pacific, in order to compare the relative contribution of each of these precursors in forcing wind variability, and assess its potential for predicting the following ENSO event. Results show:

- that the predictability captured by the 1^{st} SVD modes in these analyses mainly reflect the effect of the previous state of ENSO,
- the importance for ENSO of tropical IO SST anomalies, during the previous boreal fall in the West IO, and during early boreal spring in the South IO, which seem to mainly reflect the biennial tendency of the Indo-Pacific climate system,
- the existence of intrinsic sources of predictability in subtropical regions of the South IO and North Pacific ocean, linked to local dipolar SST variability excited by mid-latitude atmospheric variability in early boreal spring. These patterns are captured by the 2^{nd} SVD modes, but are weaker in the model.

Finally, the last SVD analyses performed between each precursor and ENSO in Section 3, highlight again the importance of extratropical variability, and support the existence of promising predictors for ENSO in the South IO (SIO) and North Pacific ocean (NPO). An article on the importance of this extratropical forcing on ENSO has been submitted to the Geophysical Research Letters journal, and is detailed in Appendix C.

Results from Part I of this chapter are summarized in Table IV.8 below, and show that the NPO has the best predicting skills for both El Niño and La Niña events, while the SIO is mostly effective in the forecast of El Niño events.

	El Niño events	La Niña events
Observations	NPO SIO	NPO W-IOD
Model	NPO SIO IOB	NPO

Table IV.8: Performance of each percursor in the prediction of El Niño and La Niña events in observations and in the model.

Numerical experiments are carried in the second part of this chapter (PART II), to examine the respective role of these precursors identified in the model (*i.e.* NPO, SIO and IOB) and to test their robustness as ENSO predictors.

PART II

Robustness of SST precursors in the SINTEX-F coupled model

IV.6 Introduction

Results from Part I have shown that the SINTEX-F model is quite realistic in its representation of ENSO and of some of its main precursors in the Indo-Pacific region: from the conventional heat content (Z20) or zonal wind (USTR) predictors along the equatorial Pacific during boreal spring, to SST precursors from the previous boreal fall to spring over the tropical IO (IOD and IOB) or the subtropical South IO (SIO) and North Pacific Ocean (NPO). In addition to the conventional ENSO precursors, the SVD analyses have highlighted the importance of the NPO 2^{nd} mode, the SIO 1^{st} and 2^{nd} modes, and the IOB 1^{st} mode for the prediction of El Niño events in the model (see Table IV.8).

As demonstrated in the previous section, the most important problem is the long-range predictability of El Niño events, the predictability of La Niña events being less critical due to the asymmetric relationship between El Niño and La Niña events. The purpose of this part is thus to examine the respective role of these SST modes and test more carefully their robustness as *El Niño* predictors by performing sensitivity experiments with the coupled model, rather than using sophisticated statistical methods on its control simulation.

To do so, we will start by selecting specific El Niño years from the control run and analyze their main characteristics in terms of the precursory signals highlighted in Part I. This will illustrate that these precursory signals exist for the *strongest* El Niño events in the control simulation, and are not dependent on the use of sophisticated statistical analyses such as the SVD (Section 7). Ensemble perturbed simulations will then be carried out for each selected year in Section 8, in order to test the robustness of these precursory signals and their relative importance for the following ENSO event in the control run.

IV.7 Selection and case study of specific El Niño events in the model

IV.7.1 Selection of El Niño years

Figure IV.24 displays the evolution of Niño3.4 SST anomalies during individual El Niño events in the model: here an El Niño event is occurring if the 5-month running means Niño3.4 SST anomalies exceed a 0.8 standard deviation for a period of 6 months or more [*Trenberth*, 1997]. Note that we slightly adapted the definition of *Trenberth* [1997] to our 110 year control run by replacing the original threshold of 0.4°C by 0.8 standard deviation.

The control run shows a variety of 20 El Niño events based on this selection criteria, with Niño3.4 SST anomalies ranging from approximately 0.6°C to above 2°C for the strongest El Niño in year 11. A majority of these events peak between October and March, although a few weaker episodes also

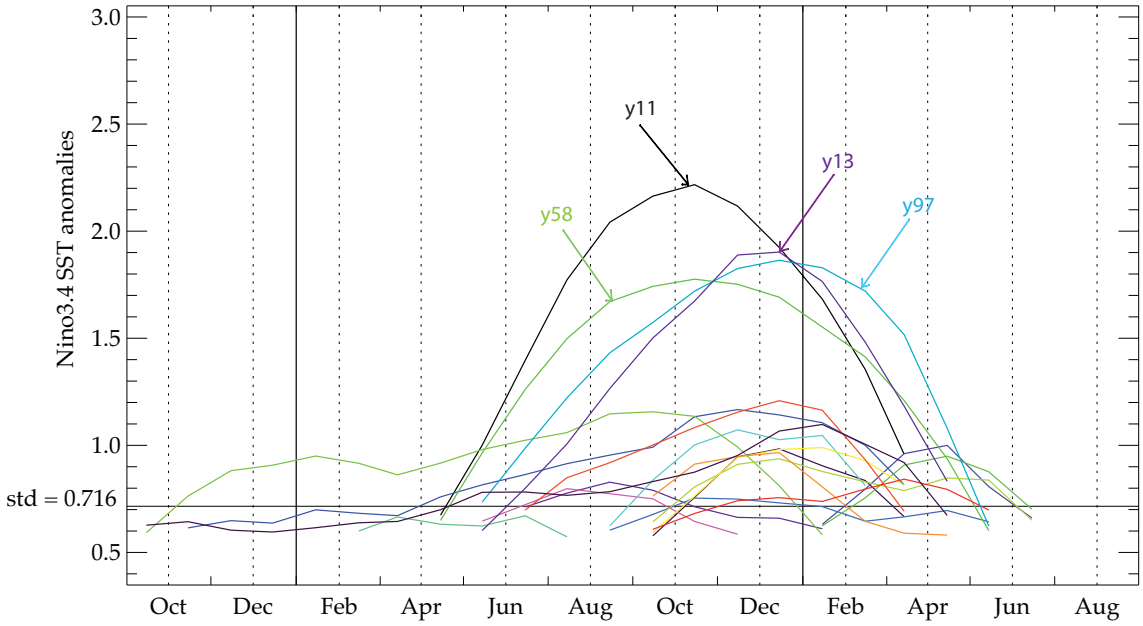

Figure IV.24: Niño3.4 SST anomalies during individual El Niño events, selected by the criteria defined in [*Trenberth*, 1997] in the SINTEX-F control simulation.

seem to peak around boreal spring or summer: these 'spring-type' El Niño events are a well-known bias of the SINTEX-F model [*Guilyardi et al.*, 2003; *Terray et al.*, 2005a].

In this study, we have decided to focus on the El Niño events peaking during boreal winter (as they correspond to the majority of El Niño events found in the real climate) and have selected the four events which stand out as the strongest in the control run, namely years 11, 13, 58 and 97 (Fig IV.24).

IV.7.2 Characteristics of these events

In the following subsections, we will be describing the characteristics of these selected events in terms of El Niño SST conditions, and their associated precursors during boreal spring. To compare the four events and examine the relative importance of each precursor, we will use the SVD tools we developed in Part I, and project for each selected year, the winter SST anomalies in the tropical Pacific, and the anomalous precursory fields (Z20, USTR or SST), onto the left and right singular vectors of the corresponding SVD modes. The details of these various projections are given in Table IV.9. Note that, to be consistent with Part I, we have examined the role of SST precursors through the window of zonal wind variability, *i.e.* by considering the SST modes derived from the SVD between each SST precursor and the zonal wind variability during FMA (*and not the winter SST*

variability as it is the case for the conventional Z20 and USTR precursors).

	Projection of	onto singular vectors	of corresponding SVD mode	See Fig. in Part 1:
a)	monthly SST anomalies in tropical Pacific	SST	SVD between Z20 in JFM (or USTR in FMA) and SST in ONDJF *(1^{st} mode)*	Fig IV.3 (or Fig. IV.5)
b)	Z20 anomalies in JFM in tropical Pacific	Z20	SVD between Z20 in JFM and SST in ONDJF *(1^{st} mode)*	Fig IV.3
b)	USTR anomalies in FMA in equatorial Pacific	USTR	SVD between USTR in FMA and SST in ONDJF *(1^{st} mode)*	Fig. IV.5
c)	SST anomalies in JFM in IOB, SIO or NPO regions (defined in Table IV.4)	SST	SVD between SST in JFM and USTR in FMA *(1^{st} mode for IOB and SIO, 2^{nd} mode for SIO and NPO)*	Fig. IV.12 (IOB) Fig. IV.13 (SIO) Fig. IV.15 (NPO)

Table IV.9: List and details of the projections performed in this section for each selected El Niño year in the control run. The figures showing the corresponding SVD patterns in Part I are given in the last column.

a - El Niño SST conditions during boreal winter

To begin with, we compare the evolution and amplitudes of the four El Niño events in years 11, 13, 58 and 97 in the delayed oscillator and zonal wind frameworks (*i.e.* with the help of the SVD analyses between Z20 and SST anomalies, and between USTR and SST anomalies in the tropical Pacific, see Table IV.9a). To do so, we have projected, for each selected year, the monthly SST anomalies in the tropical Pacific onto the SST singular vectors associated with the 1^{st} mode of these two SVD analyses.

Fig IV.25a shows the monthly projected values for the 1^{st} Z20-SST mode, and illustrates how the events in years 11, 58 and 97 are very similar in their development from a neutral state to a warm El Niño phase, with peaking SST anomalies ranging from 0.8°C (for year 58) to a maximum of 1.1°C (for year 11) during boreal winter. The El Niño of year 13, however, is weaker (0.5°C peaking SST anomalies in December), and is preceded by opposite La Niña conditions during the previous boreal winter.

Projections for the 1^{st} USTR-SST mode are similar in all respects, since the SST singular vectors of these two SVD analyses are almost identical (*i.e.* see the corresponding homogenous SVD patterns in Figs IV.3 and IV.5).

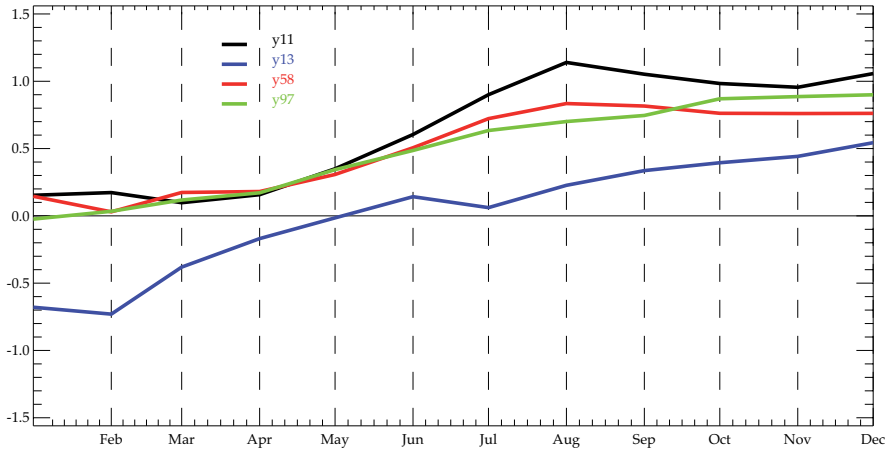

Figure IV.25: Projection of monthly SST anomalies in the tropical Pacific onto the SST singular vectors of the 1^{st} SVD(Z20-SST) mode (similar results obtained with the 1^{st} SVD(USTR-SST) mode), for each selected El Niño year.

b - Heat content in JFM and zonal wind variability in FMA

We now examine the heat content preconditioning and zonal wind variability associated with each of these events during the previous boreal spring (Fig IV.26b-c). For each year, we have projected the Z20 anomalies in JFM onto the Z20 singular vectors of the 1^{st} SVD (Z20-SST) mode, and the USTR anomalies in FMA onto the USTR singular vectors of the 1^{st} SVD (USTR-SST) mode (see Table IV.9b). Results from these seasonal projections are shown in the form of histograms, in order to easily compare the contribution of each precursor from one El Niño event to the other. The standardized Z20 and USTR expansion coefficient time series derived from these SVD analyses are also plotted in the left panels of Fig IV.26a and b respectively. The values for years 11, 13, 58 and 97 are marked by a colored star, and correspond well, as we would expect, to the projected bar plots represented in the right panels of this figure.

Overall, the positive values and bar plots in this figure illustrate how the El Niño events of years 11, 13, 58 and 97 are all 'preconditioned' with positive heat content anomalies in the western Pacific (see Z20 pattern in Fig IV.3) and are marked by westerly wind anomalies in the western tropical Pacific (see USTR pattern in Fig IV.5) during the previous boreal spring. Interestingly, the El Niño of year 97 is only weakly preconditioned in Z20 compared to the other events (Fig IV.26a), but seems related to stronger USTR anomalies (Fig IV.26b). It seems worth noting here that, although the El Niño events of years 58 and 97 in the control run have a very similar evolution (see Fig IV.25), they differ markedly in terms of Z20 and USTR preconditioning during the previous boreal winter and early spring: indeed, one event is strongly preconditioned in heat content (year 58), while the other seems more linked to enhanced zonal wind activity over the western equatorial Pacific in FMA (year 97). Nevertheless, these selected El Niño events do not correspond to the *strongest* occurrence

a) Z20 precursor - mode 1

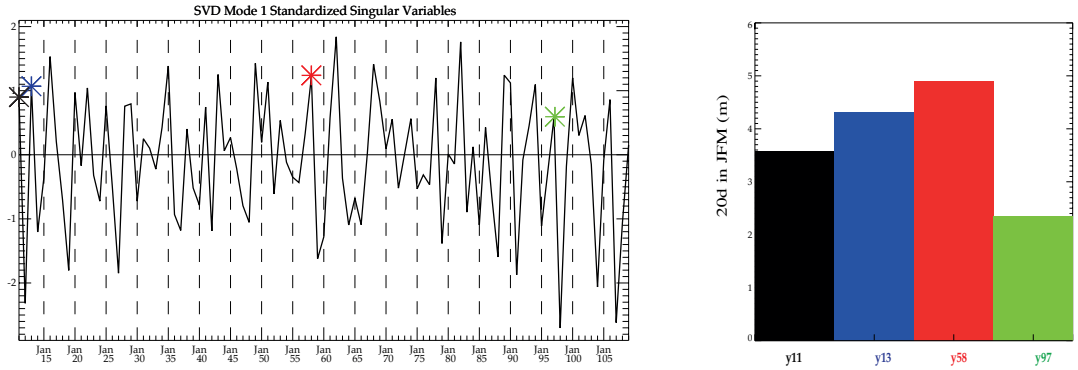

b) USTR precursor - mode 1

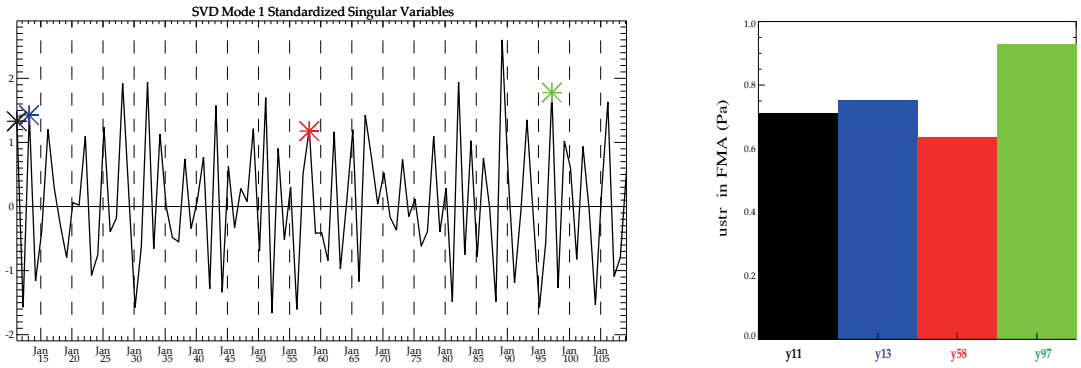

Figure IV.26: **(a)** Expansion coefficient time series of Z20 singular variables from the 1^{st} SVD(Z20-SST) mode *(left)*, and projection of Z20 anomalies in the tropical Pacific in JFM onto the Z20 singular vectors of this mode *(right)* **(b)** Expansion coefficient time series of USTR singular values from the 1^{st} SVD(USTR-SST) mode *(left)* and projection of USTR anomalies in the tropical Pacific in FMA onto the USTR singular vectors of this 1^{st} mode *(right)*, for each selected El Niño years.

of the Z20 or USTR expansion coefficients time series (Fig IV.26a-b). The moderate values observed in years 11, 13, 58 and 97 suggest that other/additional factors may be playing a significant role and forcing these strong El Niño events in the control run.

In order to distinguish these El Niño events and explore these potential sources of forcing, we will now examine the contribution of other precursory SST signals during boreal spring, in the same SVD framework.

c - SST precursors during JFM

As mentioned above, and in accordance with Part I, we will be focusing here on the IOB 1^{st} SVD mode, the SIO 1^{st} and 2^{nd} modes and the NPO 2^{nd} mode, as they have been identified as being the most important for El Niño predictability in the model. As demonstrated in Part I, the IOB and SIO 1^{st} modes mainly reflect an influence from the previous ENSO event, while the SIO and NPO 2^{nd} modes capture the existence of intrinsic sources of predictability in extratropical regions.

To examine the potential role played by these precursors during each of our selected years, we have thus projected the JFM SST anomalies in the IOB, NPO and SIO regions onto the SST singular vectors of the corresponding SVD modes (see Table IV.9c). Once again, the standardized SST expansion coefficient time series derived from these SVD analyses are plotted for each mode in the left panels of Fig IV.27(a-d).

Overall, these projections illustrate the key importance of ***intrinsic*** sources of **predictability in extratropical regions** for the development of El Niño events in the model. Indeed, the strongest El Niño events selected in the control run are here associated with the largest time expansion coefficients for the SIO and NPO 2^{nd} modes (Fig IV.27c-d), and not necessarily for the Z20 or USTR 1^{st} modes as we would initially expect (see Fig IV.26a-b). As an illustration, the strongest value of the 2^{nd} SIO SST expansion coefficients time series occurs during year 97 (Fig IV.27c), while the strongest occurrence in the 2^{nd} NPO SST expansion coefficients time series is observed in year 58 (Fig IV.27d). In the model, the SIO and NPO extratropical precursors can thus either play separately (*e.g.* year 97 for the SIO 2^{nd} mode; years 13 and 58 for the NPO 2^{nd} mode), or together (*e.g.* year 11) depending on the El Niño event (Fig IV.27c-d).

There also seems to be a *more or less* constant, but moderate contribution from the 1^{st} IOB mode for all the selected El Niño events (Fig IV.27a). However, the time expansion coefficients for this 1^{st} IOB mode are only weak to moderate, and most of the peak values in the time series are not even associated with El Niño events in the following months. Contribution from the 1^{st} SIO mode seems even weaker (Fig IV.27b), except during year 13. Indeed, the El Niño event during this year 13 is

a) IOB precursor - mode 1

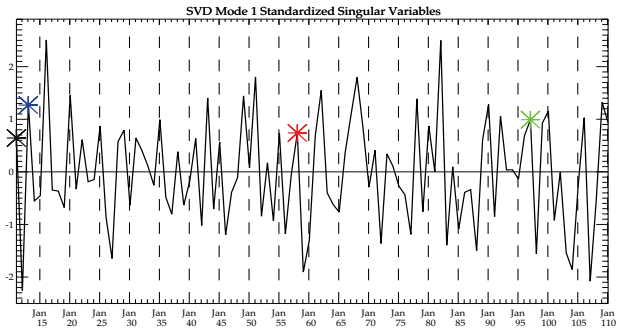

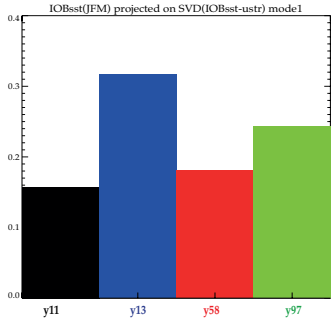

b) SIO precursor - mode 1

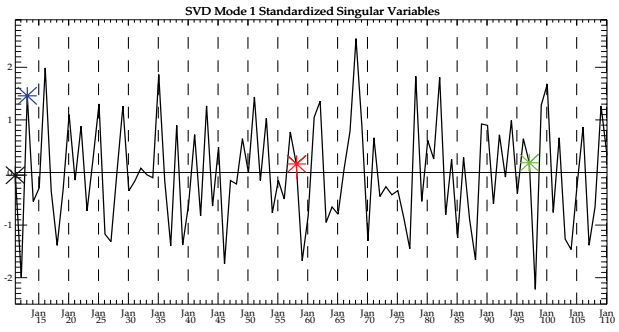

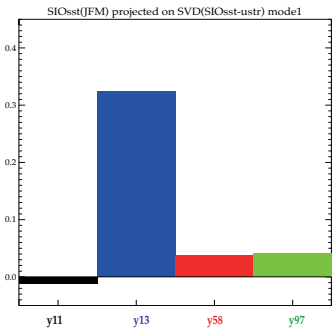

c) SIO precursor - mode 2

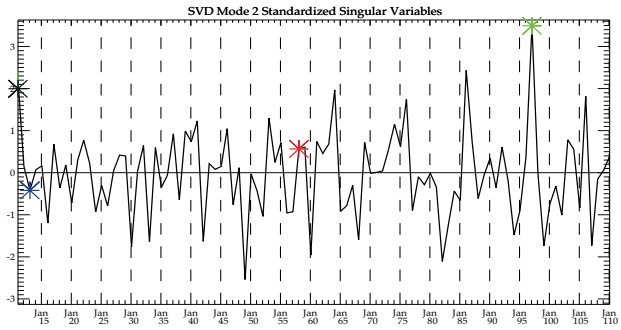

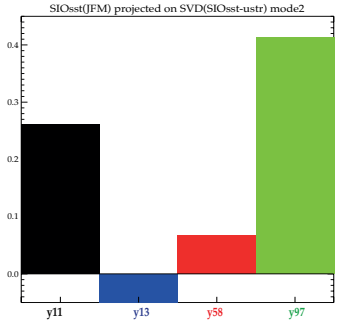

d) NPO precursor - mode 2

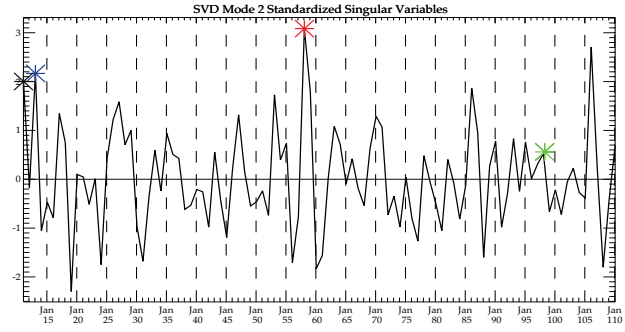

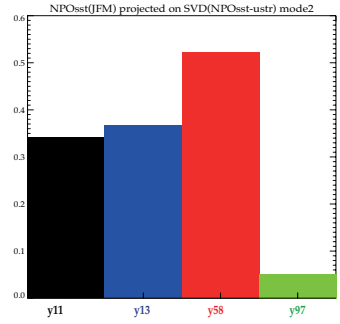

Figure IV.27: Expansion coefficient time series associated with each SST precursor *(left)* and projection of SST anomalies in JFM of each selected El Niño year onto the corresponding SVD mode *(right)*, for **(a)** IOB, **(b-c)** SIO and **(d)** NPO precursor (see Table IV.3 for the spatial definition of these SST precursors).

marked by particularly strong values of the 1^{st} IOB and SIO modes, which is consistent with the fact that this is the only selected El Niño preceded by a La Niña event during the previous boreal winter (see Fig IV.25). Interestingly, the SIO SST precursor in this analysis plays a prominent role during both years 13 and 97, but in one case this effect is due to the previous ENSO event (the 1^{st} SIO mode, year 13), while in the other it is linked to a more intrinsic source of forcing (the 2^{nd} SIO mode, year 97).

Table IV.10 below summarizes the characteristics of the selected El Niño years in the control run in terms of ENSO precursors.

	El Niño characteristics	**'Conventional' predictors**		**Dominant SST precursors**			
		Z20	USTR	IOB *(mode1)*	SIO *(mode1)*	SIO *(mode2)*	NPO *(mode2)*
Year 11	strongest El Niño	moderate	moderate	X		**X**	**X**
Year 13	weakest El Niño previous La Niña	stronger than year 11	stronger than year 11	**X**	**X**		X
Year 58	strong El Niño (similar to y97)	strongest	weakest	X			**X**
Year 97	strong El Niño (similar to y58)	weakest	strongest	X		**X**	

Table IV.10: Characteristics of the selected years 11, 13, 58 and 97 in the control run, in terms of El Niño SST conditions during boreal winter, and precursory heat content (Z20), zonal wind (USTR) and SST signals during the previous boreal spring. The X symbol indicates the most dominant SST mode(s) prior to each El Niño event.

IV.8 Ensemble perturbed runs experiment

The purpose of this numerical experiment is to further test the importance and robustness of the precursory signals identified in Section 7 as playing an important role in the evolution of the four selected El Niño events.

IV.8.1 Experimental Protocol

To test our hypothesis on the role of traditional USTR and Z20 and SST precursors, we performed a suite of numerical experiments for each selected El Niño year, where we added a SST perturbation to the global SST field in the January restarts of the coupled GCM (*e.g.* one year before the peak phase of the selected Niño events). This added global perturbation follows a Gaussian distribution with a zero mean and a standard deviation proportional to the local SST variability at each grid point

(10% of the local SST standard deviation in January), but is uncorrelated in space. An example of the spatial structure of this perturbation is shown in Fig IV.28b. Note here the close resemblance with the global structure of the SST standard deviation, shown in Fig IV.28a for the month of January in the control run. For each selected year, the coupled model was then integrated, with ten different SST initial conditions in January, and each time for a 1-year period, in order to study the impact of this SST perturbation on the ongoing El Niño event. By partly destroying the SST spatial structure associated with each SST precursor and by comparing both the perturbed and control runs, we have the hope to isolate implicitly some of the effects of these precursors on the following El Niño event.

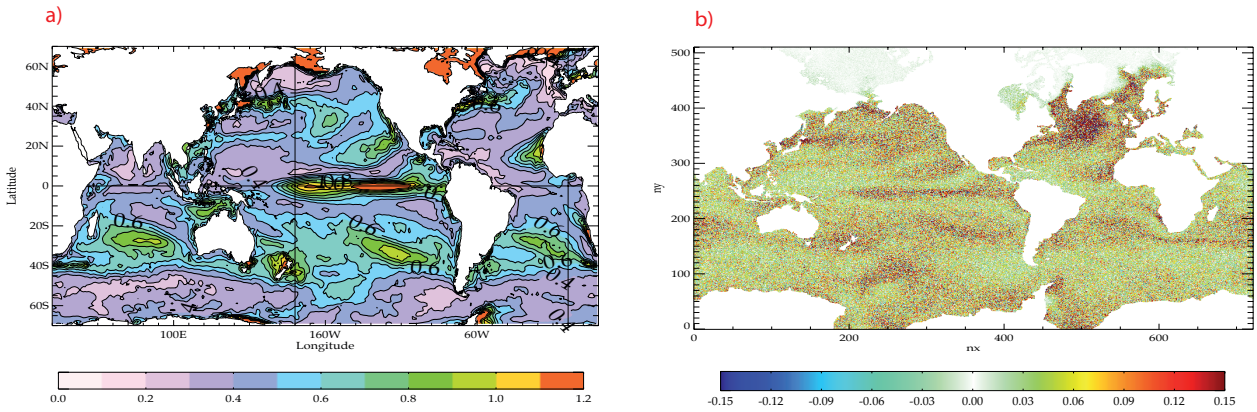

Figure IV.28: **(a)** Standard deviation of global SST anomalies in January, **(b)** example of noise structure (SST perturbation in °K) added to the January SST fields in the experiment.

IV.8.2 Results

Results from these sensitivity experiments will be analyzed separately for year 11, 13, 58 and 97, in terms of the **impact of the initial SST perturbation on the characteristics of each year** summarized in Table IV.10. We will be particularly interested in answering (if possible) the following questions:

(i) Does each of these perturbed runs still develop into El Niño conditions during the following winter?

(ii) If so, are these events linked to the same precursory signals during the previous spring as those identified in the control run?

(iii) If not, what are the "missing" signals, which may explain the aborted El Niño events in the perturbed experiments?

a - El Niño SST conditions during boreal winter

The Niño3.4 SST time series of each selected year for the control run (in black), and the 10 perturbed experiments (in colour) are shown in Fig IV.29. This figure gives a first broad overview of

the impact of the initial SST perturbations on the evolution of the various El Niño events considered in these sensitivity experiments.

For the El Niño event occurring in year 11 — which is the strongest event in the control run (see Fig IV.24) and is characterized by a strong extratropical signal with *an intrinsic origin* in both the NPO and SIO (see Fig. IV.27c-d) — most of the perturbed runs also develop into El Niño conditions, but with a much weaker amplitude than in the control run. Two of the perturbed runs also begin to develop warm conditions in the tropical Pacific, but suddenly diverge in June and evolve towards opposite La Niña conditions during the following winter (*e.g.* the blue curves in Fig IV.29a). In many respects, this particular El Niño event in the control run is reminiscent of the 1997-98 El Niño event in observations: the strongest El Niño of the 20^{th} century which was also marked by intense and concomitant SIO and NPO signals during JFM (see Figs IV.22 and IV.23 in Part I and also [*Terray*, 2011]). The weakening of the event in all the perturbed runs here points towards a possible role of extratropical SST forcing in the exceptional strength of the El Niño event in year 11 of the control run.

For the El Niño event in year 13, which is representative of the biennial tendency of the simulated ENSO (see Fig IV.25), the perturbation of the initial La Niña state in January seems to have a more diverse impact on the following Niño3.4 SST conditions, since only 3 perturbed runs develop into a similar El Niño state as the control run. One of the runs (*e.g.* the red curve in Fig IV.29b) develops even into a much stronger El Niño event from April onwards, while the 7 others evolve towards weaker or neutral SST conditions during winter.

The El Niño event occurring in year 58 seems much more robust as those discussed above: as *all* the perturbed runs develop into mature El Niño phases, with either weaker and stronger amplitudes than the initial event in the control simulation (Fig IV.29c). Note that this event in the control run is also characterized by a very strong signal in the NPO (Fig IV.27d).

Finally, for the El Niño in year 97, there is a more continuous spread of winter SST conditions, ranging from La Niña to neutral and El Niño states, but all the Niño3.4 SST time series simulated in the perturbed runs remain below the initial values of Niño3.4 SSTs in the control run (black curve, Fig IV.29d). In this respect, this event is similar to the very strong El Niño in year 11 discussed above. This year 97 is also characterized by the highest precursory signal, with a possible intrinsic origin, in the SIO extratropical domain, although the NPO signal in this case is not significant (see Fig IV.27c-d). This highlights again the possible influence of extratropical SSTs on the triggering or amplification mechanisms involved in the evolution of ENSO in the control run, which will be more thoroughly discussed below.

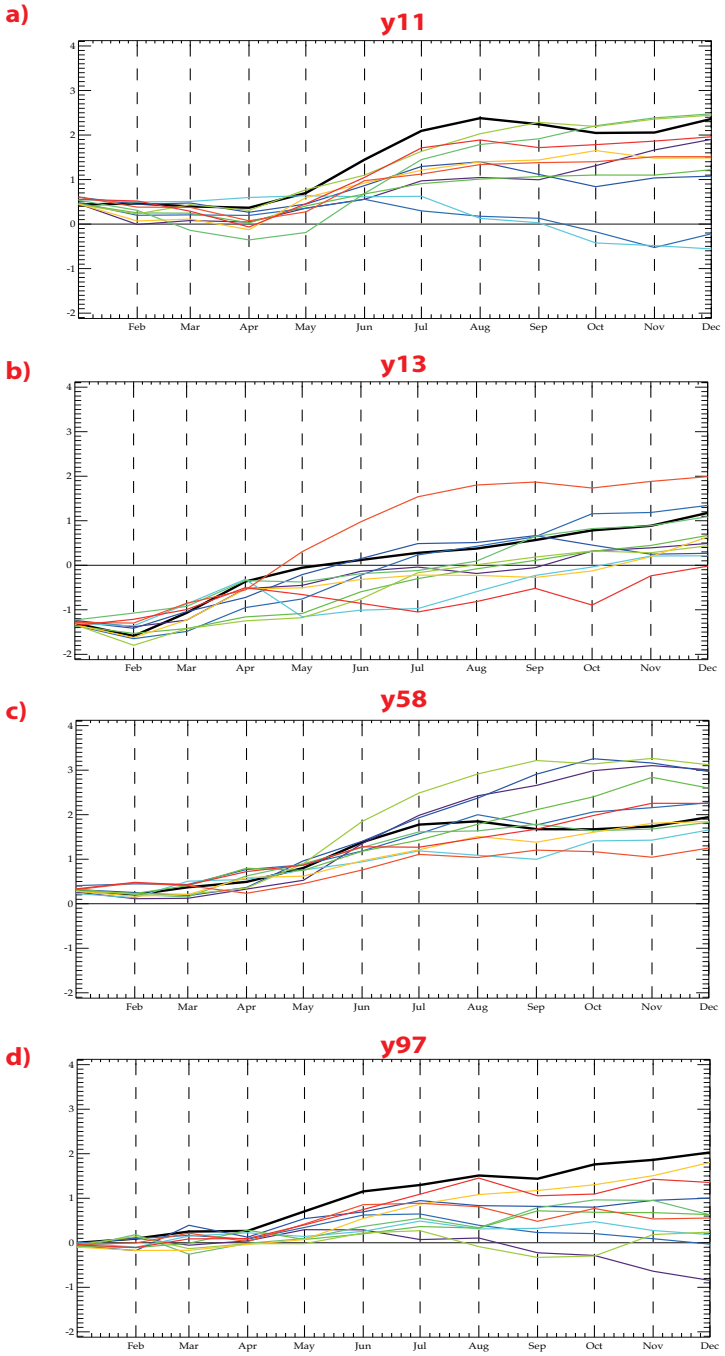

Figure IV.29: Monthly Niño3.4 SST timeseries (°K) in the control run (in black) and perturbed runs (in colour) for the selected years **(a)** 11, **(b)** 13, **(c)** 58 and **(d)** 97.

In order to facilitate a detailed and robust comparison of the perturbed runs for each El Niño event, and from one event to another, we have also presented these results in the alternative form of bar plots for each year involved in the sensitivity experiments (as in Fig IV.26). In Fig. IV.30, each bar represents the projection of SST anomalies in OND (control run in black, perturbed runs in colour), onto the SST singular vector associated with the 1^{st} SVD (USTR-SST) mode (computed from the control run), thereby showing the impact of the initial SST perturbation on the tropical SSTs this time *only during the following winter*. Similar results are obtained with the projection onto the SST singular vector associated with the 1^{st} SVD (Z20-SST) mode or with any of the SST precursors, since all the SST singular vectors of these modes are all very similar (see Part I).

Once again, year 58 stands out as the most robust event, as the initial El Niño is able to persist in 100% of the simulations (Fig IV.30c). Although initially stronger, the El Niño of year 11 persists only in 80% of these simulations (Fig.IV.30a). Finally, years 13 and 97 seem 'more easily perturbed' in the sensitivity experiments (Figs IV.30b and d), although the evolution of El Niño in year 97 is very similar to the event occurring in year 58 in the control run (Fig IV.25).

How can similar El Niño events respond so differently to a global SST perturbation? What causes this large spread of tropical Pacific SST conditions simulated during the following winter in the perturbed runs of each year, and from one event to the other? In an attempt to understand the diversity of El Niño responses in our sensitivity experiments, we will now examine in more detail the behavior of the precursory signals during the previous boreal spring (identified in Part I) in each of these perturbed runs. This is done, as previously, by projecting the time series produced in the perturbed runs onto the SVD modes associated with the Z20, USTR and SST precursors.

b - Heat content in JFM and zonal wind precursor in FMA

The projection of Z20 anomalies in JFM onto the Z20 singular vector of the 1^{st} SVD (Z20-SST) mode, and of USTR anomalies in FMA onto the USTR singular vector of the 1^{st} SVD (USTR-SST) mode are shown in Fig IV.31a and b, respectively.

In these bar plots, the more or less constant values of Z20 anomalies in the perturbed runs clearly contrast with the scattered bars associated with the USTR precursor, and this for each selected year. As it may be expected, the zonal wind anomalies in FMA are more easily perturbed than heat content anomalies in these sensitivity experiments, and may thus be largely responsible for the modulation of El Niño events in the perturbed runs (see Fig IV.30). As a first illustration, in year 13, the perturbed run producing a much stronger El Niño event than the control run (see the dark orange line in Fig IV.29b or bar in Fig IV.30b) has also the highest loading in the projections onto the USTR singular vector of the 1^{st} SVD (USTR-SST) mode (see Fig IV.31b), while the corresponding loading for the

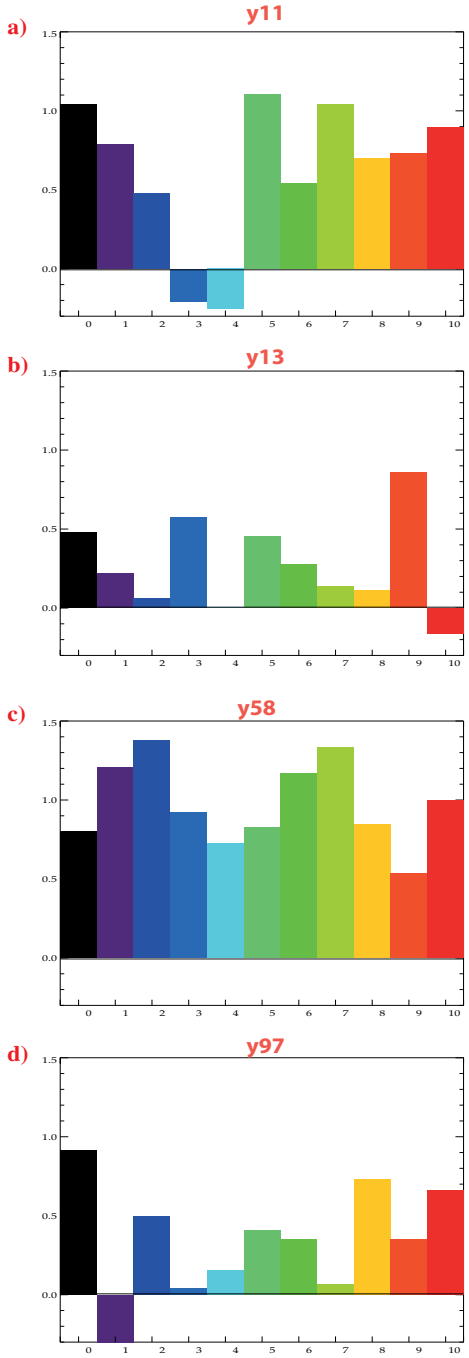

Figure IV.30: Projection of SST anomalies in the tropical Pacific during OND for **a)** y11, **b)**13, **c)** 58 and **d)** y97 of the control run (black bar) and perturbed runs (coloured bars), onto the SST singular vectors of the 1^{st} of SVD (USTR-SST) mode.

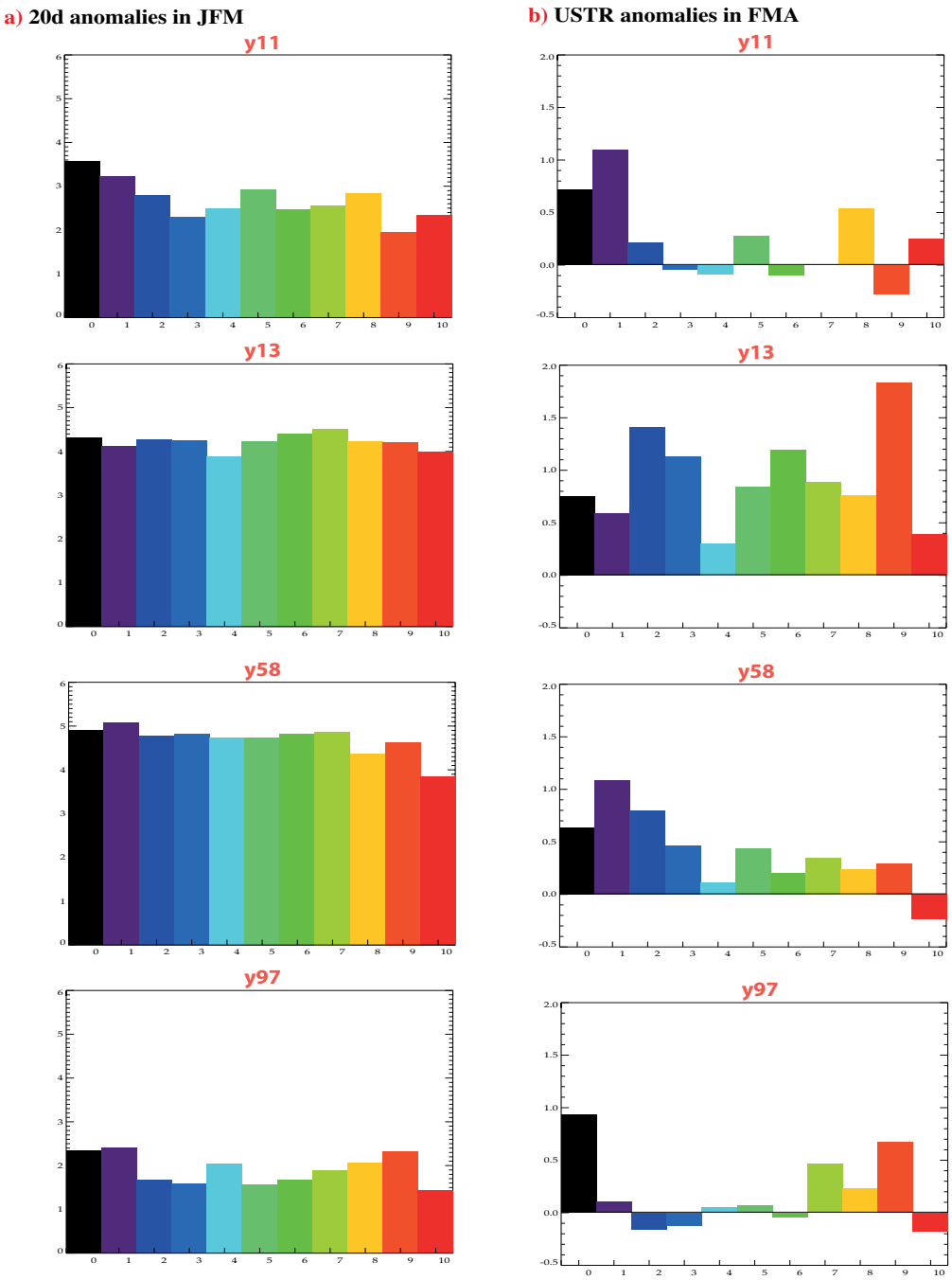

Figure IV.31: Projection of **(a)** Z20 anomalies in JFM onto the Z20 singular vectors of the 1^{st} SVD(Z20-SST) mode and **(b)** USTR anomalies in FMA onto the USTR singular vectors of the 1^{st} SVD(USTR-SST) mode, for each year in the control run (black bar) and perturbed runs (colored bars).

Z20 projection is roughly at the same level as the one associated with the control run. Similarly, in year 97, the only perturbed run evolving into a La Niña state (see purple case in Figs IV.29d and IV.30d) has the highest loading in the Z20 projections, but a very low loading in the USTR projections. Finally, for year 11, the strongest El Niño event in the control run, the two perturbed runs evolving into a neutral state in the following winter (*e.g.* the two blue lines or bars in Fig IV.29a and IV.30a, respectively) are also characterized by negative loadings in the USTR projections, even though these projections are not the most negative ones in the set of 10 perturbed experiments for this event.

These results seem to highlight the key importance of wind variations over the (western) Pacific during boreal spring in the simulated El Niño events. This hypothesis justifies that, so far, we have been examining the SST precursors through the channel of the zonal wind variability, *i.e.* by considering the SST modes derived from the SVD analyses between these SST precursors and the zonal wind variability over the equatorial Pacific during FMA (see Part I).

In the next section, we will thus examine the impact of the imposed SST perturbation on the SST precursors during boreal spring, by using the SVD analyses between the SIO, IOB and NPO precursors in JFM and the zonal wind anomalies over the equatorial Pacific during FMA. However, similar results are obtained if we consider the SVD analyses between these SST precursors in JFM and Pacific SSTs in the following winter (in ONDJF).

c - SST precursors in JFM

Figure IV.32 shows, for each run, the projection of SST anomalies associated with each SST precursor in JFM onto the SST singular vector of the corresponding SVD (SST precursor-USTR) mode. These results will here be analyzed for each selected year in two prospects:

- first, in terms of the **relative importance** of each SST precursor for the following El Niño event,
- and secondly, in terms of the **robustness** of these SST precursors in the face of the initial SST perturbation in the control simulation.

As already described in the previous section, the SIO and NPO SST precursors (2^{nd} SVD modes in each case) seem to play an important role in the very strong El Niño occurring in year 11 of the control run (see Table IV.10 and the black bars in the 1^{st} line of Fig IV.32c-d). This hypothesis is largely confirmed here by the concomitant large decrease of the El Niño amplitude (see Fig IV.29a) and of the loadings associated with these SST precursors in many of the perturbed runs in Fig IV.32

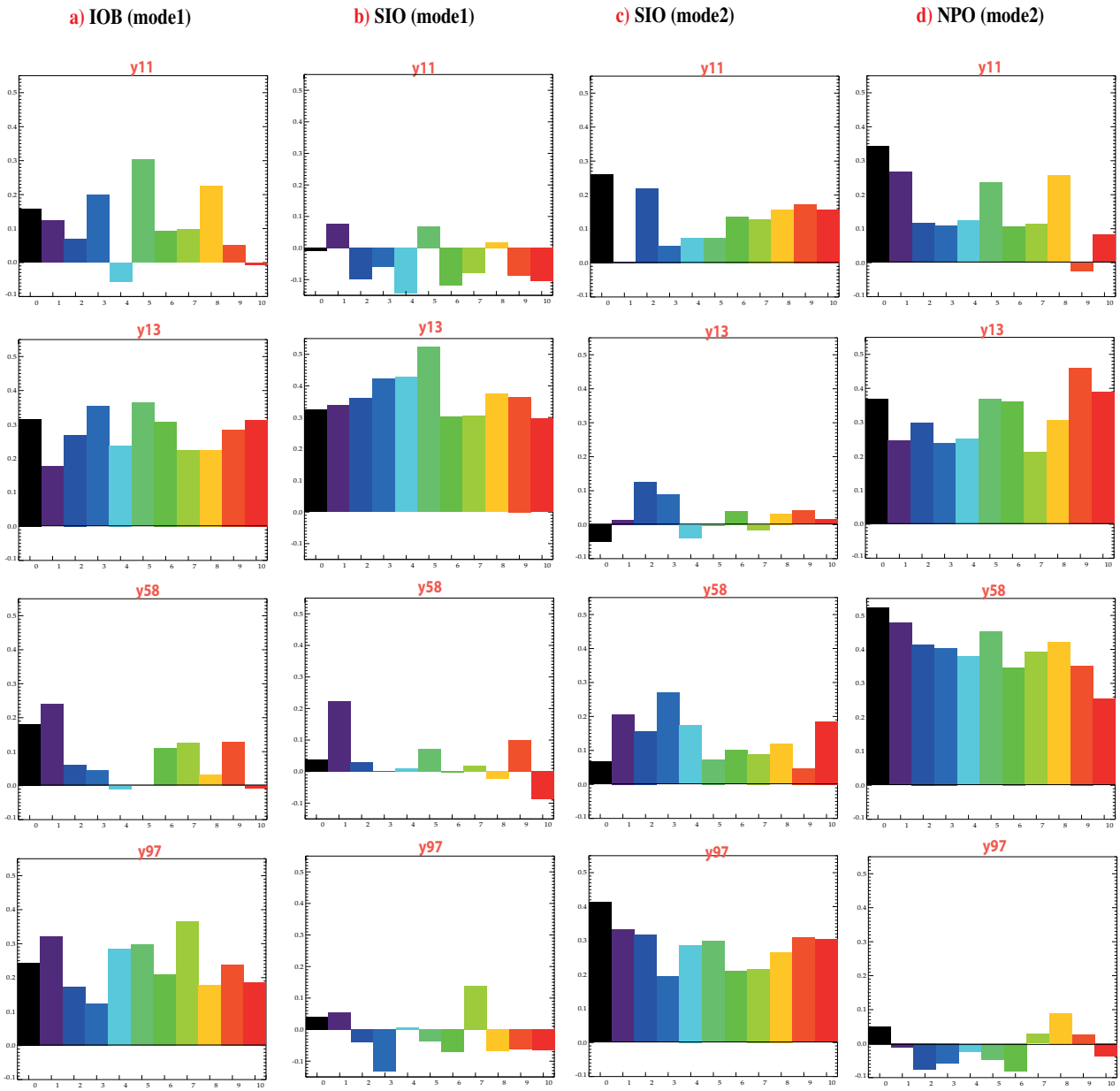

Figure IV.32: Projection of **(a)** IOB, **(b-c)** SIO and **(d)** NPO SST anomalies in JFM onto the SST singular vectors of the **(a)** 1^{st} SVD(IOB-USTR) mode **(b)** 1^{st} SVD(SIO-USTR) mode **(c)** 2^{nd} SVD(SIO-USTR) mode and **(d)** 2^{nd} SVD(NPO-USTR) mode, for each El Niño year of the control run (black bar) and the perturbed runs (colored bars).

(1^{st} line). Given that the heat content recharge preconditioning is not maximized for this event in the control run, but is also not fundamentally perturbed in the sensitivity experiments (see the Z20 projections for year 11 in Fig IV.31a), the exceptional strength of this El Niño event in year 11 can be largely attributed to the extratropical signals in the NPO and SIO domains. Besides, the synchronous decrease of the loadings associated with the USTR, NPO and SIO precursors for this particular event are consistent with the hypothesis that these extratropical signals play a fundamental role in the modulation of the wind anomalies over the western Pacific during boreal spring (*i.e.* near the onset of the event).

The results for year 13 are entirely different, as the important SST precursors for this event, namely the IOB, SIO (1^{st} mode) and the NPO (see Table IV.10), have projection loadings of the same order of magnitude in the control and perturbed runs (Fig IV.32). This is consistent with the high loadings found for the USTR precursor in many of the perturbed runs in year 13 (see Fig IV.31b), and highlights again the importance of the Indian and North Pacific oceans SSTs for modulating the low-frequency wind anomalies over the western Pacific during spring. However, the overall robustness of the ENSO signal and of the various wind and SST precursors in year 13 are probably mainly linked to the large heat content recharge and the previous La Niña state observed in the equatorial Pacific before the onset of the event year 13 (Figs IV.29b and IV.31a).

Year 58 is also a very interesting case, in which the heat content recharge is maximum out of all the cases studied here (Fig IV.31a), but not linked to a previous La Niña state as year 13 discussed above (Fig IV.29c). During this event, the NPO precursor is by far the most dominant SST signal (Fig IV.32d), despite a very modest signal for the USTR precursor in the control run (Fig IV.31b). Indeed, the NPO mode remains rather unperturbed during JFM of year 58 (Fig IV.32d), and the following El Niño event stands out as being particularly robust, as it is the only El Niño event able to persist in all the perturbed runs of our experiment (Figs IV.29c and IV.30c).

Finally, year 97 presents yet another interesting case study, with the weakest heat recharge preconditioning before the onset of the El Niño event (Fig IV.31a), but at the same time the largest USTR precursory signal over the Pacific in the control run (Fig IV.31b). Although the El Niño event in this case may be largely flawed by its weaker heat content preconditioning (see Table IV.10), the El Niño amplitude observed during the next boreal winter is at the same level or even stronger than in years 13 and 58, in which the heat content preconditioning is optimal (Fig IV.29). Besides, the significant zonal wind signal during year 97 seems to be mostly associated with SST precursors over the Indian Ocean in the control run, namely the SIO (2^{nd} mode) and to a much lesser extent the IOB (1^{st} mode) (see Fig IV.32, last line). This dominant role played by the SIO SST precursor (2^{st} mode) is corroborated by the results of our perturbed experiments since, in all

the perturbed runs, we observe a large decrease of the El Niño signal preceded by a concomitant weakening of both the SIO and USTR precursory signals during boreal spring (Figs IV.31b and IV.32c).

Overall, the various bar plots in Fig IV.32 suggest that the SIO, NPO and to a lesser extent IOB are robust precursors in the model, as they are only weakly perturbed during the years when they have been shown to play a significant role (see Table IV.10). This is the case of the 1^{st} IOB and SIO modes in year 13, the 2^{nd} NPO mode in year 58, and the 1^{st} IOB mode and 2^{nd} SIO modes for year 97. Indeed, for these precursors, the projections associated with most of the perturbed runs (coloured bars) yield values that are positive and quite comparable to the projection values obtained from the control run (black bar, Fig IV.32). Moreover, when there is a large decrease in the projection loadings of these significant SST precursors for a particular year in the perturbed runs, we generally observe a weakening of the ongoing El Niño event, as well as a concomitant decrease of the projection loading associated with the zonal wind (USTR) precursor during boreal spring. This is again consistent with the key role of the SST precursors studied here for the ENSO evolution in the coupled model.

But which of these SST modes is the most important for the following ENSO? If we focus on the two last columns of Fig IV.32, we can notice that the NPO and SIO 2^{nd} SVD modes, alone, seem able to explain a considerable part of the modulated El Niño conditions observed each year in Fig IV.30: this stresses the importance of extratropical modes of variability for the ENSO evolution in the model, through the channel of zonal wind anomalies over the western equatorial Pacific before the El Niño onset. The IOB plays a non-negligible role during each year, however it seems difficult to evaluate its respective contribution based on this simple analysis, taking into account that the loadings associated with the IOB are of moderate values and always weaker than those found for at least one of the other SST precursors (see Fig IV.32). Finally, these results seem to highlight the importance and robustness of the NPO precursor for El Niño prediction in the model, as it stands out as a dominant player in 3 of 4 of the El Niño years examined here (years 11, 13 and 58), in both the control and perturbed runs (see Fig IV.32).

IV.9 Conclusion

Results from the sensitivity experiments have shown that the IOB, SIO and NPO SST precursors all play an important role during the four selected El Niño events, in addition to the traditional ENSO precursors, namely the Z20 and USTR precursors. Furthermore, these results suggest that the main effects of the SST precursors outside the tropical Pacific seem to rely on the modulation of the wind variations over the western equatorial Pacific, as suggested in the previous observational studies [*Terray*, 2011; *Vimont et al.*, 2003a].

The IOB 1^{st} mode contributes only moderately to each of these events, however this mode captures the effect of the previous ENSO state, and may also combine different sources of local SST forcing in the IO. Further work is needed to be able to distinguish each of these potential contributions to the following El Niño event.

The SIO and NPO extratropical modes play a key-role in the El Niño evolution simulated by the SINTEX-F model. These SST precursors can act either separately or together depending on the El Niño event, and in complement of the heat content recharge state of the ocean before the onset of the event. The SIO signal exerts a significant control on the zonal wind variations over the equatorial Pacific and plays a fundamental role in 2 out of the 4 selected El Niño years (years 11 and 97). However, the NPO stands out as the most robust SST precursor studied here, for 3 out of 4 of these El Niño events (years 11, 13 and 58).

In order to unravel in more details the relative contribution of each of these SST precursors, we will need to carry out additional numerical experiments. For instance, we could perform similar ensemble run simulations during the same four El Niño years, but this time we could add the initial SST perturbations (perhaps of a greater amplitude) only to precise/key regions, which have been identified as the most significant for each of the selected years in the control run. This would allow us to test, individually, and more precisely the role, as well as the robustness of each of these precursors.

Chapter V

CONCLUSION and PERSPECTIVES

Contents

V.1 Conclusion

This thesis takes part in a global effort to improve our understanding of the potential predictability of ISM rainfall and ENSO, by exploring the large-scale teleconnections associated with the whole monsoon-ENSO system on interannual timescales and the role played by leading modes of coupled variability, particularly in tropical and extra-tropical parts of the Indo-Pacific region. In this work, our intention is not to detail the small-scale processes inherent to the monsoon or to ENSO, but rather to approach this problem from a *global* point of view, and focus, as a preliminary step, on the importance of ocean-atmospheric coupling and fast atmospheric teleconnections for the predictability of the monsoon and ENSO [*Dommenget*, 2010; *Clement et al.*, 2011; *Luo*, 2011].

In the scientific community, there is a general and accepted consensus that ENSO represents an important source of predictability for tropical and mid-latitudes in both the northern and southern hemispheres; but these extratropical latitudes, in return, are believed to exert a relatively weaker influence on the interannual variability of tropical phenomena such as ENSO or the Asian Monsoon [*Alexander et al.*, 2002]. However, this potential extratropical influence has so far received only too little attention. This thesis follows some of the most recent works from Vimont and colleagues [*Vimont et al.*, 2001, 2003a, 2009; *Chang et al.*, 2007] or Terray [*Terray et al.*, 2003, 2005a, 2007; *Terray*, 2011], and attempts to bridge in a single coherent framework, some of the fragmented (and at times contradictory) and recent results on the forcing from mid-latitude to tropical regions, in observations and in coupled model simulations. A major outcome from this work is that these mid-latitudes are also a very significant source of predictability for tropical regions, particularly for major climatic phenomena such as the Indian Summer Monsoon or ENSO, and that this forcing most likely occurs through fast atmospheric teleconnections.

V.1.1 ISM predictability in observations

For India's population, climate is a deciding factor in the subsistence of everyday life, since droughts and floods associated with the interannual variation of the seasonal monsoon rainfall (from June to September) have devastating effects on the people, agriculture and economy of the region. The most recent Indian drought in 2009 brought to the fore the poor skill of the current seasonal forecast models, and once again stressed the need for accurate seasonal prediction of rainfall over India [*Francis and Gadgil*, 2010]. This prediction is not only important because of its socioeconomic impact on the Indian subcontinent, but also because of the monsoon's interaction with other components of the global climate system, in particular with slowly varying events such as ENSO events.

In the first part of this thesis, we have examined the variability and predictability of ISM rainfall, by exploring its relationship with global SST modes of variability, and evaluating the possible changes in these teleconnections before and after the 1976-77 climate shift in observations [*Boschat et al.*, 2011a,b].

The first paper (**Chapter 2**) focuses on the recent 1979-2007 period, and compares the respective merits of key SST indices in the Indo-Pacific region, which have already been proposed as ISM predictors in the literature [*Webster et al.*, 1998; *Saji et al.*, 1999; *Yang et al.*, 2007; *Terray et al.*, 2003, 2007; *Krishnan and Swapna*, 2009]. The relevance of each SST index for the monsoon is assessed in terms of its statistical association with ISM rainfall and its dynamical properties, *i.e.* the mechanisms through which it may impact Indian rainfall during the following summer. The originality of this work lies in the fact that we have gathered these various pre-defined SST indices in a *single* framework, and examined their relative role *on* the monsoon: a comparison which had never really been carried out in the literature. Another original perspective from this work, is that we considered these ISM-SST teleconnections on both a seasonal and monthly timescale during JJAS: this showed us that the ISM interannual variability was significantly affected by the timing of rainfall onset and withdrawal (in June and September), thereby questioning the validity of using here the conventional *seasonal* ISM rainfall index (*i.e.* during JJAS). By considering this subseasonality, and by evaluating the effect of each SST index on the *timing* of monsoon onset and withdrawal as well as the *amount* of rainfall, we were able to show that ISM predictability is significantly different for the early and late summer season, and that, surprisingly, both ENSO and local IO SST indices (in tropical *and* subtropical regions of the IO) give rise to prospects of higher predictability for ISM onset, and for the amount of rainfall during August-September.

An important problem about ISM teleconnections and predictability is the stationnarity of the observed relationships on longer periods. Therefore, these results are confirmed in the larger and more objective framework proposed in our 2^{nd} paper [*Boschat et al.*, 2011b], where ISM-SST relationships are examined on a global spatial scale, and during both 1950-1976 and 1979-2006 time periods (see **Chapter 3**). The purpose of this analysis is to test the robustness and stability of the predictive relationships proposed in [*Boschat et al.*, 2011a], and its originality resides in the decomposition of ISM-SST relationships on two levels: during the 1^{st} and 2^{nd} part of the ISM season (in JJ and AS), and during El Niño and La Niña years. This approach has offered new and interesting perspectives in terms of *(i)* ISM predictability and *(ii)* in our understanding of the ISM-ENSO relationship.

(i) ISM predictability

Indeed, our results corroborate the existence of higher predictability for AS rainfall, but here stress the **importance of *extratropical* forcing on the monsoon**, as the most robust SST precursors

stem from the South IO and North Pacific Ocean during the previous boreal winter and spring. These are well-known precursors of ENSO, and may thus affect the monsoon indirectly through their forcing on ENSO [*Vimont et al.*, 2003a, 2009; *Terray and Dominiak*, 2005], as well as their direct forcing on the monsoon system [*Terray et al.*, 2007; *Peings et al.*, 2009].

(ii) ENSO-monsoon relationship

The distinction between JJ and AS rainfall also suggests the occurrence of a **'phase-shift' rather than a weakening of the ENSO-monsoon relationship in recent decades** [*Kumar et al.*, 1999; *Kinter et al.*, 2002]. Indeed, JJ and AS Indian rainfall are always strongly related to ENSO, but after 1979, AS rainfall becomes more significantly linked to the decaying phase of ENSO, and no longer to its development! This AS phase shift suggests that ENSO has become a significant *precursor* for the monsoon in recent decades.

The El Niño-La Niña decomposition provides a possible explanation for this inter-decadal modulation, by showing that opposite processes may be occurring during the 1^{st} and 2^{nd} part of the ISM season and affecting the seasonal ISM-ENSO relationship. Indeed, JJ Indian rainfall seems mostly sensitive to ENSO, but in AS, local IO feedbacks come into play and may counteract this effect of ENSO on ISM rainfall. A recent enhancement of these local IO feedbacks in AS could be the main cause to an *apparent* weakening of the ENSO-monsoon relationship on a seasonal scale.

This hypothesis will be discussed in more detail in the perspectives section of this chapter.

V.1.2 ENSO predictability in observations and in the SINTEX-F coupled model

Finally, in this last part of the thesis, we have further examined the predictability offered by this common extratropical forcing on the monsoon-ENSO system, but this time through the window of ENSO variability, and with the help of both observations and the SINTEX-F coupled model. Our motivation in this last chapter is similar to the previous monsoon analyses: *(i)* to assess the respective role of various tropical and extratropical SST precursors which have been suggested to impact ENSO onset in the literature ([*Clarke and Van Gorder*, 2003; *Kug and Kang*, 2006; *Vimont et al.*, 2009; *Izumo et al.*, 2010; *Terray*, 2011] among many others), and also *(ii)* to test the robustness of these predictors through numerical experiments.

However, our approach is here somewhat different and based on a more sophisticated statistical analysis (*i.e.* Singular Value Decomposition method), which consists in identifying leading modes of covariability with relevant information for ENSO, and then classifying these potential predictors according to their predicting skill for El Niño or La Niña events. This SVD methodology here seeks objectivity, and is applied to large spatial and temporal frames, in order to sidestep the biases linked to the choice of specific indices to represent climatic modes of variability and potential precursors in both observations and numerical climate simulations. In order to distinguish the SST signal reflecting

the effect of the *previous* ENSO state from that indicating a potential *'intrinsic'* source of forcing for ENSO, we also considered several SVD modes for each precursor, and then determined which of these modes carried the best predicting skill for the following ENSO state. Overall, this SVD method has proved itself to be quite relevant for the study of ENSO predictability, as it has allowed us *(i)* to compare in a single conceptual framework various potential sources of ENSO forcing, with some *quantitative* insight into their respective merit for ENSO forecast, and *(ii)* to overcome the challenging problem of the spring predictability barrier of ENSO-related SST indices. We began by elaborating and defining this set of metrics in observations, and ensuring that the SINTEX-F model was realistic in its representation of ENSO and of its relationship with 'conventional' precursors during boreal spring (*e.g.* tropical Pacific heat content and low-frequency wind variability). We were then able to apply these SVD metrics to both the SINTEX-F control run and observations, in order to identify other key regions for ENSO prediction: in the tropical IO (*e.g.* IOB or IOD modes) and in extratropical regions of the South IO (SIO mode) or North Pacific Ocean (NPO mode).

Our main results show that, in both observations and model, predictability for ENSO can stem from the **biennial tendency of ENSO itself**, or from intrinsic sources of predictability in subtropical regions of the South IO and North Pacific ocean, linked to local dipolar SST variability excited by **mid-latitude atmospheric variability** in early spring (similar to the variability affecting the monsoon). Our analysis highlights the importance of this extratropical forcing, and shows that these SIO and NPO modes are the most promising SST predictors outside the tropical Pacific for both El Niño and La Niña events. This extratropical variability could be emerging in the 'stationary' form of coupled ocean-atmospheric modes, similar to the seasonal SST dipoles described in [*Vimont et al.*, 2003a; *Terray*, 2011], or in the form of atmospheric 'pulsations' linked to higher frequency blocking phenomena (*e.g.* Mascarene High in the SIO, Aleutian Low in the NPO). In either case, these SIO and NPO modes carry predictability for ENSO and stand out as the most robust precursors in the model (with the IOB to a lesser extent), since results from our sensitivity experiments (ensemble perturbed runs) show that these precursory modes either remain stable during the El Niño years when they have been shown to play a significant role, or else when they are effectively perturbed and weakened, this often leads to a concomitant decay of the ongoing El Niño signal. These SST precursors can play either separately or together (*e.g.* as in the 1997-98 El Niño) depending of the type of El Niño event, and their main effect on ENSO essentially relies on the modulation of the wind variations over the western equatorial Pacific, as suggested in previous observational studies [*Vimont et al.*, 2003a; *Terray*, 2011]. Although this effect is not systematic, our numerical experiment reveals that the occurrence and strength of these precursory extratropical signals in the North Pacific and South IO can largely affect the amplitude of ENSO in our coupled simulation. This result has interesting implications concerning the role of extratropical atmospheric teleconnections for the predictability of ENSO, and is consistent with challenging new ideas on this matter from *Clement*

et al. [2011].

V.2 Perspectives

The work in this thesis opens up many perspectives in the field of predictability of the monsoon-ENSO system, in particular concerning the role of tropical-extratropical teleconnections, the underlying physical mechanisms, their representation in global coupled models, and how they may evolve in a future warmer climate.

V.2.1 An increasing influence from extratropics on the ISM-ENSO system?

To begin with, we have shown evidence that extratropical variability exerts a significant control on the recent ENSO-monsoon system at the interannual timescale. A first important question is whether this forcing is stationary in time, or if it is a unique characteristic of the recent period.

In 2005, Terray and Dominiak presented the South IO SST as a key precursor in predicting El Niño evolution, but showed that this statistical relationship was highly significant only after the 1976-77 climate shift. The predictive relationship between extratropical precursors and the ISM seems to have also strengthened since the late 1970s, as it is illustrated here by the steady increase in the sliding correlations between ISM rainfall and the 'extratropical' predictors currently used by the Indian Meteorological Department in their statistical seasonal forecasts of ISM rainfall (red curve in Fig V.1).

Is this increasing influence from the extratropics intrinsically non-deterministic and driven by stochastic effects from the atmosphere? Or is it linked to the anthropogenic global warming of the planet? In order to examine the possibility of a link between these enhanced tropical-extratropical interactions and climate change, it would be interesting to reproduce the set of analyses carried out in this thesis for the monsoon and for ENSO, using the CMIP5 panel of models (driven by Greenhouse Gases (GHG) climate scenarios for the 21^{st} century).

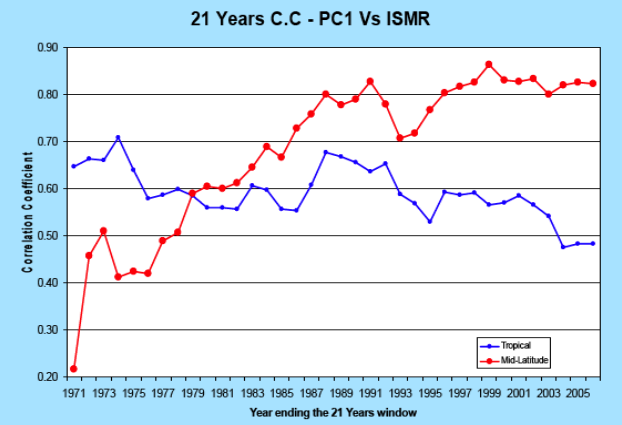

Figure V.1: Sliding correlations on a 21-year moving window between ISM rainfall and the 1^{st} principal component of the tropical (blue curve) and extratropical (red cruve) precursors used by the Indian Department of Meteorology in their seasonal forecasts based on statistical methods/empirical models (Courtesy of Dr. Rajeevan).

V.2.2 What physical processes are behind these extratropical-tropical teleconnections?

Given the importance of this extratropical forcing on the whole ISM-ENSO system, it now seems essential to gain a better understanding of the physical processes linked to each of these potential predictors (*e.g.* in the North Pacific or South IO).

ENSO precursors

Results in this thesis have suggested that extratropical SST precursors in the North Pacific and South IO may affect ENSO through fast atmospheric teleconnections, involving a modulation of zonal wind variations in the west equatorial Pacific during boreal spring. However, these NPO and SIO modes have obtained higher predicting scores for ENSO in the *direct* SVD analysis with tropical Pacific SST anomalies during boreal winter (rather than with the intermediate SVD with zonal wind stress during boreal spring, see Tables IV.4 and IV.6 in **Chapter 4**), which suggests that these predictors may affect ENSO through different or additional means than this spring wind modulation. The NPO and SIO - ENSO mechanisms evidently deserve further study, and this could be investigated through sensitivity experiments with the SINTEX-F coupled model. As an example, we could perform similar perturbed ensemble runs as in **Chapter 4**, but add SST perturbations only to precise locations and at specific times during each El Niño year. Sensitivity experiments could also be designed during the same El Niño years, but where, this time, positive/negative SST anomalies (of various amplitudes) are inserted in the key SIO or NPO regions during early boreal spring, as to examine the impact of each type of SST anomaly on the following ENSO, and then compare this with the evolution of the initial ENSO event in the control run.

Besides, these numerical experiments could also be used in an attempt to examine the *interdependence* of these various predictors for the ISM-ENSO system. This issue is particularly at stake in the IO, where the SIO mode at the end of boreal winter has been shown to be quite intimately linked with other IO SST modes of variability (*e.g.* IOB during the following spring or IOD mode during the previous fall). It would be interesting to examine the interactions between these tropical and extratropical modes of variability in the IO, without excluding the possibility of a 'cross-hemispheric' link also between the extratropical SIO and NPO modes.

Finally, it seems important to point out that we have not included the Atlantic basin in our SVD analysis of ENSO predictability, although recent studies suggest this ocean also exerts a significant influence on the ISM-ENSO system [*Kucharski et al.*, 2008, 2009; *Rodriguez-Fonseca et al.*, 2009]. Our analysis of ISM predictability showed no convincing contribution from Atlantic SSTs on ISM [*Boschat et al.*, 2011b], however its potential effect on ENSO variability remains to be tested. This could be done by applying the same methodology developed in this thesis to precursory SST signals in tropical or extratropical regions of the Atlantic Ocean.

ISM precursors

Meanwhile, the recognition of *common* precursors for ISM and ENSO also raises the question of whether the extratropics have a *direct* impact on the monsoon, or whether their influence mainly relies on an *indirect* forcing on ENSO.

Boschat et al. [2011b] have highlighted the importance of these NPO and SIO extratropical precursors for ISM rainfall even before the 1976-77 climate shift, though the SIO precursor during the same period shows no significant predicting skill for ENSO [*Terray and Dominiak*, 2005]. This result tends to support the hypothesis that at least a part of this extratropical forcing on the monsoon occurs 'independently' from ENSO. The physical processes inherent to this direct forcing need to be examined, and this could be done through similar numerical experiments as those proposed for ENSO (or analogous to what has already been done for the SIO mode in [*Terray et al.*, 2007]), using a coupled model which is able to realistically simulate the ISM mean state and interannual variability.

Besides, we need to bear in mind that, in observations, ISM predictability is significantly different for the early and late summer season, and global monsoon teleconnections seem to be largely affected by subseasonal features of the monsoon (*e.g.* timing of ISM onset and withdrawal, see [*Boschat et al.*, 2011a,b]). It thus seems important to be able to assess the impact of these timescale interactions on ISM predictability. In this perspective, it would be interesting to examine and compare to what extent, the 1^{st} and/or 2^{nd} part of the ISM season may be affected by this increasing influence of the extratropical SIO and NPO modes.

V.2.3 Impact of global warming on the ISM-ENSO relationship?

Finally, this thesis has suggested that the ISM-ENSO relationship has experienced an AS phase-shift rather than a weakening in recent decades, and that this could be linked to a recent enhancement of local feedbacks in the IO during the late summer season [*Boschat et al.*, 2011b]. But why would the IO ocean-atmosphere interactions be stronger in recent decades? Several works have suggested a more frequent occurrence of extreme IOD events, possibly due to global warming [*Ihara et al.*, 2008, 2009; *Cai et al.*, 2009b,c] or a natural decadal fluctuation of the tropical system [*Zheng et al.*, 2010], developing in association with strong El Niño events. We suspect this change of nature or 'phase-shift' in the ENSO-monsoon relationship may be related to a sustained warming of the IO occurring in response to global climate change. This impact of climate change is illustrated in Fig V.2, in terms of SST trends observed from 1960 to 2005 over the Indo-African region, which shows that the tropical IO is marked by a clear expansion of the Indian warm pool. It is argued here that the change in SST mean state, particularly in the west part of the basin, may lead to an increase in the intensity of local ocean-atmospheric interactions (due to an increase in SST values above which the non linear relationship between convection and SST becomes pronounced). This question could be further addressed in the framework for climate change experiments, which will soon be provided by the CMIP5 simulations.

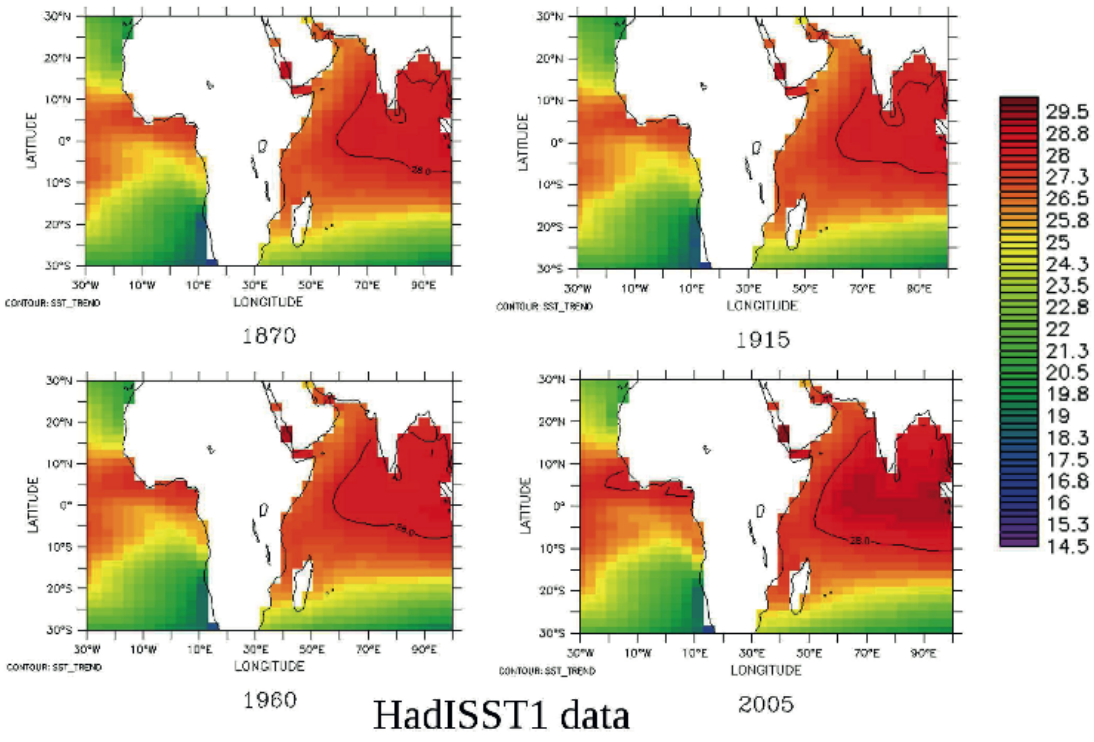

Figure V.2: SST trends in the West Indo-African region, calculated from HadISST1 dataset and using the STL filtering method over the 1871-2006 period, and shown here for four specific years in 1870, 1915, 1960 and 2005. The contour shows the position of the 28°C isotherm for each year (Courtosy of Ms. Gaëlle Drouot).

Appendix A

ISM teleconnection and precursory patterns in the SINTEX-F coupled model

A.1 Description of the SINTEX-F coupled model

The results of **Chapter 4** are based on the global coupled ocean-atmosphere general circulation model (CGCM) called SINTEX-F2, an upgraded version of SINTEX-F1 [*Luo et al.*, 2003; *Masson et al.*, 2005; *Luo et al.*, 2005b] that is very close to the model used by *Park et al.* [2009] but with higher resolutions in the ocean and the atmosphere. This CGCM, developed in the framework of an European Union-Japan collaboration, is based on ECHAM5.2 [*Roeckner et al.*, 2003], NEMO 3.2 [*Madec*, 2008] and OASIS3 [*Valcke*, 2006].

The physics of the atmospheric model is very close to the one used in SINTEX-F1 and we will not go into details in this thesis. ECHAM5 includes the *Tiedtke* [1989] bulk mass flux formula for cumulus convection with modifications for penetrative convection according to *Nordeng* [1994], and the *Morcrette et al.* [1986] radiation code. See [*Luo et al.*, 2005a,b] for a more complete description of the physics of the atmosphere. The atmospheric grid has a relatively high horizontal resolution of about 1.1°by 1.1°(T106, same as in SINTEX-F1). A hybrid sigma-pressure vertical coordinate (31 levels instead of 19 for SINTEX-F1) is used with the highest resolution near the earth's surface [*Roeckner et al.*, 2004].

The oceanic component uses OPA [*Madec*, 2008] for the oceanic dynamical core and LIM2 [*Timmermann et al.*, 2005] for sea-ice model (SINTEX-F1 had no sea-ice model). We use the configuration known as "ORCA05" (DRAKKAR 2007) which is a tri-polar global grid with a resolution of 0.5°by

0.5°cos(latitude). The default vertical resolution is 31 levels with a layer thickness of about 10m meter in the first 100 meters. Following *Barnier et al.* [2006], we use the combination of an energy enstrophy conserving scheme for momentum advection with a partial step representation of the bottom topography. Viscosity is parameterized with the help of a horizontal biharmonic operator (-8.5e+11 m4/s), whereas tracer diffusivity operator is an isopycnal laplacian (500m2/s). The parameterization of *Gent and McWilliams* [1990] is used to reproduce the effect of eddies on tracer advection (500m/s). Tracer advection is parameterized using the Total Variance Dissipation (TVD) formulation [*Zalesak*, 1979]. The vertical eddy viscosity and diffusivity coefficients are computed from a turbulent closure model based on a prognostic equation of the turbulent kinetic energy (TKE) including a dependence of near surface mixing length on the surface wave field [*Bernie et al.*, 2007]. The ocean is started from rest, and initialized by a mean Levitus T–S field.

The coupling information, without any flux correction, is exchanged by means of the OASIS 3 coupler [*Valcke*, 2006] in its pseudo-parallel configuration. Our physical interface for the air-sea coupling differs from the one described by *Park et al.* [2009] in only 2 points. First, we do not send the surface sea-ice temperature to the atmosphere and we do not send the runoff and the calving to the ocean. Instead we have used, in the ocean, monthly climatological values ensuring a realistic outflow of major tropical rivers (the Ganges for example). Secondly, heat and freshwater fluxes over sea-ice are weighted by the fraction of sea-ice in order to preserve the total fluxes sent by the atmosphere regardless of the changes of sea-ice cover during the coupling period. The coupling frequency between the ocean and the atmosphere is 2 hours.

A.2 Validation of the model

A thorough validation of the coupled model's mean state and seasonal cycle is given in [*Masson et al.*, 2011]. Besides, the characteristics of the ISM, ENSO and IOD signals in the control simulation have also been analyzed in a recent study by *Terray et al.* [2011].

In this section, we are simply interested in comparing and confronting the results from our observational diagnoses to the SINTEX-F control simulation, in particular those regarding the ISM-SST teleconnections (in **Chapter 2** and **Chapter 3**). We will also illustrate the model's skill in representing ENSO, through the correlation between the Niño3.4 index and global SST. This will justify the use of the SINTEX-F coupled model for our analysis of ENSO variability and predictability in **Chapter 4** of this thesis.

To begin with, the correlation between ISM rainfall in JJAS, JJ and AS in the control simulation (Fig A.1) suggests that the seasonal rainfall over India is strongly linked to rainfall averages in JJ (0.80 correlation), and in AS (0.72 correlation). However, there is a rather weak correlation between the 1^{st} and 2^{nd} part of the monsoon in the model (0.16 between JJ and AS rainfall, close to the 0.11 correlation obtained in observations, in Fig II.1), which points towards the existence of a **comparable JJ-AS rainfall dichotomy** as in observations.

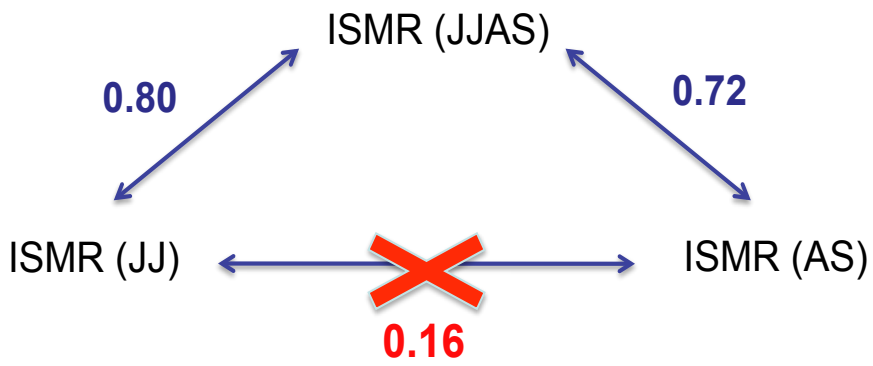

Figure A.1: Correlation between ISM rainfall in JJ, AS and JJAS in the 110-year SINTEX-F control run.

Main ISM-SST and ISM-AS teleconnections:

To examine ISM-SST and ISM-SLP relationships in the model, we have examined the correlation between bimonthly SST/SLP maps and the ISM rainfall in JJ (Fig A.2) and in AS (Fig A.3), and compared these results to Figures 3 to 6 in [*Boschat et al.*, 2011b]. We were then able to evaluate the impact of the JJ-AS dichotomy on the ISM-ENSO-IOD relationship in the model. This has simply consisted in reproducing the ISM-SST and ISM-SLP correlation analyses performed during El Niño and La Niña years in Section 5 of [*Boschat et al.*, 2011b].

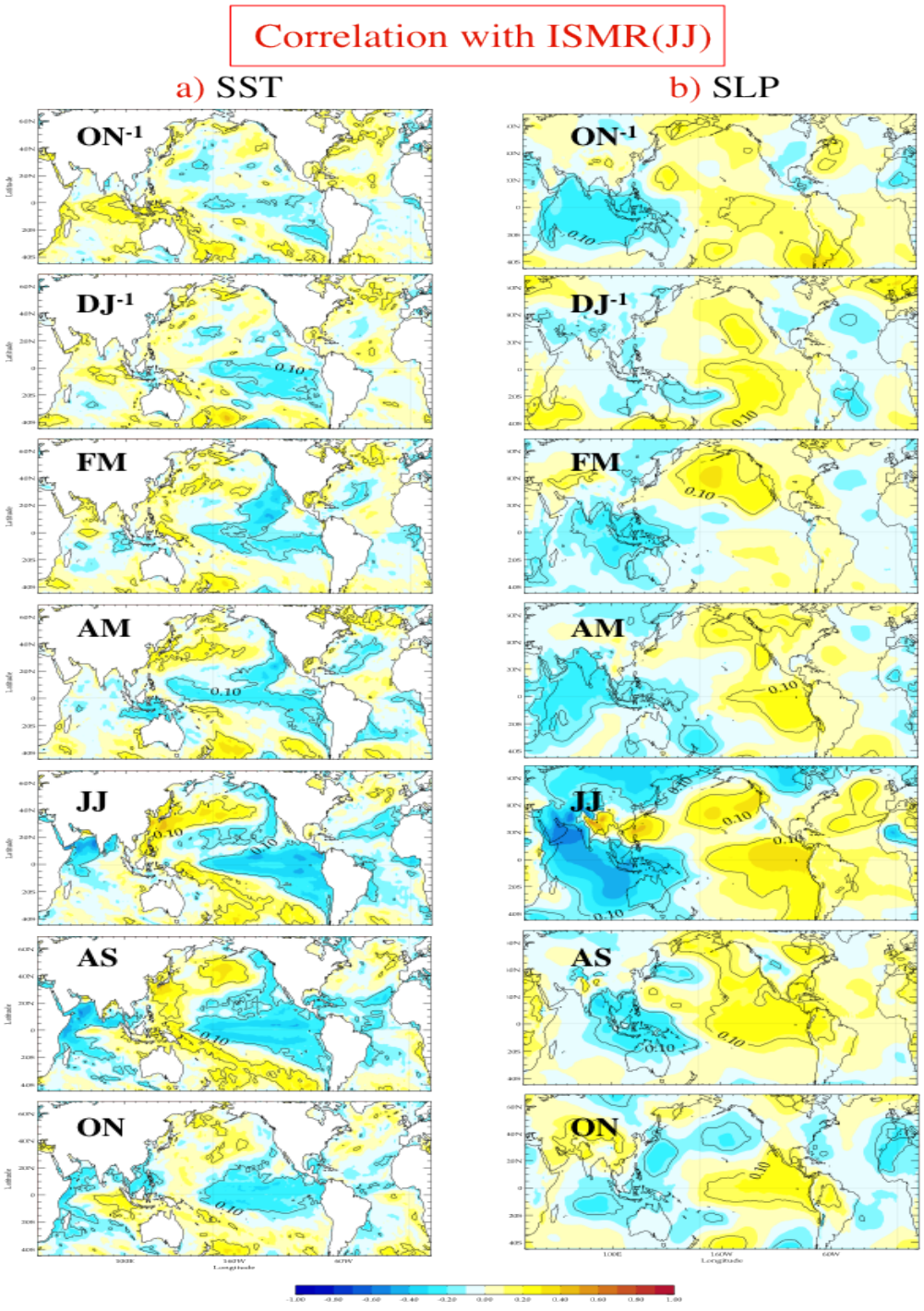

Figure A.2: Lead-Lag correlation between bimonthly **(a)** SST **(b)** SLP anomalies and ISM rainfall index in JJ in the model control simulation. Correlations significant at the 90% confidence level according to a two-tailed student-t test are encircled.

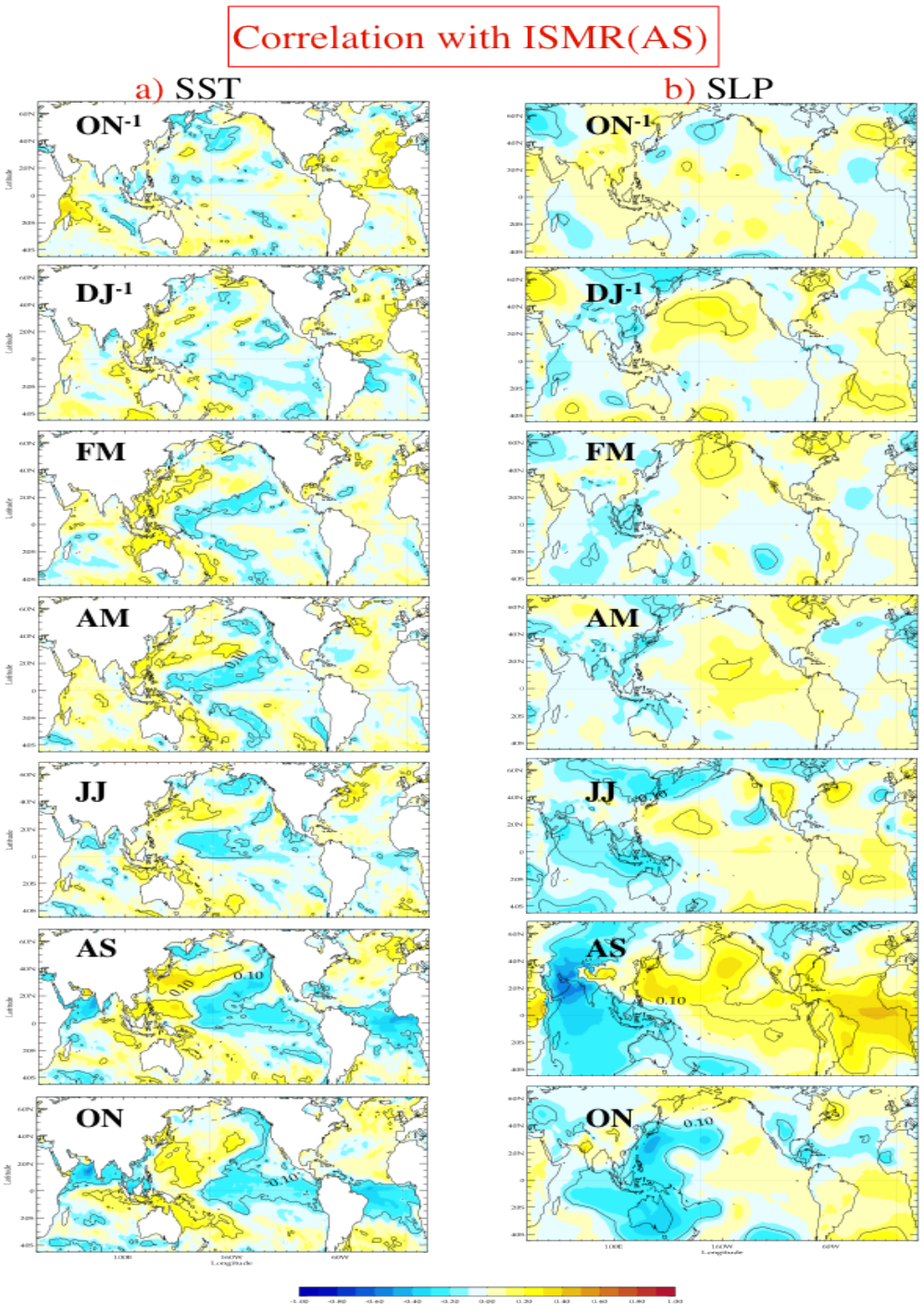

Figure A.3: Lead-Lag correlation between bimonthly **(a)** SST **(b)** SLP anomalies and ISM rainfall index in AS in the model control simulation. Correlations significant at the 90% confidence level according to a two-tailed student-t test are encircled.

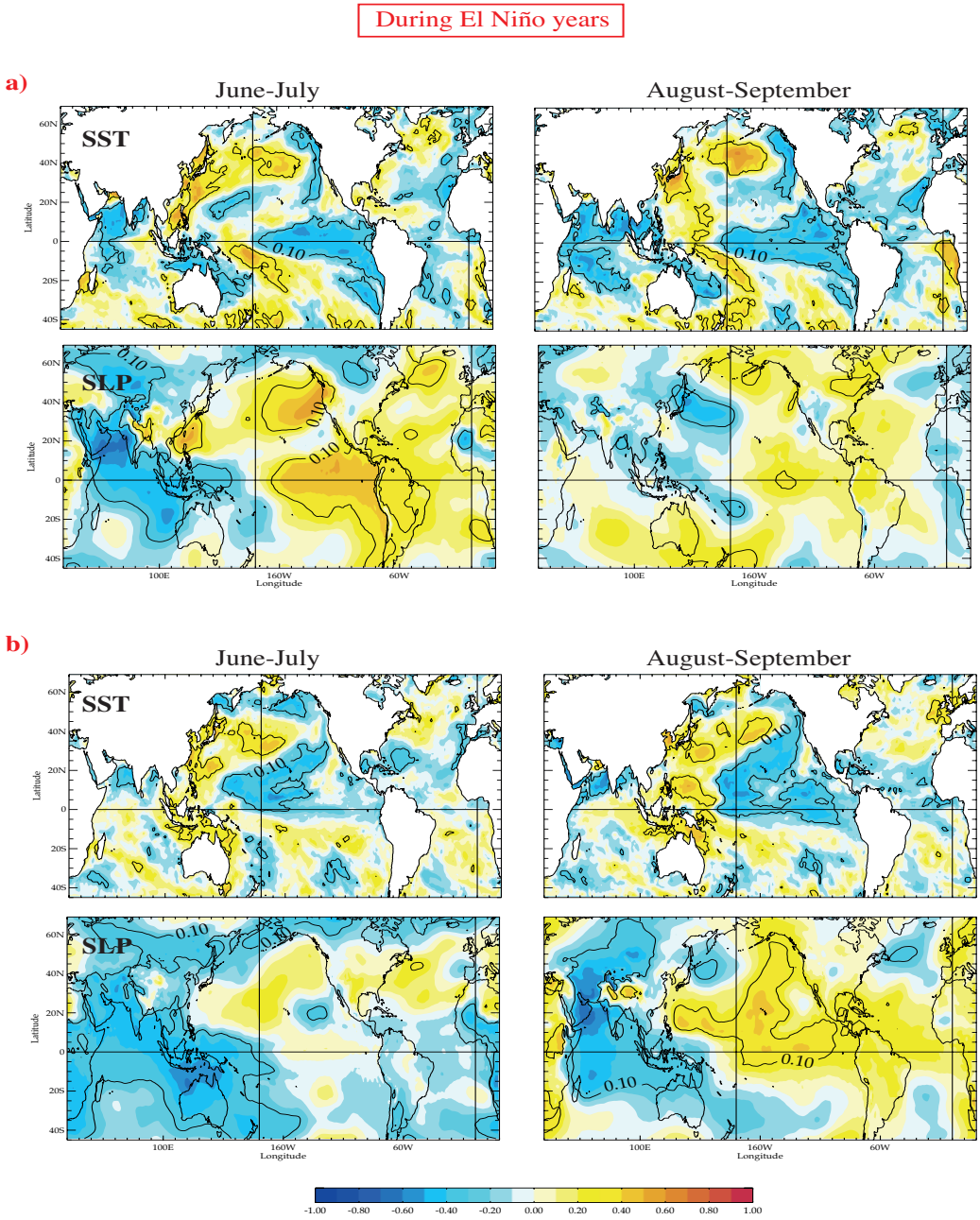

Figure A.4: Correlation of summer SST *(top panels)* and SLP anomalies *(bottom panels)* with **a)** ISM rainfall in JJ and **b)** ISMR rainfall in AS, during El Niño years selected in the SINTEX-F control simulation (upon a 0.5 standard deviation of the Niño3.4 SST index in December-January). Correlations significant at the 90% confidence level according to a two-tailed student-t test are encircled.

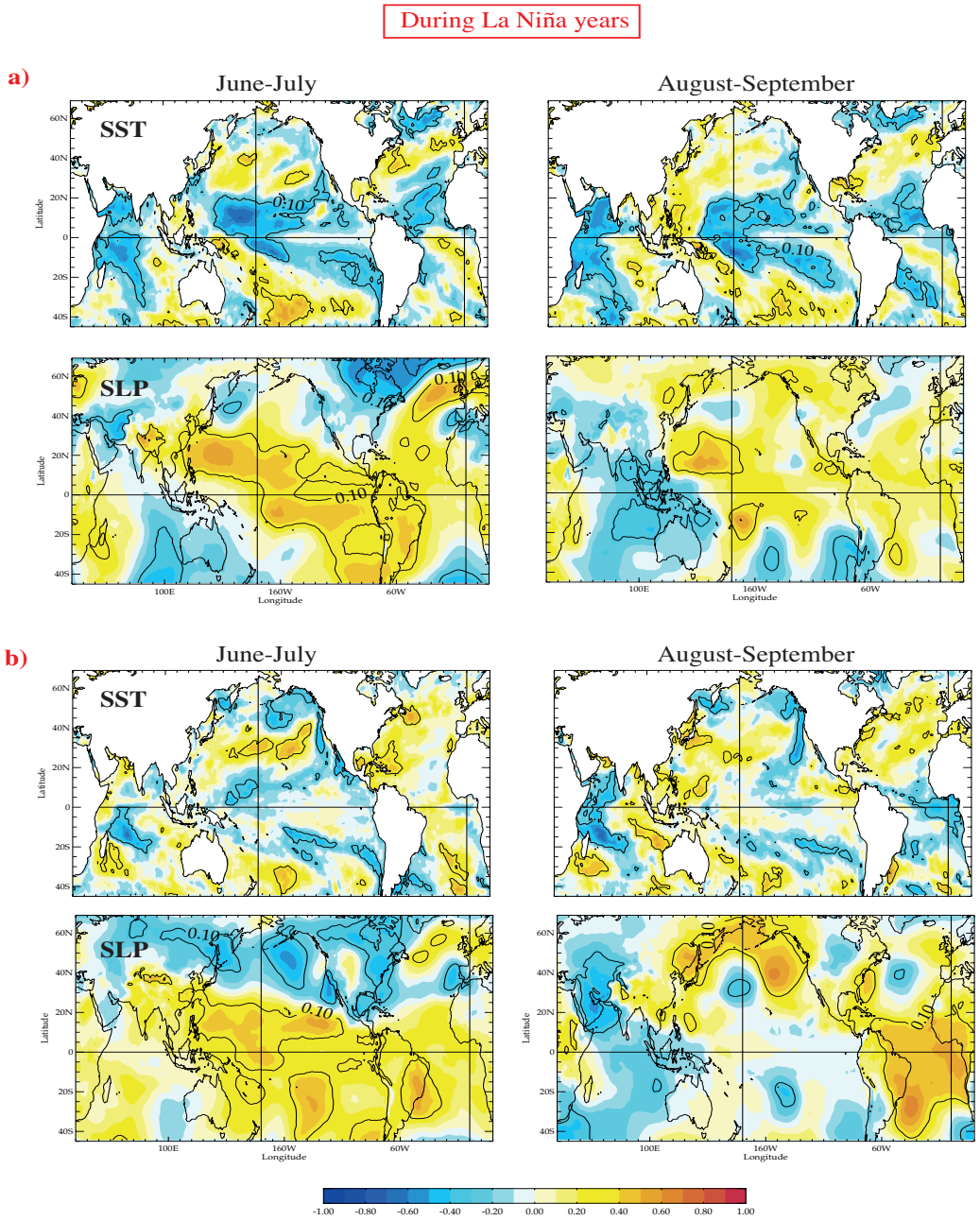

Figure A.5: Correlation of summer SST *(top panels)* and SLP anomalies *(bottom panels)* with **a)** ISM rainfall in JJ and **b)** ISMR rainfall in AS, during La Niña years selected in the SINTEX-F control simulation (upon a -0.5 standard deviation of the Niño3.4 SST index in December-January). Correlations significant at the 90% confidence level according to a two-tailed student-t test are encircled.

Results are displayed in Figs A.4 and A.5, and illustrate how the model is quite successful in reproducing the **impact of ENSO on ISM rainfall during the 1^{st} part of the season** in JJ (Figs A.4a and A.5a). However, during El Niño years, this ENSO signal persists in the correlation with AS rainfall, which suggests that the 2^{nd} part of the monsoon is also mainly governed by the effect of ENSO (Fig A.4b). The model here fails to reproduce the key-role played by local processes (in the eastern IO) in the modulation of AS rainfall (see Fig 8b in the paper). On the other hand, during La Niña years, correlation with AS rainfall yields results that are very similar to those obtained in observations (see Fig 9b in the paper), and the SST and SLP patterns in AS are consistent with a more active role of local processes in the southeast IO for the enhancement of AS rainfall.

Overall, the model is quite successful in reproducing the modulation of ISM rainfall by ENSO and by local processes in the South IO. Based on these model skills, and on the importance of common extratropical precursors for the whole ENSO-monsoon system suggested in [*Boschat et al.*, 2011b], we have decided to focus more on the interannual variability and predictability of ENSO in the SINTEX-F model (in **Chapter 4**). Indeed, Fig A.6 illutrates how this model is successful in reproducing the structure and evolution of ENSO in the control run, along with the main precursory patterns observed before these events (*e.g.* significant SST precursory signals in the South IO and North Pacific Ocean during the previous boreal winter and spring).

Correlation between SST and Nino3.4 SST index in DJ:

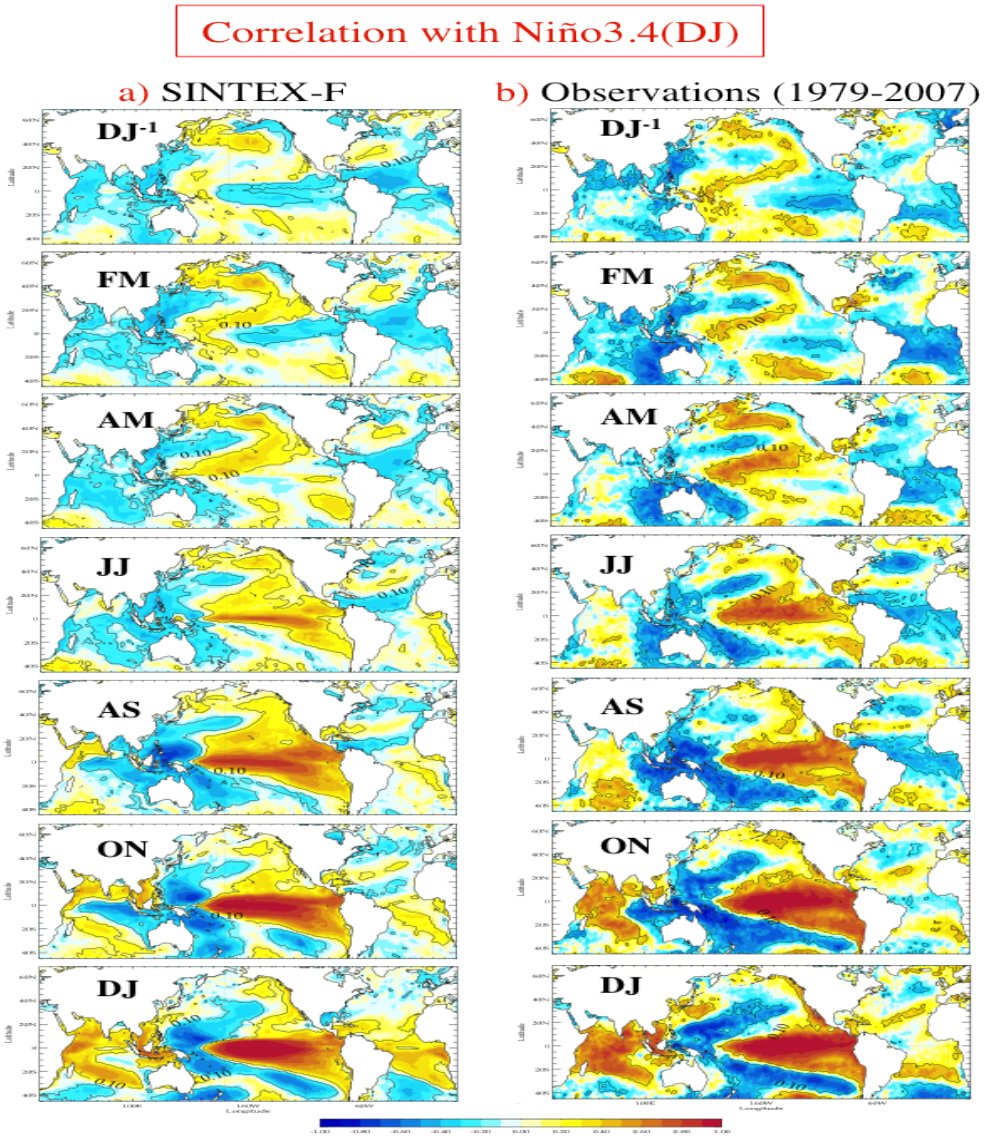

Figure A.6: Lagged correlation of bimonthly SST anomalies with Niño3.4 SST index in December-January **a)** in the model **b)** in recent observations (1979-2007). Correlations significant at the 90% confidence level according to a two-tailed student-t test are encircled.

Appendix B

SVD Methodology

The observational datasets used in this thesis, and the main analysis methods we have followed, have already been detailed in each corresponding chapter or in the article it refers to (see Data and Method section in [*Boschat et al.*, 2011b,a]). Since the focus of this thesis is on the interannual variability, we filtered out any long-term, multi-decadal and seasonal variability in all of the observed and simulated monthly time series, by using the Seasonal-Trend decomposition procedure based on Loess (STL), which breaks down the series into a trend, a seasonal signal, and a residual component, as it is illustrated in Fig B.1 ([*Cleveland et al.*, 1990], for further detail see [*Terray*, 2011] or [*Boschat et al.*, 2011a]). The statistical diagnoses were then performed on the residual component of these STL-filtered fields, which corresponds to the interannual variability.

The purpose of this appendix is to briefly describe the **Singular Value Decomposition (SVD)** methodology we have applied to filtered observations and coupled model outputs in **Chapter 4**, in an attempt to identify and compare potential precursors of ENSO.

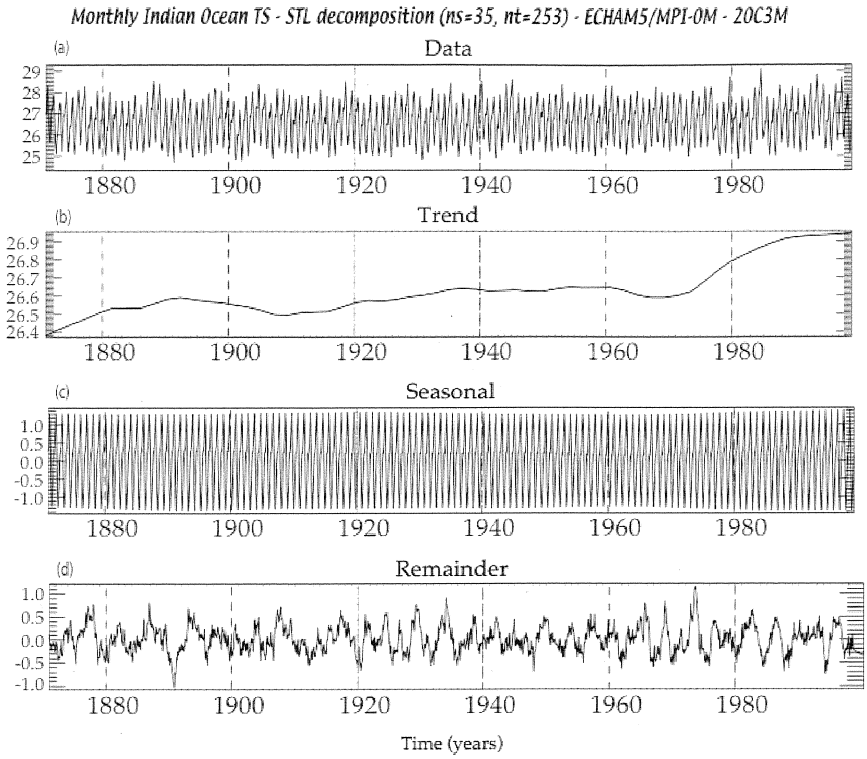

Figure B.1: Example of STL analysis performed on a SST time series in the tropical IO (40°E-120°E; 30°S-30°N), from a 20th century simulation from the ECHAM5/MPI-OM coupled model. **(a)** SST time series from 1870 to 2000 from the coupled simulation, **(b)** seasonal component, **(c)** low-frequency component and **(d) residual** component from the time series shown in (a). (from *"Rôle de l'océan Indian dans le système couplé mousson-El Niño Oscillation Australe"* by Pascal Terray (HDR in 2006))

The SVD method, also known as Maximum Covariance Analysis (MCA), is a useful tool for detecting coupled patterns between two different climatic fields. This method can be considered as a generalization of the Empirical Orthogonal Function (EOF) analysis [*Bretherton et al.*, 1992]. However, unlike the EOF which is used to decompose a space and time distributed data matrix of a *single* field, the SVD technique is applied to *two* data matrices of *two* jointly analyzed fields to identify pairs of the coupled spatial pattern and their respective temporal variations. To perform the SVD method, we start by estimating the covariance matrix between the two (filtered) fields, and then compute the SVD of this matrix, which yields two spatially orthogonal sets of singular vectors (spatial patterns analogous to the eigenvectors or EOFs, but one for each variable) and a set of singular values associated with each pair of vectors (analogous to the eigenvalues). Each pair of spatial patterns describes a fraction of the square covariance (SC) between the two variables. The 1^{st} pair of patterns (*i.e.* 'mode 1') describes the largest fraction of the SC and each succeeding pair describes a maximum fraction of the SC that is unexplained by the previous pairs. This decomposition thereby allows the extraction of dominant modes of coupled covariability between the two analyzed fields.

In **Chapter 4**, several SVD analyses are performed to identify (and compare) leading modes of co-variability between tropical Pacific SST anomalies during boreal winter (*i.e.* representing ENSO) and precursory anomalous patterns during the previous boreal spring (*e.g.* zonal wind stress or SST anomalies selected in various key regions, see Table IV.3). These SVD computations have been performed with the STATPACK set of tools developed by Pascal TERRAY at the LOCEAN, and are based on temporal covariance matrices weighted by cosine of the latitude so that equal areas carry equal weights.

The SVD methodology helps us identify linear functions of these two variables where they are most strongly related to each other. For example, if we apply the SVD to SST and Zonal Wind Stress (USTR) anomalies, these fields can be represented by the following linear combinations:

$$SST(x,y,t) = \sum_n \alpha_n(t) e_n(x,y) \tag{B.1}$$

$$USTR(x,y,t) = \sum_n \beta_n(t) f_n(x,y) \tag{B.2}$$

where $e_n(x,y)$ are $f_n(x,y)$ are the **spatial patterns** (eigenvectors) associated with SST and USTR anomalies, respectively, and $\alpha_n(t)$ and $\beta_n(t)$ denote the **expansion coefficients** associated with the SST and USTR anomalies respectively.

The kth Expansion Coefficient (EC) time series for each variable is obtained by projecting the original monthly interannual anomalies onto the kth singular vector of the SVD of the covariance matrix. Using the ECs from the SVD, two types of regression maps can be generated:

- the kth *homogenous vector*, which is the regression map between a given data field and its kth EC (see Fig B.2a for the USTR field, B.2b for the SST field),
- and the kth *heterogeneous vector*, which is the regression map between a given data field and the kth EC of the other field (see Fig B.2c for the USTR field, B.2d for the SST field). The kth heterogeneous vector indicates how well the grid point anomalies of one field can be predicted from the kth EC time series of the other field.

Fig B.2 shows an example of the spatial patterns and time series obtained with this SVD between observed USTR anomalies in boreal spring and SST anomalies during the following winter in the tropical Pacific.

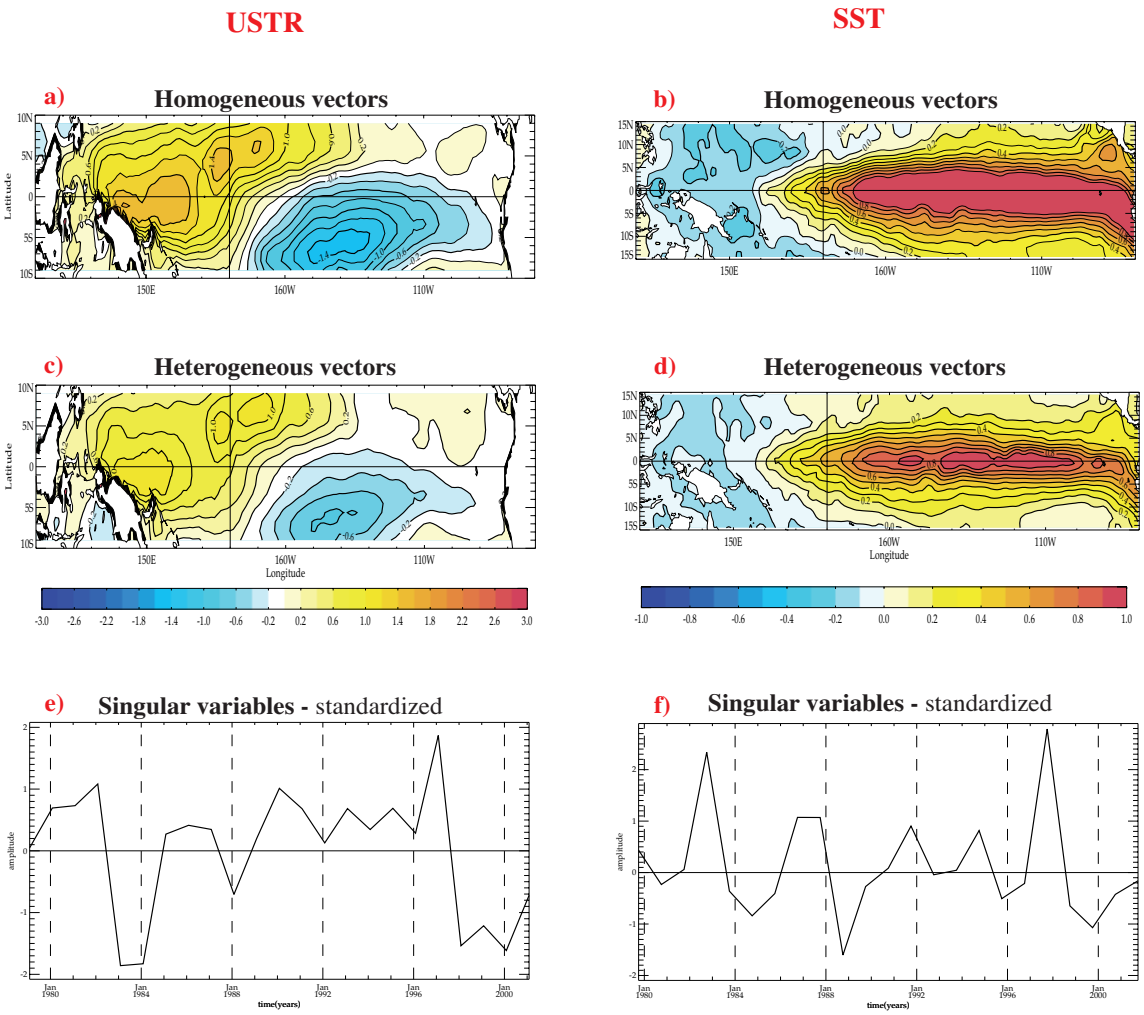

Figure B.2: Spatial patterns and expansion coefficient time series of the 1^{st} SVD mode (which explains a maximum of 90.9% of square covariance between boreal winter SST and spring USTR in the tropical Pacific region, see Chapter IV). Spatial patterns are presented as *homogeneous* maps for USTR **(a)** and SST **(b)**, and *heterogeneous* maps for USTR **(c)** and SST **(d)**. The standardized *time series* for this mode are also shown for USTR **(e)** and SST **(f)**.

This methodology allows us **to quantify the strength of the coupling** between the two fields, and also to sidestep the biases linked to the choice of *fixed* boxes, such as Niño3, Niño4 or Niño34 to account for ENSO variability (particularly in the model). The statistics provided by this SVD calculation are also very efficient tools for assessing and **comparing** the strength of these relationships and their relevance for the prediction of ENSO in **Chapter 4**. The Squared Covariance Fraction (SCF) is a first simple measure of the relative importance of each mode in the relationship between the precursory field and the SST anomalies in the tropical Pacific during the following winter (*i.e.* ENSO). However, our results have shown that the 1^{st} SVD mode doesn't always offer the best predictability for the following ENSO event. In order to examine the pertinence of each potential precursor, we are particularly interested in comparing how much of winter SST variance each SVD mode is able to explain, or how well this selected SVD mode is correlated with the Niño3.4 index during the following winter. This gives us an indication of the potential predicting skill of each SVD mode for the following ENSO event, and allows us to compare and classify the various precursors according to these SVD statistical criteria (see Table IV.4 for an example of these statistics).

Appendix C

Article submitted: Extratropical forcing of ENSO

Extratropical forcing of ENSO

Ghyslaine Boschat[1], Pascal Terray[2], Sébastien Masson[3]

LOCEAN/IPSL, CNRS/IRD/UPMC/MNHN, Paris, France

To be submitted to *Geophysical Research Letters*

June 2012

[1] Corresponding author: Ghyslaine Boschat, LOCEAN-IPSL,
Université Pierre et Marie Curie, BP100 – 4 place Jussieu, 75252 Paris cedex 05, France.
Tel : +33 1 44 27 23 29
E-mail : gbolod@locean-ipsl.upmc.fr

[2] Pascal TERRAY, LOCEAN-IPSL, UMR 7617 CNRS/IRD/UPMC/MNHN
Université Pierre et Marie Curie, BP 100 - 4 Place Jussieu 75252 Paris cedex 05 France
Tel : +33 1 44 27 70 78
E-mail : pascal.terray@locean-ipsl.upmc.fr

[3] Sébastien MASSON, LOCEAN-IPSL,
Université Pierre et Marie Curie, BP100 – 4 place Jussieu, 75252 Paris cedex 05, France.
Tel : +33 1 44 27 27 48
E-mail : sebastien.masson@locean-ipsl.upmc.fr

1. Abstract

We present evidence that Sea Surface Temperatures (SSTs) in the North Pacific, South Atlantic and Indian Oceans (AO and IO, respectively) during early boreal spring, offer another important source of predictability for El Niño Southern Oscillation (ENSO). This new SST predictor provides accurate prediction of the *amplitude* of ENSO events before their onset, for both El Niño and La Niña events, and especially for the extreme warm events, which occurred during recent decades.

2. Introduction

According to many studies, the crucial set of information for ENSO forecasts lies in the spatial variation of the thermocline depth or heat content (Meinen and McPhaden, 2000; McPhaden 2003) and the low-frequency wind variability in the tropical Indo-Pacific region (Clarke and Van Gorder, 2003). An influence from high-frequency wind variability in the western Pacific region has also been suggested, but so far the most robust leading relationship has been observed with the Madden Julian Oscillation activity in late boreal spring or early summer, therefore after the ENSO onset period (Hendon et al., 2007).

Nevertheless, there has been growing evidence in the literature, that other tropical and extratropical regions may also be playing an important role for ENSO. First, a number of studies suggested a close link with SST anomalies in the tropical IO or AO, which may induce modulations of the Walker circulations (Kug et al., 2005; Dommenget et al., 2006; Jansen et al., 2009; Rodriguez-Fonseca et al., 2009; Izumo et al., 2010; Frauen and Dommenget, 2012). Recently, there has also been a rising interest in the predictability offered by *extratropical* climate modes of variability. Vimont et al. (2003) and Wang et al. (2012) have implied a connection between the mid-latitude

and tropical Pacific, whereby the winter atmospheric variability in the North Pacific impacts subtropical SST variability and western Pacific equatorial wind anomalies, which may be responsible for exciting subsequent El Niño events. Several recent studies also emphasized the role of mid-latitude coupled variability in the South AO and IO during late boreal winter (Terray and Dominiak, 2005; Terray, 2011).

However, several open questions remain regarding the *pertinence* or added value of these new 'extratropical' precursors for the forecast of ENSO, compared to the conventional Pacific wind or heat content predictors, or the other tropical SST predictors. In this study, we combine the newly proposed sources of ENSO predictability in the North Pacific, South AO and IO, and evaluate the efficiency of this new SST predictor in predicting ENSO onset and amplitude across the "spring predictability barrier" (Webster and Yang, 1992). We present evidence, through statistical analyses of observations and a coupled ocean-atmosphere model simulation, that this new SST precursor offers an important source of predictability for ENSO, by adding pertinent information regarding the *amplitude* of events, especially for the extreme warm events (Takahashi et al., 2011).

3. Data and Methods

We compare three precursors of ENSO in early boreal spring: the upper-ocean heat content (Z20 precursor) and low-frequency zonal wind stress variability (USTR precursor) in the tropical Pacific, and SST variability in the North Pacific, South AO and IO (new SST precursor). We focus our analysis on the recent period after 1979, since records of tropical Pacific heat content and SST in the South AO and IO are either sparse or inexistent before this date.

The depth of the 20°C isotherm (Z20) is used as a proxy of the thermocline depth or heat content in the tropical Pacific Ocean, and is extracted from the Simple Ocean Data Assimilation (SODA) reanalysis (Carton and Giese, 2008; SODA version 2.2.4), available until 2008. We examine atmospheric fields (zonal wind stress (USTR), sea level pressure (SLP), and 850hPa winds) from the ERA-Interim reanalysis (Dee et al., 2011) and SST fields from the Hadley Centre Global Sea Ice and Sea Surface Temperature (HadISST1.1) dataset (Rayner et al. 2003), both available until 2011. For each field, monthly anomalies are calculated by applying the Seasonal-Trend decomposition procedure based on Loess (Cleveland et al., 1990), which filters out any long-term trends and annual cycle in the initial data.

Our goal is to predict the ENSO peak phase, which is defined by SST anomalies averaged from October to the following February (ONDJF) over the *entire* equatorial Pacific. The precursors are taken either from January to March (JFM) or February to April (FMA), 9 or 10 months prior to this typical ENSO peak phase. Sensitivity analyses have been performed with the precursors taken successively in JFM, FMA or from March to May (MAM), and for each case, we have chosen the season which offers the best skill for the following ENSO.

In order to compare the Z20, USTR and new SST precursors, we use the Singular Value Decomposition (SVD) method (Bretherton et al., 1992), which we apply separately between each precursory field during its peaking season and the following tropical Pacific SST field during boreal winter. Results are shown for the 1st SVD mode associated with each precursor in terms of the corresponding Expansion Coefficient (EC) time series, the 'homogeneous' map for the precursor (i.e regression map between the precursory field and its corresponding EC time series) and 'heterogeneous' map for the predicted ENSO field (i.e regression map between the

tropical Pacific SST and the EC time series of the precursory field, indicating how well the grid point anomalies of the ENSO field can be predicted from the precursor's EC time series). The statistics provided by the SVD are also efficient tools for quantifying the relevance of each ENSO precursor. The Squared Covariance Fraction (SCF) measures the relative importance of each SVD mode in reconstructing the covariance matrix between the precursory field and tropical Pacific SSTs. The correlation coefficient (r) between the EC time series of the two fields indicate how strongly related the coupled patterns are. Finally, we computed how much of Pacific SST variance each SVD mode explains, and the correlations between the SVD modes and the Niño3.4 SST time series during the following winter.

To test the robustness of our results, we also performed similar SVD analyses on a 110-year control simulation of the SINTEX-F2 global coupled ocean-atmosphere general (CGCM) model, since it exhibits a realistic ENSO (Masson et al., 2012).

4. Analysis and Results

4.1 Heat content and zonal wind predictors

We here examine the conventional Z20 and USTR predictors and assess their predicting skill for the following ENSO event, within our SVD framework (Fig. 1 and Table 1). During the 1979-2008 period, the 1st SVD mode between the Z20 precursor and ENSO is consistent with the predicting potential of heat content in the context of ENSO forecasting (McPhaden, 2003). Indeed, the Z20 pattern in Fig. 1 is marked by positive Z20 anomalies in the west-central tropical Pacific in spring and appears as a mixture of the two leading Empirical Orthogonal Functions (EOFs) of Pacific Z20 variability (see Meinen and McPhaden, 2000); while the corresponding SST pattern (Fig. 1b) illustrates a typical El Niño peak phase during the following winter

(consistent with figure 5 in McPhaden, 2003). This SST pattern also suggests that the performance of the Z20 precursor is degraded in the far eastern equatorial Pacific.

The statistics of this 1st SVD mode (shown in Table 1) confirm that Z20 anomalies during boreal spring are strongly correlated with SST anomalies in the tropical Pacific during the following winter (r=0.71), and that this 1st SVD mode accounts for a significant 77.1% of tropical Pacific SST variance during winter. Consistently, the Z20 expansion coefficients are highly correlated with the Niño3.4 SST time series in December-January (0.76 correlation, see Table 1), and with the C index, which was recently defined by Takahashi et al. (2011) to describe the regime of cold and moderately warm ENSO events (0.77 correlation, see Table 1). Note, however, that its performance is only modest for the E index of Takahashi et al. (2011), which accounts for the extreme warm events in the eastern Pacific (e.g. the 1982-83 El Niño event). In Fig. 1c, the correspondence between the standardized Z20 EC and Niño3.4 SST time series illustrates how well this Z20 precursor is able to anticipate ENSO variability and forecast the occurrence of many El Niño (4 out of 8) and La Niña (5 out of 6) events during 1979-2008. This predictor is particularly successful in predicting the transition from El Niño to La Niña phases (e.g in 1983-84, 1987-88-89, 1998-99), but seems less skillful in capturing the amplitude of some extreme events, such as the 1997-98 El Niño, and also those occuring since the early 2000s (see Fig. 1c and McPhaden, 2012).

The SVD analysis between the USTR precursor over the [110°E-70°W; 10°S-10°N] domain in FMA and ENSO during the 1979-2011 period yields results that are also consistent with previous works (Kug et al., 2005), and illustrates that westerly wind anomalies in the western Pacific during boreal spring are associated with a typical El Niño peak phase during the following winter, similar to the SST pattern in

Fig. 1b (not shown). Results (detailed in Table 1) suggest that this USTR precursor is also an efficient predictor for the 'canonical' type of ENSO events. Indeed, the corresponding 1st SVD mode accounts for a significant 78.4% of the SST variance in winter, and the highest correlation is once again obtained with the Niño3.4 and C indices (0.74 and 0.62 correlation, respectively).

4.2 New combined extratropical SST predictor

We now examine the predicting potential for ENSO which stems from extratropical SSTs. Results from the SVD between the new SST predictor and ENSO during the 1979-2011 period are shown in Fig. 2 and Table 1. The precursory fields (Fig. 2a) are characterized by anomalous SST dipoles in the North Pacific, South AO and IO during early boreal spring, consistent with patterns described in recent works from Vimont et al (2003), Wang et al (2012) and Terray (2011). These extratropical features are associated with a typical El Niño peak phase during the following winter (Fig. 2b), similar although slightly warmer than the SST pattern in Fig. 1b, and with maximum SST anomalies reaching further east in the Pacific.

In terms of statistics, the results are also very promising for ENSO predictability. Although this 1st SVD mode explains one of the least variances during boreal spring in the precursory region (13.1% in Table 1), it manages to explain the largest portion of winter SST variability in the tropical Pacific (79.6%), reaches a maximum of 0.80 correlation with the Niño3.4 SST timeseries in winter (Table 1), and thereby achieves an even higher predicting score than the traditionnal Z20 (and USTR) predictors! Compared to the Z20 predictor, this new SST predictor manages to predict *both* the timing and amplitude of ENSO events, and this not only in the transition from El Niño to La Niña events, but also when an El Niño develops from a previous neutral or La Niña state in the tropical Pacific (see Fig. 2c, e.g. in 1982-83, 1995-96). Although its

performance seems also degraded since the early 2000s, this SST predictor is particularly successful in capturing the amplitude of *extreme* El Niño events (both in 1982-83 and 1997-98). These results are consistent with the higher and significant correlation value obtained with the E index (0.48 in Table 1), and thus reflect the potential added value of extratropical SSTs for the predictability of extreme warm ENSO regimes (Takahashi et al., 2011).

4.3. Robustness of the predictive relationships

In view of the short observational record, we performed similar SVD analyses with the simulated fields from the SINTEX-F2 CGCM (Table 1; Figs.2d-f). Overall, results are quite consistent with observations, as this model exhibits a realistic simulation of the predictive relationships of ENSO with both the Z20 and USTR precursors, and the new SST precursor. In Fig. 2d, the precursory SST pattern displays similar dipole structures as in Fig. 2a (although the simulated SST signal is weaker in the South AO and shifted westwards in the North Pacific), and is also associated with an El Niño peak phase during the following winter, with warm SST anomalies mostly confined to the equatorial central Pacific compared to observations (Fig. 2e). The statistics for the CGCM are also consistent with a higher predicting score of the new combined SST precursor compared to the Z20 and USTR predictors, although they miss the observed relationship between extratropical SSTs and the E index (see Table 1).

By definition, the high values of the statistics in Table 1 may also partly result from the optimization problem solved by the SVD. In order to provide another test of the usefulness of extratropical SSTs for the prediction of ENSO, Fig A (in auxiliary material) presents the 1st and 2nd EOF modes from the same domain used in the SVD, in both observations and the CGCM. Since the results of this EOF analysis are globally similar in observations and the model (see Fig. A), we will restrict our

discussion to observations. Overall, these two EOFs provide some additional insight into the *nature* of the predictability offered by these extratropical SST regions during the 1979-2011 period. Indeed, although both EOF modes seem useful for ENSO prediction (0.27 and 0.59 correlation with the Niño3.4 SST index during the next winter, see Table A), the predictability offered by the 1st EOF mode is mostly linked to the biennial component of ENSO itself (-0.85 and 0.60 correlations with the concurrent Niño3.4 SST and Z20 EC time series, respectively), whereas the 2nd EOF mode captures a more *intrinsic* extratropical source of predictability, which is independent from the previous ENSO state (0.03 correlation with the concurrent Niño3.4 SST) and moderately linked to the Z20 EC time series (0.5 correlation). Surprisingly, this 2nd EOF has a higher predicting skill than the 1st EOF, and is also a significant precursor of the E and C indices, as the 1st SVD mode (Table A). It manages to provide an accurate prediction of the winter Niño3.4 SST time series, despite of the fact that this EOF is not computed to maximize the relationship between extratropical SSTs and Pacific SSTs several months later, as is the 1st SVD mode. Interestingly, the spatial correlations between these first two EOF modes (Fig. Aa and b) and the 1st SST SVD mode (in Fig. 2a) are 0.35 and 0.80, respectively. Consistently, the 1st SVD mode is more correlated with the 2nd EOF time series (0.82) than with the 1st EOF (0.46). Thus, the source of ENSO predictability offered by the 1st SVD mode "combines" both the effects of the ENSO cycle itself and the extratropics, but seems to mainly stem from extratropical variability.

Finally, we developed various regression models for forecasting winter Niño3.4 SST anomalies, using the USTR, Z20 and SST predictors and tested the accuracy of these models with a cross-validation procedure (Clarke and Van Gorder, 2003). In these cross-validation experiments, we selected the EOF modes for each precurory

field which offered the best prediction for the following ENSO: the 1st and 2nd EOF modes for extratropical SSTs (Fig. Aa-b), the 1st EOF mode for tropical Pacific wind anomalies and 2nd EOF mode for Z20 anomalies (same mode as shown in Meinen and McPhaden, 2000). To assess the forecast potential of each model, we then compared the observed Niño3.4 SST with the values calculated from regression equations based successively on all years within the common 1979-2008 time span, except the forecast year. The correlation coeffficient between the observed and forecast Niño3.4 SST and the Root-Mean-Square-Error (RMSE) for each model are shown in Table 2, and overall support the proposition that extratropical SSTs may be a crucial parameter in ENSO forecasts. Indeed, the regression model with the SST predictor as sole input achieves a higher correlation score and lower RMSE than the model which uses both USTR and Z20 predictors (0.64 compared to 0.61 correlation, 0.75 compared to 0.78 RMSE). When combining these 3 predictors, the performance of the multiple regression model is significantly improved (with 0.71 correlation and 0.69 RMSE). Finally, when removing the USTR, the performance of the model is not degraded (see Table 2). This regression exercice thus illustrates how the inclusion of extratropical SSTs may improve the statistical models currently used to predict ENSO.

3.4 Atmospheric variability associated with the new SST predictor

In order to explore the predicting paths of the SST predictor, we have regressed the SST and atmospheric anomalies from the previous summer to the following boreal winter onto the first two leading EOFs of extratropical SSTs in observations. As expected, the regression of SST, SLP and 850 hPa wind anomalies onto the 1st EOF mode depicts the rapid transition from La Niña to El Niño (or El Niño to La Niña since the analysis is linear) and the related changes in teleconnection patterns

elsewhere (see Fig. B in auxiliary material). Note, however, that the ENSO signal predicted by this mode is of limited amplitude and only marginally significant.

Fig. 3 displays the maps of SST, SLP and 850 hPa wind anomalies regressed onto the 2nd EOF of JFM extratropical SSTs. During the previous JAS season, no coherent SST or SLP patterns are found in the tropics, nor in the extratropics, except in the South Pacific (Fig. 3a and g). From boreal fall to winter, a significant anomalous SLP dipole emerges in the central North Pacific (Fig. 3b) consistent with the "Seasonal Footprinting Mechanism" of Vimont et al. (2003), followed one season later by large anticyclonic anomalies over the South AO and IO, which reflect the occurrence of blocking events during early boreal spring in the Southern Hemisphere (Fig. 3c). These atmospheric phenomena lead to the emergence of a boomerang warm SST structure (Fig. 3i-j) in the North Pacific (Vimont et al. 2003) and to subtropical SST dipoles in the South AO and IO (Hermes and Reason, 2005). Figs. 3c and i also suggest that the extratropical cold SST anomalies over the eastern IO and western North Pacific promote persistent westerly wind anomalies over the western equatorial Pacific from boreal winter to spring (Xu and Chan, 2001; Wang et al., 2012). This westerly equatorial wind signal is a possible trigger of El Niño onset, as it can induce eastward-propagating downwelling Kelvin waves along the thermocline, leading to an El Niño warming several months later.

However, there are also suggestions of additional predicting paths, not restricted to surface wind variability over the western equatorial Pacific. Indeed, from the JFM/AMJ season (Fig. 3c), a significant pattern emerges over the South Pacific, characterized by a weakening of the southeast trade winds and the development of an expanded trough. This slowdown of the Walker circulation induced by South Pacific atmospheric variability may be involved in El Niño onset (Van Loon, 1984; Clement

et al., 2011). South AO and IO anomalies could also be involved in this by remotly impacting the southwest Pacific through a modulation of the regional Hadley cell in boreal spring (Terray and Dominiak, 2005; Terray, 2011). By exciting Rossby waves, these modulations can induce a displacement of the westerly jet stream and low-level circulation in the South Pacific (Trenberth et al., 1998) and lead to the development of the southern branch of the traditional 'horseshoe' El Niño pattern (Fig. 3k-l).

5. Conclusions and future work

In this work, we demonstrate that, in addition to well-recognized precursors of El Niño onsets, extratropical SSTs in the North Pacific, South AO and IO during early boreal spring may provide some important information for the forecast of ENSO events, particularly for extreme warm events. This new 'combined' SST precursor achieves a higher predicting score than the traditional heat content and wind predictors during the post-1979 period, with a potential *added value* in the prediction of the *amplitude* of these events. We have further tested the performance of these predictors through various cross-validation experiments and shown that these promising predictive relationships are also quite well reproduced in a comprehensive CGCM.

Our regression analyses confirm that extratropical SST variability may be impacting ENSO through a modulation of wind variability in the western equatorial Pacific during boreal spring (Vimont et al., 2003; Terray, 2011; Wang et al., 2012), but not only. Our results also suggest that the extratropical atmospheric variability may play a significant role in ENSO development by modulating the southeast trades in the South Pacific during boreal spring, particularly for the extraordinary warm events, consistent with several recent studies (Chang et al., 2007; Clement et al., 2011).

Given the suspected importance of this extratropical forcing on ENSO, it now seems essential to gain a better understanding of the physical processes operating between extratropical and tropical latitudes before the onset of ENSO events, as well as the relative contribution of each hemisphere in this prediction. Do each of these extratropical sectors play separately, and independently? Or does this important source of predictability for ENSO result from an interaction between the different basins? In order to examine how the intrinsic coupled variability in the South AO, IO and in the North Pacific relate to the following ENSO variability, we have repeated our cross-validation experiments by using the SST in each basin as sole input to the regression model. The correlation and RMSE scores obtained show that all the three basins contribute to the ENSO predictability.

Another important question raised by this work is whether the observed relationship between extreme warm events and extratropical SSTs during recent decades is a future characteristic of a global warming climate.

Acknowledgments:

This work has been financially supported by the EMBRACE EU project (N°228320).

Simulations were performed on the IDRIS super computer.

References

Bretherton, C., C. Smith, and J. Wallace (1992), An intercomparison of methods for finding coupled patterns in climate data, *J. Clim., 5,* 541–560.

Carton, J. A. and B. S. Giese (2008), A Reanalysis of Ocean Climate Using Simple Ocean Data Assimilation (SODA), *Mon. Weather Rev.*, *136,* 2999-3017.

Chang, P., et al. (2007), Pacific meridional mode and El Niño–Southern Oscillation. *Geophys. Res. Lett., 34,* L16608, doi:10.1029/2007GL030302.

Clarke, A. J., and S. Van Gorder (2003), Improving El Niño prediction using a space-time integration of Indo-Pacific winds and equatorial Pacific upper ocean heat content, *Geophys. Res. Lett, 30,* 1399.

Clement, A., P. DiNezio, and C. Deser (2011), Rethinking the ocean's role in the Southern Oscillation, *J. Clim, 24,* 4056-4072.

Cleveland, R. B., et al. (1990) A Seasonal-Trend Decomposition Procedure Based on Loess (with Discussion). *J Official Statistics, 6*, 3-73.

Dee and co-authors (2011) The ERA-Interim reanalysis: configuration and performance of the data assimilation system. *Quart. J. R. Met. Soc.*, 137, 553-597.

Dommenget, D., V. Semenov, and M. Latif (2006), Impacts of the tropical Indian and Atlantic oceans on ENSO, *Geophys. Res. Lett, 33,* L11, 701.

Ebisuzaki, W. (1997), A method to estimate the statistical significance of a correlation when the data are serially correlated, *J. Clim., 10,* 2147-2153.

Frauen, C., and D. Dommenget (2012), Influences of the tropical Indian and Atlantic Oceans on the predictability of ENSO, *Geophys. Res. Lett, 39,* L02706.

Hermes, J. C., and C. J. C. Reason (2005), Ocean model diagnosis of interannual coevolving SST variability in the South Indian and South Atlantic Oceans, *J. Clim., 18,* 2864-2882.

Izumo, T., et al. (2010), Influence of the state of the Indian Ocean Dipole on the following years El Niño, *Nature Geoscience, 3,* 168–172.

Jansen, M. F., D. Dommenget, and N. Keenlyside, Tropical atmosphere-ocean interactions in a conceptual Framework (2009), *J. Clim., 22,* 550–567.

Kug, J. S., S. I. An, F. F. Jin, and I. S. Kang (2005), Preconditions for El Niño and La Niña onsets and their relation to the Indian ocean, *Geophys. Res. Lett., 32,* L05, 706.

Masson, S., et al. (2012), Impact of intra-daily SST variability on ENSO characteristics in a coupled model, *Clim. Dyn*., *39*, 729-754.

McPhaden, M. J. (2003), Tropical Pacific Ocean heat content variations and ENSO persistence barriers, *Geophys. Res. Lett, 30,* 1480.

Meinen, C. S., and M. J. McPhaden (2000), Observations of Warm Water Volume changes in the equatorial pacific and their relationship to El Niño and La Niña, *J. Clim., 13,* 3551–3559.

Rayner, N. A., et al. (2003), Global analyses of sea surface temperature, sea ice, and night marine air temperature since the late nineteenth century, *J. Geophys. Res., 108*(D14), 4407, doi:10.1029/2002JD002670.

Rodriguez-Fonseca, B., et al. (2009), Are Atlantic Niños enhancing Pacific ENSO events in recent decades, *Geophys. Res. Lett., 36,* L20, 705.

Takahashi, K., A. Montecinos, K. Goubanova, and B. Dewitte (2011), ENSO regimes: Reinterpreting the canonical and Modoki El Niño. *Geophys. Res. Lett., 38,* L10704.

Terray, P., and S. Dominiak (2005), Indian Ocean Sea Surface Temperature and El Niño-Southern Oscillation: a new perspective, *J. Clim., 18,* 1351–1368.

Terray, P. (2011), Southern hemisphere extra-tropical forcing: a new paradigm for El Niño-Southern Oscillation, *Clim. Dyn., 36,* 2171–2199.

Trenberth, K.E., et al. (1998), Progress during TOGA in understanding and modeling global teleconnections associated with tropical sea surface temperatures, *J. Geophys. Res., 103,* 14291-14324.

Van Loon, H. (1984) The Southern Oscillation. Part III: Associations with the trades and with the trough in the westerlies of the South Pacific Ocean, *Mon. Wea. Rev.*, *112,* 947-954.

Vimont, D. J., D. S. Battisti, and A. C. Hirst (2003), The seasonal footprinting mechanism in the CSIRO general circulation models, *J. Clim., 16,* 2653–2667.

Wang, S.-Y., et al. (2012) ENSO prediction one year in advance using Western North Pacific sea surface temperatures, *Geophys. Res. Lett., 39,* L05702.

Webster, P. J., and S. Yang (1992), Monsoon and ENSO: Selectively interactive systems, *Q. J. R. Meteorol. Soc., 118,* 877–926.

Xu J. and J. C .L. Chan (2001), The Role of the Asian-Australian Monsoon System in the Onset Time of El Niño Events, *J. Clim., 14*, 418-433.

Table 1: Statistics associated with the 1st SVD modes between Z20, USTR or the new 'combined' SST precursor during boreal spring and ENSO SST anomalies in the tropical Pacific during the following winter. The last 3 columns give the correlation between each SVD mode and various ENSO indices during the next December-January season: the Niño3.4 SST index, the C and E indices used in Takahashi et al. (2011). Results are given for observations (in red) and for the model (in blue). The correlation coefficients exceeding the 10%, 5% and 1**%** confidence levels according to the phase-scrambling bootstrap test of Ebisuzaki (1997) are followed by one asterisk (*), two asterisks (**) and three asterisks (***), respectively.

SVD results / ***Precursor***	**SCF** (%)		**r**		**Precursor var** (%)		**ENSO var** (%)		**Cor Niño3.4**		**Cor C index**		**Cor E index**	
Z20	84.5	87	0.71	0.56	12.9	24.3	77.1	63.3	0.76***	0.55***	0.77***	0.52***	0.35	0.22**
Ustr	89.3	84.9	0.64	0.53	21.1	21.5	78.4	67.1	0.74***	0.54***	0.62***	0.54***	0.32	0.21*
'combined' SST	90.8	83.1	0.78	0.71	13.1	8.1	79.6	69	**0.80*****	**0.71*****	0.67***	0.70***	0.48**	0.11

* **P**<0.1, ****P**<0.05, *****P**<0.01

Table 2: Forecast skill of simple linear regression models using two (A and B), three (D) or four (C) predictors in JFM as inputs for the prediction of the Niño3.4 time series during the following December-January. As input for each model, we select the EOF modes associated with the Z20, USTR and SST precursors, which offer the best prediction for the following ENSO. The forecast skill of each model is assessed by the cross-validated correlation and root-mean-square-error (RMSE) calculated between the observed and forecast Niño3.4 time series, without involving the forecast year.

Regression models	*Selected EOF mode*	*Correlation*	*RMSE*
A) with SST predictors	SST (eof m1) + SST (eof m2)	0.64	0.75
B) with Z20 and USTR predictors	Z20 (eof m2) + USTR (eof m1)	0.61	0.78
C) with SST, Z20 and USTR predictors	SST (eof m1) + SST (eof m2) + Z20 (eof m2) + USTR (eof m1)	0.71	0.69
D) with SST and Z20 predictors	SST (eof m1) + SST (eof m2) + Z20 (eof m2)	0.72	0.68

Figure 1 : Observed 1st SVD mode between Z20 precursor over [110°E-70°W; 20°S-20°N] and tropical Pacific SST over [120°E-80°W; 15°S-15°N] during 1979-2008: **(a)** Z20 homogeneous map in JFM, **(b)** Pacific SST heterogeneous map in ONDJF, and **(c)** standardized Z20 EC time series in JFM (black curve) superimposed with the standardized Niño3.4 SST time series in the following December-January season (red curve). The blue (green) crosses indicate the number of predicted El Niño (La Niña) events (e.g. when both time series exceed a 0.75 standard deviation threshold).

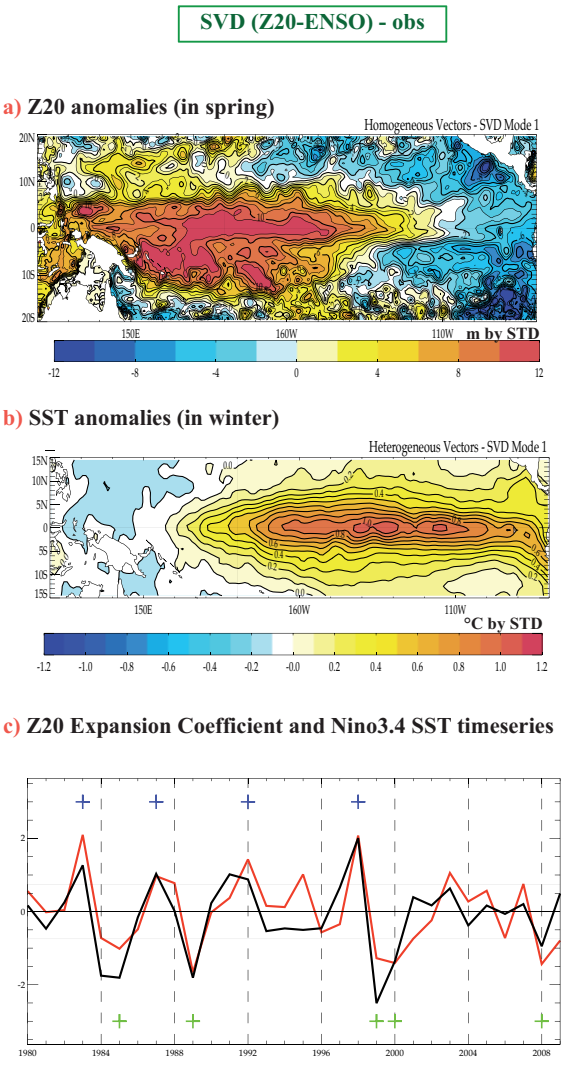

Figure 2 : As in Figure 1, but for the observed 1st SVD mode between the JFM extratropical SST precursor (over the North Pacific [110°E-90°W; 10°N-50°N], South Indian [25°E-150°E; 10°S-50°S] and South Atlantic [50°W-25°E; 10°S-50°S] Oceans) and winter tropical Pacific SST during the 1979-2011 period (**panels a,b,c**) and the SINTEX-F2 simulation (**panels d,e,f**). The SST EC time series manages to predict 12 out of the 20 El Niño events, and 14 out of the 24 La Niña events in this control simulation.

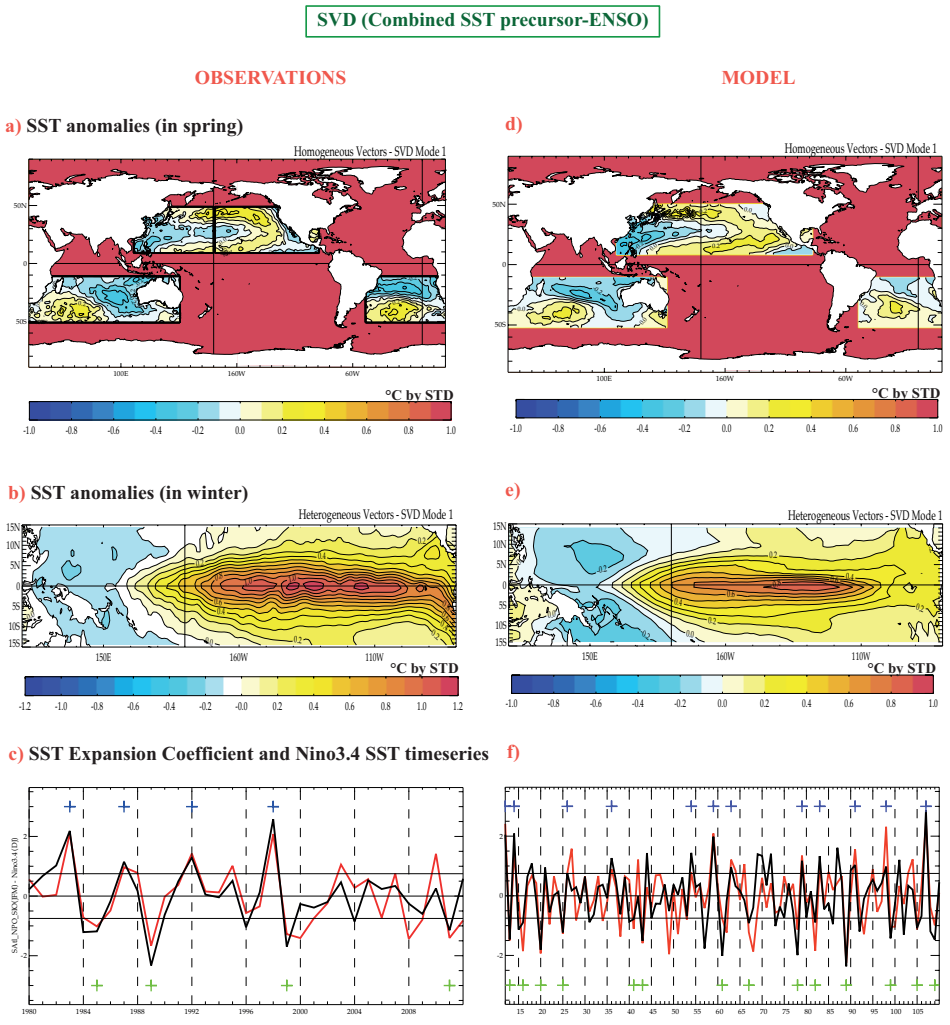

Figure 3 : SLP (shading) and 850hPa wind (vectors) anomalies (**a to f**) and SST anomalies (**g to l**) regressed onto the 2nd EOF time series of extratropical SST in JFM (over the 1979-2011 period). Maps are shown from the previous boreal summer to the following boreal winter. The black contours and the wind vectors denote that the corresponding correlation coefficients are above the 90% confidence level following a phase-scrambling procedure with 999 samples (Ebisuzaki, 19**97).**

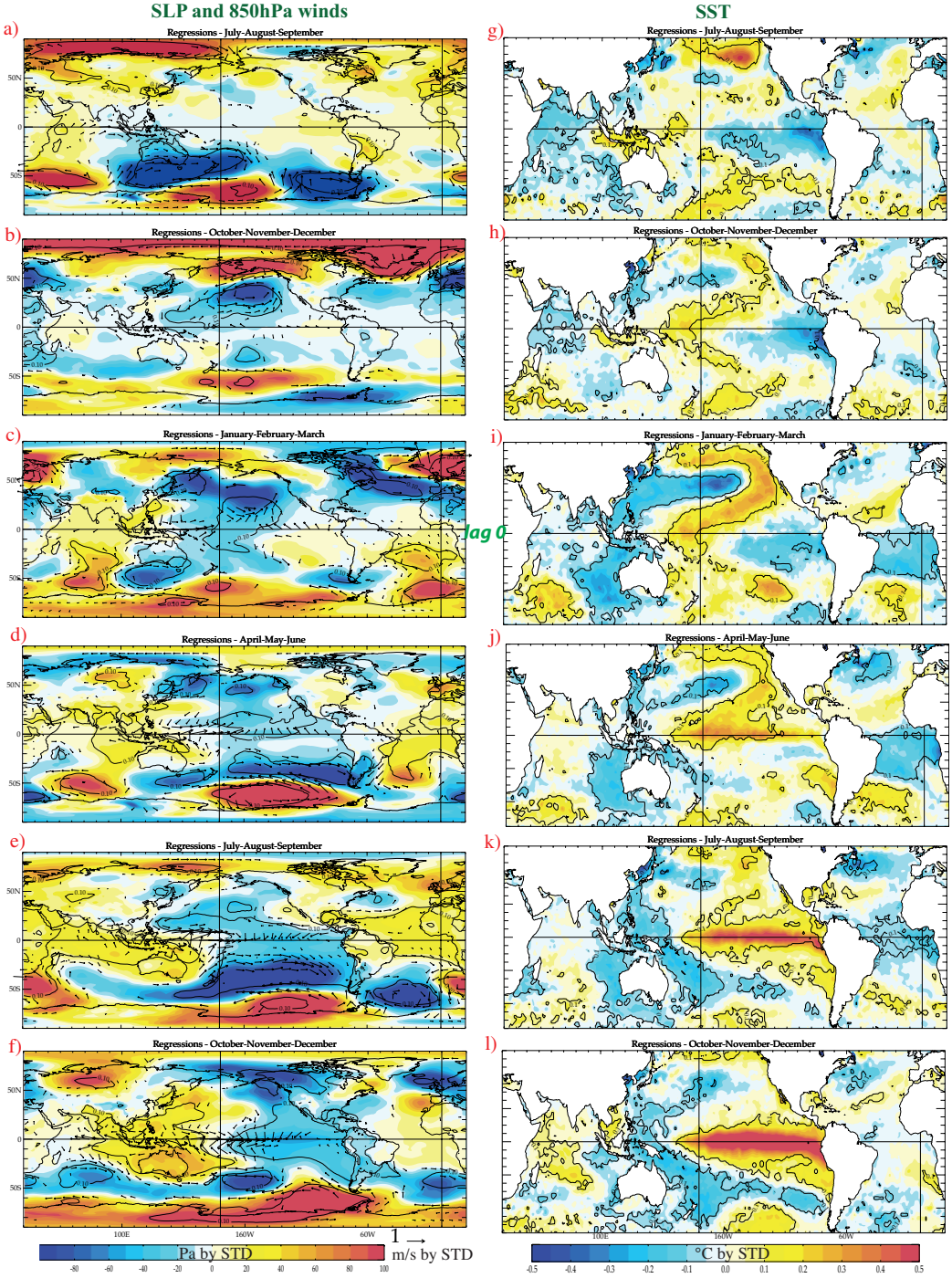

Supplementary Figures:

Figure A: Spatial patterns of the (**a**) 1st and (**b**) 2nd leading EOF modes of extratropical SST anomalies in JFM over the South Indian, Atlantic and North Pacific sectors in observations. (**c**) and (**d**), same as (a) and (b) but for the model.

Figure B: Global SLP (shading) and 850hPa wind (vectors) anomalies (**a** to **f)** and SST anomalies (**g** to **l**) regressed onto the 1st EOF time series of extratropical SST in JFM. Maps are shown from the previous boreal summer to the following boreal winter (top to bottom). The black contours and the wind vectors shown in these maps denote that the corresponding correlation coefficients are above the 90% confidence level following a phase-scrambling procedure with 999 samples.

Supplementary Tables:

Table A: Correlation of the 1st and 2nd EOF time series of extratropical SST in JFM, with the Z20 EC time series in JFM (see Fig. 1), and with various ENSO indices: the Niño3.4 SST index (during the previous and following December-January season) and the C and E indices used in Takahashi et al. (2011). Results are given separately for observations (in red) and for the model (in blue). The correlation coefficients exceeding the 10%, 5% and 5% confidence levels according to the phasescrambling bootstrap test of Ebisuzaki (1997) with 999 samples are followed by one asterisk (*), two asterisks (**) and three asterisks (***), respectively.

Figure A (Supplementary Material) :

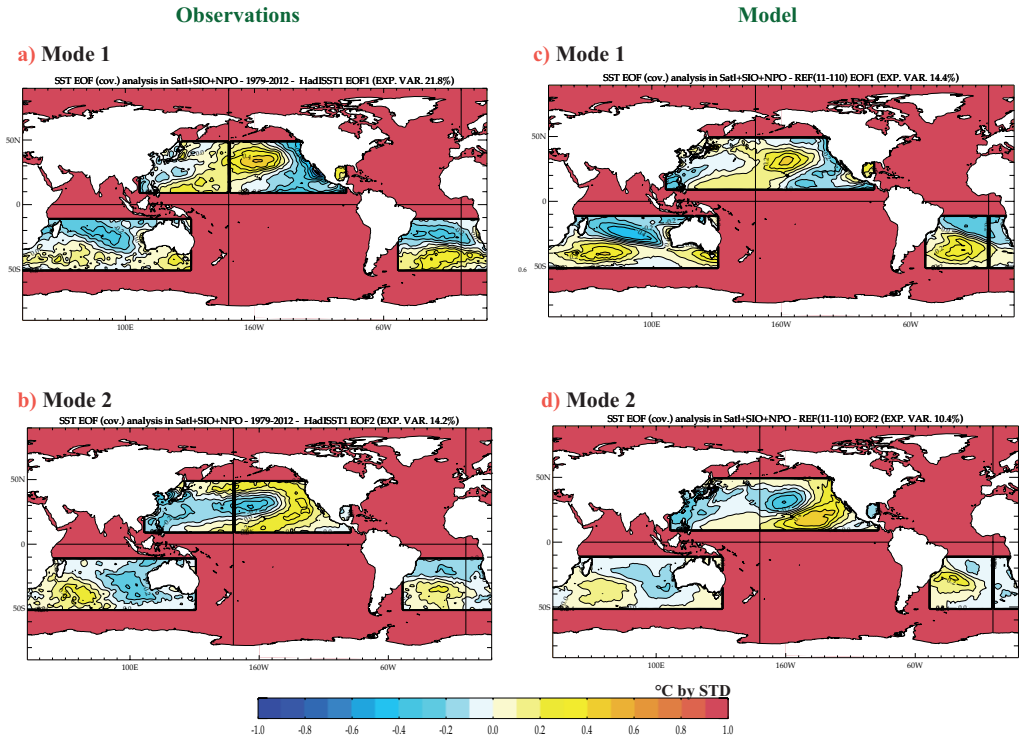

Table A (Supplementary Material) :

	Cor Niño3.4(0)		Cor Niño3.4(+1)		Cor C index		Cor E index	
Mode1	**-0.85*****	-0.80***	0.27*	0.21*	0.25	0.21*	0.05	-0.20*
Mode 2	0.03	0.06	**0.59*****	0.33**	**0.48****	0.35**	**0.40****	0.11

Figure B (Supplementary Material)

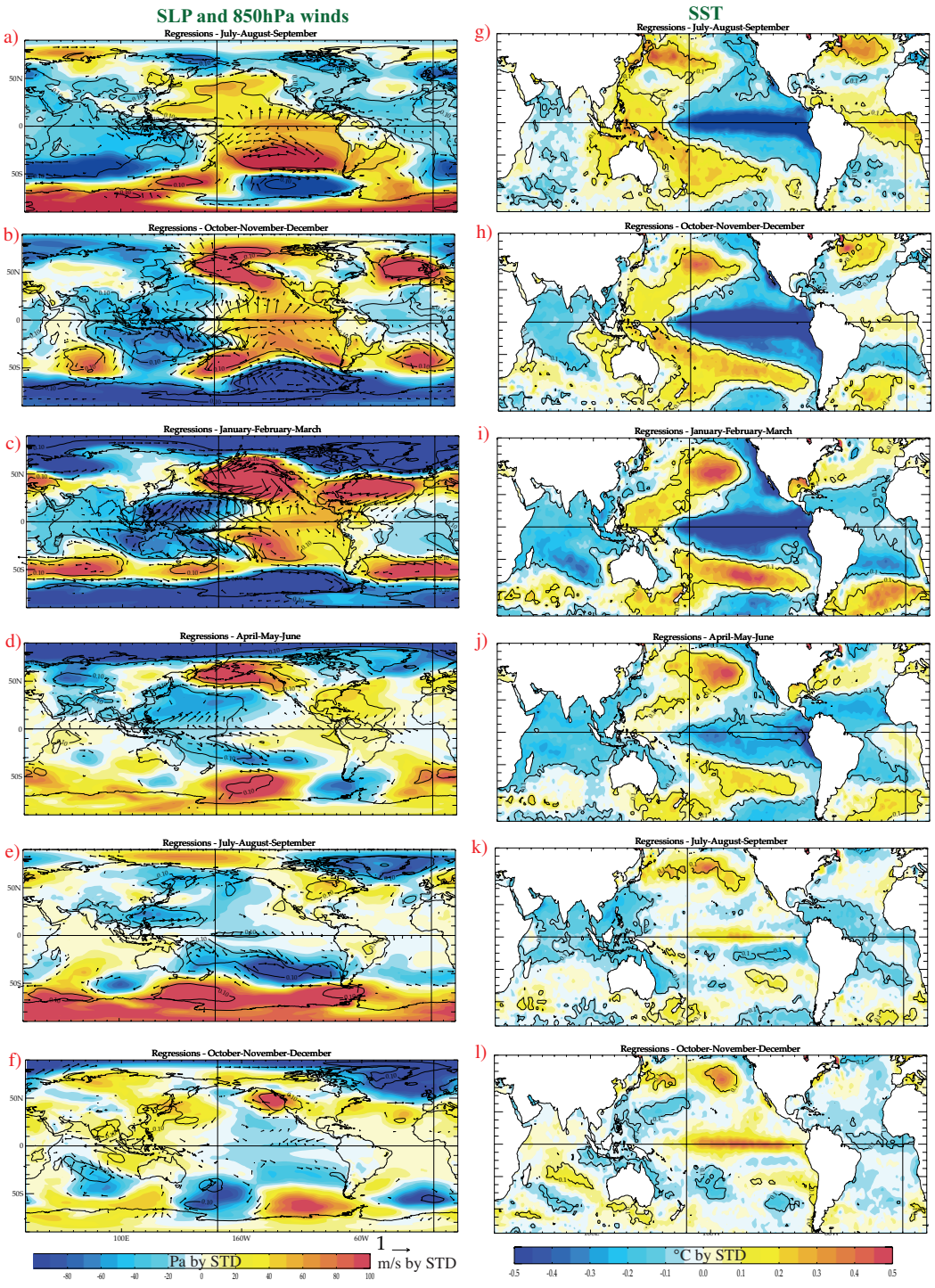

Bibliography

Abram, N. J., M. K. Gagan, J. E. Cole, W. S. Hantoro, and M. Mudelsee, Recent intensification of tropical climate variability in the indian ocean., *Nature Geoscience*, *1*, 849–853, 2008.

AchutaRao, K., and K. Sperber, Simulation of the el niño southern oscillation: Results from the coupled model intercomparison project, *Climate Dynamics*, *19*, 191–209, 2002.

Alexander, M. A., I. Bladé, M. Newman, J. R. Lanzante, N. C. Lau, and J. D. Scott, The atmospheric bridge: The influence of enso teleconnections on air-sea interaction over the global oceans, *Journal of Climate*, *15*, 2205–2232, 2002.

Alexander, M. A., I. Bladé, M. Newman, J. R. Lanzante, N. C. Lau, and J. D. Scott, The impact of extra tropical atmospheric variability on enso: testing the seasonal foot printing mechanism using coupled model experiments., *Journal of Climate*, *23*, 2885–2901, 2010.

Annamalai, H., and P. Liu, Response of the asian summer monsoon to changes in el nino properties, *Quarterly Journal of the Royal Meteorological Society*, *131*, 805–831, 2005.

Annamalai, H., and J. M. Slingo, Active/break cycles: diagnosis of the intraseasonal variability of the asian summer monsoon., *Climate Dynamics*, *18*, 85–102, 2001.

Annamalai, H., P. Liu, and S. P. Xie, Southwest indian ocean sst variability: Its local effect and remote influence on asian monsoons, *Journal of climate*, *18*, 4150–4167, 2005a.

Annamalai, H., S. P. Xie, J. P. McCreary, and R. Murtugudde, Impact of indian ocean sst on developing el niño., *Journal of Climate*, *18*, 302–319, 2005b.

Ashok, K., Z. Guan, and T. Yamagata, Impact of the indian ocean dipole on the relationship between the indian monsoon rainfall and enso, *Geophysical Research Letters*, *28*, 4499–4502, 2001.

Ashok, K., Z. Guan, N. H. Saji, and T. Yamagata, Individual and combined influences of enso and the indian ocean dipole on the indian summer monsoon, *Journal of Climate*, *17*, 2004.

Barnier, B., G. Madec, T. Penduff, J. M. Molines, A. M. Treguier, J. Le Sommer, A. Beckmann, A. Biastoch, and C. Böning, Impact of partial steps and momentum advection schemes in a global ocean circulation model at eddy-permitting resolution., *Ocean Dynamics*, *56*, 543–567, 2006.

Barnston, A. G., M. H. Glantz, and Y. He, Predictive skill of statistical and dynamical climate models in sst forecasts during the 1997–98 el niño episode and the 1998 la niña onset, *Bull. Amer. Meteor. Soc*, *80*, 217–24, 1999.

Battisti, D. S., and A. C. Hirst, Interannual variability in the tropical atmosphere-ocean model: influence of the basic state, ocean geometry and nonlinearity., *Journal of the Atmospheric Sciences*, *45*, 1687–1712, 1989.

Behera, S. K., and T. Yamagata, Subtropical sst dipole events in the southern indian ocean, *Geophysical research letters*, *28*, 327–330, 2001.

Bernie, D. J., E. Guilyardi, G. Madec, J. M. Slingo, S. J. Woolnough, and J. Cole, Impact of resolving the diurnal cycle in an ocean–atmosphere gcm. part 1: a diurnally forced ogcm., *Climate Dynamics*, *29*, 575–590, 2007.

Bjerknes, J., A possible response of the atmospheric hadley circulation to equatorial anomalies of ocean temperature., *Tellus*, *19*, 551–559, 1966.

Bjerknes, J., Atmospheric teleconnections from the equatorial pacific 1, *Monthly Weather Review*, *97*, 163–172, 1969.

Boschat, G., P. Terray, and S. Masson, Interannual relationships between indian summer monsoon and indo-pacific coupled modes of variability during recent decades, *Climate dynamics*, *37*, 1019–1043, 2011a.

Boschat, G., P. Terray, and S. Masson, Robustness of sst teleconnections and precursory patterns associated with the indian summer monsoon, *Climate Dynamics*, *1*, 155, 2011b.

Bretherton, C., C. Smith, and J. Wallace, An intercomparison of methods for finding coupled patterns in climate data., *Journal of Climate*, *5*, 541–560, 1992.

Cai, W., T. Cowan, and A. Sullivan, Recent unprecedented skewness towards positive indian ocean dipole occurrences and its impact on australian rainfall, *Geophysical Research Letters*, *36*, L11,705, 2009a.

Cai, W., A. Sullivan, and T. Cowan, Climate change contributes to more frequent consecutive positive indian ocean dipole events, *Geophysical Research Letters*, *36*, L23,704, 2009b.

Cai, W., A. Sullivan, and T. Cowan, Rainfall teleconnections with indo-pacific variability in the wcrp cmip3 models, *Journal of Climate*, *22*, 5046–5071, 2009c.

Chang, C. P., and T. Li, A theory for the tropical tropospheric biennial oscillation., *Journal of the Atmospheric Sciences*, *57*, 2209–2224, 2000.

Chang, P., L. Zhang, R. Saravanan, D. J. Vimont, J. C. H. Chiang, L. Ji, H. Seidel, and M. K. Tippett, Pacific meridional mode and el nino-southern oscillation, *Geophysical Research Letters*, *34*, 16,608, 2007.

Chang, P., et al., Climate fluctuations of tropical coupled systems-the role of ocean dynamics, *Journal of Climate*, *19*, 5122–5174, 2006.

Charney, J. G., and J. Shukla, *Monsoon Dynamics*, chap. Predictability of Monsoons, pp. 99–108, Cambridge University Press, Cambridge, 1981.

Chiodi, A. M., and D. E. Harrison, Mechanisms of summertime subtropical southern indian ocean sea surface temperature variability: On the importance of humidity anomalies and the meridional advection of water vapor*, *Journal of Climate*, *20*, 4835–4852, 2007.

Clark, C. O., J. E. Cole, and P. J. Webster, Indian ocean sst and indian summer rainfall: Predictive relationships and their decadal variability., *Journal of Climate*, *13*, 2503–2519, 2000.

Clarke, A. J., *An introduction to the dynamics of El Niño and the southern oscillation*, Academic Press, 2008.

Clarke, A. J., and S. Van Gorder, Improving el nino prediction using a space-time integration of indo-pacific winds and equatorial pacific upper ocean heat content, *Geophys. Res. Lett*, *30*, 1399, 2003.

Clement, A., P. DiNezio, and C. Deser, Rethinking the ocean's role in the southern oscillation, *Journal of Climate*, *24*, 4056–4072, 2011.

Cleveland, R. B., W. S. Cleveland, J. E. McRae, and I. Terpenning, Stl: A seasonal-trend decomposition procedure based on loess, *Journal of Official Statistics*, *6*, 3–73, 1990.

Collins, M., The impact of global warming on the tropical pacific and el niño., *Nature Geoscience*, *3*, 391–397, 2010.

Delecluse, P., M. Davey, Y. Kitamura, S. Philander, and M. Suarez, co-authors, 1998. toga review paper: coupled general circulation modeling of the tropical pacific, *J. Geophys. Res*, *103*, 357–14, 1998.

Ding, Y. H., and C. L. Chan, The east asian summer monsoon: an overview., *Meteorology and Atmospheric Physics*, *89*, 117–142, 2005.

Dommenget, D., The slab ocean el niño, *Geophys. Res. Lett*, *37*, L20,701, 2010.

Dommenget, D., V. Semenov, and M. Latif, Impacts of the tropical indian and atlantic oceans on enso, *Geophysical research letters*, *33*, L11,701, 2006.

Du, Y., S. P. Xie, G. Huang, and K. M. Hu, Role of air-sea interaction in the long persistence of el niño-induced north indian ocean warming., *Journal of Climate*, *22*, 2023–2038, 2009.

Ebisuzaki, W., A method to estimate the statistical significance of a correlation when the data are serially correlated, *Journal of Climate*, *10*, 2147–2153, 1997.

Fischer, A. S., P. Terray, E. Guilyardi, S. Gualdi, and P. Delecluse, Two independent triggers for the indian ocean dipole/zonal mode in a coupled gcm, *Journal of Climate*, 2005.

Francis, P. A., and S. Gadgil, Towards understanding the unusual indian monsoon in 2009, *Journal of Earth System Science*, *119*, 397–415, 2010.

Gadgil, S., The indian monsoon and its variability, *Annual Review of Earth and Panetary Sciences*, *31*, 429–467, 2003.

Gent, P. R., and J. C. McWilliams, Isopycnal mixing in ocean circulation models., *Journal of Physical Oceanography*, *20(1)*, 150–155, 1990.

Gershunov, A., N. Schneider, and T. Barnett, Low-frequency modulation of the enso-indian monsoon rainfall relationship: Signal or noise?, *Journal of Climate*, *14*, 2486–2492, 2001.

Goswami, B. N., Interannual variations of indian summer monsoon in a gcm: External conditions versus internal feedbacks., *Journal of Climate*, *11*, 501–522, 1998.

Goswami, B. N., South asian summer monsoon: An overview in the global monsoon system: Research and forecast, 2005.

Graham, N. E., Decadal-scale climate variability in the tropical and north pacific during the 1970s and 1980s: Observations and model results, *Climate Dynamics*, *10*, 135–162, 1994.

Guilyardi, E., El niño–mean state–seasonal cycle interactions in a multi-model ensemble, *Climate Dynamics*, *26*, 329–348, 2006.

Guilyardi, E., P. Delecluse, S. Gualdi, and A. Navarra, Mechanisms for enso phase change in a coupled gcm, *Journal of Climate*, *16*, 2003.

Guilyardi, E., A. Wittenberg, A. Fedorov, M. Collins, C. Wang, A. Capotondi, G. J. Van Oldenborgh, and T. Stockdale, Understanding el nino in ocean–atmosphere general circulation models, *Bull. Amer. Meteor. Soc*, *90*, 325–340, 2009.

Halley, E., *A historical account of the trade-winds and monsoons observable in the seas between and near the tropics with an attempt to assign the physical cause of said winds.*, vol. 26, 1686.

Harzallah, R., and R. Sadourny, Observed lead-lag relationships between indian summer monsoon and some meteorological variables., *Climate Dynamics*, *13*, 635–648, 1997.

Hasegawa, T., and K. Hanawa, Heat content variability related to enso events in the pacific, *Journal of physical oceanography*, *33*, 407–421, 2003.

Ihara, C., Y. Kushnir, and M. A. Cane, Warming trend of the indian ocean sst and indian ocean dipole from 1880 to 2004, *Journal of Climate*, *21*, 2035–2046, 2008.

Ihara, C., Y. Kushnir, M. A. Cane, and V. H. de La Peña, Climate change over the equatorial indo-pacific in global warming, *Journal of Climate*, *22*, 2678–2693, 2009.

Izumo, T., J. Vialard, M. Lengaigne, C. de Boyer Montegut, S. K. Behera, J. J. Luo, S. Cravatte, S. Masson, and T. Yamagata, Influence of the state of the indian ocean dipole on following year's el niño, *Nature Geoscience*, *3*, 168–172, 2010.

Jansen, M. F., D. Dommenget, and N. Keenlyside, Tropical atmosphere-ocean interactions in a conceptual framework., *Journal of Climate*, *22*, 550–567., 2009.

Jin, F. F., An equatorial ocean recharge paradigm for enso. part i: Conceptual model, *Journal of the atmospheric sciences*, *54*, 811–829, 1997.

Ju, J., and J. M. Slingo, The asian summer monsoon and enso., *Quarterly Journal of the Royal Meteorological Society*, *121*, 1133–1168, 1995.

Kessler, W. S., Is enso a cycle or a series of events?, *Geophysical Research Letters(0094-8276)*, *29*, 40–1, 2002.

Kinter, J. L., K. Miyakoda, and S. Yang, Recent change in the connection from the asian monsoon to enso, *Journal of Climate*, *15*, 1203–1215, 2002.

Kripalani, R. H., and A. A. Kulkarni, Climatic impact of el niño/la niña on the indian monsoon: A new perspective., *Weather*, *52*, 39–46, 1997.

Kripalani, R. H., A. A. Kulkarni, S. S. Sabade, J. V. Revadekar, S. K. Patwardhan, and J. R. Kulkarni, Intraseasonal oscillations during monsoon 2002 and 2003., *Current Science*, *87*, 325–331, 2004.

Krishnamurthi, T., M. Kanamitsu, W. Koss, and J. Lee, Tropical east-west circulations during the northern winter., *Journal of the Atmospheric Sciences*, *30*, 780–787, 1973.

Krishnan, R., and P. Swapna, Significance influence of the boreal summer monsoon flow on the indian ocean response during dipole events., *Journal of Climate*, *22*, 5611–5634, 2009.

Kucharski, F., A. Bracco, J. H. Yoo, and F. Molteni, Low-frequency variability of the indian monsoon-enso relationship and the tropical atlantic: The weakening of the 1980s and 1990s, *Journal of Climate*, *20*, 4255–4266, 2007.

Kucharski, F., A. Bracco, J. H. Yoo, and F. Molteni, Atlantic forced component of the indian monsoon interannual variability, *Geophys. Res. Lett*, *35*, 2008.

Kucharski, F., A. Bracco, J. H. Yoo, A. M. Tompkins, L. Feudale, P. Ruti, and A. Dell'Aquila, A gill–matsuno-type mechanism explains the tropical atlantic influence on african and indian monsoon rainfall, *Quarterly Journal of the Royal Meteorological Society*, *135*, 569–579, 2009.

Kug, J. S., and I. S. Kang, Interactive feedback between enso and the indian ocean, *Journal of climate*, *19*, 1784–1801, 2006.

Kug, J. S., S. I. An, F. F. Jin, and I. S. Kang, Preconditions for el nino and la nina onsets and their relation to the indian ocean, *Geophys. Res. Lett*, *32*, L05,706, 2005.

Kug, J. S., F. F. Jin, K. P. Sooraj, and I. S. Kang, State-dependent atmospheric noise associated with enso, *Geophys. Res. Lett*, *35*, L05,701, 2008.

Kug, J. S., F. F. Jin, and S. I. An, Two types of el niño events: cold tongue el niño and warm pool el niño, *Journal of Climate*, *22*, 2010.

Kumar, K. K., B. Rajagopalan, and M. A. Cane, On the weakening relationship between the indian monsoon and enso, *Science*, *284*, 2156–2159, 1999.

Kumar, K. K., B. Rajagopalan, H. Hoerling, B. G., and M. Cane, Unraveling the mystery of indian monsoon failure during el niño., *Science*, *314*, 115–119, 2006.

Lau, N. C., and M. J. Nath, Impact of enso on the variability of the asian-australian monsoons as simulated in gcm experiments, *Journal of climate*, *13*, 4287–4309, 2000.

Lau, N. C., and M. J. Nath, Atmosphere-ocean variations in the indo-pacific sector during enso episodes, *Journal of climate*, *16*, 3–20, 2003.

Lau, N. C., and M. J. Nath, Coupled gcm simulation of atmosphere-ocean variability associated with zonally asymmetric sst changes in the tropical indian ocean., *Journal of Climate*, *17*, 245–265, 2004.

Lengaigne, M., E. Guilyardi, J. P. Boulanger, C. Menkes, P. Delecluse, P. Inness, J. Cole, and J. Slingo, Triggering of el niño by westerly wind events in a coupled general circulation model, *Climate dynamics*, *23*, 601–620, 2004.

Li, T., C. W. Tham, and C. P. Chang, A coupled air-sea-monsoon oscillator for the tropospheric biennial oscillation., *Journal of Climate*, *14*, 752–764, 2001a.

Li, T., Y. S. Zhang, C. P. Chang, and B. Wang, On the relationship between indian ocean sst and asian summer monsoon., *Geophysical Research Letters*, *28*, 2843–2846, 2001b.

Loschnigg, J., G. A. Meehl, P. J. Webster, J. M. Arblaster, and G. P. Compo, The asian monsoon, the tropospheric biennial oscillation, and the indian ocean zonal mode in the ncar csm*, *Journal of climate*, *16*, 1617–1642, 2003.

Luo, J. J., Ocean dynamics not required?, *Nature*, *477*, 544–546, 2011.

Luo, J. J., S. Masson, S. Behera, P. Delecluse, S. Gualdi, A. Navarra, and T. Yamagata, South pacific origin of the decadal enso-like variation as simulated by a coupled gcm., *Geophysical Research Letters*, *30*, 2250, 2003.

Luo, J. J., S. Masson, S. Behera, S. Shingu, and T. Yamagata, Seasonal climate predictability in a coupled oagcm using a different approach for ensemble forecasts., *Journal of Climate*, *18*, 2344–2360, 2005a.

Luo, J. J., S. Masson, E. Roeckner, G. Madec, and T. Yamagata, Reducing climatology bias in an ocean-atmosphere cgcm with improved coupling physics., *Journal of Climate*, *18*, 2344–2360, 2005b.

Luo, J. J., S. Masson, E. Roeckner, G. Madec, and T. Yamagata, Reducing climatology bias in an ocean-atmosphere cgcm with improved coupling physics, *Journal of climate*, *18*, 2344–2360, 2005c.

Luo, J. J., S. Masson, S. K. Behera, and T. Yamagata, Extended enso predictions using a fully coupled ocean-atmosphere model, *Journal of Climate*, *21*, 84–93, 2008.

Luo, J. J., R. Zhang, S. K. Behera, Y. Masumoto, F. F. Jin, R. Lukas, and T. Yamagata, Interaction between el nino and extreme indian ocean dipole, *Journal of Climate*, *23*, 726–742, 2010.

Madec, G., "nemo ocean engine". note du pole de modélisation, institut pierre-simon laplace (ipsl), Institut Pierre-Simon Laplace (IPSL), France, No 27 ISSN No 1288-1619., 2008.

Masson, S., J. J. Luo, G. Madec, J. Vialard, F. Durand, S. Gualdi, E. Guilyardi, S. Behera, and P. Delecluse, Impact of barrier layer on winter-spring variability of the southeastern arabian sea., *Geophysical Research Letters*, *32*, 2005.

Masson, S., P. Terray, G. Madec, J. J. Luo, T. Yamagata, and K. Takahashi, Impact of intra-daily sst variability on enso characteristics in a coupled model., *Climate Dynamics*, 2011.

McPhaden, M. J., Genesis and evolution of the 1997-98 el niño, *Science*, *283*, 950, 1999.

McPhaden, M. J., Tropical pacific ocean heat content variations and enso persistence barriers, *Geophys. Res. Lett*, *30*, 1480, 2003.

McPhaden, M. J., S. E. Zebiak, and M. H. Glantz, Enso as an integrating concept in earth science., *Science*, *314*, 1740–1745, 2006.

Meehl, G. A., The annual cycle and interannual variability in the tropical pacific and indian ocean regions., *Monthly Weather Review*, *115*, 1987.

Meehl, G. A., The south asian monsoon and the tropospheric biennial oscillation (tbo), *Journal of Climate*, *10*, 1921–1943, 1997.

Meehl, G. A., and J. M. Arblaster, The tropospheric biennial oscillation and the asian-australian monsoon rainfall, *Journal of Climate*, *15*, 722–744, 2002a.

Meehl, G. A., and J. M. Arblaster, Indian monsoon gcm sensitivity experiments testing tropospheric biennial oscillation transition conditions., *Journal of Climate*, *15*, 923–944, 2002b.

Meehl, G. A., J. M. Arblaster, and J. Loschnigg, Coupled ocean-atmosphere dynamical processes in the tropical indian and pacific oceans and the tbo., *Journal of Climate*, *16*, 2138–2158, 2003.

Meinen, C. S., and M. J. McPhaden, Observations of warm water volume changes in the equatorial pacific and their relationship to el niño and la niña, *Journal of Climate*, *13*, 3551–3559, 2000.

Morcrette, J. J., L. Smith, and Y. Fouquart, Pressure and temperature dependence of the absorption in longwave radiation parameterizations., *Beitr Phys Atmos*, *59*, 1986.

Neelin, J. D., D. S. Battisti, A. C. Hirst, F. F. Jin, Y. Wakata, T. Yamagata, and S. E. Zebiak, Enso theory, *Journal of Geophysical Research*, *103*, 14,261–14, 1998.

Nitta, T., and S. Yamada, Recent warming of tropical sea surface temperature and its relationship to the northern hemisphere circulation, *Meteorological Society of Japan, Journal*, *67*, 375–383, 1989.

Nordeng, T. E., *Extended versions of the convective parameterization scheme at ECMWF and their impact on the mean and transient activity of the model in the tropics. Technical Memorandum 206.*, ECMWF, Reading, UK, 1994.

Ohba, M., and H. Ueda, An impact of sst anomalies in the indian ocean in acceleration of the el niño to la niña transition, *J Meteorol Soc Japan*, *85*, 335–348, 2007.

Pai, D. S., and M. Rajeevan, Indian summer monsoon onset: Variability and prediction, *Tech. rep.*, National Climate Centre, Office of the additional director general of meteorology (research), Indian Meteorological Department, PUNE, 2007.

Park, H., J. C. Chiang, and B. R. Lintner, The delayed effect of major el niño events on indian monsoon rainfall, *Journal of Climate*, *23*, 932–946, 2010.

Park, W., N. Keenlyside, M. Latif, A. Ströh, R. Redler, E. Roeckner, and G. Madec, Tropical pacific climate and its response to global warming in the kiel climate model., *Journal of Climate*, *22*, 71–92, 2009.

Parthasarathy, B., A. A. Munot, and D. R. Kothawale, All-india monthly and seasonal rainfall series: 1871–1993, *Theoretical and Applied Climatology*, *49*, 217–224, 1995.

Peings, Y., H. Douville, and P. Terray, Extented winter pacific north america oscillation as a precursor of the indian summer monsoon rainfall, *Geophys. Res. Lett*, *36*, 2009.

Philander, S. G., *El Niño, La Niña, and the southern oscillation*, vol. 46, Academic Pr, 1990.

Picaut, J., F. Masia, and Y. du Penhoat, An advective-reflective conceptual model for the oscillatory nature of the enso, *Science*, pp. 663–666, 1997.

Rajeevan, M., and L. Sridhar, Inter-annual relationship between atlantic sea surface temperature anomalies and indian summer monsoon., *Geophysical Research Letters*, *35*, 2008.

Rajeevan, M., D. S. Pai, R. Anil Kumar, and B. Lal, New statistical models for long-range forecasting of southwest monsoon rainfall over india., *Climate Dynamics*, *28*, 813–828, 2006.

Randall, D., S. Bony, R. Wood, and R. Colman, *Climate Models and Their Evaluation*, Climate Change 2007: The Physical Science Basis. Contribution of Working Group I to the Fourth Assessment Report of the Intergovernmental Panel on Climate Change, 2007.

Rasmusson, E. M., and T. H. Carpenter, Variations in tropical sea surface temperature and surface wind fields associated with the southern oscillation/el niño, *Mon. Wea. Rev*, *110*, 354–384, 1982.

Rayner, N. A., D. E. Parker, E. B. Horton, C. K. Folland, L. V. Alexander, D. P. Rowell, E. C. Kent, and A. Kaplan, Global analyses of sea surface temperature, sea ice, and night marine air temperature since the late nineteenth century, *J. Geophys. Res*, *108*, 4407, 2003.

Rodriguez-Fonseca, B., I. Polo, J. Garcia-Serrano, T. Losada, E. Mohino, C. R. Mechoso, and F. Kucharski, Are atlantic niños enhancing pacific enso events in recent decades, *Geophys. Res. Lett*, *36*, L20,705, 2009.

Roeckner, E., G. Bäuml, L. Bonaventura, R. Brokopf, M. Esch, M. Giorgetta, and S. Hagemann, The atmospheric general circulation model echam5: Part 1: Model description., Max-Planck-Institut für Meteorologie, Hamburg, 2003.

Roeckner, E., R. Brokopf, M. Esch, M. Giorgetta, S. Hagemann, L. Kornblueh, E. Manzini, U. Schlese, and U. Schulzweida, *The atmospheric general circulation model ECHAM5 Part II: Sensitivity of simulated climate to horizontal and vertical resolution.*, Max-Planck-Institute for Meteorology, MPI-Report 354, 2004.

Saji, N. H., B. N. Goswami, P. N. Vinayachandran, and T. Yamagata, A dipole mode in the tropical indian ocean., *Nature*, *401*, 360–3, 1999.

Selvaraju, R., Impact of el niño-southern oscillation on indian foodgrain production., *International Journal of Climatology*, *23*, 187–206, 2003.

Srivastava, A. K., M. Rajeevan, and R. Kulkarni, Teleconnection of olr and sst anomalies over atlantic ocean with indian summer monsoon., *Geophysical Research Letters*, *29*, 2002.

Terray, P., An evaluation of climatological data in the indian ocean area, *Journal of the Meteorological Society of Japan*, *72*, 359–385, 1994.

Terray, P., Southern hemisphere extra-tropical forcing: a new paradigm for el niño-southern oscillation, *Climate dynamics*, *36*, 2171–2199, 2011.

Terray, P., and S. Dominiak, Indian ocean sea surface temperature and el niño-southern oscillation: a new perspective, *Journal of climate*, *18*, 1351–1368, 2005.

Terray, P., P. Delecluse, S. Labattu, and L. Terray, Sea surface temperature associations with the late indian summer monsoon, *Climate dynamics*, *21*, 593–618, 2003.

Terray, P., S. Dominiak, and P. Delecluse, Role of the southern indian ocean in the transitions of the monsoon-enso system during recent decades, *Climate dynamics*, *24*, 169–195, 2005a.

Terray, P., E. Guilyardi, A. S. Fischer, and P. Delecluse, Dynamics of the indian monsoon and enso relationships in the sintex global coupled model., *Climate Dynamics*, *24*, 2005b.

Terray, P., F. Chauvin, and H. Douville, Impact of southeast indian ocean sea surface temperature anomalies on monsoon-enso-dipole variability in a coupled ocean–atmosphere model, *Climate dynamics*, *28*, 553–580, 2007.

Terray, P., K. Kakitha, S. Masson, G. Madec, A. K. Sahai, J. J. Luo, and T. Yamagata, The role of the intra-daily sst variability in the indian monsoon variability and monsoon-enso–iod relationships in a global coupled model., *Climate Dynamics*, 2011.

Tiedtke, M., A comprehensive mass flux scheme for cumulus parameterization in large-scale models., *Monthly Weather Review*, *117*, 1779–1800, 1989.

Timmermann, R., H. Goosse, G. Madec, T. Fichefet, C. Ethe, and V. Duliere, On the representation of high latitude processes in the orca-lim global coupled sea ice-ocean model., *Ocean Modelling*, *8(1-2)*, 175–201, 2005.

Torrence, C., and P. J. Webster, The annual cycle of persistence in the el niño-southern oscillation, *Quarterly Journal of the Royal Meteorological Society*, *124*, 1985–2004, 1998.

Trenberth, K., G. Branstator, and D. Karoly, Progress during toga in understanding and modeling global teleconnections associated with tropical, *Journal of Geophysical Research*, *103*, 14–291, 1998.

Trenberth, K. E., The definition of el niño, *Bulletin of the American Meteorological Society*, *78*, 2771–2778, 1997.

Trenberth, K. E., J. W. Hurrell, and D. P. Stepaniak, *The Asian Monsoon: Global perspectives.*, Praxis Publishing Ltd., Chichester, UK, 2006.

Uppala, S. M., et al., The era-40 re-analysis, *Quarterly Journal of the Royal Meteorological Society*, *131*, 2961–3012, 2005.

Valcke, *OASIS3 User Guide (prism2-5). CERFACS Technical Report TR/CMGC/06/73, PRISM Report No 3, 60 pp*, Toulouse, France, 2006.

Vimont, D. J., D. S. Battisti, and A. C. Hirst, Footprinting: A seasonal connection between the tropics and mid-latitudes, *Geophys. Res. Lett*, *28*, 3923–3926, 2001.

Vimont, D. J., D. S. Battisti, and A. C. Hirst, The seasonal footprinting mechanism in the csiro general circulation models*, *Journal of climate*, *16*, 2653–2667, 2003a.

Vimont, D. J., J. M. Wallace, and D. S. Battisti, The seasonal footprinting mechanism in the pacific: Implications for enso., *Journal of Climate*, *16*, 2668–2675, 2003b.

Vimont, D. J., M. Alexander, and A. Fontaine, Midlatitude excitation of tropical variability in the pacific: The role of thermodynamic coupling and seasonality*, *Journal of Climate*, *22*, 518–534, 2009.

Walker, G. T., Correlation in seasonal variations of weather, iv, a further study of world weather., *Mem. Indian. Meteorol. Dept.*, 1924.

Wang, B., Interdecadal changes in el niño onset in the last four decades., *Journal of Climate*, *8*, 267–285, 1995.

Wang, B., *The Asian Monsoon*, 787 pp., Praxis Publishing Ltd., Chichester, UK, 2006a.

Wang, B., and Q. Zhang, Pacific-east asian teleconnection. part ii: How the philippine sea anomalous anticyclone is established during el niño development*, *Journal of climate*, *15*, 3252–3265, 2002.

Wang, C., An overlooked feature of tropical climate: Inter-pacific-atlantic variability, *Geophys. Res. Lett*, *33*, L12,702, 2006b.

Wang, C., and J. Picaut, Understanding enso physicsa review, *Earths Climate: The Ocean-Atmosphere Interaction, Geophys. Monogr*, *147*, 21–48, 2004.

Watanabe, M., and F. F. Jin, Role of indian ocean warming in the development of philippine sea anticyclone during enso., *Geophysical Research Letters*, *29*, 2002.

Webster, P. J., and C. D. Hoyos, Beyond the spring barrier?, *Nature Geoscience*, *3*, 152–153, 2010.

Webster, P. J., and S. Yang, Monsoon and enso: Selectively interactive systems, *Quarterly Journal of the Royal Meteorological Society*, *118*, 877–926, 1992.

Webster, P. J., V. O. Maga a, T. N. Palmer, J. Shukla, R. A. Tomas, M. Yanai, and T. Yasunari, Monsoons: Processes, predictability, and the prospects for prediction, *Journal of Geophysical Research*, *103*, 14,451–14,510, 1998.

Weisberg, R. H., and C. Wang, A western pacific oscillator paradigm for the el niño-southern oscillation, *Geophysical research letters*, *24*, 779–782, 1997.

Wu, R., and B. P. Kirtman, Understanding the impacts of the indian ocean on enso variability in a coupled gcm, *Journal of climate*, *17*, 4019–4031, 2004.

Wu, R., and B. Wang, A contrast of the east asian summer monsoon-enso relationship between 1962–1977 and 1978–93., *Journal of Climate*, *15*, 3266–3279, 2002.

Wyrtki, K., Water displacements in the pacific and the genesis of el niño cycles, *Journal of Geophysical Research*, *90*, 7129–7132, 1985.

Xavier, P. K., C. Marzin, and B. N. Goswami, An objective definition of the indian summer monsoon season and a new perspective on the enso-monsoon relationship, *Quarterly Journal of the Royal Meteorological Society*, *133*, 749–764, 2007.

Xie, S. P., H. Annamalai, F. A. Schott, and J. P. McCreary, Structure and mechanisms of south indian ocean climate variability, *Journal of Climate*, *15*, 864–878, 2002.

Xie, S. P., J. Hafner, H. Tokinaga, Y. Du, T. Sampe, and H. G. Hu KaiMing, Indian ocean capacitor effect on indo-western pacific climate during the summer following el nino, *Journal of Climate*, *22*, 730–747, 2009.

Yamagata, T., S. K. Behera, J. J. Luo, S. Masson, M. Jury, and S. Rao, Coupled ocean-atmosphere variability in the tropical indian ocean., in *Earth climate: the ocean-atmosphere interaction.*, edited by C. Wang, S. P. Xie, and J. A. Carton, pp. 189–212, Geophys Monogr Ser 147, AGU, Washington, DC., 2004.

Yang, J., Q. Liu, S. P. Xie, Z. Liu, and L. Wu, Impact of the indian ocean sst basin mode on the asian summer monsoon, *Geophysical research letters*, *34*, 2708, 2007.

Yasunari, T., The monsoon year - a new concept of the climatic year in the tropics., *Bulletin of the American Meteorological Society*, *72*, 1331–1338, 1991.

Yu, J. Y., C. R. Mechoso, J. C. McWilliams, and A. Arakawa, Impacts of the indian ocean on the enso cycle, *Geophysical research letters*, *29*, 46–1, 2002.

Yu, J. Y., S. P. Weng, and J. D. Farrara, Ocean roles in the tbo transitions of the indian-australian monsoon system., *Journal of Climate*, *16*, 3072–3080, 2003.

Zalesak, S. T., Fully multidimensional flux-corrected transport algorithms for fluids., *Journal of Computational Physics*, *31*, 335–362, 1979.

Zebiak, S. E., and M. A. Cane, A model el nino-southern oscillation, *Monthly Weather Review*, *115*, 2262–2278, 1987.

Zhang, Y., J. R. Norris, and J. M. Wallace, Seasonality of large-scale atmosphere-ocean interaction over the north pacific, *Journal of Climate*, 1998.

Zheng, X. T., S. P. Xie, G. A. Vecchi, Q. Liu, and J. Hafner, Indian ocean dipole response to global warming: Analysis of ocean-atmospheric feedbacks in a coupled model*, *Journal of Climate*, *23*, 1240–1253, 2010.

ACRONYMS

ISM	Indian Summer Monsoon
ENSO	El Niño Southern Oscillation
IO	Indian Ocean
SST	Sea Surface Temperature
SLP	Sea Level Pressure
JJAS	June-July-August-September
JJ	June-July
AS	August-September
IOD	Indian Ocean Dipole
IOB	Indian Ocean Basin
SEIO	South East Indian Ocean
NPO	North Pacific Ocean
SIO	South Indian Ocean
TBO	Tropical Biennial Oscillation
ITCZ	InterTropical Convergence Zone
GCM	Global Coupled Model
SVD	Singular Value Decomposition
Z20	20°C isotherm depth
USTR	Zonal Wind Stress
JFM	January-February-March
FMA	February-March-April
ONDJF	October-November-December-January-February
CMIP5	Coupled Model Intercomparison Project Phase 5